



The  
University  
Of  
Sheffield.

**A study on the synthesis of gold nanoparticles by  
*Escherichia coli* and *Shewanella oneidensis***

**By:**

Juliano Bertozzi Silva

A thesis submitted in partial fulfilment of the requirements for the  
degree of  
Doctor of Philosophy

The University of Sheffield  
Faculty of Engineering  
Department of Chemical and Biological Engineering

November 2020



“They won’t believe that You’re talking to me, Jesus—not without seeing a miracle or a sign” . . . Suddenly a peal of thunder blasted . . . “Jesus is saying that he gave you thunder so you would listen to his messages and not ask for miracles that have no meaning . . . because your *lives* are miracles. A true miracle is a child in the womb; a mother’s love is a miracle; a forgiving heart is a miracle. Your lives are filled with miracles, but you are too distracted by material things to see them . . . Stop looking to the sky for miracles. Open your heart to God; true miracles occur in the heart.”

**The Boy Who Met Jesus, by Immaculée Ilibagiza.**

In this passage, Segatashya – a boy from Rwanda who claimed to have apparitions of Jesus Christ – was experiencing a vision of Jesus and addressed His answer to a large crowd in Kibeho that had been asking for a sign to help them believe.

*To Larissa – my beloved wife  
who I love, admire and cherish  
with all my heart*

---

## S u m m a r y

---

Gold nanoparticles (AuNPs) are fascinating structures extensively studied for applications in a variety of fields, including electronics, biomedical and catalysis. Currently, chemical reduction is the main route for their synthesis because it is simple, cost-effective and reliable. Microbial synthesis of nanoparticles is a relatively new field of research that comes with the advantages of not requiring high temperatures, manipulation of harsh chemicals and allowing the concomitant bioremediation of toxic heavy metals. Nevertheless, although promising, utilising microorganisms has a major disadvantage – lack of controllability of the process.

The present study aimed to improve the controllability of microbial synthesis of AuNPs. For that, nanoparticles fabricated by *Escherichia coli* and *Shewanella oneidensis* were evaluated. In the case of *E. coli*, strain BL21(DE3) was utilised, and for *S. oneidensis*, strain MR-1 as well as a mutant lacking *c*-type cytochromes and a range of mutants containing deletions of components from the Mtr pathway (a group of proteins and *c*-type cytochromes responsible for the conduit of electrons from the inner membrane to electron acceptors located outside the cell) were adopted. The study confirmed that, although not required for the synthesis, *c*-type cytochromes influence the process. Most importantly, it has been found that absence of specific cytochromes yielded a better control of the characteristics of the biofabricated AuNPs. Also of interest, the cytochrome MtrF was found to be the most active in the aerobic formation of nanoparticles.

It has also been observed that the methods favourable for the biosynthesis of gold nanoparticles were lethal for the cultures. Additional tests were then carried out attempting to have living cells making nanoparticles. In all cases no AuNPs were detected through spectrophotometry. Although not conclusive yet, the results indicated that it is not possible to have living cells of *E. coli* and *S. oneidensis* synthesising gold nanoparticles.

*Page intentionally left blank*

---

# A c k n o w l e d g m e n t s

---

Fully aware that it is not possible to acknowledge everybody who directly or indirectly contributed to this outcome, I will try in this section to humbly express my gratitude to as many people who helped me during this journey as possible. I do apologise in advance to those who should have been named here, but, by some mistake, were not. The surnames of non-academic persons have been omitted because I do not believe there is a need to reveal the identities of my supporters to the general public. I am certain that those who were acknowledged here will be able to recognise themselves.

My initial and deepest gratitude is certainly addressed to the Almighty God, Jesus Christ and Holy Mary. I am convinced that the journey throughout my PhD programme had ultimately a religious purpose. All the ups and downs, the moments of joy, enlightenment and flourishing, and – most importantly – the moments of suffering, blurriness and despair, have contributed to my faith reinforcement. It is delightful to learn that I have never been, and will never be, abandoned.

My spouse Larissa, mother of my most beloved children, is undoubtedly the most important person behind this thesis. Without her on my side none of this would have ever been possible. Her endless source of love, strength and inspiration makes her the hidden secret behind my success – and I am deeply grateful for that. Thank you for being part of my life.

My family in Brazil also contributed immensely, mostly indirectly, to this accomplishment in my life and deserve a special acknowledgement. Although far away in distance they know they are close in my heart.

A huge thank you is addressed to Professor Phillip C. Wright, my former supervisor. He trusted me with this challenge and provided fundamental guidance. Kindness, intelligence and diligence are aspects of his nature that are sources of inspiration to my personal and professional development.

Immense appreciation is also given to Dr. Jagroop Pandhal, who became my substitute first supervisor. He took the project over in a final and critical stage of its development and was able to skilfully conduct it to success.

Professor Iain Todd, my second supervisor, Dr. Gregory Fowler and Dr. Stephen Jaffe were also directly involved in this research and were crucial for this accomplishment. Their contributions are deeply appreciated.

Professor Jeffrey Gralnick from the University of Minnesota and Dr. Matthew Marshall from the Pacific Northwest National Laboratory are also acknowledged for providing the mutant strains applied in this work.

I would also like to express big gratitude to my colleagues from the Wright and Pandhal groups for keeping the atmosphere at work more friendly and enjoyable. Appreciation is also given to them for direct contributions to my project.

My friends in the department were also very important for the success of my PhD programme. Unfortunately, I will not be able to thank all of them name by name, but certainly one of the most important accomplishments of this journey was that I could build true friendships that – I hope – will last for a long time.

I would also like to thank all the technicians and student support staff from the department. They play a vital role in keeping all the scientific activities within the department ongoing smoothly. Likewise, many thanks are addressed to Dr. Svetomir Tzokov from the electron microscopy facilities in the Department of Molecular Biology and Biotechnology, Dr. Peng Zeng and Dr. Colm O'Regan from the Sorby Centre for Electron Microscopy, Dr. Nicola Green from the Kroto Imaging Facility and the staff from the Mathematics and Statistics Help (MASH) Centre for directly helping me in specific points of my research.

My Brazilian friends from Sheffield, Dr. Martins and Natalia, as well as those living in Brazil were certainly indirect contributors to this thesis. Their friendship makes life more colourful and festive. Special praise is given to my dear friend Tamires – who sadly is not among us anymore.

Thank you very much everybody!



---

# Table of contents

---

<b>1</b>	<b>General overview .....</b>	<b>3</b>
<b>2</b>	<b>Aims of the study and chapter breakdown .....</b>	<b>5</b>
<b>3</b>	<b>Literature review .....</b>	<b>9</b>
3.1	Biotechnology .....	9
3.2	Nanotechnology .....	12
3.3	Nanobiotechnology .....	20
3.4	Nanoparticles .....	20
3.4.1	Metallic nanoparticles .....	21
3.4.1.1	Properties of metallic nanoparticles .....	21
3.4.1.2	Methods for characterising metallic nanoparticles .....	25
3.4.1.3	Methods for synthesising metallic nanoparticles .....	29
3.4.1.3.1	<i>Chemical methods .....</i>	<i>31</i>
3.4.1.3.2	<i>Physical methods .....</i>	<i>31</i>
3.4.1.3.3	<i>Biological methods .....</i>	<i>32</i>
3.4.1.4	Synthesis of metallic nanoparticles by microorganisms .....	33
3.4.1.4.1	<i>Mechanisms involved in the synthesis of metallic nanoparticles by microorganisms .....</i>	<i>36</i>
3.4.1.4.2	<i>Advantages and disadvantages of using microorganisms for the synthesis of metallic nanoparticles .....</i>	<i>39</i>
3.4.1.4.3	<i>The chemistry involved in the microbial synthesis of gold nanoparticles .....</i>	<i>40</i>
3.5	Bacteria used in the present study .....	43
3.5.1	<i>Shewanella oneidensis</i> MR-1 .....	44
3.5.2	<i>Escherichia coli</i> BL21(DE3) .....	48
3.6	Synthesis of metallic nanoparticles by <i>Escherichia coli</i> and <i>Shewanella oneidensis</i> .....	50
3.6.1	<i>Escherichia coli</i> .....	50

3.6.2	<i>Shewanella oneidensis</i> .....	54
3.6.3	The choice for <i>Escherichia coli</i> BL21(DE3) and <i>Shewanella oneidensis</i> MR-1 .....	58
<b>4</b>	<b>Materials and methods .....</b>	<b>61</b>
4.1	Microorganisms and culture media .....	61
4.1.1	Microorganisms .....	61
4.1.2	Culture media.....	62
4.2	Methods for the microbial synthesis of gold nanoparticles.....	64
4.2.1	Method I .....	64
4.2.2	Method II .....	65
4.2.3	Method III .....	66
4.2.4	Method IV .....	67
4.3	Analyses of spectrophotometry .....	68
4.3.1	Analysis of optical density.....	68
4.3.2	Analysis of visible spectra .....	68
4.4	Adsorption of gold ions from solution .....	69
4.5	Analyses adopting electron microscopy.....	70
4.5.1	Transmission electron microscopy.....	70
4.5.2	Selected-area electron diffraction .....	70
4.5.3	Energy dispersive X-ray spectroscopy.....	70
4.5.4	Determining sizes and shapes.....	71
4.6	Determining specific productivity of gold nanoparticles .....	74
4.7	Cell viability assays .....	76
4.8	Minimum inhibitory concentration .....	79
4.9	Statistical analyses .....	80
4.9.1	Experiments in chapter 5 .....	80

4.9.2	Experiments in chapter 6 .....	80
4.9.3	Experiments in chapter 7 .....	81
<b>5</b>	<b>Comparing the gold nanoparticles synthesised by <i>Escherichia coli</i> and <i>Shewanella oneidensis</i>.</b> .....	<b>85</b>
5.1	Abstract .....	85
5.2	Introduction.....	85
5.3	Results .....	87
5.4	Discussion .....	93
5.5	Conclusion .....	98
<b>6</b>	<b>Comparing the gold nanoparticles synthesised by <i>Shewanella oneidensis</i> wild-type and mutants containing deletions in cytochromes.</b> .....	<b>101</b>
6.1	Abstract .....	101
6.2	Introduction.....	102
6.3	Results .....	103
6.3.1	Results from the experiments conducted under aerobic conditions (method I).....	103
6.3.2	Results from the experiments conducted under anaerobic conditions (method II).....	113
6.4	Discussion .....	122
6.4.1	Correlation between surface plasmon bands and the other variables measured .....	122
6.4.2	Influence of the c-type cytochromes under investigation in the synthesis of gold nanoparticles .....	124
6.4.3	Additional observations .....	125
6.5	Conclusion .....	127
<b>7</b>	<b>Tests of methods aiming to have cultures of <i>Escherichia coli</i> and <i>Shewanella oneidensis</i> actively synthesising gold nanoparticles</b> .....	<b>131</b>

7.1	Abstract .....	131
7.2	Introduction .....	131
7.3	Results .....	132
7.4	Discussion.....	138
7.5	Conclusion .....	144
<b>8</b>	<b>Future studies .....</b>	<b>147</b>
<b>9</b>	<b>Conclusion .....</b>	<b>151</b>
<b>10</b>	<b>References.....</b>	<b>155</b>
<b>11</b>	<b>Appendix I .....</b>	<b>191</b>
<b>12</b>	<b>Appendix II .....</b>	<b>201</b>
<b>13</b>	<b>Appendix III .....</b>	<b>263</b>
13.1	Materials and methods .....	263
13.1.1	Microorganisms and culture media .....	263
13.1.2	Procedures for growing the cells .....	263
13.1.3	Monitoring growth.....	264
13.1.3.1	Optical density .....	264
13.1.3.2	Colony counting.....	264
13.1.3.3	Camera pictures and microscope images.....	264
13.2	Results .....	265
13.2.1	Aerobically grown cultures .....	265
13.2.2	Anaerobically grown cultures .....	268
<b>14</b>	<b>Appendix IV .....</b>	<b>280</b>

---

## List of tables

---

<b>Table 3.1:</b> Historical development of biotechnology (reproduced from Smith (2009) with permission of The Licensor through PLSclear).....	10
<b>Table 3.2:</b> Applications of biotechnology in different areas (adapted from Bhatia and Goli (2018) © IOP Publishing. Adapted with permission. All rights reserved).....	13
<b>Table 3.3:</b> Milestones of nanoscience and nanotechnology. Adapted from Godale and Sharon (2019) with permission.....	18
<b>Table 3.4:</b> Common investigation techniques for the characterisation of nanoparticles. Reproduced from Kumar and Kumbhat (2016) with permission.....	26
<b>Table 3.5:</b> A representative list of microorganisms used for the synthesis of nanoparticles and their applications. This table was adapted from tables 1, 2, 3 and 4 of the article by Gahlawat and Choudhury (2019) - Published by The Royal Society of Chemistry; licensed under a Creative Commons Attribution-NonCommercial 3.0 Unported Licence.....	34
<b>Table 4.1:</b> List of bacteria used and relevant information about them. The Mtr pathway on the right side was reproduced from <b>Figure 3.7</b> . ....	63
<b>Table 4.2:</b> Comparison of different parameters adopted in methods I to IV. ....	67
<b>Table 11.1:</b> Primers used for checking deletions in the mutant strains of <i>Shewanella oneidensis</i> MR-1.....	192
<b>Table 11.2:</b> Polymerase chain reactions carried out for checking the deletions in the mutant strains of <i>Shewanella oneidensis</i> MR-1.....	192

---

## List of figures

---

- Figure 3.1:** The Lycurgus Cup. The left photo shows the cup illuminated from outside, thus reflecting the jade colour; and the right photo shows the cup illuminated from inside, thus transmitting the ruby colour. © **The Trustees of the British Museum**. Shared under a Creative Commons Attribution-NonCommercial-ShareAlike 4.0 International (CC BY-NC-SA 4.0) licence. ....15
- Figure 3.2:** A sequence of scanning transmission microscope images taken during the construction of a patterned array of xenon atoms on a nickel (110) surface. a, The surface after xenon dosing. b-f, Various stages during the construction. Each letter is 50 angstroms long from top to bottom. Reproduced from Eigler and Schweizer (1990). Reprinted by permission from Springer Nature Customer Service Centre GmbH. ....17
- Figure 3.3:** Visual explanation of localised surface plasmon resonance. Panel 1: schematic illustration of LSPR. Upon incidence of electromagnetic waves at specific wavelengths, the cloud of free electrons in the nanoparticle oscillates in resonance. Panel 2: pictures of aqueous solutions containing spherical AuNPs (upper pictures) and rod-shaped AuNPs (lower pictures). The corresponding transmission electron microscopy images of the nanoparticles are shown (all scale bars are 100 nm). The size of the spheres varies from 4 to 40 nm (images (a) to (e)) and the aspect ratio of the rods varies from 1.3 to 20 (images (f) to (k)). LSPR is the cause of the difference in colour of the solutions. The figure in panel 2 was reprinted from figure 2 of the article by Mody et al. (2010) with permission. ....24
- Figure 3.4:** Visible spectra of spherical AuNPs with mean sizes 51 nm for panels (A) and (B), 76 nm for (C) and (D), 88 nm for (E) and (F), 155 nm for (G) and (H), and 237 nm for (I) and (J) – the insets show size distribution of the particles. Note how different the surface plasmon bands can be depending on the size of the AuNPs. The left column shows the

spectra measured experimentally and the right column shows the spectra calculated using Mie theory. The calculated spectra detailed the total extinction (scattering plus absorption, solid lines) and the contribution from each, scattering (open circles) and absorption (dashed lines). The figure was reprinted with permission from Tcherniak et al. (2010).

Copyright (2019) American Chemical Society. .... 30

**Figure 3.5:** Schematic representation of bacterial synthesis of nanoparticles; both intracellular and extracellular processes are included. The figure was reproduced from the article by Fang et al. (2019) with permission under the Creative Commons Attribution 4.0 International Public License (<https://creativecommons.org/licenses/by/4.0/legalcode>).

..... 37

**Figure 3.6:** Speciation diagrams for the Au-Cl-OH system. The graphs contain the relative concentration of the different Au(III) chlorohydroxo complexes formed in aqueous solution at 298 K, in varying pH and at different total Au concentrations ((a)  $10^{-3}$  M, (b)  $10^{-2}$  M, (c)  $10^{-1}$  M and (d) 1 M). The figure was reprinted from figure 1 of the article by del Río et al. (2014) with permission from Elsevier. .... 41

**Figure 3.7:** Schematic illustrations of some of the anaerobic respiration pathways of *S. oneidensis* MR-1. Panel 1 shows an illustration of the pathways and the cytochromes involved in the anaerobic respiration of (left to right) dimethyl sulfoxide (DMSO), nitrate, nitrite, electrodes and extracellular soluble and insoluble metals (Mtr pathway), fumarate and trimethylamine N-oxide (TMAO). Some cytochromes were represented as high-resolution structures and some others as cartoons. Panel 2 shows a cartoon illustration of the Mtr pathway – highly relevant to the present study. OM and CM mean outer membrane and cytoplasmic membrane, respectively. Each red circle represents a heme group in the cytochromes. The figure in panel 1 was republished with permission of Royal Society from figure 3 of the article by Breuer et al. (2015); permission conveyed through Copyright Clearance Center, Inc. .... 47

<b>Figure 4.1:</b> Example of a TEM picture with a grid of 10 x 10 small squares of equal sizes. ....	71
<b>Figure 4.2:</b> Images of nanoparticles exemplifying the six categories of shapes adopted in this study. a) circular, b) triangular, c) rectangular, d) trapezoid, e) hexagonal and f) pentagon.....	72
<b>Figure 4.3:</b> Schematic illustration of the method used for determining productivity. (A) is the amount of dry bacteria without nanoparticles in a sample; (B) is the amount of bacterial ashes generated from (A); (C) is the amount of dry bacteria (E) with gold ions and gold nanoparticles (G) in a sample – the change in colour to yellow represent the gold ions adsorbed on the cells; (D) is the amount of bacterial ashes (F) with gold ions and gold nanoparticles (G).....	77
<b>Figure 5.1:</b> Bacterial adsorption of gold ions during incubation in 1 mM HAuCl <sub>4</sub> solution at 30 °C and 180 rpm for 48 h. Error bars indicate the standard deviation of three independent replicates. ....	88
<b>Figure 5.2:</b> Visible spectra of BL21(DE3) and MR-1 monitored during the implementation of method I. Graph a) shows the spectra of BL21(DE3) during incubation in HAuCl <sub>4</sub> solution, b) has the spectra of MR-1 during incubation in HAuCl <sub>4</sub> solution, c) shows the spectra of BL21(DE3) during incubation in DI water, and d) has the spectra of MR-1 during incubation in DI water. Graph e) shows the spectra of graph a) after baseline correction and graph f) has the spectra of graph b) after baseline correction. Graph g) shows the peaks of the curves in graphs e) and f). The asterisk symbol was used for the cases where plasmon bands were not detected, and the connection between the data shows the result of the statistical analysis (only the 48-h measurements were evaluated). Measurements are average of three independent replicates. For clarity of the graphs containing the spectra, error bars were not shown ( <b>Figure 12.2</b> contains spectra with error bars for graph a), <b>Figure 12.3</b> contains spectra for graph b), <b>Figure 12.4</b> for graph c), <b>Figure 12.5</b> for graph d), <b>Figure 12.6</b> for graph e) and <b>Figure 12.7</b> for graph f)).....	89



**Figure 5.3:** TEM images and determination of sizes and shapes of the gold nanoparticles synthesised by BL21(DE3) and MR-1 through method I. The images on top correspond to TEM images of the cultures after incubation in 1 mM HAuCl<sub>4</sub>. For additional images of these cultures as well as of cells after incubation in DI water (control) see **Figure 12.10**. Graph a) contains a histogram of the frontal area of the nanoparticles synthesised by the two cultures. Graph b) contains a histogram with bin range of 0 to 1000 nm<sup>2</sup> and bin width of 100 nm<sup>2</sup>. Both graphs have the same data, but graph b) was built to provide a detailed breakdown of the first bin in graph a), which contained the majority of the particles. Graph c) shows violin plots of the frontal area of the nanoparticles synthesised by both strains. The median and the quartiles are represented by the dashed and dotted lines, respectively. Note that the y-axis is in log scale. Graph d) shows a histogram depicting the categorisation of the nanoparticles according to shape. The connections between the data show the pairs that are significantly different. The results in graphs a) to d) were determined by measuring 300 particles per strain (100 per independent replicate). ..... 92

**Figure 5.4:** Specific productivity of gold nanoparticles by BL21(DE3) and MR-1 as determined from TGA measurements. Note that the values determined are a sum of gold ions adsorbed and gold nanoparticles produced. Results are average of two independent replicates. The connection between the data shows the results of the statistical analysis (ns stands for not significant)..... 94

**Figure 6.1:** Bacterial adsorption of gold ions during aerobic incubation in 1 mM HAuCl<sub>4</sub> solution at 30 °C and 180 rpm for 48 h (method I). The data of abiotic control and MR-1 are the same as those of **Figure 5.1**. Results are average of three independent replicates. For clarity of the graph, error bars were not shown (**Figure 12.11** shows the curves with error bars displayed for individual strains)..... 104

**Figure 6.2:** Visible spectra of the cultures monitored during the implementation of method I (aerobic synthesis of gold nanoparticles). The data of MR-1 are the same as those of graph b) of **Figure 5.2**. Results are

average of three independent replicates. For clarity of the graphs, error bars were not shown (**Figure 12.12** to **Figure 12.21** show the spectra with error bars). ..... 105

**Figure 6.3:** Peaks of the normalised surface plasmon bands monitored during the implementation of method I (aerobic synthesis of gold nanoparticles). The asterisk symbol was used for the cases in which plasmon bands were not detected. Results are average of three independent replicates. Graph k) shows the peaks of the 48-h measurements only. The table presents the pairs in graph k) that are significantly different. .... 107

**Figure 6.4:** TEM images of the cultures after implementation of method I (aerobic synthesis of gold nanoparticles). The image of MR-1 is the same as the image in **Figure 5.3**. For additional images of MR-1 see images g), h) and i) of **Figure 12.10**, for the other strains see **Figure 12.40** to **Figure 12.48**. .... 109

**Figure 6.5:** Frontal area of the gold nanoparticles synthesised through method I. Graph a) contains a histogram of the frontal area of the nanoparticles synthesised by the different cultures. Graph b) contains a histogram with bin range of 0 to 1000 nm<sup>2</sup> and bin width of 100 nm<sup>2</sup>. Both graphs have the same data, but graph b) was built to provide a detailed breakdown of the first bin in graph a), which contained the majority of the particles. Graph c) shows a violin plot of the frontal area of the nanoparticles synthesised by the strains. The median and the quartiles are represented by the dashed and dotted lines, respectively. Note that the y-axis is in log scale. The data for MR-1 is the same as the data in **Figure 5.3**. The table presents the pairs in graph c) that are significantly different. Results were determined by measuring 300 particles per strain (100 per independent replicate). .... 110

**Figure 6.6:** Histogram depicting the categorisation of the gold nanoparticles synthesised through method I according to shape. The data for MR-1 is the same as the data in **Figure 5.3**. The table presents the pairs

that are significantly different for each shape. Results were determined by categorising 300 particles per strain (100 per independent replicate). .. 112

**Figure 6.7:** Specific productivity of gold nanoparticles by each strain as determined from TGA measurements after the implementation of method I. Note that the values determined are a sum of gold ions adsorbed and gold nanoparticles produced. The data for MR-1 is the same as the data in **Figure 5.4**. Results are average of two independent replicates. The table presents the pairs that are significantly different. .... 113

**Figure 6.8:** Visible spectra and peaks of the surface plasmon bands generated by the cultures during the implementation of method II (anaerobic synthesis of gold nanoparticles). Graphs a) to f) show the visible spectra of the cultures. Results are average of three independent replicates. Some error bars cannot be visualised because they are smaller than the thickness of the curves. Graph g) shows peaks of the normalised plasmon bands at the 48-h measurements. Graph h) shows the peaks at the 48-h measurements comparing the results from the aerobic and anaerobic experiments. The connections between the data present the pairs that are significantly different. Statistical analyses in graph g) evaluated all strains, whereas in graph h) only the same strains (aerobically vs. anaerobically) were analysed. .... 115

**Figure 6.9:** TEM images of the cultures after implementation of method II (anaerobic synthesis of gold nanoparticles). For additional images see **Figure 12.51 to Figure 12.56**. .... 117

**Figure 6.10:** Frontal area of the gold nanoparticles synthesised through method II. Graph a) contains a histogram of the frontal area of the nanoparticles synthesised anaerobically by the different cultures. Graph b) contains a histogram with bin range of 0 to 1000 nm<sup>2</sup> and bin width of 100 nm<sup>2</sup>. Both graphs have the same data, but graph b) was built to provide a detailed breakdown of the first bin in graph a), which contained the majority of the particles. Graph c) shows violin plots of the frontal area of the nanoparticles synthesised anaerobically by the strains. The median and the quartiles are represented by the dashed and dotted lines, respectively.

Note that the y-axis is in log scale. The table presents the pairs in graph c) that are significantly different. Graph d) shows violin plots comparing the results from the aerobic and anaerobic experiments. The connections between the data present the pairs that are significantly different. Statistical analyses in graph c) evaluated all strains, whereas in graph d) only the same strains (aerobically vs. anaerobically) were analysed. Results were determined by measuring 300 particles per strain (100 per independent replicate).....118

**Figure 6.11:** Histograms depicting the categorisation of the gold nanoparticles according to shape. Graph a) shows the histogram of the nanoparticles synthesised anaerobically through method II. The table presents the pairs in graph a) that are significantly different for each shape. Graphs b) to g) compare the shapes of the particles synthesised aerobically and anaerobically. The connections between the data present the pairs that are significantly different. Statistical analyses in graph a) evaluated all strains, whereas in graphs b) to g) only the same strains (aerobically vs. anaerobically) were analysed. Results were determined by categorising 300 particles per strain (100 per independent replicate). ....120

**Figure 6.12:** Specific productivity of gold nanoparticles. Graph a) shows the productivity by anaerobic strains as determined from TGA measurements after the implementation of method II. Results are average of three independent replicates. Statistical analyses determined that the pairs are not significantly different. Graph b) shows comparisons of specific productivity obtained from aerobic and anaerobic experiments. The connections between the data present the pair that is significantly different. Statistical analyses in graph a) evaluated all strains, whereas in graph b) only the same strains (aerobically vs. anaerobically) were analysed. Note that the values determined are a sum of gold ions adsorbed and gold nanoparticles produced. ....121

**Figure 7.1:** Images of the viability tests carried out with BacLight™ assay for BL21(DE3) (a), b) and c)) and MR-1 (d), e) and f)) at different stages of method I. a) and d) are cells after growth in LB; b) and e) are cells after the

washing steps with sterile DI water; and c) and f) are cells after incubation in 1 mM H<sub>AuCl</sub><sub>4</sub> solution for 30 min. The green and red fluorescence dots correspond to living and dead cells, respectively..... 133

**Figure 7.2:** Viability tests carried out with PrestoBlue®. The upper panel shows results for BL21(DE3) and the lower panel shows results for MR-1. Samples were collected at five different stages of method I: after overnight growth in LB, after the washing steps with sterile DI water, and after 30 min, 24 h and 48 h of incubation in 1 mM H<sub>AuCl</sub><sub>4</sub>. The same procedures were conducted in cultures that were resuspended and incubated in sterile DI water with pH 3.17. The samples were added on top of the viability reagent on a 96-well plate and the plate was left incubating at 30 °C and 180 rpm for 24 h. After 1 h, 6 h and 24 h of incubation, fluorescence readings were taken. Error bars indicate the standard deviation of three independent replicates. The connections between the data present the pairs that are significantly different. Note that only the 24-h measurements were evaluated statistically. .... 134

**Figure 7.3:** TEM images and visible spectra of autoclaved BL21(DE3) and MR-1 measured during the implementation of method I. The images were taken after incubation of the cultures in 1 mM H<sub>AuCl</sub><sub>4</sub> solution. Results of the visible spectra are average of three independent replicates. For clarity of the graphs containing the spectra, error bars were not shown (**Figure 12.63** contains additional TEM images of BL21(DE3) and spectra with error bars from graph a) and **Figure 12.64** contains additional TEM images of MR-1 and spectra with error bars from graph b))...... 135

**Figure 7.4:** Experiments on minimum inhibitory concentration (MIC) of gold ions. Graph a) shows MIC results for BL21(DE3) and MR-1 cultures growing in LB added with H<sub>AuCl</sub><sub>4</sub> at different concentrations. Error bars indicate the standard deviation of three independent replicates. The connections between the data present the pairs that are significantly different. Graphs b) and c) show measurements of visible spectra of samples collected after the MIC assays. The samples analysed were the controls (only LB) of both strains, the cases of BL21(DE3) growing in 0.5

mM H<sub>AuCl</sub><sub>4</sub> and MR-1 growing in 0.1 mM H<sub>AuCl</sub><sub>4</sub>, and the cases in which BL21(DE3) and MR-1 did not grow – 1 mM and 0.5 mM H<sub>AuCl</sub><sub>4</sub>, respectively. Results are average of two independent replicates. Some error bars cannot be visualised because they are smaller than the thickness of the curves.....137

**Figure 7.5:** Visible spectra of cultures during implementation of method III (aerobic cultures at OD<sub>600</sub> of 1.25 resuspended in anaerobic LB containing H<sub>AuCl</sub><sub>4</sub> at non-lethal concentrations). a) BL21(DE3) in LB with 0.1 mM H<sub>AuCl</sub><sub>4</sub>; b) BL21(DE3) in LB with 0.01 mM H<sub>AuCl</sub><sub>4</sub>; c) MR-1 in LB with 0.1 mM H<sub>AuCl</sub><sub>4</sub>; d) MR-1 in LB with 0.01 mM H<sub>AuCl</sub><sub>4</sub>; e) BL21(DE3) in LB; f) MR-1 in LB; g) LB with 0.1 mM H<sub>AuCl</sub><sub>4</sub> (abiotic control); h) LB with 0.01 mM H<sub>AuCl</sub><sub>4</sub> (abiotic control). Measurements are average of three independent replicates. For clarity of the graphs, error bars were not shown (**Figure 12.65 to Figure 12.72** show the spectra with error bars).....139

**Figure 7.6:** Visible spectra of cultures during implementation of method IV (aerobic cultures at OD<sub>600</sub> of 2.5 left incubating in anaerobic LB for 24 h before addition of H<sub>AuCl</sub><sub>4</sub>; measurements were taken after the incorporation of gold ions). Graph a) shows results for BL21(DE3), graph b) shows results for MR-1 and graph c) shows results for abiotic control. Measurements are average of three independent replicates. For clarity of the graphs, error bars were not shown (**Figure 12.73 to Figure 12.75** show the spectra with error bars).....140

**Figure 12.1:** Examples of real TGA measurements. These examples demonstrate the reason for adopting different time in the burning step at 600 °C for the cases of samples with (24 h) and without (60 h) gold nanoparticles. Graphs a), b) and c) are the cases without nanoparticles; and graphs d), e) and f) are the cases with nanoparticles. Time zero corresponds to the moment the TGA starts raising the temperature from 105 °C to 600 °C. Therefore, at time zero samples were already dry. After reaching 600 °C, the temperature was then kept constant for 24 h or 60 h, depending on the sample. For cases a), b) and c) it took ca. 2000, 1700 and 3200 minutes for the samples to reach a constant weight, respectively; for

cases d), e) and f) it took ca. 300, 350 and 250 minutes for the samples to reach a constant weight, respectively. Hence, it can be seen that for the cases of samples containing gold nanoparticles the burning process reach weight stabilisation much faster than for the cases without nanoparticles. The substantial contribution of the nanoparticles to the final weight of the ashes is hypothesised to be the cause of this difference. .... 201

**Figure 12.2:** Visible spectra from graph a) of **Figure 5.2** divided into individual measurements. Results are average of three independent replicates. Some error bars cannot be visualised because they are smaller than the thickness of the curves. .... 202

**Figure 12.3:** Visible spectra from graph b) of **Figure 5.2** divided into individual measurements. Results are average of three independent replicates. Some error bars cannot be visualised because they are smaller than the thickness of the curves. .... 203

**Figure 12.4:** Visible spectra from graph c) of **Figure 5.2** divided into individual measurements. Results are average of three independent replicates. Error bars cannot be visualised because they are smaller than the thickness of the curves. .... 204

**Figure 12.5:** Visible spectra from graph d) of **Figure 5.2** divided into individual measurements. Error bars indicate the standard deviation of three independent replicates. .... 205

**Figure 12.6:** Spectra from graph e) of **Figure 5.2** divided into individual measurements. Results are average of three independent replicates. Some error bars cannot be visualised because they are smaller than the thickness of the curves. .... 206

**Figure 12.7:** Spectra from graph f) of **Figure 5.2** divided into individual measurements. Results are average of three independent replicates. Some error bars cannot be visualised because they are smaller than the thickness of the curves. .... 207

**Figure 12.8:** Visible spectra of 1 mM H<sub>AuCl</sub><sub>4</sub> solution incubated under aerobic conditions at 30 °C and 180 rpm for 48 h – abiotic control of method I. Results are average of three independent replicates. Error bars

cannot be visualised because they are smaller than the thickness of the curves.....208

**Figure 12.9:** Picture of a shake flask with BL21(DE3) culture after incubation in 1 mM HAuCl<sub>4</sub> solution for 48 h. Cell accumulation on the meniscus line is indicated by the white arrow. Picture b) shows a zoom of the film formed inside the flask, also containing accumulated cells.....209

**Figure 12.10:** TEM images of BL21(DE3) and MR-1 after implementation of method I. Images a), b) and c) show BL21(DE3) cultures after incubation in 1 mM HAuCl<sub>4</sub> solution; images d), e) and f) show BL21(DE3) cultures after incubation in sterile DI water (control); images g), h) and i) show MR-1 cultures after incubation in 1 mM HAuCl<sub>4</sub> solution; and images j), k) and l) show MR-1 cultures after incubation in sterile DI water (control).....210

**Figure 12.11:** Adsorption curves from **Figure 6.1** divided into individual cultures. Error bars indicate the standard deviation of three independent replicates. Some error bars cannot be visualised because they are smaller than the symbols.....211

**Figure 12.12:** Visible spectra from graph a) of **Figure 6.2** divided into individual measurements. Error bars indicate the standard deviation of three independent replicates. ....212

**Figure 12.13:** Visible spectra from graph b) of **Figure 6.2** divided into individual measurements. Error bars indicate the standard deviation of three independent replicates. ....213

**Figure 12.14:** Visible spectra from graph c) of **Figure 6.2** divided into individual measurements. Error bars indicate the standard deviation of three independent replicates. ....214

**Figure 12.15:** Visible spectra from graph d) of **Figure 6.2** divided into individual measurements. Error bars indicate the standard deviation of three independent replicates. ....215

**Figure 12.16:** Visible spectra from graph e) of **Figure 6.2** divided into individual measurements. Error bars indicate the standard deviation of three independent replicates. ....216



<b>Figure 12.17:</b> Visible spectra from graph f) of <b>Figure 6.2</b> divided into individual measurements. Error bars indicate the standard deviation of three independent replicates. ....	217
<b>Figure 12.18:</b> Visible spectra from graph g) of <b>Figure 6.2</b> divided into individual measurements. Results are average of three independent replicates. Some error bars cannot be visualised because they are smaller than the thickness of the curves.....	218
<b>Figure 12.19:</b> Visible spectra from graph h) of <b>Figure 6.2</b> divided into individual measurements. Error bars indicate the standard deviation of three independent replicates. ....	219
<b>Figure 12.20:</b> Visible spectra from graph i) of <b>Figure 6.2</b> divided into individual measurements. Error bars indicate the standard deviation of three independent replicates. ....	220
<b>Figure 12.21:</b> Visible spectra from graph j) of <b>Figure 6.2</b> divided into individual measurements. Error bars indicate the standard deviation of three independent replicates. ....	221
<b>Figure 12.22:</b> Visible spectra of SmA monitored during aerobic incubation in DI water (control of method I). Error bars indicate the standard deviation of three independent replicates.....	222
<b>Figure 12.23:</b> Visible spectra of SmC monitored during aerobic incubation in DI water (control of method I). Results are average of three independent replicates. Some error bars cannot be visualised because they are smaller than the thickness of the curves.....	223
<b>Figure 12.24:</b> Visible spectra of SmF monitored during aerobic incubation in DI water (control of method I). Results are average of three independent replicates. Some error bars cannot be visualised because they are smaller than the thickness of the curves.....	224
<b>Figure 12.25:</b> Visible spectra of DmAC monitored during aerobic incubation in DI water (control of method I). Results are average of three independent replicates. Error bars cannot be visualised because they are smaller than the thickness of the curves. ....	225

**Figure 12.26:** Visible spectra of DmAF monitored during aerobic incubation in DI water (control of method I). Error bars indicate the standard deviation of three independent replicates. ....226

**Figure 12.27:** Visible spectra of DmCF monitored during aerobic incubation in DI water (control of method I). Results are average of three independent replicates. Some error bars cannot be visualised because they are smaller than the thickness of the curves.....227

**Figure 12.28:** Visible spectra of TmACF monitored during aerobic incubation in DI water (control of method I). Results are average of three independent replicates. Some error bars cannot be visualised because they are smaller than the thickness of the curves.....228

**Figure 12.29:** Visible spectra of MmOP monitored during aerobic incubation in DI water (control of method I). Results are average of three independent replicates. Error bars cannot be visualised because they are smaller than the thickness of the curves.....229

**Figure 12.30:** Visible spectra of CcmC<sup>-</sup> monitored during aerobic incubation in DI water (control of method I). Results are average of three independent replicates. Some error bars cannot be visualised because they are smaller than the thickness of the curves.....230

**Figure 12.31:** Spectra of SmA after baseline correction. The original visible spectra are shown in graph b) of **Figure 6.2**. Results are average of three independent replicates. Some error bars cannot be visualised because they are smaller than the thickness of the curves.....231

**Figure 12.32:** Spectra of SmC after baseline correction. The original visible spectra are shown in graph c) of **Figure 6.2**. Results are average of three independent replicates. Some error bars cannot be visualised because they are smaller than the thickness of the curves.....232

**Figure 12.33:** Spectra of SmF after baseline correction. The original visible spectra are shown in graph d) of **Figure 6.2**. Results are average of three independent replicates. Some error bars cannot be visualised because they are smaller than the thickness of the curves.....233

<b>Figure 12.34:</b> Spectra of DmAC after baseline correction. The original visible spectra are shown in graph e) of <b>Figure 6.2</b> . Results are average of three independent replicates. Some error bars cannot be visualised because they are smaller than the thickness of the curves. ....	234
<b>Figure 12.35:</b> Spectra of DmAF after baseline correction. The original visible spectra are shown in graph f) of <b>Figure 6.2</b> . Results are average of three independent replicates. Some error bars cannot be visualised because they are smaller than the thickness of the curves. ....	235
<b>Figure 12.36:</b> Spectra of DmCF after baseline correction. The original visible spectra are shown in graph g) of <b>Figure 6.2</b> . Results are average of three independent replicates. Some error bars cannot be visualised because they are smaller than the thickness of the curves. ....	236
<b>Figure 12.37:</b> Spectra of TmACF after baseline correction. The original visible spectra are shown in graph h) of <b>Figure 6.2</b> . Results are average of three independent replicates. Some error bars cannot be visualised because they are smaller than the thickness of the curves. ....	237
<b>Figure 12.38:</b> Spectra of MmOP after baseline correction. The original visible spectra are shown in graph i) of <b>Figure 6.2</b> . Results are average of three independent replicates. Some error bars cannot be visualised because they are smaller than the thickness of the curves. ....	238
<b>Figure 12.39:</b> Spectra of CcmC <sup>-</sup> after baseline correction. The original visible spectra are shown in graph j) of <b>Figure 6.2</b> . Results are average of three independent replicates. Some error bars cannot be visualised because they are smaller than the thickness of the curves. ....	239
<b>Figure 12.40:</b> Additional TEM images of SmA after implementation of method I (aerobic synthesis of gold nanoparticles).....	240
<b>Figure 12.41:</b> Additional TEM images of SmC after implementation of method I (aerobic synthesis of gold nanoparticles).....	240
<b>Figure 12.42:</b> Additional TEM images of SmF after implementation of method I (aerobic synthesis of gold nanoparticles).....	240
<b>Figure 12.43:</b> Additional TEM images of DmAC after implementation of method I (aerobic synthesis of gold nanoparticles).....	241

<b>Figure 12.44:</b> Additional TEM images of DmAF after implementation of method I (aerobic synthesis of gold nanoparticles). .....	241
<b>Figure 12.45:</b> Additional TEM images of DmCF after implementation of method I (aerobic synthesis of gold nanoparticles). .....	241
<b>Figure 12.46:</b> Additional TEM images of TmACF after implementation of method I (aerobic synthesis of gold nanoparticles). .....	242
<b>Figure 12.47:</b> Additional TEM images of MmOP after implementation of method I (aerobic synthesis of gold nanoparticles). .....	242
<b>Figure 12.48:</b> Additional TEM images of CcmC <sup>-</sup> after implementation of method I (aerobic synthesis of gold nanoparticles). .....	242
<b>Figure 12.49:</b> Spectra of the anaerobic cultures after baseline correction. The original visible spectra are shown in graphs a) to f) of <b>Figure 6.8</b> . Results are average of three independent replicates. Some error bars cannot be visualised because they are smaller than the thickness of the curves.....	243
<b>Figure 12.50:</b> Visible spectra of anaerobic 1 mM H <sub>AuCl</sub> <sub>4</sub> solution incubated under anaerobic conditions at 30 °C and 180 rpm for 48 h – abiotic control of method II. Error bars indicate the standard deviation of three independent replicates.....	244
<b>Figure 12.51:</b> Additional TEM images of MR-1 after implementation of method II (anaerobic synthesis of gold nanoparticles). .....	245
<b>Figure 12.52:</b> Additional TEM images of SmA after implementation of method II (anaerobic synthesis of gold nanoparticles). .....	245
<b>Figure 12.53:</b> Additional TEM images of SmC after implementation of method II (anaerobic synthesis of gold nanoparticles). .....	245
<b>Figure 12.54:</b> Additional TEM images of SmF after implementation of method II (anaerobic synthesis of gold nanoparticles). .....	246
<b>Figure 12.55:</b> Additional TEM images of DmAC after implementation of method II (anaerobic synthesis of gold nanoparticles). .....	246
<b>Figure 12.56:</b> Additional TEM images of DmAF after implementation of method II (anaerobic synthesis of gold nanoparticles). .....	246

**Figure 12.57:** EDS measurement of nanoparticles made anaerobically by MR-1 through method II (anaerobic synthesis of gold nanoparticles). ..... 247

**Figure 12.58:** EDS measurement of nanoparticles made anaerobically by SmA through method II (anaerobic synthesis of gold nanoparticles)..... 247

**Figure 12.59:** EDS measurement of nanoparticles made anaerobically by SmC through method II (anaerobic synthesis of gold nanoparticles). ..... 247

**Figure 12.60:** EDS measurement of nanoparticles made anaerobically by SmF through method II (anaerobic synthesis of gold nanoparticles)..... 248

**Figure 12.61:** EDS measurement of nanoparticles made anaerobically by DmAC through method II (anaerobic synthesis of gold nanoparticles).... 248

**Figure 12.62:** EDS measurement of nanoparticles made anaerobically by DmAF through method II (anaerobic synthesis of gold nanoparticles). ... 248

**Figure 12.63:** Additional TEM images of autoclaved BL21(DE3) after implementation of method I and visible spectra from graph a) of **Figure 7.3** divided into individual measurements. Results are average of three independent replicates. Some error bars cannot be visualised because they are smaller than the thickness of the curves..... 249

**Figure 12.64:** Additional TEM images of autoclaved MR-1 after implementation of method I and visible spectra from graph b) of **Figure 7.3** divided into individual measurements. Error bars indicate the standard deviation of three independent replicates. .... 250

**Figure 12.65:** Visible spectra from graph a) of **Figure 7.5** divided into individual measurements. Results are average of three independent replicates. Some error bars cannot be visualised because they are smaller than the thickness of the curves..... 251

**Figure 12.66:** Visible spectra from graph b) of **Figure 7.5** divided into individual measurements. Results are average of three independent replicates. Some error bars cannot be visualised because they are smaller than the thickness of the curves..... 252

**Figure 12.67:** Visible spectra from graph c) of **Figure 7.5** divided into individual measurements. Results are average of three independent replicates. Some error bars cannot be visualised because they are smaller

than the thickness of the curves. For improved clarity of the graphs, the scale in the y-axis was modified in relation to the scale in **Figure 7.5**. .....253

**Figure 12.68:** Visible spectra from graph d) of **Figure 7.5** divided into individual measurements. Results are average of three independent replicates. Some error bars cannot be visualised because they are smaller than the thickness of the curves. For improved clarity of the graphs, the scale in the y-axis was modified in relation to the scale in **Figure 7.5**. .....254

**Figure 12.69:** Visible spectra from graph e) of **Figure 7.5** divided into individual measurements. Results are average of three independent replicates. Some error bars cannot be visualised because they are smaller than the thickness of the curves.....255

**Figure 12.70:** Visible spectra from graph f) of **Figure 7.5** divided into individual measurements. Results are average of three independent replicates. Some error bars cannot be visualised because they are smaller than the thickness of the curves. For improved clarity of the graphs, the scale in the y-axis was modified in relation to the scale in **Figure 7.5**. .....256

**Figure 12.71:** Visible spectra from graph g) of **Figure 7.5** divided into individual measurements. Results are average of three independent replicates. Some error bars cannot be visualised because they are smaller than the thickness of the curves. For improved clarity of the graphs, the scale in the y-axis was modified in relation to the scale in **Figure 7.5**. .....257

**Figure 12.72:** Visible spectra from graph h) of **Figure 7.5** divided into individual measurements. Results are average of three independent replicates. Some error bars cannot be visualised because they are smaller than the thickness of the curves. For improved clarity of the graphs, the scale in the y-axis was modified in relation to the scale in **Figure 7.5**. .....258

**Figure 12.73:** Visible spectra from graph a) of **Figure 7.6** divided into individual measurements. Error bars indicate the standard deviation of three independent replicates. ....259

**Figure 12.74:** Visible spectra from graph b) of **Figure 7.6** divided into individual measurements. Results are average of three independent

replicates. Some error bars cannot be visualised because they are smaller than the thickness of the curves..... 260

**Figure 12.75:** Visible spectra from graph c) of **Figure 7.6** divided into individual measurements. Results are average of three independent replicates. Some error bars cannot be visualised because they are smaller than the thickness of the curves. For improved clarity of the graphs, the scale in the y-axis was modified in relation to the scale in **Figure 7.6**. .... 261

**Figure 12.76:** Visible spectra of MR-1 monitored during the implementation of method I with the variation of cells being resuspended and incubated in gold solution which had the pH corrected to 7. Error bars indicate the standard deviation of three independent replicates..... 262

**Figure 13.1:** Regression analysis comparing OD<sub>600</sub> measurements carried out with Helios Epsilon by Thermo Spectronic and UV-10 by Thermo Scientific. The data points were collected from three different experiments in duplicate: BL21(DE3) growing in LB and in M9, and MR-1 growing in LB. The dashed line corresponds to the linear regression..... 265

**Figure 13.2:** Monitoring growth of BL21(DE3) and MR-1 in LB and M9 at 30 °C and 180 rpm. Graphs a), c), e) and g) show data for BL21(DE3) and graphs b), d), f) and h) show data for MR-1. Graphs a) and b) show growth in LB monitored through OD<sub>600</sub>; graphs c) and d) show growth in LB monitored through colony counting; graphs e) and f) show regression analyses comparing the data of OD<sub>600</sub> and colony counting in LB; and graphs g) and h) show growth in M9 monitored through OD<sub>600</sub>. The insets in graphs a), b), g) and h) present the same data as in the original graphs, but as log OD<sub>600</sub> vs. time. Error bars indicate the standard deviation of three independent replicates. .... 267

**Figure 13.3:** Monitoring growth of MR-1 in anaerobic media. a), c) and e) are images of cells under the microscope and b), d) and f) are pictures of the cultures after centrifugation. a) and b) show samples at time 0 h, c) and d) show samples at time 6 h, and e) and f) show samples at time 24 h. .... 269

**Figure 13.4:** Monitoring growth of SmA in anaerobic media. a), c) and e) are images of cells under the microscope and b), d) and f) are pictures of the cultures after centrifugation. a) and b) show samples at time 0 h, c) and d) show samples at time 6 h, and e) and f) show samples at time 24 h.  
.....270

**Figure 13.5:** Monitoring growth of SmC in anaerobic media. a), c) and e) are images of cells under the microscope and b), d) and f) are pictures of the cultures after centrifugation. a) and b) show samples at time 0 h, c) and d) show samples at time 6 h, and e) and f) show samples at time 24 h.  
.....271

**Figure 13.6:** Monitoring growth of SmF in anaerobic media. a), c) and e) are images of cells under the microscope and b), d) and f) are pictures of the cultures after centrifugation. a) and b) show samples at time 0 h, c) and d) show samples at time 6 h, and e) and f) show samples at time 24 h.  
.....272

**Figure 13.7:** Monitoring growth of DmAC in anaerobic media. a), c) and e) are images of cells under the microscope and b), d) and f) are pictures of the cultures after centrifugation. a) and b) show samples at time 0 h, c) and d) show samples at time 24 h, and e) and f) show samples at time 48 h.  
.....273

**Figure 13.8:** Monitoring growth of DmAF in anaerobic media. a), c) and e) are images of cells under the microscope and b), d) and f) are pictures of the cultures after centrifugation. a) and b) show samples at time 0 h, c) and d) show samples at time 6 h, and e) and f) show samples at time 24 h.  
.....274

**Figure 13.9:** Monitoring growth of DmCF in anaerobic media. a), c) and e) are images of cells under the microscope and b), d) and f) are pictures of the cultures after centrifugation. a) and b) show samples at time 0 h, c) and d) show samples at time 24 h, and e) and f) show samples at time 48 h.  
.....275

**Figure 13.10:** Monitoring growth of TmACF in anaerobic media. a), c) and e) are images of cells under the microscope and b), d) and f) are pictures



of the cultures after centrifugation. a) and b) show samples at time 0 h, c) and d) show samples at time 24 h, and e) and f) show samples at time 48 h.

..... 276

**Figure 13.11:** Monitoring growth of MmOP in anaerobic media. a), c) and e) are images of cells under the microscope and b), d) and f) are pictures of the cultures after centrifugation. a) and b) show samples at time 0 h, c) and d) show samples at time 24 h, and e) and f) show samples at time 48 h.

..... 277

**Figure 13.12:** Monitoring growth of CcmC<sup>-</sup> in anaerobic media. a), c) and e) are images of cells under the microscope and b), d) and f) are pictures of the cultures after centrifugation. a) and b) show samples at time 0 h, c) and d) show samples at time 24 h, and e) and f) show samples at time 48 h.

..... 278

**Figure 14.1:** Pictures of a) 1 mM HAuCl<sub>4</sub> solution (abiotic control) after incubation at 30 °C and 180 rpm for 48 h; b) BL21(DE3) biomass after incubation in DI water at 30 °C and 180 rpm for 48 h; c) MR-1 biomass after incubation in DI water at 30 °C and 180 rpm for 48 h; d) BL21(DE3) biomass after incubation in 1 mM HAuCl<sub>4</sub> solution at 30 °C and 180 rpm for 48 h; e) MR-1 biomass after incubation in 1 mM HAuCl<sub>4</sub> solution at 30 °C and 180 rpm for 48 h. .... 280

**Figure 14.2:** TEM images of nanoparticles present in 1 mM HAuCl<sub>4</sub> solution after incubation for 48 h at 30 °C and 180 rpm (abiotic control of method I). The inset corresponds to the SAED measurement of image c). ..... 281

**Figure 14.3:** TEM images of nanoparticles present in 1 mM HAuCl<sub>4</sub> solution after incubation for 48 h at 30 °C and 180 rpm (abiotic control of method I). The carbon grid was not plasma treated for these analyses. .... 282

**Figure 14.4:** TEM images of DI water after incubation for 48 h at 30 °C and 180 rpm. The insets in images b) and c) correspond to the SAED measurements of images b) and c), respectively. .... 283

**Figure 14.5:** EDS measurements of a) nanoparticles present in 1 mM HAuCl<sub>4</sub> solution after incubation for 48 h at 30 °C and 180 rpm (abiotic control of method I); b) nanoparticles made by BL21(DE3) after incubation

in 1 mM HAuCl<sub>4</sub> solution for 48 h at 30 °C and 180 rpm; c) nanoparticles made by MR-1 after incubation in 1 mM HAuCl<sub>4</sub> solution for 48 h at 30 °C and 180 rpm. ....284

---

# List of abbreviations and nomenclatures

---

AAS – atomic absorption spectroscopy/spectrometer

AD – Anno Domini

ANOVA – analysis of variance

ATCC® – American type culture collection

BC – Before Christ

bp – base pairs

CCD – charge-coupled device

CM – cytoplasmic membrane

DI – deionised

DLS – dynamic light scattering

DMSO – dimethyl sulfoxide

DNA – deoxyribonucleic acid

EDS, EDX or EDXS – energy-dispersive X-ray spectroscopy

EET – extracellular electron transfer

EINPs – NPs is the abbreviation for nanoparticles and EI for element. Hence, EINPs is the abbreviation for nanoparticles of any element, for example AuNPs, AgNPs, PdNPs, etc.

EPLS – elliptically polarised light scattering

EPS – extracellular polymeric substances

FHL – formate hydrogenlyase

FMR – ferromagnetic resonance

FTIR – Fourier transform infrared spectroscopy

GLD – glycerol dehydrogenase

LB – Luria-Bertani culture medium

LSPR – localised surface plasmon resonance

MIC – minimum inhibitory concentration

NAD – nicotinamide adenine dinucleotide

NAD<sup>+</sup> – oxidised form of NAD  
NADH – reduced form of NAD  
NASA – National Aeronautics and Space Administration  
OD<sub>600</sub> – optical density at wavelength of 600 nm  
OFN – oxygen-free nitrogen  
OM – outer membrane  
OMC – outer membrane cytochrome  
ORF – open reading frame  
<sup>31</sup>P-NMR – phosphorus nuclear magnetic resonance  
PBS – phosphate-buffered saline  
PC – phytochelatin  
PCR – polymerase chain reaction  
PEC – periplasmic electron carrier  
PG – peptidoglycan  
QSE – quantum size effect  
RNA – ribonucleic acid  
ROI – region of interest  
RPM – rotations per minute  
SAED – selected-area electron diffraction  
SAXS – small angle X-ray scattering  
SEM – scanning electron microscope  
TEM – transmission electron microscope  
TMAO – trimethylamine N-oxide  
TGA – thermogravimetric analysis/analyser  
WT – wild-type  
XPS – X-ray photoelectron spectroscopy  
XRD – X-ray diffraction  
UV-vis – ultraviolet-visible

# *I n t r o d u c t i o n*

*Then Jesus went on to say to the Jews who had believed him:*

*“If you remain in my word, you are really my disciples,  
and you will know the truth, and the truth will set you free.”*

*John 8:31-32*



# 1 General overview

---

Nanoparticles are small solid objects with at least one dimension measuring less than 100 nm (Guo et al., 2014). In general, nanoparticles can be classified according to their composition: carbon, ceramics, semiconductor, lipids, polymer or metal (Khan et al., 2017). The peculiar properties and vast applications of metallic particles make them an important group of nanoparticles – and gold nanoparticles (AuNPs) are major representatives of this group. One of the reasons why AuNPs are so relevant is because they are one of the few metals that display localised surface plasmon resonance when at nanoscale (Amendola et al., 2017). This and other properties of nanoparticulate gold make them suitable for applications in a range of fields, such as diagnostics, sensing and catalysis (Eustis and El-Sayed, 2006).

There are a variety of techniques used to synthesise metallic nanoparticles, each with its advantages and disadvantages. Chemical reduction, the most common method, has the advantages of high productivity, low cost fabrication and simple preparation (Kim et al., 2004). One relevant disadvantage of this method is that it often involves harsh chemicals and elevated temperatures (Reza Ghorbani et al., 2011). The synthesis through the application of organisms (directly or through cell extracts) is relatively simple, cost-effective and does not require toxic chemicals and high energy consumption (Schröfel et al., 2014). However, biosynthesis has disadvantages as well, with lack of controllability on the synthesis process and on the characteristics of the particles made being the main ones (Li et al., 2011).

*Escherichia coli* and *Shewanella oneidensis* – the two strains utilised in the present work – are well-known strains highly relevant for biotechnology. *E. coli* is possibly the most studied bacterium and is a model Gram-negative organism; and, *S. oneidensis* is renowned for its remarkable respiratory ability: it is capable of respiring an impressive variety of electron acceptors and is endowed with the Mtr pathway – a group of proteins and cytochromes responsible for the

respiration of a range of extracellular electron acceptors (Heidelberg et al., 2002, Naurú Idalia and Bernardo, 2017).

Both species, as well as several other microorganisms, have been shown to be capable of producing a wide variety of metallic nanoparticles, including AuNPs (Gahlawat and Choudhury, 2019). Unfortunately, the mechanisms involved in the synthesis process is still poorly understood. It is known, however, that the process starts with the adsorption (and/or absorption) of the metallic ions by the organism, followed by chemical reduction performed by biomolecules (Li et al., 2011). The main reason for the lack of knowledge on the process is that an enormous range of biomolecules have the potential to interact and react with the metallic ions. Therefore, it remains a challenge to flag the exact cell components that drive the synthesis process.



## 2 Aims of the study and chapter breakdown

---

The main aims of this thesis were: 1 – to test if specific *c*-type cytochromes, from the Mtr pathway, of *S. oneidensis* are involved, or have an influence, in the synthesis of gold nanoparticles; and, 2 – to verify if deletions in these specific cytochromes can provide a better tuning of the process (improve controllability). Interestingly, when planning and performing the experiments aiming to address these aims, several new intriguing questions and objectives have opened. Important additional goals that resulted from the work to address these aims included: 1 – the development of a methodology that reliably evaluates the performance of each bacterial strain in the synthesis of AuNPs; 2 – the confirmation that the method employed for biofabrication indeed resulted in the successful synthesis of nanoparticles; 3 – determining if the methods applied for the synthesis of nanoparticles sustain living conditions for the cultures; and, 4 – testing if it is possible to have living cells making AuNPs.

The aims and objectives of this study were addressed in three research chapters (and in appendix sections). A brief description of each research chapter is given below:

In the first research chapter – chapter 5 – a methodology for comparing the synthesis of gold nanoparticles by different strains was successfully employed in cultures of *E. coli* BL21(DE3) and *S. oneidensis* MR-1. The variables compared were amount of gold ions adsorbed from solution, size and shape of the nanoparticles, surface plasmon bands generated and specific productivity. The objectives of the chapter were to consolidate the comparison platform and to characterise the two strains according to the applications to which the biofabricated nanoparticles are more suitable for. In essence, the results in this chapter evaluated statistically the organism that produced more nanoparticles, of larger size and of specific shapes.

In the following chapter, chapter 6, the platform of comparison was adopted for comparing the synthesis of gold nanoparticles by *S. oneidensis* wild-type and mutants containing deletions of specific *c*-type cytochromes from the

Mtr pathway. That comparison allowed the categorisation of the strains according to the characteristics of the nanoparticles fabricated and the evaluation of the influence that *c*-type cytochromes have in the synthesis process. Essentially, the results of the chapter made it possible to choose a culture that synthesises particles with specifications more suitable for a particular application.

Chapter 7 revealed that the methods adopted in the previous chapters for the synthesis of gold nanoparticles do not sustain survival conditions for the cultures. The chapter then shows a range of tests carried out aiming to have active cells making nanoparticles. Although not conclusive, the results from the experiments indicated that it is not possible to have living cells of *E. coli* and *S. oneidensis* synthesising AuNPs.

# *Literature review*

*But John, having heard in jail about the works of the Christ,  
sent his disciples to ask him:*

*"Are you the Coming One, or are we to expect a different one?"*

*In reply Jesus said to them:*

*"Go and report to John what you are hearing and seeing:*

*The blind are now seeing and the lame are walking,  
the lepers are being cleansed and the deaf are hearing,  
the dead are being raised up and the poor are being told the good news."*

*Matthew 11:2-5*



### 3 Literature review

---

The study of the present thesis – the synthesis of gold nanoparticles by bacterial strains – lies in the interface between biotechnology and nanotechnology. Putting in simple terms, biotechnology can be described as technology using biological systems and nanotechnology as technology on the nanoscale (Mayer, 1993, Nasrollahzadeh et al., 2019). Some authors prefer to treat the intersection between these two areas as a new, third field, known as bionanotechnology, nanobiotechnology or nanobiology. A better explanation on the meaning and significance of the three fields is given below.

#### 3.1 Biotechnology

Biotechnology is defined by The European Federation of Biotechnology as “the integrated use of biochemistry, microbiology and engineering sciences in order to achieve technological (industrial) application of the capabilities of microorganisms, cultured tissue cells and parts thereof” (Scragg, 1988). The name was introduced in 1919 by Károly Ereky, a former Minister of Food of Hungary (Stockwell, 2017). Curiously, for a number of years biotechnology had been applied to describe two distinct areas of knowledge, industrial fermentation and efficiency in the workplace (currently known as ergonomics) (Arora, 2007). The ambiguity ended in 1961 with the renaming of the Journal of Microbiological and Biochemical Engineering and Technology to Biotechnology and Bioengineering. Although biotechnology is seen as a modern field of study, mankind has been benefiting from it for thousands of years, when ancient peoples fermented raw materials for the production of foods and drinks (Bhatia and Goli, 2018). **Table 3.1** presents some of the important historical milestones that contributed to the development of biotechnology.

Scragg (1988) divided the history of biotechnology in five eras: the pre-Pasteur era, the Pasteur era, the antibiotic era, the post-antibiotic era and the era of new biotechnology.

**Table 3.1:** Historical development of biotechnology (reproduced from Smith (2009) with permission of The Licensor through PLSclear).

---

**Biotechnological production of foods and beverages**

Sumarians and Babylonians were drinking beer by 6,000 BC, they were the first to apply direct fermentation to product development; Egyptians were baking leavened bread by 4,000 BC; wine was known in the Near East by the time of the book of Genesis. Microorganisms were first seen in the seventeenth century by Anton van Leeuwenhoek who developed the simple microscope; the fermentative ability of microorganisms was demonstrated between 1857 and 1876 by Pasteur – *the father of biotechnology*; cheese production has ancient origins, as does mushroom cultivation.

---

**Biotechnological processes initially developed under non-sterile conditions**

Ethanol, acetic acid, butanol and acetone were produced by the end of the nineteenth century by open microbial fermentation processes. Waste-water treatment and municipal composting of solid wastes represents the largest fermentation capacity practised throughout the world.

---

**Introduction of sterility to biotechnological processes**

In the 1940s complicated engineering techniques were introduced to the mass production of microorganisms to exclude contaminating microorganisms. Examples include the production of antibiotics, amino acids, organic acids, enzymes, steroids, polysaccharides, vaccines and monoclonal antibodies.

---

**Applied genetics and recombinant DNA technology**

Traditional strain improvement of important industrial organisms has long been practised; recombinant DNA techniques together with protoplast fusion allow new programming of the biological properties of organisms.

---

In the first era, biotechnology was unconsciously applied for the preparation of important artefacts such as beer, wine, vinegar and cheese. For the case of beer, there are reports of its preparation in Egypt, Sumer, Babylonia and Assyria – with evidences dating back to the Predynastic era in Egypt (Hornsey, 2003). Regarding wine production, chemical evidence of wine was

found in pottery jar from 5400 – 5000 BC, the Neolithic period (McGovern et al., 1996). In addition, it is now well known that the Egyptians, Greeks and Romans practiced sophisticated viniculture (McGovern and Mondavi, 2007). As for vinegar, it was already consumed by the Babylonians, Assyrians and Egyptians (Rehm and Prave, 1987). Production of cheese also started in the remote past, but not as remote as these other biotechnological items. According to Donnelly (2014), cheese was first made in the first century BC in the mountainous regions of the Alps.

In the nineteenth century, the pioneering work of Louis Pasteur and other scientists allowed the recognition that physiological metabolic reactions in microorganisms actively contributes to processes such as brewing, wine making and food spoilage (Rehm and Prave, 1987, Scragg, 1988). Such discoveries initiated the second era of biotechnology, which permitted the development of processes for manufacturing primary metabolic products, such as acetone, butanol, glycerol and citric acid. Out of these processes, some were especially remarkable for the field. Examples include the Weizmann process – which used *Clostridium acetobutylicum* for the production of acetone and butanol, the Neuberg process for the production of glycerol using *Saccharomyces cerevisiae*, and the defined adaptation of biomass for activated sludge (Brown et al., 1987, Bu'Lock, 1987). Because these processes involved the application of selected microbes, some authors like to characterise these developments as the real beginnings of biotechnology (Bu'Lock, 1987, Scragg, 1988).

The following era – the antibiotic era – is defined by the discovery and production of antibiotics. Alexander Fleming discovered the penicillin in 1928 by observing the inhibitory activity of the fungus *Penicillium notatum* towards *Staphylococcus aureus* (Durand et al., 2019). Interestingly, the industrial-scale manufacturing of the molecule took place only in 1940, with the development of aseptic biotechnological processes (Rehm and Prave, 1987). Major contribution to the discovery of antibiotics was also given by Selman Waksman. He not only led the discovery of a range of antibiotics, the main one being streptomycin, but was also responsible for the development of a screening methodology for identifying antagonistic activity between microbial species (Woodruff, 2014).

This 'platform' yielded the discovery of several other antibiotics (Durand et al., 2019).

Next enters the post-antibiotic era. In this phase the world experienced a boom in diversity of products made through biotechnology (Scragg, 1988). Items that were introduced to the market included vitamins, nucleotides, amino acids, enzymes and hormones (Brown et al., 1987, Suzuki, 2013, Sych et al., 2016, Patel et al., 2017). This period has also witnessed major improvements in the engineering side of production (Rehm and Prave, 1987).

The era of new biotechnology is our contemporary period. Scragg (1988) described two developments as the main accomplishments of this era: hybridoma technology and genetic engineering. Obviously, as over 30 years has passed since the publication of the book by Scragg, many other achievements were obtained afterwards. Protein engineering, tissue engineering, gene therapy, stem cell therapy, genomics, transcriptomics and proteomics, are few examples of recent important advances in biotechnology (Berthiaume et al., 2011, Wu and Izpisua Belmonte, 2016, Dunbar et al., 2018, Lutz and Iamurri, 2018, Manzoni et al., 2018).

Biotechnology as a science has come of age and has proved its importance. It has not only diversity in its interdisciplinary structure, but has also diversity in the areas of contribution. Some examples of application of biotechnology in different fields are found in **Table 3.2**. Because society recognises – for the most part – the importance of biotechnology, it is likely that the list of areas benefited by biotechnology will continue to increase throughout the years.

## **3.2 Nanotechnology**

The Royal Society of Great Britain defines nanotechnology as the design, characterisation, production and implementation of structures, mechanisms and systems by monitoring shape and size at the nanometric scale (Wautelet, 2009). Nanoscience, on the other hand, is the study of phenomena and the



**Table 3.2:** Applications of biotechnology in different areas (adapted from Bhatia and Goli (2018) © IOP Publishing. Adapted with permission. All rights reserved).

---

#### **Animal biotechnology**

- Biopharmaceuticals: production of hormones, growth factors, interferons, enzymes, recombinant proteins, vaccines, blood components, oligonucleotides, transcription factor-based drugs;
- Antibiotics;
- Diagnostics: antibodies, biosensors;
- Gene therapy;
- Stem cell therapy;
- Animal tissue culture: cell, tissue and organ culture;
- Gene cloning: genetic engineering, transgenic animals, xenotransplantation.

---

#### **Agricultural biotechnology**

- Horticultural biotechnology, tree biotechnology, plant biotechnology (photosynthesis improvers, bio-fertilizers, stress-resistant crops, bio-insecticides and biopesticides), food biotechnology.

---

#### **Environmental biotechnology**

- Environmental monitoring: diagnosis of environmental problems via biotechnology;
- Waste management: bioremediation is the use of microbes to break down organic molecules or environmental pollutants;
- Pollution prevention: renewable resources, biodegradable products, alternative energy sources.

---

#### **Industrial biotechnology**

- Metabolite production (acetone, butanol, alcohol, antibiotics, enzymes, vitamins, organic acids), anaerobic digestion, fermentation of food products, bio-based fuel and energy, biotechnology in the galvanizing industry, recovery of metals and minerals, sugars from starches.
-

manipulation of material at the atomic, molecular, macromolecular scale, where the properties differ notably from the properties at a bigger scale (Wautelet, 2009). It can be perceived from the definitions that the most important factor involving nanotechnology and nanoscience is the scale (nano represents  $10^{-9}$ ). Hence, the rational manipulation of matter at the atomic or molecular levels is key for obtaining the effects important for nanotechnology.

In a similar manner to biotechnology, nanotechnology had also been unconsciously applied by ancient peoples. For example, in the fourteenth and thirteenth centuries BC, in Egypt and Mesopotamia, metallic nanoparticles were adopted in glass-making for colouring glasses (Schaming and Remita, 2015). Another example is the application of PbS nanotechnology by the Greco-Romans for hair dyeing, around 2000 years ago (Walter et al., 2006). Nevertheless, the Lycurgus Cup (**Figure 3.1**), a sophisticated Roman glass vessel from the fourth or fifth century AD, is possibly the most famous ancient nanotechnological object (Harden and Toynebee, 1959). It depicts six mythological characters portraying the scene of the death of King Lycurgus (Scott, 1995). Undoubtedly, the most remarkable feature of the cup is its dichroism: when illuminated from outside it reflects an opaque jade green colour tone, whereas when illuminated from the inside it transmits a translucent ruby colour (Schaming and Remita, 2015) (see the dichroism of the Cup in **Figure 3.1**). This unusual phenomenon was found to be caused by the presence of nanoparticles of silver-gold alloy measuring 50-100 nm (Freestone et al., 2007).

Michael Faraday, a physicist renowned for works on electro-magnetism, was a pioneer in conducting systematic studies to try to understand the unusual behaviour of metals at the nanoscale. In 1857 Faraday published a paper entitled *experimental relations of gold (and other metals) to light* where he described in detail several experiments carried out with gold, silver, copper and other metals in which the metals went through a series of treatments (chemical, thermal, pressure and even explosion) and the resulting interaction with light (especially change in colour) was monitored (Faraday, 1857). To some authors, these investigations conducted by Faraday marked the birth of modern colloidal chemistry (Thompson, 2007).



**Figure 3.1:** The Lycurgus Cup. The left photo shows the cup illuminated from outside, thus reflecting the jade colour; and the right photo shows the cup illuminated from inside, thus transmitting the ruby colour. © **The Trustees of the British Museum**. Shared under a Creative Commons Attribution-NonCommercial-ShareAlike 4.0 International (CC BY-NC-SA 4.0) licence.

Another scientist that investigated and advanced the understanding of metallic nanoparticles was Richard Zsigmondy. His importance to the field extended from systematic studies on colloidal gold to the invention (together with Henry Siedentopf) of the ultramicroscope, which allowed the indirect visualisation of colloids and other small entities (James, 1993). In addition, he introduced the gold number – the least amount (in milligrams) of protective colloid required to prevent the precipitation of 10 cubic centimetres of gold sol when added with 1 cubic centimetre of 10 % sodium chloride solution – and was the first person to coin the term nanometer for characterising particle size (Goel, 2006, Hulla et al., 2015).

Important contributions to the field also came from Gustav Mie. In 1908 he published an article entitled *beiträge zur optik trüber medien, speziell*

*kolloidal metallösungen (contributions to the optics of diffuse media, especially colloidal metal solutions)* where he elucidates the interaction of electromagnetic waves with spherical metallic particles of equal or smaller size than the wavelength of light (Mie, 1908). Mie's theoretical approach adopted Maxwell equations on the electromagnetic light theory in spherical coordinates of particles of certain refractive index, providing an elegant analytical explanation of absorption and scattering of light by particles, and, consequently, the distinct colours presented by colloids when at nanometric sizes (Horvath, 2009). Applications of his theory in experimental results were performed by him in his publication of 1908 and by other researchers (Mie, 1908, Tcherniak et al., 2010). In all cases, a good fit was achieved.

The efforts of all of these and many other scientists allowed the birth of modern nanotechnology, which – according to several authors – took place in 1959 when the physicist, and future Nobel prize winner, Richard Feynman gave a speech entitled *there is plenty of room at the bottom* at Caltech (Feynman, 1960, Godale and Sharon, 2019). In the talk Feynman attempted to instigate the audience into thinking about the miniaturisation of things: “What I want to talk about is the problem of manipulating and controlling things on a small scale.”. The presentation is seen as a milestone because it predicted several developments in miniaturisation that later became reality. For example, Feynman proposed the manipulation of individual atoms: “What would happen if we could arrange the atoms one by one the way we want them (within reason, of course; you can't put them so that they are chemically unstable, for example)?”. Years later, scientists at IBM Research Division accomplished the task by moving individual xenon atoms on a single-crystal nickel surface to “draw” the word IBM (Eigler and Schweizer, 1990). The atomic “writing” can be seen in **Figure 3.2**. In the lecture Feynman even issued a challenge: “It is my intention to offer a prize of 1,000 dollars to the first guy who can take the information on the page of a book and put it on an area 1/25,000 smaller in linear scale in such manner that it can be read by an electron microscope.”. Later on, the prize was claimed by scientists at Stanford Solid State Laboratories (Newman et al., 1987).

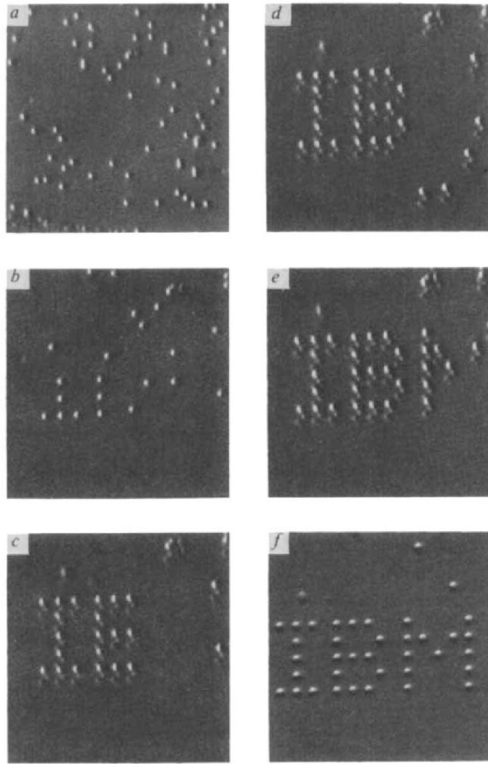


**Figure 3.2:** A sequence of scanning transmission microscope images taken during the construction of a patterned array of xenon atoms on a nickel (110) surface. a, The surface after xenon dosing. b-f, Various stages during the construction. Each letter is 50 angstroms long from top to bottom. Reproduced from Eigler and Schweizer (1990). Reprinted by permission from Springer Nature Customer Service Centre GmbH.

Although Norio Taniguchi was the first person to coin the term “nanotechnology” (Taniguchi, 1974), it was Eric Drexler who popularised it with the book *engines of creation: the coming era of nanotechnology* (Drexler, 1986). This imaginative and visionary book was important because it informed the general public about the potential capabilities of technology in general, but mainly nanotechnology. Drexler proposed the construction of nanomachines named assemblers, which, according to him, would “be able to bond atoms together in virtually any stable pattern, adding a few at a time to the surface of a workpiece until a complex structure is complete... they (the assemblers) will let us build almost anything we can design – including more assemblers.”. Such devices do

not exist yet, but researchers, including myself, are taking small steps on a daily basis that will eventually lead to their development.

**Table 3.3** presents a compilation of milestones important for the field of nanotechnology.

**Table 3.3:** Milestones of nanoscience and nanotechnology. Adapted from Godale and Sharon (2019) with permission.

Year	Advances
1857	M. Faraday synthesised gold colloids of nano size.
1931	E. Ruska and M. Knoll developed the first electron microscope.
1951	E. Müller developed the field ion microscope, which enabled the imaging of atoms from the tip of metallic samples.
1959	R. Feynman delivered his very famous talk “There’s plenty of room at the bottom”.
1968	A. Y. Cho developed molecular beam epitaxy technique for layer-by-layer growth of materials.
1970	L. Esaki demonstrated the quantum size effect (QSE).
1974	N. Taniguchi originally coined the term “nano-technology” in his paper on ion-sputter machining.
1980	A. I. Akimov showed QSE in CdS and CdSe particles dispersed in glass, triggering research on nanoparticles.
1981	G. Binnig and H. Rohrer developed the scanning tunnelling microscope by which atomic resolution could be obtained.
1985	R. F. Curl, H. W. Kroto and R. E. Smalley synthesised sixty atom carbon molecules, later known as buckyball or fullerene.
1986	K. Eric Drexler developed and popularised the concept of nanotechnology and founded the field of molecular nanotechnology in his book <i>engines of creation: the coming era of nanotechnology</i> .
1986	Atomic force microscopy was invented.
1988	First university course on nanotechnology started in the U. S.

1990	D. M. Eigler and E. K. Schweizer wrote the letters “IBM” using xenon atoms.
1991	S. Iijima discovered carbon nanotubes.
1996	The National Aeronautics and Space Administration (NASA) began work in computational nanotech.
1998	First safety guidelines for use of “nano” were made.
1999	C. A. Mirkin’s group developed dip-pen nanolithography.
2000	President Clinton announced U. S. National Nanotechnology Initiative.
2006	J. Tour and colleagues at Rice University built a nanoscale car made of oligo(phenylene ethynylene) with alkynyl axles and four spherical C <sub>60</sub> fullerene wheels.
2007	Synthesis and characterisation of graphene by Geim and Novoselov.
2010	DNA-based “robotic” assembly by N. Seeman and colleagues at New York University.

As a general rule, nanostructures can be fabricated with two different methods: the top-down approach and the bottom-up approach (Poole Jr. and Owens, 2003). The former utilises tools, such as photolithography and electron beam lithography, to build the desired devices through the manipulation of bulk materials at a small scale; and the latter deals with the construction of objects from the direct assembly of atoms or molecules (Biswas et al., 2012). Both approaches have advantages and disadvantages. For instance, while top-down is currently the method of choice for manufacturing most nanodevices, this technology is reaching a limitation of miniaturization at a competitive cost; whereas in bottom-up techniques, they tend to produce less waste, but have more issues in terms of controllability and reproducibility (Teo and Sun, 2006, Biswas et al., 2012).

Nowadays, nanotechnology is already benefiting society in several different fronts. These include the areas of electronics (Durkan, 2019), medicine (Bayford et al., 2017), agriculture (Khot et al., 2012), construction (Lee et al., 2010) and transportation (Mathew et al., 2018), to name a few.

### **3.3 Nanobiotechnology**

As previously explained, bionanotechnology is a convergent technology endowed with elements from biotechnology and nanotechnology. Therefore, theoretically, any system that incorporate both technologies will fall within the scope of nanobiotechnology. According to Niemeyer and Mirkin (2004), “nanobiotechnology concerns the refinement and application of instruments, originally designed to generate and manipulate nanostructured materials, to basic and applied studies of fundamental biological processes.”

One important aspect of the field is its multidisciplinary approach. A broad range of professionals, spanning from biochemists and physicians to engineers and physicists, collaborate for the advancement of nanobiology. Equally important are the insights from industries, ethicists and regulatory bodies. The contribution of these various professionals is allowing the development of this promising and fast-growing industry – according to Maine et al. (2014) the number of companies selling nanobiotechnological devices increased 51 % between 2005 and 2008.

Technologies within the scope of nanobiotechnology include nanodevices for gene therapy, nanoscale systems for drug delivery, nanostructured scaffolds for tissue engineering, nanoparticles as contrast agents for bioimaging, nanofluidic devices for analysis of individual biomolecules, protein nanobiochips, nanobiosensors and, obviously, the synthesis of nanoparticles by biological entities (subject of the present thesis) (Jain, 2007, Greque de Morais et al., 2014).

### **3.4 Nanoparticles**

Many accomplishments of nanotechnology are achieved through the employment of nanoparticles (NPs). These are small solid objects with at least one dimension measuring less than 100 nm (Guo et al., 2014). The most appealing aspect of nanoparticles is their high surface area-to-volume ratio, which often yields a modification to the chemical, electronic, magnetic and



mechanical properties of the material in relation to the bulk counterpart (Akbari et al., 2011). This and other attractive characteristics of nanoparticles have fostered scientists to synthesise and test an enormous variety of particles in order to study and fine-tune their unique properties (Xia et al., 2009).

There are several ways nanoparticles can be classified – synthesis method, field of application and physical and chemical properties are some examples (Ealias and Saravanakumar, 2017). The categorisation according to the structural materials that compose the particles is one interesting approach relevant for this thesis. Khan et al. (2017) has described six different categories following this classification: carbon-based NPs, metal NPs, ceramics NPs, semiconductor NPs, polymeric NPs and lipid-based NPs. All these categories are important for nanotechnology and have potential applications in a variety of fields; however, since the particles of interest in the present study are made of gold, more focus in this thesis is going to be directed towards the class of metallic nanoparticles.

### **3.4.1 Metallic nanoparticles**

As the name suggests, metallic nanoparticles are nanosized particulate matter composed of metals. This is a group of nanoparticles with large importance because the majority of the periodic table is composed of metallic elements. In addition, these nanoparticles can be constructed with individual or multiple metallic elements and can be further conjugated with a variety of molecules, such as surfactants, polymers and antibodies (Sih and Wolf, 2005, Arruebo et al., 2009, Heinz et al., 2017). These and other characteristics (some of which will be further discussed) explain why metallic nanoparticles are among the most studied NPs.

#### **3.4.1.1 Properties of metallic nanoparticles**

The fact that nanoparticles are extremely small and, consequently, have a large proportion of their atoms on the surface of the structure can cause them to present different mechanical, chemical, magnetic, electrical and biological

properties in relation to the bulk counterparts (Moeinzadeh and Jabbari, 2017). In other words, when some structures have sizes smaller than lengths critical for characterising relevant physical phenomena their properties will change (Poole Jr. and Owens, 2003). And this is the case for various metallic nanoparticles.

One property that is directly affected by the size of the particle is magnetism. In the case of iron, for instance, a particle with size smaller than around 100 nm becomes single domain and fully magnetised – which translates into a more powerful magnetic behaviour (Binns, 2010). The magnetic properties of nanoparticles make them attractive to a range of applications. For example, magnetic separation is overall a high-throughput and low-cost alternative to most standard methods of separation (Leong et al., 2016). Genetic material, cells, proteins and catalysts were all already tested for separation by magnetic nanoparticles (Kudr et al., 2017). In addition, the magnetic delivery of drugs and the application as contrast agents for magnetic resonance imaging are also topics of intense research (Lu et al., 2007).

The antimicrobial property of materials is also enhanced when the structure is at the nano size. That is due to the high surface area-to-volume fraction and the capability of some nanoparticles to enter the cells and damage them internally (Binns, 2010). Major interest has risen towards this type of investigation mainly because of the concerning rise of antibiotic resistance (Lee et al., 2019). The mechanisms of action of metallic nanoparticles against microorganisms include inhibition of the electron transport chain, formation of reactive oxygen species and damage in the membrane, proteins and DNA (Wang et al., 2017). A variety of metallic nanoparticles, such as CuO, Al<sub>2</sub>O<sub>3</sub> and ZnO, have been tested for their antimicrobial effect, however Ag is the element most studied for this application (Li, 2014).

The high surface area-to-volume ratio of metallic nanoparticles is also favourable for chemical reactivity. This is especially advantageous for the field of catalysis (Kumar and Kumbhat, 2016). In fact, most catalysts are nanoparticles (Binns, 2010). Metallic elements routinely adopted in catalysis, such as palladium and platinum, tend to be the particles of choice for this area of study, however researchers are also turning attention to other metals, such as gold, that lack

catalytic activity in the bulk state, but that present enhanced reactivity when diminished to the nanoscale (Valden et al., 1998, Narayanan and El-Sayed, 2008, Moma et al., 2016).

Some metallic nanoparticles, such as gold, silver and copper, display a quantum-size phenomenon called localised surface plasmon resonance (LSPR). The phenomenon happens when the mean free path of the conduction electrons in the bulk material is bigger than the particle radius (Mulvaney, 1996). It is characterised by a collective oscillation of the free electrons in the metal when excited by incident photons (Yeh et al., 2012). In other words, the electric field of incident electromagnetic wave polarises the conduction electrons of the particle and cause their displacement from the positively charged lattice; then, a restoring force pulls the electrons back to the lattice (Amendola et al., 2017). In some metallic nanoparticles, including gold, the resonance takes place at the visible region of the electromagnetic spectrum, and, therefore, the particles exhibit bright colours in transmitted and reflected light (Maier, 2007). It is important to note that LSPR is dependent on several variables: the properties of the particles (size, shape, surface ligand and core charge), dielectric constants of the surrounding material, temperature, and proximity towards other nanoparticles (Eustis and El-Sayed, 2006). Therefore, particles with different properties, such as size and shape, will present different LSPR response. **Figure 3.3** shows a schematic illustration of LSPR as well as pictures demonstrating the influence of LSPR in the colours of particles.

Usually, the most important variables for distinguishing metallic nanoparticles, besides composition, are size and shape. That is because the chemical and structural properties of the particles vary greatly with changes in size and shape (Cao et al., 2016). It is important to point out, however, that size and shape of nanoparticles are not variables that categorise the particles by quality. In other words, smaller nanoparticles are not necessarily better than larger nanoparticles. Likewise, rod-shaped nanoparticles are not better than the round-shaped ones. Depending on the application, rod-shaped nanoparticles with larger size might be more effective than small round-shaped particles and vice-versa. For example, in a study on the activity of gold-ceria nanorods,

nanocubes and nanopolyhedra in catalysing water-gas shift reaction, Si and Flytzani-Stephanopoulos (2008) found a remarkable difference in performance between the particles, with the rods achieving almost 100 % conversion and the cubes reaching less than 20 %.

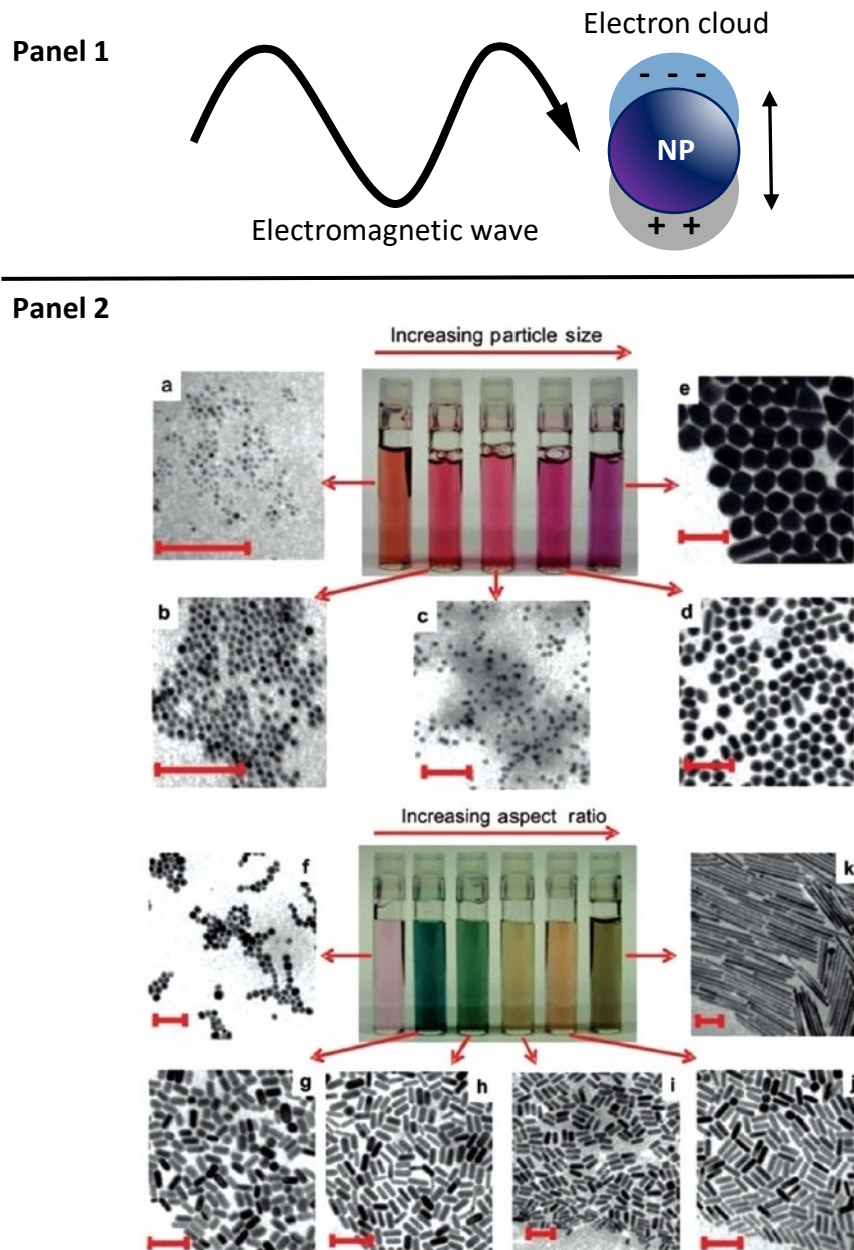


**Figure 3.3:** Visual explanation of localised surface plasmon resonance.

Panel 1: schematic illustration of LSPR. Upon incidence of electromagnetic waves at specific wavelengths, the cloud of free electrons in the nanoparticle oscillates in resonance. Panel 2: pictures of aqueous solutions containing spherical AuNPs (upper pictures) and rod-shaped AuNPs

(lower pictures). The corresponding transmission electron microscopy images of the nanoparticles are shown (all scale bars are 100 nm). The size of the spheres varies from 4 to 40 nm (images (a) to (e)) and the aspect ratio of the rods varies from 1.3 to 20 (images (f) to (k)). LSPR is the cause of the difference in colour of the solutions. The figure in panel 2 was reprinted from figure 2 of the article by Mody et al. (2010) with permission.

Because gold nanoparticles display LSPR, are easy to synthesise and functionalise, and have low toxicity, these particles are possibly the most studied metallic nanoparticles (Kong et al., 2017). All these properties make them highly versatile materials with the potential for usage in a variety of fields. For instance, they are currently being investigated for application as labelling agents for cancer diagnostics, contrast agents for cancer imaging, building blocks for nanoelectronics, detection helper in diagnostics, agents for cancer theragnosis, delivery vehicle for genes and agents for photothermal ablative therapy (El-Sayed et al., 2005, Aydogan et al., 2010, Homberger and Simon, 2010, Dykman and Khlebtsov, 2011, Kwon et al., 2017, Lee et al., 2017, Yang et al., 2017).

#### **3.4.1.2 Methods for characterising metallic nanoparticles**

Undoubtedly, the advances in nanotechnology were only possible because of the developments and improvements in the methods for measuring the properties of nanostructured materials. In particular, two inventions released in the 1980s were revolutionary for opening the doors to the nanoworld – scanning tunneling microscope and atomic force microscope (Kumar and Kumbhat, 2016). Nowadays, an immense variety of techniques are available for characterising nanoparticles, each with its strengths and limitations.

Parameters of nanoparticles important to be determined include size and shape, degree of aggregation, crystal structure and surface chemistry (surface charge, functional groups and catalytic activity) (Kumar and Kumbhat, 2016). A combinatorial characterisation approach is commonly adopted in order to reliably determine a specific parameter (Mourdikoudis et al., 2018). A list of

techniques regularly used for measuring properties of nanoparticles is described in **Table 3.4**.

**Table 3.4:** Common investigation techniques for the characterisation of nanoparticles. Reproduced from Kumar and Kumbhat (2016) with permission.

<b>Techniques</b>	<b>Characterisation parameters</b>
Dynamic light scattering/particle size analyser	Size and size distribution of nanoparticles suspended in a liquid phase.
Zeta potential analyser	Surface charge of nanoparticles in aqueous solutions or suspensions.
Scanning electron microscopy	Shape and surface structure.
Transmission electron microscopy	Size, shape and morphology (including internal structure), especially useful for biological specimen.
Atomic force microscopy	Shape and surface morphology of nanoparticles with high lateral and vertical resolutions.
Scanning tunnelling microscopy	Surface images with atomic-scale lateral resolution; modification of material at atomic/molecular/nanometer scale with high precision.
Laser scanning confocal microscopy	Noninvasive technique provides information about migration of nanoparticles into bio-barrier; 3D morphology of nanoparticles.
Brunauer-Emmett-Teller technique	Surface area analysis, porosity and adsorption capability.
X-ray diffraction technique	Crystal structure, phase and average particle size.

X-ray photoelectron spectroscopy	Chemical composition (both elemental and chemical states) information on nanoparticle's surface.
Fourier transform infrared spectroscopy	Assisted analytical tool for chemical composition.
Differential scanning calorimetry	Thermal analysis and phase transition studies.
High-performance liquid chromatography	Detection, separation and quantification of nanoparticles/nanomaterials with different particle size.

Electron microscopy, as transmission electron microscope (TEM) and scanning electron microscope (SEM), is the most common tool applied for determining size of nanoparticles, although other techniques, as dynamic light scattering (DLS) and X-ray diffraction (XRD), are also regularly adopted (Poole Jr. and Owens, 2003, Khlebtsov and Khlebtsov, 2011, Ealias and Saravanakumar, 2017). In electron microscopy an image is formed by the interaction of the specimen with a beam of electrons that had passed through lenses made of magnetic fields in an environment with high vacuum (Goodhew et al., 2001). The size is then obtained by a simple measurement of the particles in the image. For the case of DLS, the intensity of light from a monochromatic beam scattered by the sample is monitored over time, and the size of the particles is determined by the correlation that the diffusion caused by Brownian motion has with the hydrodynamic radius (Carvalho et al., 2018). The XRD technique measures the diffraction angles generated from the incidence of a collimated beam of X-rays onto the sample, and the average grain size of the nanoparticles is determined from the analysis of the widths of the Bragg peaks obtained in the scan (Poole Jr. and Owens, 2003).

Advanced microscopy is also the most used technique for determining shapes of nanoparticles; elliptically polarised light scattering (EPLS) and ferromagnetic resonance (FMR) are methods that can be applied for this purpose as well (Mourdikoudis et al., 2018). EPLS characterise the properties of particles

by measuring the intensity and polarisation state of light scattered by a sample upon incidence of a pre-treated laser beam, and FMR by measuring the absorption of an applied magnetic field (microwave, in general) by NPs made by a material with strongly exchange coupled electrons (Bhagat, 1986, Saltiel et al., 2004).

For determining degree of aggregation, DLS and electron microscopy are the methods most commonly adopted, however other techniques, such as zeta potential, are also utilised (Hondow et al., 2012, Mourdikoudis et al., 2018). Zeta potential is the potential at the shear plane (the plane at which a fluid moves tangentially with respect to the particle) of a particle under electrokinetic effects (Tadros, 2015). Zeta potential is determined by applying an electrical field to the particles and measuring their electrophoretic mobility (Bhattacharjee, 2016).

Crystal structure of nanoparticles can be characterised by various methods, including XRD, electron diffraction and small angle X-ray scattering (SAXS) (Ida, 2007, Vollath, 2013). In electron diffraction a beam of electrons, which behaves like a wave, is directed towards the sample and the interference pattern created by the crystal lattice is measured (Asadabad and Eskandari, 2016). Crystallographic information from electron diffraction can be obtained with different techniques – low-energy electron diffraction, reflection high-energy electron diffraction and electron microscopy (Poole Jr. and Owens, 2003). SAXS is a method that determines the crystal structure (and other properties) of materials by recording the elastic scattering of X-rays generated by a sample at small and very small angles (Kumar and Kumbhat, 2016).

For characterisation of parameters related to surface chemistry a broad range of methods is available, energy-dispersive X-ray spectroscopy (EDS, EDX or EDXS), X-ray photoelectron spectroscopy (XPS) and Fourier transform infrared spectroscopy (FTIR) are three examples (Mourdikoudis et al., 2018). EDS is an elemental analysis method performed by electron microscopes endowed with specific detectors (Scimeca et al., 2018). Upon incidence of the primary electron beam, the atoms in the specimen that undergo ionization release excess energy, in the form of low-energy *Auger* electron, X-ray or visible photon, to relax back to the ground state; and the energies of the X-rays released are then measured by



the detector to determine the elements present in the sample (Brydson, 2007). XPS allows the quantitative characterisation of surface composition as well as the chemical and electronic states of the elements (Kumar and Kumbhat, 2016). It works based on the photoelectric effect, where soft X-rays photoionise atoms in the sample's surface and the number and kinetic energy of photoelectrons emitted in the relaxation process are determined (Wren et al., 2011). In FTIR the absorption at specific frequencies of energy by the sample upon the incidence of radiation in the infrared spectrum is monitored and computed (converted into absorption spectrum) with Fourier transformation (Petit and Madejova, 2013). As absorption in the infrared spectrum is mainly carried out by vibrational frequency of functional groups, this technique is useful for detecting constituents and structural differences between components in a sample (Che Man et al., 2010).

One characterisation method relevant for gold nanoparticles is the measurement of their absorption and scattering of ultraviolet and visible light by UV-vis spectroscopy (Kumar and Kumbhat, 2016). This technique allows the detection of LSPR, where a characteristic plasmon band is built up at the wavelength region where the condensation (extinction) of the absorbed light is more intense (Burda et al., 2005). Different materials present plasmon bands at different regions of the spectrum. For example, the absorption peaks for gold and silver nanoparticles in water are typically observed at the wavelengths of 550 nm and 382 nm, respectively (Mulvaney, 1996, Haiss et al., 2007). It is important to note, though, that the factors influencing LSPR – described in section 3.4.1.1 – also affect the plasmon bands. **Figure 3.4** demonstrates visible spectra of gold nanoparticles yielding surface plasmon bands.

### **3.4.1.3 Methods for synthesising metallic nanoparticles**

Overall, the methods for synthesising metallic nanoparticles can be grouped into three categories: chemical, physical and biological methods (Iravani et al., 2014). The first involves chemical reactions, the second deals with physical manipulation of matter and the third relates to the use of organisms and/or their

extracts for biochemical reactions. A brief explanation of each category is presented below.

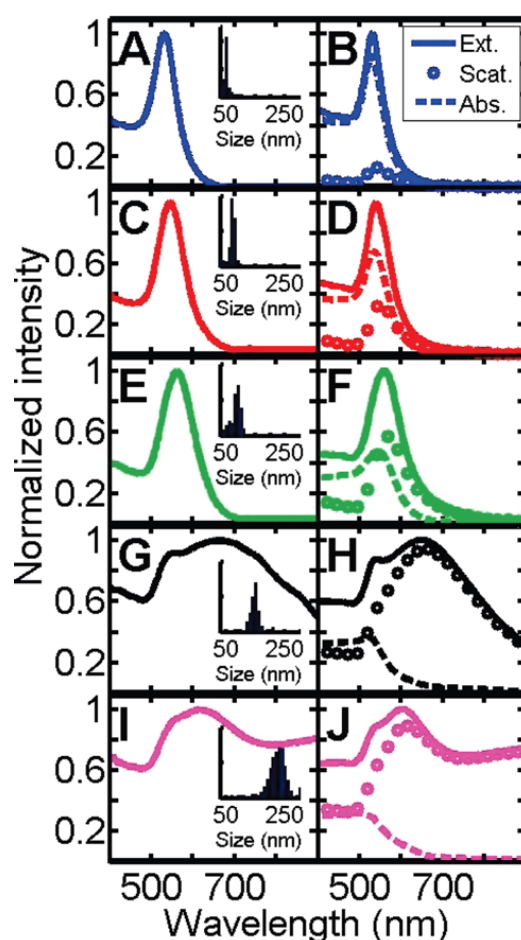


**Figure 3.4:** Visible spectra of spherical AuNPs with mean sizes 51 nm for panels (A) and (B), 76 nm for (C) and (D), 88 nm for (E) and (F), 155 nm for (G) and (H), and 237 nm for (I) and (J) – the insets show size distribution of the particles. Note how different the surface plasmon bands can be depending on the size of the AuNPs. The left column shows the spectra measured experimentally and the right column shows the spectra calculated using Mie theory. The calculated spectra detailed the total extinction (scattering plus absorption, solid lines) and the contribution from each, scattering (open circles) and absorption (dashed lines). The figure was reprinted with permission from Tcherniak et al. (2010). Copyright (2019) American Chemical Society.

#### 3.4.1.3.1 Chemical methods

Chemical synthesis is the preferable method for fabricating metallic nanoparticles (Reza Ghorbani et al., 2011). In general, this approach is relatively simple, scalable and provides good controllability over size, shape and composition of nanoparticles (Nikam et al., 2018). On the other hand, this method can raise concerns for human and environmental safety because of the regular adoption of toxic chemicals (Sardar et al., 2014).

One classic technique for the chemical synthesis of metallic nanoparticles is the sol-gel method. In this approach synthesis typically occurs by hydrolysis and polycondensation of metal alkalooids, followed by ageing and drying (Hench and West, 1990). Simplicity, efficiency and cost competitiveness are appealing aspects of this method (Parashar et al., 2020).

Hydrothermal and solvothermal methods are well-known for making nanoparticles at high temperatures and pressures (Adschiri et al., 2001, Yang et al., 2007). Typically, autoclaves or bombs are adopted for the reaction (Ansari et al., 2010). The synthesis process usually involves two steps: crystal nucleation and crystal growth; with the first step taking place when the solution becomes supersaturated and the second when growth units are further incorporated into the crystals (Li et al., 2016). The hydrothermal method utilises water as solvent and the solvothermal uses organic or mixed water-organic solvents (Canu and Buscaglia, 2017). The advantages of these methods include simplicity and good controllability (Ye et al., 2018).

The route most used for nanoparticle fabrication is chemical reduction (Kumar and Kumbhat, 2016). This method involves the reduction of metallic ions in solution by a chemical reagent, generally in the presence of a stabiliser to prevent particle aggregation (Daniel and Astruc, 2004). It has the advantages of low cost fabrication, simple preparation and high productivity (Kim et al., 2004).

#### 3.4.1.3.2 Physical methods

In physical methods pressure, radiation, thermal energy and/or electrical energy are applied to synthesise the nanoparticles (Dhand et al., 2015). Lack of need for solvents and wide size distribution of the particles made are advantages

and disadvantages of physical techniques, respectively (Toshima, 2004, Iravani et al., 2014). Typical synthesis methods include high energy ball milling, laser ablation and inert gas condensation.

In high energy ball milling mechanical energy is applied by vigorous shaking or high-speed rotation of steel or tungsten carbide balls, causing plastic deformation, grinding, fracturing, mixing, cold welding and thermal shock of bulk material (Tavakoli et al., 2007). Despite being a process easy to perform and highly versatile in terms of materials suitable for grinding, the final particles tend to have broad size and shape distribution (Scudino et al., 2009).

For the case of laser ablation a solid material – placed in an ambient with gas or liquid – is targeted with a laser beam which vaporises the material and generates the nanoparticles through the formation of a laser-induced plasma plume (Kim et al., 2017). Material's optical properties, laser wavelength and pulse width are parameters important for this technique, as they affect the amount of material ablated in a single laser pulse (Kumar and Kumbhat, 2016). This method has the advantages of utilising bulk material instead of metal salts, requiring low manual operation and producing minimum waste; on the other hand, the equipment is pricy, production rate is low and the properties of the particles are not easily controllable (Amendola and Meneghetti, 2009).

Inert gas condensation is a technique in which the metal is vaporised into a cooler low density gas, which causes its high supersaturation and the subsequent nucleation and growth of nanoparticles (Simchi et al., 2007). Raffi et al. (2007) reported that shape, particle mean size, agglomeration state and size distribution are directly affected by process parameters as evaporation temperature and inert gas pressure. Advantages and disadvantages of the method include high purity of the particles synthesised and low production rate, respectively (Simchi et al., 2007, Wen and Xia, 2018).

#### 3.4.1.3.3 Biological methods

In biological processes metal ions are turned into metallic nanoparticles through reactions with biomolecules. In general, the process consists of adding cells or cell-derivative biomolecules into solution containing metallic ions. After

some period of incubation, the ions are reduced and nanoparticles are formed. According to Pantidos and Horsfall (2014), biological synthesis can be divided into two categories, bioreduction and biosorption. In bioreduction metal ions are reduced enzymatically and in biosorption nanoparticles are formed as a consequence of the binding of ions onto the organism. Synthesis at standard temperature and pressure, and requirement of sample purification are examples of advantages and drawbacks of biological methods (Schröfel et al., 2014).

Multiple organisms were already investigated for their capability to synthesise various metallic nanoparticles, such as AuNPs, AgNPs, PtNPs, PdNPs. These include bacteria, fungi, algae, plants and even human cells (Gardea-Torresdey et al., 2002, Anshup et al., 2005, Castro-Longoria et al., 2012, Courtney et al., 2016, da Silva Ferreira et al., 2017). Comprehensive reviews on the investigations conducted for this field can be found in the articles by Rai et al. (2013), Iravani et al. (2014), Pantidos and Horsfall (2014), and Schröfel et al. (2014).

#### **3.4.1.4 Synthesis of metallic nanoparticles by microorganisms**

It has been already mentioned that bacteria, fungi and algae were shown to be able to synthesise metallic nanoparticles. For each of these domains, and others, several species have been tested for their capacity to form nanoparticles. For example, the bacteria *Pseudomonas aeruginosa*, *Rhodopseudomonas capsulata* and *Bacillus* sp., the fungi *Verticillium* sp., *Colletotrichum* sp. and *Neurospora crassa*, and the microalgae *Rhizoclonium hieroglyphicum*, *Tetraselmis suecica* and *Chlorella vulgaris* are all of microorganisms capable of synthesising AuNPs from gold ion precursors (Mukherjee et al., 2001, Karthikeyan and Beveridge, 2002, Shankar et al., 2003, He et al., 2007, Chakraborty et al., 2009, Shakibaie et al., 2010, Castro-Longoria et al., 2011, Annamalai and Nallamuthu, 2015, Roshmi et al., 2015). Li et al. (2011), Park et al. (2016), Fang et al. (2019), and Gahlawat and Choudhury (2019) published interesting reviews on the microbial synthesis of nanoparticles. A list of some representative metallic nanoparticles synthesised by microorganisms can be found in **Table 3.5**.

**Table 3.5:** A representative list of microorganisms used for the synthesis of nanoparticles and their applications. This table was adapted from tables 1, 2, 3 and 4 of the article by Gahlawat and Choudhury (2019) - Published by The Royal Society of Chemistry; licensed under a Creative Commons Attribution-NonCommercial 3.0 Unported Licence.

Microorganism	Metal	Size (nm)	Shape	Applications	Reference
<b>Bacteria</b>					
<i>Bacillus cereus</i>	Silver	20-40	Spherical	Antibacterial activity	(Sunkar and Nachiyar, 2012)
<i>Deinococcus radiodurans</i>	Silver	4-50	Spherical	Antibacterial activity, anti-biofouling agent and anticancer activity	(Kulkarni et al., 2015)
<i>Pseudomonas aeruginosa</i> JP-11	Cadmium sulphide	20-40	Spherical	Removal of cadmium pollutant from aqueous solution	(Raj et al., 2016)
<b>Actinomycetes</b>					
<i>Streptacidiphilus durhamensis</i>	Silver	8-48	Spherical	Antibacterial and anticancer activity	(Buszewski et al., 2018)
<i>Streptomyces griseoruber</i>	Gold	5-50	Spherical, hexagonal and triangular	Degradation of methylene blue	(Ranjitha and Rai, 2017)
<b>Fungi</b>					
<i>Penicillium diversum</i>	Silver	10-50	Roughly spherical	Antimicrobial activity	(Ganachari et al., 2012)
<i>Trichoderma harzianum</i>	Cadmium sulfide	3-8	Spherical	Photocatalytic activity	(Bhadwal et al., 2014)
<i>Fusarium oxysporum</i> 405	Silver	10-50	Spherical	Colloidal stability	(Rajput et al., 2016)
<b>Yeast</b>					

<i>Candida lusitanae</i>	Silver and silver chloride	2-10	Cubical, cuboctahedral, icosahedral and spherical	Antiproliferative and microbicidal activity	(Eugenio et al., 2016)
<i>Magnusiomyces ingens</i> LH-F1	Gold	20.3-28.3	Spherical and pseudo-spherical	Catalyst for nitrophenols reduction	(Qu et al., 2018)
<i>Saccharomyces cerevisiae</i>	Palladium	32	Hexagonal	Degradation of textile dyes	(Sriramulu and Sumathi, 2018)
<b>Algae</b>					
<i>Tetraselmis kochinensis</i>	Gold	5-35	Spherical and triangular	nd	(Senapati et al., 2012)
<i>Scenedesmus sp.</i>	Silver	15-20	Spherical crystalline	Antibacterial assay	(Jena et al., 2014)
<i>Chlorella vulgaris</i>	Gold	2-10	Spherical self assembled cores	Anti-pathogenic activity	(Annamalai and Nallamuthu, 2015)
<b>Viruses</b>					
Tobacco mosaic virus	Gold	5	Spherical	Building block for chiral meta-molecules	(Kobayashi et al., 2012)
M13 virus	Titanium dioxide	20-40	Mesoporous nanowires	Photo-electrochemical properties	(Chen et al., 2015)

Another important group of bacteria involved in the synthesis of metallic (metaloxide) nanoparticles are the magnetotactic bacteria. These are Gram-negative motile aquatic bacteria capable of performing magnetotaxis – motility caused by a magnetic field (Blakemore, 1982). Magnetotaxis is possible because these cells produce magnetosomes – intracellular organelles composed of iron oxide (magnetite, Fe<sub>3</sub>O<sub>4</sub>) or iron sulphide (greigite, Fe<sub>3</sub>S<sub>4</sub>) nanocrystals surrounded by a phospholipid bilayer (Lower and Bazylinski, 2013). The most relevant differences in the synthesis of nanoparticles by this type of microbe in

relation to the other microorganisms are that magnetotactic bacteria oxidise (and not reduce) the metallic ions and that they are endowed with special machinery dedicated for the formation of nanoparticles.

*Escherichia coli* and *Shewanella oneidensis*, the two bacteria adopted in the present study, have also been previously investigated for their capability to synthesise metallic nanoparticles. A more detailed description of some of these studies is given below, in section 3.6.

#### 3.4.1.4.1 Mechanisms involved in the synthesis of metallic nanoparticles by microorganisms

Certainly, the most well characterised mechanism involved in the microbial synthesis of metallic nanoparticles is the one which results in the formation of magnetosomes. This is not because magnetotactic bacteria are more important or more studied than the other microorganisms, instead it is because – as previously explained – these bacteria have specialised machinery for making nanomagnets. Therefore, once this machinery was discovered it was possible to narrow down the scope of the investigation and focus on determining the function and structure of each component of the machinery. For the case of the other microbes, the mechanisms involved in the synthesis process are still mostly unknown and, therefore, the scope of the investigation is still broad.

A series of complex processes and reactions not entirely known are involved in the synthesis of magnetosomes. In a brief explanation, four steps must be completed for the biofabrication of these organelles: formation of the magnetosome vesicle, uptake of iron ions, transport of the ions into the vesicles and controlled biomineralization of the ions into  $\text{Fe}_3\text{O}_4$  or  $\text{Fe}_3\text{S}_4$  (Bazylinski and Frankel, 2004). Four clusters of operons were found to be involved in the formation of magnetosomes: *mamAB*, *mamGFDC*, *mamXY* and *mms6*; however, only the first has been shown to be essential for the process, with the other three having accessory roles (Lohse et al., 2011). In general terms, the proteins derived from the *mamAB* cluster were found to be responsible for the formation of the vesicles and biomineralization of the ions, those composing the *mamGFDC* group are involved in the control of the sizes of the magnetosomes, the ones



from *mamXY* are responsible for the maturation of the organelles, and those from *mms6* are involved in the nucleation of the crystals (Jogler and Schuler, 2009, Murat et al., 2010, Tanaka et al., 2010, Yang et al., 2013, Staniland and Rawlings, 2016).

For the other microbes, those which are not endowed with specialised machinery for the formation of nanoparticles, the mechanisms surrounding the synthesis remains poorly understood. One fact that is known is that the process involves first the adsorption and/or absorption of metallic ions by the organism followed by biochemical reduction (Li et al., 2011). A schematic illustration of this phenomenon is represented in **Figure 3.5**. It is not entirely known if cells adsorb the metallic ions, absorb or performs both processes simultaneously. There is a general consensus, however, that the sorption process is a result of electrostatic interactions that occur between molecules on the cell envelopes, such as carboxyl and phosphate groups, and the metallic ions (Hoyle and Beveridge, 1984, Ferris and Beveridge, 1986, Lin et al., 2011, Cheng et al., 2019). For this reason, the term for sorption mostly adopted in this thesis is adsorption.

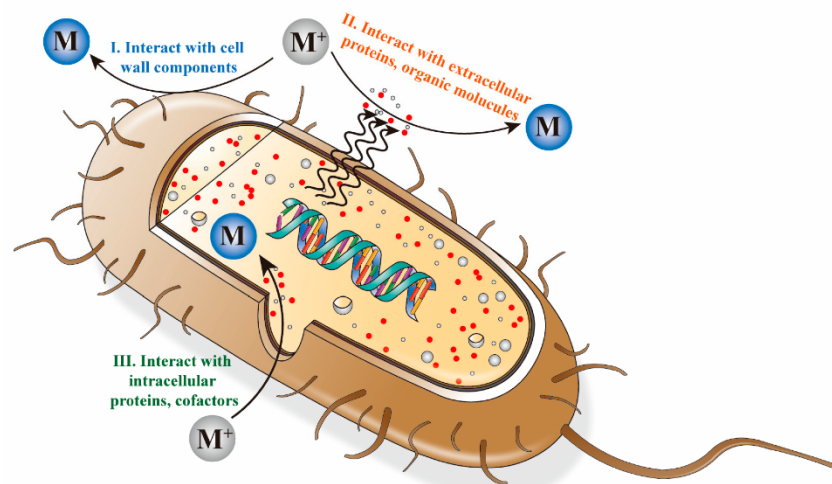


**Figure 3.5:** Schematic representation of bacterial synthesis of nanoparticles; both intracellular and extracellular processes are included. The figure was reproduced from the article by Fang et al. (2019) with

permission under the Creative Commons Attribution 4.0 International Public License (<https://creativecommons.org/licenses/by/4.0/legalcode>).

Some studies proposed mechanisms and identified biomolecules involved in the synthesis of metallic particles by microorganisms. For example, NADH-dependent nitrate reductase has been suggested to be involved in the synthesis of AuNPs by *Rhodopseudomonas capsulate* (He et al., 2007). The same enzyme was considered to be involved in the formation of gold and silver nanoparticles by *Bacillus licheniformis* (Kalimuthu et al., 2008, Kalishwaralal et al., 2008). Nitrate reductase was also suggested to participate in the fabrication of nanoparticles by the fungus *Fusarium oxysporum* (Ahmad et al., 2003, Durán et al., 2005). A corroboration for the involvement of this enzyme in the synthesis of metallic nanoparticles comes from the study by Kumar et al. (2007), which confirmed that this enzyme is capable of reducing silver ions *in vitro*.

A study on the bioremediation of technetium ions identified the hydrogenase III (Hyc) component of the formate hydrogenlyase (FHL) complex as the enzyme responsible for Tc(VII) reduction (Lloyd et al., 1997). Hydrogenases were also demonstrated that have an influence in the deposition of palladium nanoparticles by *Desulfovibrio fructosivorans*, *E. coli* and *S. oneidensis* (Mikheenko et al., 2008, Deplanche et al., 2010, Ng et al., 2013b). In addition, Marshall et al. (2008) reported that although not an absolute requirement for the reduction of Tc(VII), hydrogenases in *S. oneidensis* were essential for the rapid and complete formation of Tc(IV)O<sub>2</sub>.

The *c*-type cytochromes MtrC and OmcA of *S. oneidensis* were found to reduce Tc(VII) to Tc(IV) when coupled to the oxidation of lactate (Marshall et al., 2008). According to the study, MtrC was capable of transferring electrons to Tc(VII) more than one order of magnitude faster than OmcA. Purified MtrC and OmcA were also able to reduce Cr(VI) *in vitro* (Belchik et al., 2011). Interestingly, for the case of Cr(VI) MtrC was found to be a slower reductant than OmcA. MtrC was also demonstrated to function as terminal reductase of U(VI) (Marshall et al., 2006). Moreover, the flavocytochrome *c*-fumarate reductase FccA of *S.*

*oneidensis* was discovered to work, in conjunction with the c-type cytochrome CymA, as terminal reductase of selenite (Li et al., 2014). It should be noted, however, that selenium is not a metallic element.

Other biomolecules reported to be involved in the synthesis of metallic nanoparticles include phosphatases – which form inorganic phosphates that then react with metallic ions to make the nanoparticles; phytochelatins – peptides that have high affinity towards with heavy metal ions; and metallothioneins – metal-binding proteins of low molecular weight (Bayer and Bayer, 1991, Kang et al., 2008, Park et al., 2016, Choi et al., 2018).

#### 3.4.1.4.2 Advantages and disadvantages of using microorganisms for the synthesis of metallic nanoparticles

As it happens with all methods used for the synthesis of metallic nanoparticles, the adoption of microorganisms also present intrinsic advantages and disadvantages. The main advantages related to the use of microorganisms are that the process is conducted without the need for toxic chemicals and high energy consumption (Fang et al., 2019). Also considered as advantages are the facts that the microbial synthesis process is simple, scalable and cost-effective, it allows the formation of a wide diversity of nanoparticles, and can be coupled with environmental bioremediation (Lloyd et al., 2011, Park et al., 2016, Gahlawat and Choudhury, 2019). Suresh et al. (2010, 2011) have also suggested that microbial-made particles present higher stability over the ones fabricated through chemical routes. According to the authors, that could be due to the negative charge of the biosynthesised particles, whose electrostatic repulsive forces prevent agglomeration or clumping.

Lack of controllability of the synthesis process and particle properties is probably the main disadvantage of using microorganisms (Li et al., 2011, Park et al., 2016). Some researchers have identified ways to better control the microbial formation of particles through changes in reaction parameters, such as concentration of metallic ions, temperature, pH, culture medium and type of electron donor (Gericke and Pinches, 2006, He et al., 2007, Deplanche and Macaskie, 2008, Gurunathan et al., 2009, De Corte et al., 2011, Kaul et al., 2012).

Although enhancement can be achieved, these measures did not improve controllability to the levels seen in the other methods. It is important to note, though, that lack of knowledge of the biomolecules involved in the synthesis process is a main factor causing the lack of controllability. Once more elucidation in this matter is achieved, researchers will be able to address the issue of controllability with better precision.

#### 3.4.1.4.3 The chemistry involved in the microbial synthesis of gold nanoparticles

Because the microbial synthesis of gold nanoparticles takes place in aqueous solutions, some factors on the speciation and reduction process should be considered. Tetrachloroauric(III) acid –  $\text{HAuCl}_4$  – is the gold precursor mostly adopted in the synthesis of AuNPs, and was also the precursor used in the present study. When in aqueous acid solution, the precursor forms  $\text{AuCl}_4^-$  ions stacked along with interleaved layers of  $[(\text{H}_5\text{O}_2)^+ \cdot 2\text{H}_2\text{O}]$  (Williams and Peterson, 1969). As can be seen in the speciation diagrams of **Figure 3.6**, at 298 K  $\text{AuCl}_4^-$  is the most predominant species at pH 7 and lower in all different concentrations of  $\text{HAuCl}_4$  evaluated. In fact, according to Pan and Wood (1991),  $\text{AuCl}_4^-$  is the most common ionic form of gold in acidic aqueous solutions at temperatures up to 100 °C. This Au(III)-chloride complex has a square-planar molecular geometry with Au–Cl bonds presenting an average length of 2.27 Å (Hargittai et al., 2001).

Since the precursor ion in solution is predominantly at the Au(III) oxidation state, its reduction process into Au(0) requires three electrons, as detailed in equation 3.1. According to the CRC Handbook of Chemistry and Physics (Lide, 1993), the standard reduction potential ( $E^0$ ) for the reaction at 298 K and 1 atm is +1.002 V. The application of this value into the Nernst equation (eq. 3.2) thus allows the calculation of the redox potential for the reaction ( $E = +0.942$  V). Therefore, any biomolecule with redox properties, present in its reduced form, and having a considerably lower redox potential than +0.942 V should, theoretically, be able to reduce the Au(III)-chloride complex.

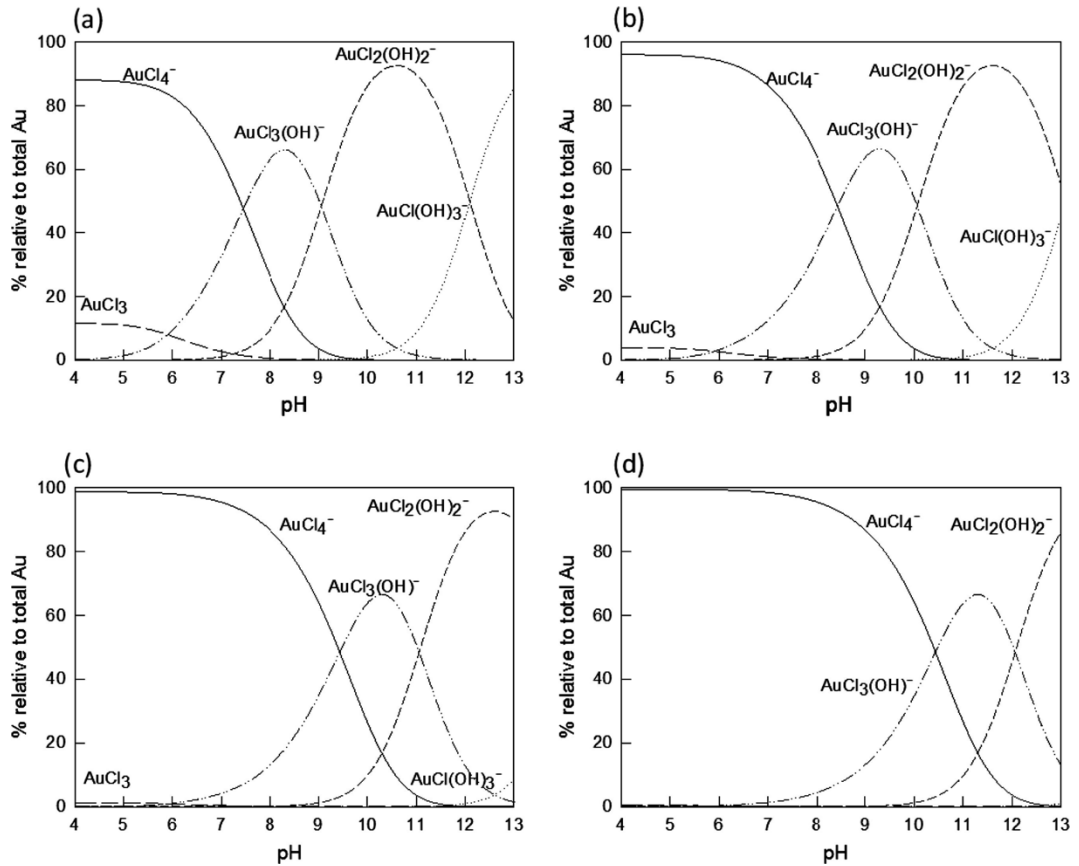


**Figure 3.6:** Speciation diagrams for the Au-Cl-OH system. The graphs contain the relative concentration of the different Au(III) chlorohydroxo complexes formed in aqueous solution at 298 K, in varying pH and at different total Au concentrations ((a)  $10^{-3}$  M, (b)  $10^{-2}$  M, (c)  $10^{-1}$  M and (d) 1 M). The figure was reprinted from figure 1 of the article by del Río et al. (2014) with permission from Elsevier.



$$E = E^0 - \frac{RT}{nF} \ln \left( \frac{[\text{Ox}]}{[\text{Red}]} \right) \quad (\text{eq. 3.2})$$

Where:

$E$  = redox potential in respect to the standard hydrogen electrode;

$E^0$  = standard reduction potential;

$R$  = ideal gas constant;

$T$  = temperature;

$n$  = number of electrons transferred in the reaction;

F = Faraday's constant;

[Ox] and [Red] = molar concentrations of oxidised and reduced gold ions.

R and F are both constants and have the values of 8.314 J/mol.K and 96,485 C/mol, respectively. n is equal to three and T is 298 K. The molar concentration of the oxidised form was obtained from graph (a) of **Figure 3.6**. At pH 4 or below and at total gold concentration of  $10^{-3}$  M the percentage of Au(III) in the form of  $\text{AuCl}_4^-$  is approximately 90 %. Therefore, [Ox] equals 0.0009 M. Because the reduced species is a solid, it has unity activity. For the case of pH 7, the presence of  $\text{AuCl}_4^-$  in solution is reduced to 60 %. In this case, E becomes +0.939 V.

Gold(III) can form stable complexes with C, N, P, S, and O-donor ligands (Gimeno, 2008). In some cases, for example in gold-thiol bonding, the interaction can have the strength of a covalent bond (Xue et al., 2014). Because several biomolecules contain these ligands, Au(III) has been found to interact with a range of cellular components, including amino acids, proteins, nucleic acids and carbohydrates (Sadler, 1976, Korobushkina et al., 1983, Savvaidis et al., 1998). With such an abundant number of bacterial components capable of binding to gold ions, it becomes difficult to identify the specific cellular functional groups responsible for adsorbing and reducing Au(III).

Nevertheless, Lin et al. (2011) have identified that the adsorption of Au(III) onto the biomass of the Gram-positive strain *Bacillus megatherium* D01 took place through an ion-exchange mechanism in which coordinate-covalent bonds between Au(III) and oxygenic- and nitrogenous-active groups of polysaccharides and proteins (primary and secondary structures) were formed. In addition, a recent study determined that the functional groups involved in the adsorption of gold ions at the cell surface of the Gram-positive strain *Bacillus licheniformis* FZUL-63 are amino, carboxyl and phosphate groups (Cheng et al., 2019). In fact, Jiang et al. (2004) demonstrated that carboxylic and phosphate groups are likely the main contributors to the negative charge and reactivity of bacterial surfaces in the pH range of 4 to 9. The authors also determined that the bulk functional group chemistry of the surfaces of both Gram-positive and Gram-

negative strains are identical. Hence, for the case of the strains used in the present study (*E. coli* and *S. oneidensis*), sorption of Au(III) probably takes place with one or more of the aforementioned functional groups. It is important to note, though, that differences in pH of the solution modify substantially the characteristics of cell walls. That is because pH alterations can change protonation state of oxygenous- and nitrogenous-active groups, induce compositional modifications on the surface of cells and trigger up- and down-regulations in the transcription of membrane-bound protein complexes (Wilks et al., 2009, Lin et al., 2011, Ramstedt et al., 2014).

Equally unknown are the exact biomolecules involved in the reduction of gold ions. Narrowing down the components involved in the reaction is further complicated by the fact that gold nanoparticles synthesised by microbes (including *E. coli* and *S. oneidensis*) were already found in the extracellular ambient, attached to the outer cell surface, in the periplasmic space as well as within the cytoplasm (Deplanche and Macaskie, 2008, De Corte et al., 2011, Suresh et al., 2011). Therefore, it is likely that, once the ions are in contact with the cell, multiple reducing biomolecules end up forming the gold nanoparticles.

It should also be noted that, depending on the concentration, Au(III) can be toxic to bacteria (Nies, 1999). It is not entirely clear the mechanisms that drive the toxicity, but a publication by Muñoz-Villagrán et al. (2020) shed a light into the matter. In a study on Au(III) toxicity towards *E. coli*, the authors found that the metal increased superoxide concentration and decreased thiol levels in the cell. This is not a surprising outcome because generation of intracellular reactive oxygen species and depletion of total cellular thiols are mechanisms of toxicity commonly observed during metal poisoning in bacteria (Lemire et al., 2013).

### **3.5 Bacteria used in the present study**

Two bacterial strains were adopted in this project, *E. coli* and *S. oneidensis*. The two are highly studied and important cells in the field of biotechnology. A detailed explanation of each organism can be found below.

### 3.5.1 *Shewanella oneidensis* MR-1

*S. oneidensis* MR-1 is a facultative aerobic Gram-negative bacterium member of the *Gammaproteobacteria* class. It was isolated from the Lake Oneida in the state of New York and designated, at the time, as *Alteromonas putrefaciens* MR-1 since the results of conventional biochemical identification tests revealed close relationship to a *A. putrefaciens* strain (Myers and Nealson, 1988). The name then changed to *Shewanella putrefaciens* MR-1 based on the proposal by MacDonell and Colwell to establish the genus *Shewanella* (MacDonell and Colwell, 1985). The final denomination of *S. oneidensis* MR-1 took place after a range of phylogenetic analyses revealed that MR-1 and *S. putrefaciens* are in fact different species – although they share 97 % similarity in their 16S rDNA sequences, DNA-DNA hybridisation test and *gyrB* sequence analysis showed 36 % and 85 % similarity between both strains, respectively (the threshold for the inclusion within a species is 70 % for the first case and 90 % for the second) (Venkateswaran et al., 1999).

*S. oneidensis* is capable of respiring an impressive variety of oxidants: dimethyl sulfoxide, sulphite, fumarate, nitrate, nitrite, Fe(III), Mn(IV) and oxygen are all electron acceptors of MR-1 (Myers and Nealson, 1988, Heidelberg et al., 2002). Even Cr(VI), a toxic substance, was found to be an electron acceptor for *S. oneidensis* (Gao et al., 2010). Such versatility in respiration is attributed in part by the vast amount of *c*-type cytochromes present in this organism (Heidelberg et al., 2002). In terms of fermentation, MR-1 was found to be capable of fermenting pyruvate for cell survival, not for growth (Pinchuk et al., 2011).

Another remarkable feature of this strain is its ability to respire electron acceptors extracellularly. This phenomenon is only possible because this cell is endowed with mechanisms dedicated for extracellular electron transfer (EET). One of these is the secretion of endogenous redox-active electron shuttles that transfer electrons from reducing agents within the cell to external substances. Flavin mononucleotide and riboflavin were found to be the main electron shuttles of *Shewanella* sp. (von Canstein et al., 2008). Marsili et al. (2008) determined that secretion of flavins is a fundamental tool for the respiration of *Shewanella* cells within a biofilm.



Another mechanism utilised by *S. oneidensis* for the extracellular electron transfer is the formation of nanowires – thin and long structures that protrude from the bacterial surface in order to attach to the surface of an electron sink (Gorby et al., 2006). Nanowires were initially thought to be pilin-like structures, but it was later proved that they are actually extensions of the outer membrane and periplasm which contain multiheme cytochromes positioned to guarantee an efficient electron transfer (Pirbadian et al., 2014).

Despite all these exquisite respiratory tools that *S. oneidensis* is endowed with and that allow extracellular electron transfer, the Mtr (metal reducing) pathway – another feature involved in extracellular respiration – is certainly the most famous attribute of MR-1. The pathway is composed by five core proteins – CymA, MtrA, MtrB, MtrC and OmcA – that act in conjunction for the efficient conduit of electrons from the inner membrane to electron acceptors located outside the cell (Kouzuma et al., 2015).

The process starts with the oxidation of quinols from the NADH-dehydrogenase by CymA, a tetraheme cytochrome *c* that catalyses the reaction and conducts the electrons generated (Kracke et al., 2015). CymA is a 21-kDa protein that is anchored to the cytoplasmic membrane through a single N-terminal transmembrane helix and that protrudes into the periplasm through a globular domain with *c* hemes (Marriott et al., 2012).

Next in the process, MtrA takes up the electrons from CymA and transfers them to MtrC and OmcA (Shi et al., 2007). MtrA is a 32-kDa decaheme *c*-type cytochrome endowed with hemes with *bis*-histidine axial ligation (Pitts et al., 2003). Although this cytochrome is water soluble, it is localised in the outer membrane of the cell – which is only possible because of its interaction with MtrB (Hartshorne et al., 2009).

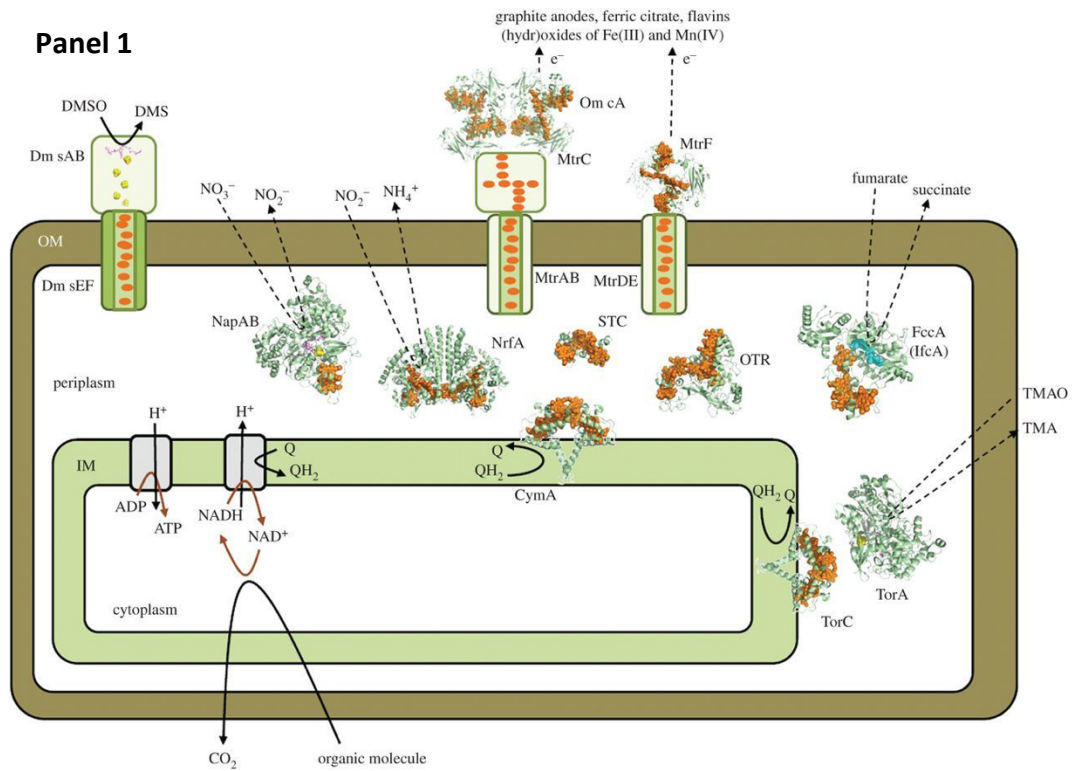
In fact, the role of MtrB in the electron transfer process is indirect, as it is not a cytochrome and cannot conduct electrons. MtrB is a transmembrane porin-type protein that acts like a sheath for MtrA and is responsible for the connection between MtrA and MtrC (Richardson et al., 2012). White et al. (2013) carried out a bioinformatics simulation of the structure of MtrB, based on its amino acid sequence, and revealed that this is a  $\beta$ -barrel protein with 28  $\beta$ -

strands and 14 long and 13 short solvent-exposed loops. The short loops, as well as a 33-amino acid N-terminus, were hypothesised to be positioned facing the external side of the membrane, and the long loops the periplasm. According to the study, the pore diameter created by this protein is estimated to be 3 to 4 nm.

The EET process ends with the reduction of a final exogenous electron acceptor (soluble or insoluble metal ions) by the extracellular terminal reductases MtrC and OmcA (Tikhonova and Popov, 2014). Both proteins are decaheme *c*-type cytochromes embedded in the outer cell membrane. MtrC has 671 amino acids and around 75 kDa (Beliaev et al., 2001). Absorption spectra and sequence alignments revealed that MtrC is composed by *bis*-histidine-ligated *c*-type hemes (Hartshorne et al., 2007). OmcA has also been found to be composed by hemes with *bis*-histidine axial ligands (Edwards et al., 2014). The *omcA* open reading frame (ORF) was reported to encode for 734 amino acids, however it has been suggested that the protein has a hydrophobic leader sequence that is cleaved during its translocation to the outer membrane; after the cleavage the mature protein presents 708 amino acids and 83 kDa (Myers and Myers, 1998).

Originally, the Mtr pathway did not include OmcA – especially because *mtrC*, *mtrA*, and *mtrB* form an operon (Beliaev et al., 2001). However, although OmcA and MtrC are paralogs and share overlapping functions, both cytochromes are known to establish a direct cross-linked interaction to form a complex for transferring electrons (Myers and Myers, 2003, Zhang et al., 2009). In fact, in a test for the ability of OmcA and MtrC to reduce Fe(III)-nitrilotriacetic acid, Shi et al. (2006) found that when combined both cytochromes presented higher reductase activity than the sum of the individual activities – suggesting a synergistic effect between them. The same study also identified that OmcA and MtrC form a heterotrimer, with a stoichiometry of two OmcA per MtrC. A schematic representation of the Mtr pathway as well as of other pathways involved in the anaerobic respiration of *S. oneidensis* MR-1 can be found in **Figure 3.7**.

It is important to point out that the periplasmic electron carrier (PEC) MtrA has three paralogs (MtrD, DmsE and SO4360), the  $\beta$ -barrel protein MtrB has also three (MtrE, DmsF and SO4359) and the outer membrane cytochrome



**Panel 2**

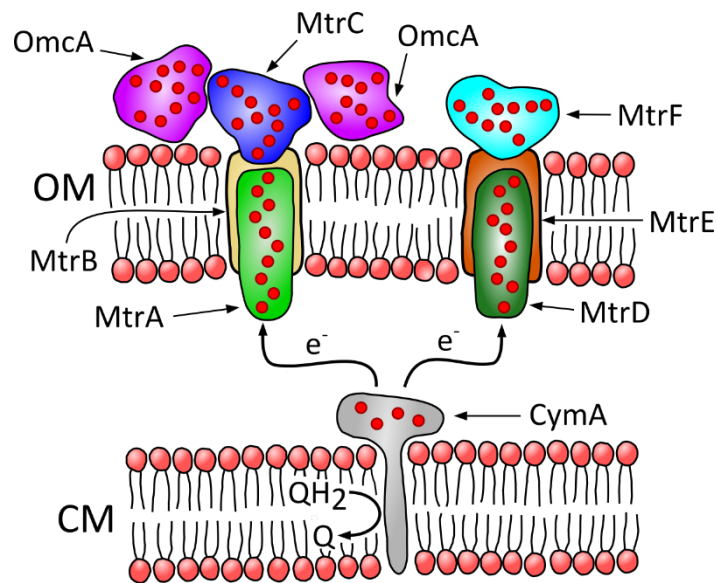


**Figure 3.7:** Schematic illustrations of some of the anaerobic respiration pathways of *S. oneidensis* MR-1. Panel 1 shows an illustration of the pathways and the cytochromes involved in the anaerobic respiration of (left to right) dimethyl sulfoxide (DMSO), nitrate, nitrite, electrodes and extracellular soluble and insoluble metals (Mtr pathway), fumarate and trimethylamine N-oxide (TMAO). Some cytochromes were represented as high-resolution structures and some others as cartoons. Panel 2 shows a cartoon illustration of the Mtr pathway – highly relevant to the present

study. OM and CM mean outer membrane and cytoplasmic membrane, respectively. Each red circle represents a heme group in the cytochromes. The figure in panel 1 was republished with permission of Royal Society from figure 3 of the article by Breuer et al. (2015); permission conveyed through Copyright Clearance Center, Inc.

(OMC) MtrC has two (MtrF and OmcA) (Heidelberg et al., 2002, Coursolle and Gralnick, 2012). Also of note, the redox potential of the MtrCAB complex ranges from 0 to  $-0.45$  V in respect to the standard hydrogen electrode (Hartshorne et al., 2009). Redox potential of individual cytochromes has also been determined:  $-0.35$  to 0 V for CymA,  $-0.4$  to  $-0.1$  V for MtrA,  $-0.4$  to  $+0.1$  V for MtrC,  $-0.4$  to  $-0.18$  V for OmcA, and  $-0.044$  to  $-0.312$  V for MtrF (Field et al., 2000, Pitts et al., 2003, Hartshorne et al., 2007, Firer-Sherwood et al., 2008, Clarke et al., 2011, Shi et al., 2012). It is also relevant to note that all proteins from the Mtr pathway contain cysteine residues in their structures. As explained in section 3.4.1.4.3 thiols are ligands with high affinity towards gold, therefore the presence of cysteine may assist the interaction between the cytochromes and gold, and consequently, contribute for the reduction process. The number of cysteine residues in the cytochromes are 8, 21, 20, 23, 25 and 25 for CymA, MtrA, MtrD, MtrC, MtrF and OmcA, respectively.

All these features of *S. oneidensis* make it an attractive microbe for a range of biotechnological applications. For instance, MR-1 has been widely studied for usage in microbial fuel cells (Kouzuma et al., 2015). In that case, the electrons originated from the anaerobic catabolism of organic substrates are transferred to an electrode in the anode for electricity generation. In addition, the extraordinary capability of MR-1 to reduce a wide variety of electron acceptors has been explored for the bioremediation of toxic substances, such as uranium (Newsome et al., 2014).

### **3.5.2 *Escherichia coli* BL21(DE3)**

*Escherichia coli* is a facultatively anaerobic chemoorganotroph Gram-negative bacterium (Madigan et al., 2012). It is the most studied Gram-negative

microorganism, making it a model strain. Major efforts have been directed towards understanding this organism, which led to the annotation of most part of *E. coli*'s genome and the construction of specialised mutant libraries of *E. coli* (Sevin et al., 2017). In one of them, clones encoding a complete set of the open reading frames of *E. coli* K-12 were generated – the ASKA library (Kitagawa et al., 2005). In another, mutants of *E. coli* K-12 containing single-gene deletions of all nonessential open reading frames in the genome were constructed – the Keio collection (Baba et al., 2006).

*E. coli* BL21(DE3), the species used in the present study, had its full circular chromosome of 4,557,508 bp sequenced (Jeong et al., 2009). Studier and Moffatt (1986) constructed this strain, harbouring an integrated T7 RNA polymerase under control of a lacUV5 promoter, to favour high-level expression of cloned genes.

*E. coli* is not capable of extracellular respiration and cannot transfer electrons to as many electron acceptors as *S. oneidensis* – *E. coli* is able to respire six different electron acceptors: oxygen, nitrate, nitrite, fumarate, dimethyl sulfoxide and trimethylamine *N*-oxide (Unden et al., 2014). Nevertheless, the strain can carry out anaerobic mixed acid fermentation – which utilise endogenous organic compounds as electron acceptors, converting them mainly into carbon dioxide, hydrogen, ethanol, formate, acetate and lactate (Sawers and Clark, 2004). Interestingly, *E. coli* cultures at high cell-density and growing in aerobic conditions and with excess glucose were found to be able to produce and release acetate (Lee, 1996). It is important to observe that these chemicals excreted by the cells can change the properties of the surrounding medium (such as pH) and influence parameters relevant for gold nanoparticle production, as Au(III) speciation.

Interestingly, some of the proteins involved in the anaerobic respiration of *S. oneidensis* share similarities with proteins of *E. coli*. For example, the tetraheme *c*-type cytochrome NapC of *E. coli* is not only a homolog of CymA, but is actually able to replace CymA in electron transfer activity (Gescher et al., 2008). It was also found that CymA shares sequence homology with *E. coli*'s pentaheme cytochrome-*c* TorC (Myers and Myers, 1997). Moreover, *S.*

*oneidensis'* MtrA was found to have sequence homology with *E. coli's* pentaheme *c*-type cytochrome nitrite reductase NrfB (Clarke et al., 2008).

Because *E. coli* is a bacterium extensively studied, considerable knowledge about it was obtained. This makes this organism more predictable and an appropriate host for the construction of novel metabolic pathways. For example, *E. coli* was the host chosen for the construct of the first bacterial image recording system (Levskaya et al., 2005). *E. coli* was also the chassis chosen to receive a genetic cassette expressing *S. oneidensis'* Mtr pathway (Jensen et al., 2010). In this study, the authors transformed *E. coli* BL21(DE3) with plasmids encoding for MtrA, MtrB, MtrC and cytochrome *c* maturation proteins. The engineered *E. coli* was found to be able to reduce iron citrate and iron oxide considerably faster than the parent strain.

### **3.6 Synthesis of metallic nanoparticles by *Escherichia coli* and *Shewanella oneidensis***

Throughout the last decades several different research groups have demonstrated the formation of metallic nanoparticles by *E. coli* and *S. oneidensis*. A large variety of nanoparticles was synthesised by both bacteria, including gold, silver and palladium. A compilation of some of these previous studies is described below.

#### **3.6.1 *Escherichia coli***

Possibly the first work demonstrating formation of nanoparticles by *E. coli* was the one conducted by Gerrard et al. (1974). The study revealed, through electron microscopy analyses, that *E. coli* grown in media containing sodium selenite was capable of reducing the selenite and forming nanoparticles – or deposits of elemental selenium accumulation, as called by the authors. Nevertheless, since selenium is not a metal, this was not the first study revealing the synthesis of metallic nanoparticles.

A study that can possibly be considered the first demonstration of metallic nanoparticles synthesised by *E. coli* was published in 1981 (Beveridge and Koval, 1981). In this study the authors added bacterial envelopes (composed of outer membrane, peptidoglycan and cytoplasmic membrane) into solutions containing 32 different metal salts individually. According to the publication, apart from lithium and vanadium, all metals tested bound to the envelopes in more or less quantities.

Later on, in 1983, the same group published a study that was conducted in a similar fashion as the previous one (Hoyle and Beveridge, 1983). In this case only the outer-membrane of *E. coli* was put to react with 19 different metal salt solutions. The study tried to compare the quantity of metals that bound to the envelope (as determined in the previous publication) to the quantity that bound to the OM, in an attempt to understand the role of each wall fraction in metal binding. Such a comparison was found to be more complex than initially predicted. One conclusion the authors stated, though, was that the OM was solely responsible for Na<sup>+</sup> capturing.

The next publication on this subject by the same group reported the reaction of peptidoglycan sacculi of *E. coli* with the same 19 metal solutions (Hoyle and Beveridge, 1984). The comparison of metal binding onto PG with the two previous articles was again complex and not conclusive. For example, peptidoglycan was also found to have great affinity for sodium ions. Fe(III) was found to form nanoparticles (iron oxide hydrate crystalloids) and this phenomenon made the authors suggest a two-step deposition process, where a nucleation site would form as a result of chemical interactions between the metal ions and the peptidoglycan, followed by accumulation of newly precipitated metal.

In a study more focused in the environmental aspect of bacterial sorption of heavy metals, Mullen et al. (1989) tested the capacity of *Bacillus cereus*, *Bacillus subtilis*, *E. coli*, and *Pseudomonas aeruginosa* to remove ions of silver, cadmium, copper and lanthanum from solution. According to the authors, all bacteria were able to remove the four ions tested and all formed Ag and La nanoparticles. Interestingly, these results present some contradictions with

another study, released in the same year, in which *E. coli* envelopes and *B. subtilis* walls were tested for the capability to remove silver, copper, cadmium, nickel, lead, zinc and chromium ions from nitrate salt solutions (Walker et al., 1989). According to this latter study, Ag, Pb and Cr nanoparticles – the only nanoparticles detected – were made solely by *B. subtilis* walls. A possible explanation for this divergence in *E. coli* results is that whole cells were used in the former study, whereas the latter used cell envelopes. Nevertheless, a third article on this topic added fuel to the contradiction. The publication, by Flemming et al. (1990), is, in essence, a continuation of the research disclosed by Walker et al. (1989), as it tested different strategies for the remobilization of Ag(I), Cu(II) and Cr(III) bound to *E. coli* envelopes and *B. subtilis* walls, as well as kaolinite and smectite clays. The controversy lies in the fact that in this third article *E. coli* envelopes were found to be able to synthesise AgNPs. The authors did not address this controversy probably because synthesis of nanoparticles was not the focus of their work.

Bayer and Bayer (1991) published a study in which lanthanum(III), terbium(III) or europium(III) were put to react with *E. coli* cells for 30s to 60s before or concomitantly to the addition of glutaraldehyde – a fixation agent. The lanthanide nanoparticles formed had predominantly the shape of patches and were located mainly in the periplasm of the cells. Lower concentration of lanthanides decreased the density, but not the distribution, of the patches. Addition of calcium reduced the size and number of particles, and NaCl in the medium favoured nanoparticle formation. Interestingly, de-energisation of the membrane through phage infection or through treatment with carbonyl cyanide *m*-chlorophenylhydrazone prevented NPs to be formed.

In a work testing the bioremediation ability of *E. coli* and *Desulfovibrio desulfuricans*, Mabbett et al. (2006) harnessed the reductive power of the bacteria for the recovery of platinum group metals (mainly palladium) from industrial waste solutions. The microbial biomass covered by bio-reduced palladium, and other metals, was then applied for the catalytic reduction of Cr(VI) to Cr(III). The results showed that the bacteria containing Pd(0) were



capable of remediating hexavalent chromium more efficiently than chemically synthesised Pd(0).

The soluble ions of Cd, Se, Zn, Te, Cs, Sr, Pr, Gd, Au, Ag, Fe, Co, Ni and Mn were incubated with *E. coli* expressing phytochelatins from *Arabidopsis thaliana* and/or metallothioneins from *Pseudomonas putida* to test if the recombinant bacterium is capable of synthesising nanoparticles (Park et al., 2010). The elements were added to the reaction either individually or in combination. According to the study, all elements tested for the biosynthesis yielded nanoparticles and even never-previously-synthesised nanoparticles, such as PrGd and SrGd, were made. Years later, the same group adopted *E. coli* DH5 $\alpha$  co-expressing metallothionein and phytochelatin synthase for the formation of a wide range of nanoparticles (Choi et al., 2018). The cells and their extracts were used in the tests, and 34 different elements were screened for the formation of single-element nanoparticulate matter and 35 (the same 34 plus sulphur) for multi-element nanoparticles. In total, 60 different nanostructured particles were synthesised, including 33 that have never been previously produced – 20 single-element and 13 multi-element.

Du et al. (2007) biosynthesised AuNPs through a 120-h incubation of biomass in aqueous solution of chloroauric acid. The bacteria coated with gold colloids were then tested for their ability to enhance electron transfer between haemoglobins and glassy carbon electrodes. Cyclic voltammogram results demonstrated that redox peaks were improved in the cases where bacteria containing AuNPs were added to the system.

Deplanche and Macaskie (2008) investigated the capability of *E. coli* and *D. desulfuricans* to reduce Au(III) using H<sub>2</sub> as electron donor. Both bacteria were able to remove the gold ions from solution (pH 7 and 2 mM H<sub>2</sub>AuCl<sub>4</sub>) in less than 140 min. The nanoparticles were formed on the outer cell surface, in the periplasm and intracellularly, with the intracellular particles being significantly smaller than those located elsewhere. Both bacteria were then individually challenged with leached waste from a gold factory and, surprisingly, both were capable of removing all soluble residual Au(III) in 100 min.

Gold nanoparticles were also synthesised by recombinant *E. coli* cells expressing glycerol dehydrogenase (GLD) (Niide et al., 2011). The authors incubated *E. coli* bacteria – which had been pre-induced for the overexpression of GLD – for 72 h in an aqueous solution of  $\text{AuCl}_4^-$  containing  $\text{NAD}^+$ , glycerol and NaOH. The synthesis mechanism proposed by the authors was that GLD catalyses  $\text{NAD}^+$  regeneration into NADH through glycerol oxidation, and NADH, in turn, reduces gold ions into Au(0). The study explored the mechanism *in vitro* and *in vivo*, and in both cases nanoparticles were formed only when all elements of the reaction were present, demonstrating a robust design of the system.

Another investigation demonstrating biosynthesis of AuNPs by *E. coli* was conducted by Srivastava et al. (2013). In this case the synthesis process did not take place through incubation of cells in solution containing gold ions. Instead, bacterial membrane fraction was used to perform the reduction. The soluble fraction of the cells was also tested for biogenesis but did not show AuNP formation. The authors further utilised the biosynthesised nanoparticles for the reduction of 4-nitrophenol – a toxic nitroaromatic pollutant of water – in the presence of  $\text{NaBH}_4$ . Addition of the biocatalyst to the reaction caused major degradation of the toxic compound within a few minutes.

A recent study tested *E. coli* for its ability to synthesise Ru and Pd/Ru nanoparticles (Gomez-Bolivar et al., 2019). Three different synthesis reactions were carried out, one in which cells were loaded solely with Ru(III), one in which cells carried 5 wt % Pd/5 wt % Ru and one where cells contained 5 wt % Pd/20 wt % Ru. The nanoparticles were further evaluated for their potential to catalyse the conversion of 5-hydroxymethyl furfural into 2,5 dimethylfuran. The results revealed that cells containing 5 wt % Pd/5 wt % Ru, the sample with the best catalytic results, outperformed even a commercial catalyst composed of Ru on carbon.

### **3.6.2 *Shewanella oneidensis***

In comparison to *E. coli* fewer studies employed *S. oneidensis* for the synthesis of nanoparticles. This is a reasonable fact considering that this bacterium was not isolated from nature until the late 80's. Yet, a considerable

amount of studies tested the capability of this versatile strain to reduce important metallic elements. Some publications on the topic are described below.

Possibly the first study on the synthesis of metallic nanoparticles by *S. oneidensis* was the one by Liu et al (2002). The work tested the capability of *Geobacter metallireducens* GS-15, *Shewanella putrefaciens* CN32, *Shewanella alga* BrY and *S. oneidensis* MR-1 to reduce Fe(III)NTA, Fe(III)citrate, Co(III)EDTA<sup>-</sup>, Cr(VI), U(VI) and Tc(VII). TEM images revealed outer membrane, periplasmic and extracellular formation of UO<sub>2</sub> precipitates by CN32 and GS-15. TcO<sub>2</sub> nanoparticles were also visualised in the bacterial surface and periplasmic space of CN32. The publication did not present any TEM picture of MR-1, but it contains an observation stating that Cr(OH)<sub>3(s)</sub> precipitates were found on the cell surface of *S. oneidensis*.

De Windt et al. (2005) utilised *S. oneidensis* MR-1 and a mutant derivative with improved autoaggregation capabilities for the biosynthesis of palladium nanoparticles from Na<sub>2</sub>PdCl<sub>4</sub> precursor. Different electron donors (H<sub>2</sub>, formate, lactate, pyruvate and ethanol) and acceptors (O<sub>2</sub> and NO<sub>3</sub><sup>-</sup>) were tested for their influence on productivity. The largest amount of nanoparticles was formed when H<sub>2</sub> and NO<sub>3</sub><sup>-</sup> were added to the reaction medium and the smallest when no donor was used and O<sub>2</sub> was the acceptor. Interestingly, cells that had been previously autoclaved were capable of removing Pd(II) from solution, but – according to the authors – PdNPs were not formed. The biomass containing Pd(0) was further applied for the catalytic dechlorination of polychlorinated biphenyls, halogenated organic pollutants. The results indicated that biomass with PdNPs was highly efficient in the decontamination and had better performance than a commercial palladium catalyst.

Another study on the synthesis of PdNPs by MR-1 was carried out by the same group (De Windt et al., 2006). The work started evaluating the viability and culturability of cells during exposure to Pd(II) in the presence and absence of electron donors. The bacteria were observed to significantly decrease in number as a consequence of higher concentration of Na<sub>2</sub>PdCl<sub>4</sub> in solution. Most interestingly, the presence of electron donors helped the strains to maintain

viability and culturability. The cells containing the biosynthesised Pd(0) were then tested for the dechlorination of 2,3,4-trichlorobiphenyl and reductive degradation of perchlorate. Intriguingly, the biomass that formed the bigger and most abundant nanoparticles was more effective in the dechlorination reaction, and the cells containing smaller and more dispersed precipitates performed better in the reduction of  $\text{ClO}_4^-$ .

*S. oneidensis* was also adopted for the biofabrication of AgNPs and AuNPs (Suresh et al., 2010, 2011). In both cases, extracellular hydrophilic homogeneous spherical nanoparticles were synthesised. Also in both cases, the nanoparticles were found to be highly stable – with no aggregation detected even months after the synthesis. Size distribution ranged from 2 to 11 nm and 2 to 50 nm for AgNPs and AuNPs, respectively. The toxicity of the particles towards *E. coli*, *S. oneidensis* and *B. subtilis* was further assessed in both studies. Gold nanoparticles were not found to be toxic at concentration as high 150  $\mu\text{M}$ , whereas silver nanoparticles presented high bactericidal activity towards the three strains tested. Interestingly, the authors reported that biogenic AgNPs had greater toxicity than chemically synthesised colloids.

MR-1 has also been shown to be able to reduce hexavalent chromium (Belchik et al., 2011). The study tested wild-type MR-1 and mutants containing deletions in *mtrC*, *omcA* and *mtrC/omcA* for their reductive capability. Experiments evaluating reduction kinetics found lower rates by all mutants in relation to WT cells. The study also found differences in the location of the nanoparticles synthesised. Precipitates formed by wild-type were present outside the cell, associated with the outer membrane and inside the cytoplasm, whereas single deletion mutants contained nanoparticles on the outer membrane and in the cytoplasm and the double deletion strain had most of the particles inside the cytoplasm.

Ng et al. (2013b) evaluated the formation of palladium nanoparticles by *S. oneidensis* WT and mutants. The mutants tested were  $\Delta\text{cymA}$ ,  $\Delta\text{mtrC}/\Delta\text{omcA}$ ,  $\Delta\text{hydA}$ ,  $\Delta\text{hyaB}$  and  $\Delta\text{hydA}/\Delta\text{hyaB}$ . HydA is a hydrogen-forming [FeFe]-hydrogenase and HyaB is a [NiFe]-hydrogenase that can either form or oxidise hydrogen. The reduction rates of the mutants lacking the cytochromes as well as

the strain without HydA were similar to those of WT, while  $\DeltahyaB$  and  $\DeltahyaA/\DeltahyaB$  presented significantly lower rates. These results suggest that CymA, MtrC, OmcA and HydA are not involved in Pd(II) reduction, as opposite to HyaB. TEM analyses of MR-1 WT with nanoparticles revealed precipitates associated with the cell membrane and in the extracellular environment.

The same group also investigated the influence that MtrC and OmcA have on size and activity of extracellular AgNPs and Ag<sub>2</sub>S NPs synthesised by *S. oneidensis* MR-1 WT and a  $\Delta mtrC/\Delta omcA$  mutant (Ng et al., 2013a). The particles produced by both strains were spherical in shape, but those made by the mutant were significantly smaller than the ones formed by the WT. Tests evaluating the toxicity of the biogenic AgNPs towards *E. coli* found that the particles produced by the mutant were more toxic than the ones made by WT. Likewise, the catalytic activity of Ag<sub>2</sub>S NPs in the reduction of methylviologen was higher for the nanoparticles made by the mutant in comparison to the ones made by the WT.

More recently, Ishiki et al. (2017) reported the synthesis of AuNPs by *S. oneidensis*. The authors resuspended cells in phosphate-buffered saline solution containing sodium formate and tetrachloroauric(III) acid and monitored synthesis of nanoparticles with UV-vis scan, zeta potential, scanning electron microscopy and transmission electron microscopy. The study points out the differences in morphology and quantity of particles made between cells incubated with gold ions for 3 h and 7 h, suggesting that the synthesis process starts with seeds generation, followed by growth and aggregation of precipitates.

Finally, in another recent study, AuNPs were synthesised by *S. oneidensis* under stimulation of light (Huang et al., 2019). The wild-type strain and mutants containing deletions in the Mtr pathway were tested for the synthesis under varying conditions of wavelength and light intensity. Interestingly, the intensity of white light was found to directly influence the concentration of AuNPs formed, with maximum productivity being achieved at the highest intensity. Likewise, wavelength was reported to affect production rate and maximum rate constant. Tests made with the mutant strains under various wavelengths of light

did not show difference in productivity – except for the cases with blue light, where most mutants formed less nanoparticles than the wild-type.

### **3.6.3 The choice for *Escherichia coli* BL21(DE3) and *Shewanella oneidensis* MR-1**

*E. coli* was chosen for the present project because it is a model strain, a widely studied bacterium with well-known properties and characteristics. Moreover, it is an organism that has been shown to be able to synthesise AuNPs. Since BL21(DE3) is a strain optimized for expression of recombinant proteins, it was the *E. coli* species chosen for this study – as it can then be easily adopted in further works involving the synthesis of metallic nanoparticles by engineered cells.

*S. oneidensis* was chosen because it is endowed with the Mtr pathway, a respiratory machinery specialised in the reduction of external electron acceptors. Not only MR-1 has been shown to be able to synthesise metallic nanoparticles, but actually members of the Mtr pathway were demonstrated to be able to reduce different metals, such as technetium, chromium and uranium. This strain was therefore applied based on the hypotheses that components of the Mtr pathway could be involved in the biofabrication of AuNPs by MR-1, and that the presence or absence of such components could potentially improve controllability of the synthesis process.

# *Materials and methods*

*“On this account I say to you:  
Stop being anxious about your lives  
as to what you will eat or what you will drink,  
or about your bodies as to what you will wear.  
Does not life mean more than food and the body than clothing?  
Observe intently the birds of heaven;  
they do not sow seed or reap or gather into storehouses,  
yet your heavenly Father feeds them.  
Are you not worth more than they are?”*

*Matthew 6:25-26*





## 4 Materials and methods

---

### 4.1 Microorganisms and culture media

#### 4.1.1 Microorganisms

The bacteria used for the experiments in this thesis were *Escherichia coli* BL21(DE3), *Shewanella oneidensis* MR-1 ATCC® 700550™ and a variety of MR-1 mutants: *S. oneidensis* JG719, which contains deletion in *omcA*; *S. oneidensis* JG731, which contains deletion in *mtrC*; *S. oneidensis* JG635, which contains deletion in *mtrF*; *S. oneidensis* JG749, which contains deletions in *omcA* and *mtrC*; *S. oneidensis* JG641, which contains deletions in *omcA* and *mtrF*; *S. oneidensis* JG636, which contains deletions in *mtrC* and *mtrF*; *S. oneidensis* JG596, which contains deletions in *omcA*, *mtrC* and *mtrF*; *S. oneidensis* JG1176, which contains deletions in the OMCs *omcA*, *mtrC* and *mtrF*, the PECs *mtrA*, *mtrD*, *dmsE* and *so4360* and the periplasmic tetraheme cytochrome *c cctA*; and *S. oneidensis* BG148, which contains a transposon insertion in *ccmC* – a heme exporter protein C involved in the maturation of cytochrome *c*.

The mutants *S. oneidensis* JG719, JG731, JG635, JG749, JG641, JG636 and JG596 were generated for the study by Coursolle and Gralnick (2010), *S. oneidensis* JG1176 was created for the study by Coursolle and Gralnick (2012), and *S. oneidensis* BG148 was revealed in the study by Bouhenni et al. (2005). *E. coli* BL21(DE3) was purchased from New England Biolabs (Hitchin, UK), *S. oneidensis* MR-1 from the American Type Culture Collection (ATCC®) repository (Manassas, VA), the JG strains were kindly provided by Professor Jeffrey A. Gralnick from the University of Minnesota, and BG148 was kindly provided by Dr. Matthew J. Marshall from the Pacific Northwest National Laboratory.

In order to facilitate the reading process, *Escherichia coli* BL21(DE3) was renamed to BL21(DE3), *Shewanella oneidensis* MR-1 ATCC® 700550™ to MR-1 and the mutants were renamed according to the number (single mutant - Sm, double mutant - Dm, triple mutant - Tm, and multiple mutant - Mm) and type (last letter of the cytochrome deleted) of deletions. Therefore, JG719 becomes SmA, JG731 becomes SmC, JG635 becomes SmF, JG749 becomes DmAC, JG641

becomes DmAF, JG636 becomes DmCF and JG596 becomes TmACF. Because JG1176 has multiple deletions in OMCs and PECs, it has been renamed to MmOP. Finally, BG148 becomes CcmC<sup>-</sup>.

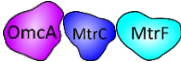
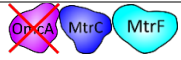
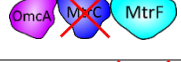
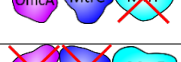
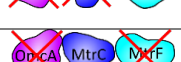
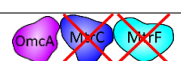
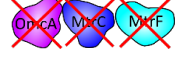
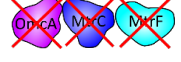
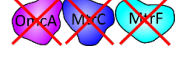

A list of the microbes used together with relevant information about them is detailed in **Table 4.1**. The mutant strains with cytochrome deletions (the JG strains) had their deletions confirmed through DNA sequencing (the results from the sequencings as well as information of the primers used can be found in Chapter 11 – Appendix I).

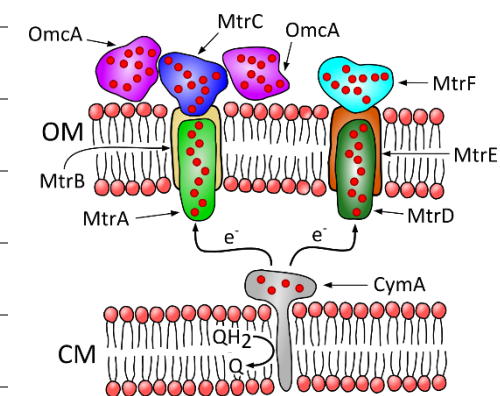
#### 4.1.2 Culture media

In all aerobic experiments bacterial growth was carried out in Luria-Bertani (LB – Fisher Scientific, Fair Lawn, NJ) and M9 minimal medium. LB broth was prepared following the instructions of the manufacturer, dissolving 25 g of the powder in 1 L of deionised (DI) water. LB agar (Fisher Scientific, Fair Lawn, NJ) was prepared by adding 40 g of the mix into 1 L of DI water, again as per the instructions of the manufacturer. M9 medium was made according to the recipe in Sambrook and Russell (2001). First, 5 × M9 was prepared by adding 64 g of Na<sub>2</sub>HPO<sub>4</sub> · 7H<sub>2</sub>O, 15 g KH<sub>2</sub>PO<sub>4</sub>, 5 g NH<sub>4</sub>Cl, 2.5 g NaCl in DI water to a final volume of 1 L. 5 × M9 and solutions of 1 M MgSO<sub>4</sub>, 1 M CaCl<sub>2</sub> and 20 g/L glucose were sterilised separately. M9 medium was then formed by mixing 200 mL of 5 × M9 with 20 mL of glucose solution, 2 mL of 1 M MgSO<sub>4</sub> and 0.1 mL of 1 M CaCl<sub>2</sub>, and completing the mix with sterile DI water to have 980 mL.

The anaerobic growth of *S. oneidensis* wild-type and mutants was carried out using anaerobic LB supplemented with 50 mM anaerobic sodium DL-lactate (≥ 99.0 %. Sigma-Aldrich, St. Louis, MO) as electron donor and 50 mM anaerobic ferric citrate (BioReagent, suitable for cell culture, Sigma-Aldrich, St. Louis, MO) with pH corrected to 7.4 with NaOH (Merck KGaA, Darmstadt, Germany) as electron acceptor. This recipe was adapted from the medium used by Bücking et al. (2012), with slight variations. The differences were the use of DI water at room temperature for dissolving ferric citrate, the use of pellets of NaOH for correcting the pH of ferric citrate solution and the centrifugation of the ferric citrate solution at 4,000 ×g and 4 °C for 10 min after pH correction. The use of

**Table 4.1:** List of bacteria used and relevant information about them. The Mtr pathway on the right side was reproduced from **Figure 3.7**.

Strain	Name adopted in the thesis	Genotypic information	Graphic information of the OMCs present/deleted
<i>Escherichia coli</i> BL21(DE3)	BL21(DE3)	Strain with T7 RNA polymerase controlled by a lacUV5 promoter	Not applicable
<i>Shewanella oneidensis</i> MR-1 ATCC® 700550™	MR-1	wild-type	
<i>S. oneidensis</i> JG719	SmA	$\Delta omcA$	
<i>S. oneidensis</i> JG731	SmC	$\Delta mtrC$	
<i>S. oneidensis</i> JG635	SmF	$\Delta mtrF$	
<i>S. oneidensis</i> JG749	DmAC	$\Delta omcA/\Delta mtrC$	
<i>S. oneidensis</i> JG641	DmAF	$\Delta omcA/\Delta mtrF$	
<i>S. oneidensis</i> JG636	DmCF	$\Delta mtrC/\Delta mtrF$	
<i>S. oneidensis</i> JG596	TmACF	$\Delta omcA/\Delta mtrC/\Delta mtrF$	
<i>S. oneidensis</i> JG1176	MmOP	$\Delta omcA/\Delta mtrC/\Delta mtrF/\Delta mtrA/\Delta mtrD/\Delta dmsE/\Delta so4360/\Delta cctA$	
<i>S. oneidensis</i> BG148	CcmC <sup>-</sup>	$\Delta ccmC$ , strain lacking cytochrome c	



pellets of NaOH was made because a considerable amount of sodium hydroxide is required to raise the pH of 50 mM ferric citrate. The use of water at room temperature and the centrifugation step were necessary to avoid the presence of undissolved ferric citrate in the final growth medium – which would jeopardise the thermogravimetric and the electron microscopy analyses. LB, sodium lactate and ferric citrate solutions were prepared separately in concentrated forms and joined together, after sparging and sterilisation, inside an anaerobic chamber (857-OTA/EXP, Plas Labs, Lansing, MI). For the sparging process, serum bottles containing the solutions were left degassing on a heated hot plate for 10 min with concomitant flushing of oxygen-free nitrogen (OFN); then, sparging of OFN continued for an extra 10 min outside the hot plate, followed by a quick bottle sealing with rubber stoppers and open-top aluminium seals.

Because BG148 has a transposon insertion, and not gene deletion, the culture media used for growing this strain had the addition of 50 µg/mL of kanamycin. Solutions containing gold ions were not added with the antibiotic.

## **4.2 Methods for the microbial synthesis of gold nanoparticles**

Four different methods for the bacterial synthesis of gold nanoparticles were tested. In order to facilitate the understanding of the tests conducted, each method was numbered. The numbers and the descriptions of the methods are given below.

### **4.2.1 Method I**

This method is an adaptation of the protocol used by Suresh et al. (2011) for the synthesis of gold nanoparticles by *S. oneidensis*. The method was used because it is straightforward and because it has been previously proved successful for the biofabrication of AuNPs by one of the strains adopted in the present study. 1 to 3 colonies in LB agar were inoculated in 250-mL shake flasks containing 50 mL LB and the flasks were incubated at 30 °C and 180 rpm for ca.

16 h. After the incubation period, the cultures had grown and reached an optical density at wavelength of 600 nm ( $OD_{600}$  – see details on the measurement of  $OD_{600}$  in section 4.3.1) above 2.5. In order to standardise cell concentration, an amount equivalent to 50 mL of cells at an  $OD_{600}$  of 2.5 was withdrawn to be used in the next steps. The cultures with standard concentration were then centrifuged at 4,000  $\times g$  and 4 °C for 10 min and the pellets were washed twice with sterile DI water (with subsequent centrifugations performed in the same conditions). Next, the pellets were resuspended in 250-mL shake flasks containing 50 mL of 1 mM gold(III) chloride trihydrate ( $H AuCl_4 \cdot 3H_2O$  – Sigma Aldrich, St. Louis, MO) solution and left incubating at 30 °C and 180 rpm for 48 h. Abiotic controls and controls without gold were also tested. In the case without gold, the exact same procedures were applied, with the exception that the cells were resuspended in sterile DI water instead of gold(III) chloride solution; in the abiotic case, 50 mL of 1 mM  $H AuCl_4$  solution in shake flasks were left incubating at the same conditions.

For tests on the capability of autoclaved cells to synthesise gold nanoparticles through method I, a slight variation of the method was made – after growth for ca. 16 h and withdrawal of an amount equivalent to 50 mL of cells at an  $OD_{600}$  of 2.5, the cultures were autoclaved at 121 °C for 15 min. The procedures afterwards remained the same: pellets were washed twice, resuspended in chloroauric acid solution and left incubating for 48 h.

#### **4.2.2 Method II**

Method II was developed to be an anaerobic version of method I. That way, a comparison of the results obtained under aerobic and anaerobic conditions is possible.

1 to 3 colonies in LB agar were inoculated in 10 mL LB in 50-mL centrifuge tubes, which were then incubated under aerobic conditions at 30 °C and 180 rpm for ca. 16 h. After the overnight incubation,  $OD_{600}$  was measured and an amount equivalent to 1 mL of cells at an  $OD_{600}$  of 1 was withdrawn with a syringe to be used in the next steps. The cultures were then injected into serum bottles containing 100 mL of anaerobic LB supplemented with sodium lactate and ferric

citrate and the bottles were left incubating at 30 °C and 180 rpm for 24 h (48 h for the case of DmAC). Because cells growing anaerobically reach a concentration much smaller than cells growing under aerobic conditions, multiple bottles (8 to 10) had to be inoculated for each of the three independent replicates. The bottles with anaerobically grown cultures were inserted into the anaerobic chamber and the contents were transferred into autoclaved KIMAX® heavy duty borosilicate glass centrifuge tubes (Kimble Chase Life Science and Research Products, Vineland, NJ). In order to allow centrifugation under anaerobic conditions, the tubes were closed with autoclaved screw caps, removed from the chamber and put to centrifuge at 3,000 ×g and 4 °C for 20 min. After centrifugation, the tubes were re-inserted into the anaerobic chamber, supernatants were discarded and the pellets that belong to the same replicate were joined together into a single centrifuge tube. The unified pellet was then resuspended with 50 mL of anaerobic sterile DI water and a sample was collected for OD<sub>600</sub> measurement. The result of the optical density test allowed the calculation of the amount equivalent to 50 mL of cells at an OD<sub>600</sub> of 2.5 to be transferred into another KIMAX® centrifuge tube, which was closed, removed from the chamber and inserted into the centrifuge for a 20-min centrifugation at 3,000 ×g and 4 °C. The tubes returned to the chamber, the supernatants were discarded and the pellets were resuspended (injected) into serum bottles containing 50 mL of anaerobic gold(III) chloride solution at 1 mM. The gold solution was made anaerobic by the injection of concentrated (100 mM) HAuCl<sub>4</sub> into anaerobic sterile DI water. The resuspended cultures were then removed from the chamber and left incubating at 30 °C and 180 rpm for 48 h. Abiotic controls (50 mL of anaerobic 1 mM HAuCl<sub>4</sub> solution left incubating at 30 °C and 180 rpm for 48 h) and controls without gold (cells incubated in anaerobic sterile DI water) were also tested.

### **4.2.3 Method III**

This method was developed to test if AuNPs can be biofabricated by cells growing anaerobically in culture medium containing non-lethal concentrations of gold(III) chloride. 1 to 3 colonies from LB agar were inoculated in 50-mL

centrifuge tubes containing 10 mL LB and were incubated under aerobic conditions for around 16 h at 30 °C and 180 rpm. The overnight cultures had their OD<sub>600</sub> measured and an amount equivalent to 500 µL of cells at an OD<sub>600</sub> of 1.25 was withdrawn and added into serum bottles containing 50 mL anaerobic LB with 0.1 mM or 0.01 mM of H<sub>2</sub>AuCl<sub>4</sub>. LB was made anaerobic through the sparging process described in section 4.1.2 and concentrated gold(III) chloride solution (100 mM) was later added into the anaerobic LB to reach the desired concentration. After the inoculation, the bottles were incubated at 30 °C and 180 rpm for 48 h. Abiotic controls and controls without gold ions (only bacteria in anaerobic LB) were also analysed.

#### 4.2.4 Method IV

Method IV is a variation of method I and was developed to check whether it is possible to have biosynthesis of nanoparticles in anaerobic culture medium (LB). 1 to 3 colonies in LB agar were inoculated in 250-mL shake flasks containing 50 mL LB and the flasks were incubated at 30 °C and 180 rpm for ca. 16 h. An amount equivalent to 50 mL of the overnight-grown cells at an OD<sub>600</sub> of 2.5 was withdrawn and the cultures were centrifuged at 4,000 ×g and 4 °C for 10 min. The pellets were washed twice with sterile DI water, resuspended in serum bottles containing 50 mL of anaerobic LB and were left incubating at 30 °C and 180 rpm for 24 h to allow them to become fully anaerobic. After the incubation period, concentrated (100 mM) chloroauric acid solution was added in an amount to reach a final concentration of 1 mM H<sub>2</sub>AuCl<sub>4</sub> and the cultures were incubated at 30 °C and 180 rpm for 48 h. Abiotic controls were also analysed.

Comparative information on parameters adopted in methods I to IV can be found in **Table 4.2**.

**Table 4.2:** Comparison of different parameters adopted in methods I to IV.

Method	Growth of overnight cultures
I	Aerobically, in 250-mL shake flasks with 50 mL LB
II	Aerobically, in 50-mL centrifuge tubes with 10 mL LB

III	Aerobically, in 50-mL centrifuge tubes with 10 mL LB
IV	Aerobically, in 250-mL shake flasks with 50 mL LB
<b>Amount and concentration of cells used for inoculation in gold(III)</b>	
I	50 mL of aerobic cells at an OD <sub>600</sub> of 2.5
II	50 mL of anaerobic cells at an OD <sub>600</sub> of 2.5
III	500 µL of aerobic cells at an OD <sub>600</sub> of 1.25
IV	50 mL of anaerobic cells at an OD <sub>600</sub> of 2.5
<b>Gold(III) chloride solution used</b>	
I	Aerobic, 50 mL of 1 mM HAuCl <sub>4</sub> in DI water
II	Anaerobic, 50 mL of 1 mM HAuCl <sub>4</sub> in DI water
III	Anaerobic, 50 mL of 0.1 mM and 0.01 mM of HAuCl <sub>4</sub> in LB
IV	Anaerobic, 50 mL of 1 mM HAuCl <sub>4</sub> in LB

## 4.3 Analyses of spectrophotometry

### 4.3.1 Analysis of optical density

Analysis of optical density at wavelength of 600 nm (OD<sub>600</sub>), or turbidity, is adopted to determine total cell mass and, thus, microbial growth. It measures the unscattered light (upon incidence, light is scattered by cells) that passes through a cell suspension (Madigan et al., 2012). For OD<sub>600</sub> analysis samples of 1 mL were added into polystyrol/polystyrene cuvettes (Sarstedt, Numbrecht, Germany) and measurements were conducted in a UV-10 spectrophotometer (Thermo Scientific, Madison, WI) at wavelength of 600 nm. The blank used in every measurement was pure culture medium.

### 4.3.2 Analysis of visible spectra

In accordance with the explanation in section 3.4.1.2, UV-vis spectroscopy – which measures absorption and scattering of ultraviolet and visible light (only visible light was measured in this study) – was employed for the determination of LSPR. UV-10 spectrophotometer and polystyrol/polystyrene cuvettes were used in the assays of visible spectra. Samples were not diluted for



the analyses and tests covered the wavelengths from 400 nm to 800 nm. DI water was used as reference/blank for all tests, with the exception of the measurements in methods III and IV, where LB was used as a blank.

In the cases where the surface plasmon bands generated by different strains were set for comparison, baseline corrections were carried out. The corrections were made with the OriginPro software.

#### **4.4 Adsorption of gold ions from solution**

In order to quantify the amount of gold ions that were adsorbed and/or absorbed from the solution by the bacteria, atomic absorption spectroscopy (AAS) was employed. AAS works based on the principle that an external light of a specific frequency excites a ground-state electron of an analyte atom (gold in this case) to an upper-energy-level state (Sanz-Medel and Pereiro, 2014).

For the analysis, 5-mL samples were collected 15 min, 4 h, 8 h, 24 h, 32 h and 48 h after the resuspension of the cells in chloroauric acid solution and were centrifuged at 4,000 ×g and 4 °C for 10 min. The pellets were discarded and the supernatants were further ultracentrifuged (Optima™ MAX-XP with MLS-50 swinging-bucket rotor, Beckman Coulter, Indianapolis, IN) at 200,000 ×g and 4 °C for 2 h to settle AuNPs and any remaining cells in solution. 1 % of nitric acid (69 % concentration) was added into the supernatants of the ultracentrifugation and these were then analysed with an atomic absorption spectrometer (AAAnalyst 400, PerkinElmer®, Shelton, CT) containing a gold (Au) hollow cathode lamp (Lumina™, PerkinElmer®) and operated by the software WinLab 32™ for AA. The measurements of time 0 h corresponded to gold(III) chloride solution before the resuspension of the cells. Abiotic controls were also carried out.

## **4.5 Analyses adopting electron microscopy**

### **4.5.1 Transmission electron microscopy**

TEM analyses were performed to visualise samples in high magnification and determine size and shape of the nanoparticles. For preparation of the specimen, 10  $\mu\text{L}$  of undiluted sample were added onto plasma-treated (glow-discharged) carbon grid. It was left adsorbing on the grids for 2 min before blotting with filter paper. Then, excess sample was removed through mild vacuum suction. Stain was not added because it has been observed that staining compromises the visualisation of smaller nanoparticles. Examination was made with a TEM (CM100, Philips, Eindhoven, NL) operating at 100 kV and images were recorded on a CCD camera (Gatan Multiscan 794 1k x 1k). This is not a high-resolution microscope, therefore it is possible that nanoparticles of minimal size were not detected by the equipment. However, AuNPs with diameter as small as 1 nm were visualised with the microscope. Hence, it is reasonable to consider 1 nm as the lower limit of the equipment.

### **4.5.2 Selected-area electron diffraction**

Selected-area electron diffraction (SAED) measurements were performed to obtain crystallographic information of the sample based on (as explained in section 3.4.1.2) the interference pattern created by the crystal lattice upon incidence of a beam of electrons. The assay was carried out in another TEM (CM200, Philips, Eindhoven, NL) also at 100 kV. For the analysis, the selected area aperture was inserted into the beam path and the operation of the microscope was switched to diffraction mode.

### **4.5.3 Energy dispersive X-ray spectroscopy**

Energy dispersive X-ray spectroscopy (EDS) was employed for elemental analysis. As detailed in section 3.4.1.2, the analysis is performed by a detector – attached to an electron microscope – that identifies the elements from the energies of the X-rays released by atoms ionised by the primary electron beam.

EDS measurements were made with a JED-2300T EDS system (JEOL Ltd., Tokyo, JP) coupled to a TEM (JEM-F200, JEOL Ltd., Tokyo, JP) operating at 200 kV.

#### 4.5.4 Determining sizes and shapes

The images from the TEM analyses were used for determining the sizes and shapes of the nanoparticles. In order to obtain a statistically valid comparison between the AuNPs synthesised by the different strains, three independent replicates were analysed under the TEM and around 10 images were taken for each replicate.

Equally important for statistical analysis was the random selection of the nanoparticles to have the sizes and the shapes determined. The method consisted in first drawing grids with 10 x 10 squares of equal size to all pictures generated by the TEM. A representation of a TEM image with a grid drawn can be found in **Figure 4.1**. Then, one of the squares was randomly chosen through a random number generator tool (random.org website) set to generate numbers from 1 to 100, and all of the particles contained in the chosen square had their sizes measured and shapes determined.

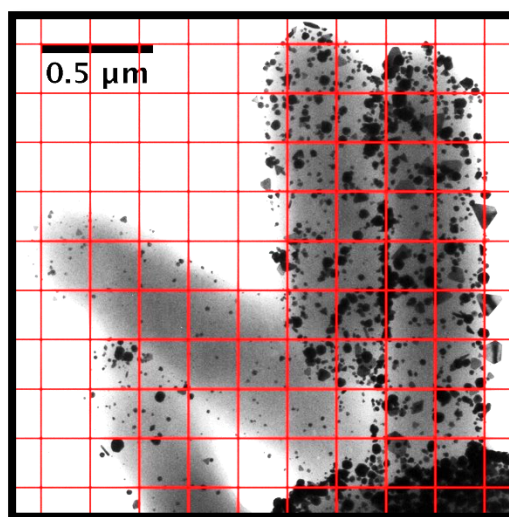


**Figure 4.1:** Example of a TEM picture with a grid of 10 x 10 small squares of equal sizes.

The shapes had to fall within one of six categories: circular, triangular, rectangular, trapezoid, hexagonal and pentagon. Squares were included in the rectangular category. Obviously, not all nanoparticles had shapes with exact geometrical forms. In these cases, their categorisation was made considering the forms they shared the highest similarity. Examples of nanoparticles categorised within the six different shapes are given in **Figure 4.2**.

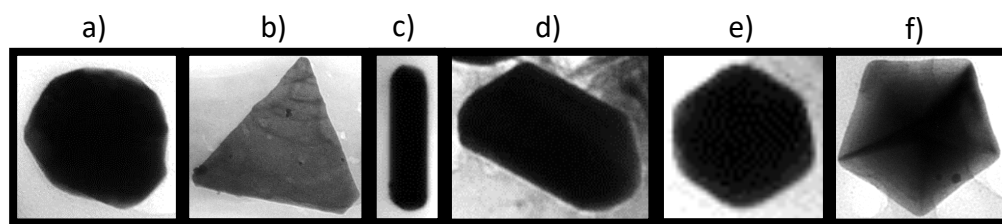


**Figure 4.2:** Images of nanoparticles exemplifying the six categories of shapes adopted in this study. a) circular, b) triangular, c) rectangular, d) trapezoid, e) hexagonal and f) pentagon.

Size measurements were utilised to calculate the frontal area of the nanoparticles. Usually, length is the variable used for comparison – diameter for circular particles and edge length for nanotriangles, for example (Shankar et al., 2004, Wu et al., 2013). However, length allows an accurate comparison only in the cases where shapes of the particles do not vary. Since in this study the particles were categorised into six different shapes, frontal area was found to be the most appropriate variable for comparison.

After counting all the particles within the randomly chosen square in the grid, the same procedures were carried out in another image from the same replicate. This process went on until 100 nanoparticles had their sizes measured and shapes categorised per replicate, making a total of 300 particles counted per strain. ImageJ was the software used for drawing the grids and measuring the sizes.

The number of 300 particles counted per strain was a round up of the result from a power-based sample size calculation (for a power of 95 %), which

yielded 246 particles. The calculation was performed using equation for parallel group trials (equation 4.1).

$$n_A = \frac{2 \left( Z_{1-\beta} + Z_{1-\frac{\alpha}{2}} \right)^2 \sigma^2}{d^2} \quad \text{(eq. 4.1)}$$

Where:

$n_A$  is the sample size.

$Z_{1-\beta}$  and  $Z_{1-\alpha/2}$  are the standardised normal distributions for power and significance.

$\sigma^2$  is the estimated population variance.

$d$  is the effect size (meaningful difference).

$d$  was defined as 5 nm<sup>2</sup>.  $\beta$  and  $\alpha$  were defined as 0.05 and 0.01, therefore  $Z_{1-\beta}$  and  $Z_{1-\alpha/2}$  were found to be 0.842 and 3.38, respectively.  $\sigma^2$  was calculated with a formula for pooled variance (equation 4.2):

$$S_p^2 = \frac{S_1^2(n_1-1) + S_2^2(n_2-1)}{n_1 + n_2 - 2} \quad \text{(eq. 4.2)}$$

Where:

$S_p^2$  is the pooled variance, or  $\sigma^2$  in this case.

$S_i^2$  is the sample variance.

$n_i$  is the sample size of the population.

$S^2$  and  $n$  were determined from preliminary size measurements performed for strains SmA and DmAC. The results of the measurements gave  $S^2$  and  $n$  as 327.6 and 300, respectively, for SmA; and 79.4 and 500, respectively, for DmAC.

To our knowledge, this is the first study applying this method for the statistical comparison of sizes and shapes of nanoparticles. Nevertheless, although innovative and reliable, the method presents some limitations and drawbacks. First, the small and the big particles tend to be counted more often than the medium-sized particles. That is because, for the case of small particles,

these are generally located in close proximity to each other, and, if the randomly chosen square in the grid falls in a region containing several of them, a large amount will be counted. On the other hand, big particles are also counted more often because they cover a larger area of the image, and, thus, have higher probability of being inside a randomly chosen square. Another disadvantage is that as most of the images have areas that are not occupied by nanoparticles, it can take a few attempts in the random number generator to hit a square with particles. Finally, and most importantly, the method has to be performed manually, is labour-intensive and has low-throughput.

#### **4.6 Determining specific productivity of gold nanoparticles**

Thermogravimetric analyses (TGA) were performed to determine specific productivity, i.e. the amount (mg) of particles synthesised per 100 mg of biomass. The assay consisted of monitoring the weight change of a sample while varying its temperature (or maintaining it under isothermal condition) and controlling the atmosphere surrounding it. The equipment specialised for this analysis, the thermogravimetric analyser, is capable of reaching extremely high temperatures and can be connected to a large variety of gas tanks for the atmosphere control.

Productivity was determined based on the concept that a burning process oxidises most of the organic matter in a sample and leaves most of the inorganic contents unreacted. Therefore, theoretically, if bacteria containing gold nanoparticles get burnt, most of the ashes contents will be composed of microbial inorganic matter, adsorbed gold ions and gold nanoparticles. Thus, if the weight of the ashes can be determined, it should be possible to calculate AuNPs productivity.

Unfortunately, previous studies quantifying productivity of metallic nanoparticles through microbial burning seem inexistent. Priestley et al. (2015) innovatively burnt bacterial cells with TGA, but the aim of the analysis was not specifically to determine productivity, but rather to obtain information on the

composition and thermal stability of samples of *E. coli* embedded with graphene oxide and PdNPs. Therefore, since dry ashing of food is a method that focus on determining the contents of inorganic matter from samples that usually contain large amount of organic matter (foodstuff), this method was used as guidance. In brief, the protocol consists of adding 5-10 g of a dry sample into a tared crucible, placing the crucible in a muffle furnace, heating the furnace up to 500-600 °C and maintaining at this temperature for 12-18 h (Marshall, 2010). Finally, the sample is cooled down and the ashes formed are weighed.

The method utilised in the present study had an adaptation to the protocol for food analysis mainly in terms of equipment used – TGA (TGA 4000, PerkinElmer®, Shelton, CT) operated by the software Pyris™ Manager (PerkinElmer®) was used instead of a muffle furnace. The adaptation was made to reduce the amount of sample needed and make the process less labour-intensive, since the TGA is programmable and can perform the drying and the burning steps without human intervention. In addition, it has the advantages of measuring the weight of samples throughout the entire process and of presenting a high resolution, 0.000001 mg.

In order for the calculation of productivity to be made, two types of samples had to be analysed in the TGA: one composed of bacteria with gold nanoparticles and adsorbed gold ions, and one of bacteria without gold ions and particles. The samples without particles were generated from the control experiments in methods I and II. After incubation of the cells in DI water for 48 h, the cultures were centrifuged at 4,000 ×g and 4 °C for 10 min to form pellets that were then ready to be loaded into the TGA. For the cases of microbes containing nanoparticles, after the incubation of the cells in HAuCl<sub>4</sub> for 48 h, the cultures were ultracentrifuged at 200,000 ×g and 4 °C for 2 h to form pellets containing cells with AuNPs and adsorbed gold ions, and nanoparticles that were somehow free in solution. After the ultracentrifugation step the pellets were ready to be added into the TGA.

The thermogravimetric analyser was programmed to heat up the sample from room temperature to 105 °C at 30 °C/min and maintain the temperature for time enough to allow the sample to reach a constant weight (generally 2 h to 4

h). This drying step is carried out with a permanent influx of nitrogen (20 mL/min) to avoid any ignition and oxidation. Next, the instrument switches the gas entering the furnace to oxygen (also 20 mL/min), heat up the sample to 600 °C at 30 °C/min and maintain the temperature for 24 h for the case of samples with nanoparticles and 60 h for samples without nanoparticles. This difference in isothermal time occurred because the generation of ashes from bacteria is a process that takes a long time to reach completion (or, at least, weight stabilisation), and for the cases of samples with particles it has been found that the contribution of the gold ions and AuNPs to the final weight of the ashes was considerably higher than that of the inorganic matter from bacteria. Therefore, it took less time for the samples to reach a constant weight – see examples of real measurements in **Figure 12.1**.

A schematic illustration of the method as well as the formulas used for the calculation can be found below, in **Figure 4.3**. The amounts of (A), (B), (C) and (D) in **Figure 4.3** are obtained experimentally. (G), which is the sum of gold ions and gold nanoparticles, can thus be determined. It is important to clarify that, although they represent the same thing, the quantities of (A) and (B) are not the same as those of (E) and (F). That is because the amount of cells added into the TGA varied from sample to sample.

It is assumed, for calculation purposes, that (for a given strain) the percentage of bacterial inorganic matter is the same regardless of the presence or absence of gold ions and gold nanoparticles. This percentage of inorganic matter is defined as (H) and is presented in equation 4.5:

## 4.7 Cell viability assays

Cell viability assays were conducted mainly to determine if gold(III) chloride solution (1 mM) is lethal to cells. Two different assays were carried out, both from commercial kits. One is the LIVE/DEAD® *BacLight*™ bacterial viability kit (L7007) (Molecular Probes Europe BV, Leiden, The Netherlands) and the other





For LIVE/DEAD® analyses, 1-mL samples were collected at three different stages of method I. The first was after overnight growth of cells in LB, the second was at the end of the washing steps with sterile DI water and the third was after the cells were resuspended and left incubating in chloroauric acid solution for approximately 30 min. The samples were centrifuged at 10,000 ×g for 10 min, the supernatants were discarded and the pellets were resuspended in 2 mL of sterile 0.85 % NaCl (saline) solution. 1 mL of the resuspended pellets were then diluted in 20-mL saline solutions and the diluted samples were left incubating for 1 h at room temperature under gentle mixing conditions in a rocker. In the meantime, equal amounts of components A (containing 1.67 mM of SYTO 9 dye and 1.67 mM of propidium iodide in DMSO) and B (containing 1.67 mM of SYTO 9 dye and 18.3 mM of propidium iodide in DMSO) of the kit were mixed in a separate tube. The samples were then centrifuged at 10,000 ×g for 10 min and the pellets were resuspended in 10 mL saline solution. Then, 0.5 µL of the mix of components A and B was added into 200 µL of the resuspended pellets, followed by a 15-min incubation in the dark before microscopy analysis. Images were obtained using an inverted widefield epifluorescent Leica microscope DM IRB (Leica Microsystems Wetzlar GmbH, Wetzlar, Germany) with an ORCA-ER CCD digital camera (Hamamatsu Photonics K.K., Hamamatsu City, Japan), and image analysis was performed using Openlab 4.0.2 software (Improvision, Image Processing & Vision Company Limited, Coventry, England).

For the analyses with PrestoBlue® samples were collected at five different stages of method I. The first collection took place after overnight growth in LB, the second was at the end of the washing steps with sterile DI water, and the third, fourth and fifth were after approximately 30 min, 24 h and 48 h of incubation in chloroauric acid solution, respectively. In order to evaluate if cells are being inactivated by gold ions or by the low pH of the solution, the same procedures were carried out in samples that were resuspended and incubated in sterile DI water with the pH lowered to 3.17 (the same pH of 1 mM H<sub>2</sub>AuCl<sub>4</sub> solution) with HCl. The samples (200 µL) were centrifuged at 4,000 ×g for 10 min and the pellets were resuspended in 200 µL of sterile phosphate-buffered saline (PBS) solutions. 180 µL of the resuspended samples were added on top of and

mixed up with 20  $\mu\text{L}$  of the viability reagent (resazurin) in the wells of 96-well plates. Wells containing only 180  $\mu\text{L}$  of PBS buffer and 20  $\mu\text{L}$  of the reagent were also measured to be used as reference (blank) for the calculations. The plates were left incubating at 30 °C and 180 rpm for 24 h. After 1 h, 6 h and 24 h of incubation, fluorescence readings were made with a plate reader (Genios-Basic operated by the software Magellan™ – Tecan, Grödig, AT) at excitation and emission wavelengths of 530 nm and 610 nm, respectively. Measurements at time zero (right after resazurin was added) were not conducted because the protocol requires an incubation time of 10 min to 2 h for a reliable fluorescence reading.

#### **4.8 Minimum inhibitory concentration**

Minimum inhibitory concentration (MIC) experiments were conducted to determine the inhibitory profile of  $\text{HAuCl}_4$  towards the bacterial strains within a range of concentrations of gold ions. MIC were also performed in 96-well plates. 200  $\mu\text{L}$  of LB containing different molar concentrations of  $\text{HAuCl}_4$  (1 mM, 0.5 mM, 0.1 mM, 0.05 mM, 0.01 mM and control – only LB) were added to each well; and some wells were inoculated with 2  $\mu\text{L}$  of cultures at an  $\text{OD}_{600}$  adjusted to 1.5 and some wells were not added with bacteria. The plate was left incubating at 30 °C for 48 h with normal agitation (terminology of the equipment) in the plate reader (Genios-Basic, Tecan) and  $\text{OD}_{595}$  measurements were taken every 15 min. The growth curves were built from the values of the readings with cells minus the readings without cells (blank) and the areas under the curves were thus obtained for each sample.

Visible spectra were measured at the end of the MIC experiments to determine if gold nanoparticles were synthesised. For the assays, the samples of 200  $\mu\text{L}$  had to be diluted in 800  $\mu\text{L}$  of fresh LB, as 1 mL is the minimum amount required for the analysis. LB was used as blank for the measurements.

## **4.9 Statistical analyses**

### **4.9.1 Experiments in chapter 5**

Independent t-test with two-tailed significance was adopted for the comparison between the peaks of the normalised surface plasmon bands generated by BL21(DE3) and MR-1 and for specific productivity. For the cases of measurements of frontal area of nanoparticles, Mann-Whitney test was adopted because the dependent variables were not normally distributed. The analysis of the data on the categorisation of the particles into six different shapes was carried out with a Pearson's chi-squared test. The significance level considered was 0.05.

### **4.9.2 Experiments in chapter 6**

One-way ANOVA followed by Tukey were the tests applied for comparing the 48-h peaks of the normalised surface plasmon bands and specific productivity. These methods were chosen because the assumptions of normal distribution on the residuals were met and the variances were assumed to be equal (Levene's tests were not significant). Exceptionally for the case of specific productivity under aerobic conditions it was not possible to conduct Levene's test because two independent replicates were analysed.

For the cases of measurements of frontal area of nanoparticles, the Kruskal-Wallis test was adopted because residuals were not normally distributed. Post-hoc analysis was carried out with Mann-Whitney test and Bonferroni correction was applied for adjustments to multiple tests.

The analyses of the data on the shapes of particles were carried out with Pearson's chi-squared test. p-value for Fisher's exact test was adopted whenever the chi-squared method was not valid – when the cells had an expected count less than 5.

For the comparisons between aerobic and anaerobic experiments, independent t-test with two-tailed significance was applied in the cases of specific productivity and 48-h peaks of normalised surface plasmon bands, and

Mann-Whitney was adopted in the violin plots – because the data were not normally distributed. In all cases the significance level considered was 0.05.

### **4.9.3 Experiments in chapter 7**

Independent t-tests with two-tailed significance were carried out for the results from the PrestoBlue® assay and minimum inhibitory concentration. The data analysed in the PrestoBlue® experiments were the 24-h measurements after growth in LB vs. all other 24-h measurements, whereas for minimum inhibitory concentration control (only LB) was compared with all other concentrations of H<sub>Au</sub>Cl<sub>4</sub>. Equal or unequal variances were assumed depending on the results from Levene's test for equality of variances. The significance level applied was 0.05.



*1<sup>st</sup>*  
*research*  
*chapter*

*"Should we pay, or should we not pay?"*

*Detecting their hypocrisy, he said to them:*

*"Why do you put me to the test? Bring me a denarius to look at."*

*They brought one, and he said to them:*

*"Whose image and inscription is this?" They said to him: "Caesar's."*

*Jesus then said: "Pay back Caesar's things to Caesar, but God's things to God."*

*And they were amazed at him.*

*Mark 12:15-17*





## 5 Comparing the gold nanoparticles synthesised by *Escherichia coli* and *Shewanella oneidensis*.

---

### 5.1 Abstract

The present chapter compared the gold nanoparticles synthesised under aerobic conditions by *E. coli* BL21(DE3) and *S. oneidensis* MR-1. Method I was implemented for the biofabrication and the comparisons involved amount of gold ions adsorbed from solution, size and shape of the nanoparticles, heights of peaks of surface plasmon bands and specific productivity (amount of gold ions adsorbed + AuNPs produced per 100 mg of dry cells). Overall, both strains responded similarly towards incubation in 1 mM gold solution for 48 h at 30 °C and 180 rpm: both cultures were able to adsorb 80 % of the gold ions in solution within 15 min of reaction and more than 99 % within 24 h, and both presented similar specific productivity, 24.47 mg for BL21(DE3) and 20.6 mg for MR-1. The differences were in the visible spectra generated by the nanoparticles and the sizes and the shapes of the particles – with MR-1 producing a significantly higher plasmon band, significantly smaller nanoparticles and significantly more round-shaped particles. BL21(DE3), on the other hand, formed significantly more trapezoid and hexagonal nanoparticles. These findings show that if a certain application of biosynthesised AuNPs requires smaller round-shaped particles, then *S. oneidensis* is a more suitable strain for the synthesis process. Likewise, if bigger and multiple-shaped particles are more appropriate, then *E. coli* is a more qualified organism.

### 5.2 Introduction

As demonstrated in section 3.5, *Escherichia coli* and *Shewanella oneidensis* are model strains subject of intense research, where *E. coli* is a model Gram-negative bacterium and *S. oneidensis* is a model strain for anaerobic respiration. Both cells have also been demonstrated to be able to synthesise a

large variety of metallic nanoparticles, including AuNPs, under various conditions – as described in section 3.6.

The study developed in this chapter evaluated and compared the gold nanoparticles fabricated by both strains using method I (see details of the method in section 4.2.1). This method, which describes the synthesis under aerobic conditions, was chosen because it has already been successfully utilised for the biofabrication of gold nanoparticles by MR-1 and because it is a simple method. The comparisons carried out included size and shape of the nanoparticles as well as other aspects of the synthesis process – amount of gold ions adsorbed from solution, specific productivity (amount of gold ions adsorbed + AuNPs produced per 100 mg of dry cells) and the surface plasmon bands generated by the particles.

Overall, the characterisation of the particles and of the synthesis process utilised techniques regularly used for this purpose (e.g. surface plasmon bands and size and shapes of the nanoparticles). However, some techniques had to be modified/improved to allow a more appropriate comparison. That was the case, for example, of the random counting of particles for their categorisation into shapes and for measurement of their sizes, and of specific productivity determined through TGA measurements. They were adapted so that reliable and unbiased statistical comparisons could be possible.

The main purpose of this chapter is to introduce methods for comparing nanoparticles produced by different strains. This comparison should thus facilitate the choice for a strain more suitable for a specific application. For instance, if larger nanoparticles are more useful for a specific catalytic reaction, then the strain that synthesises larger particles should be considered. It is important to note, however, that productivity is one characteristic that does differentiate strains in terms of quality. This means that the strain that produces more particles can be considered the best for making gold nanoparticles.

### 5.3 Results

In order to guarantee reliability of the comparison, it is important that all aspects of the biosynthesis are the same for both bacteria tested. For that reason, OD<sub>600</sub> of the strains was corrected to 2.5 before their resuspension in chloroauric acid solution. However, different microbes with the same OD<sub>600</sub> do not necessarily have the same concentration. That is because differences in physical characteristics of the strains (such as size and shape) affect turbidity of the cultures, and, consequently, scattering measurements. Chapter 13, Appendix III, presents data on the growth characteristics of both strains. As described in section 13.2.1, the concentrations of BL21(DE3) and MR-1 at OD<sub>600</sub> of 2.5 are  $8.30 \times 10^7$  cfu/mL and  $1.05 \times 10^8$  cfu/mL, respectively. Since these concentrations are similar, it was considered reasonable to adopt the same OD<sub>600</sub> for both strains.

Another background information highly relevant for the present chapter is the confirmation that both strains are capable of synthesising gold nanoparticles. This evaluation is presented in Chapter 14, Appendix IV, and it confirmed the biofabrication of AuNPs by the cells.

The pattern of adsorption/absorption of gold ions by BL21(DE3) and MR-1 as well as of the abiotic control is depicted in **Figure 5.1**. This figure reveals that both strains were capable of adsorbing gold ions at similar rates – with more than 80 % of the contents removed from solution within 15 min of reaction and with more than 99 % removed within 24 h. As expected, the abiotic control did not present any reduction in gold ion contents.

The visible spectra generated by both cultures during incubation in gold solution and DI water are shown in **Figure 5.2**. The figure also depicts the spectra and the peaks after baseline corrections. Abiotic control, 1 mM HAuCl<sub>4</sub> solution incubated at 30 °C and 180 rpm for 48 h, can be found in **Figure 12.8**.

Graphs a) and b) of **Figure 5.2** show clear formation of surface plasmon bands with peaks at around 550 nm, indicating synthesis of AuNPs. For the case of *E. coli*, the band started to be visible at the 24 h measurement, and for *S. oneidensis* it started earlier, at the 8-h measurement (see **Figure 12.2** and

**Figure 12.3** for a more accurate observation). As expected, these bands cannot be seen in graphs c) and d) of **Figure 5.2** and in the abiotic spectra depicted in **Figure 12.8**. Interestingly, graphs c) and d) presented a small band of absorption at the region around 410 nm. This band corresponds to the Soret peak of c-type cytochromes in the oxidised form (Pitts et al., 2003, Shi et al., 2006). They are more pronounced in graph d) because *S. oneidensis* is endowed with more of these cytochromes than *E. coli* (39 vs. 7) (Heidelberg et al., 2002).

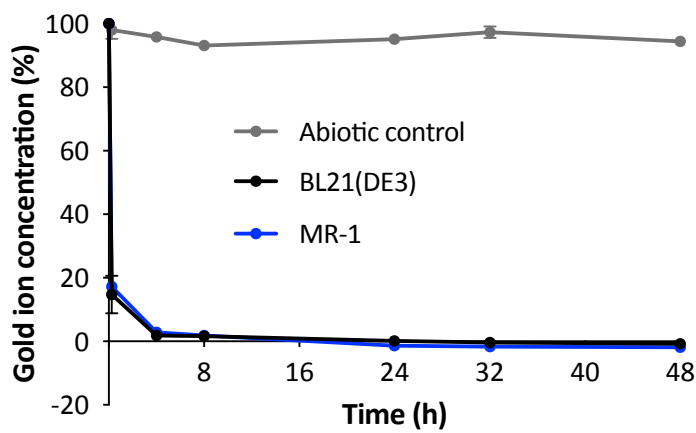


**Figure 5.1:** Bacterial adsorption of gold ions during incubation in 1 mM  $\text{HAuCl}_4$  solution at 30 °C and 180 rpm for 48 h. Error bars indicate the standard deviation of three independent replicates.

When comparing the results in graph a) with those in graph b), it can be noted that, as the time of the experiments increased, the spectra of *S. oneidensis* had an overall shift upwards (it went from 1.34 as the data point for time 0 h at the wavelength of 800 nm to 1.64 for time 48 h at the wavelength of 800 nm), whereas in the case of *E. coli* the spectra shifted downwards (it went from 1.3 as the data point for time 0 h at the wavelength of 800 nm to 1.25 for time 48 h at the wavelength of 800 nm). The shift upwards can be explained by the gain obtained in the spectra from the plasmon bands formed. It can be clearly seen in graph b) that the higher the band, the higher the shift. For the case of the shift downwards, it happened because of cell accumulation in the flasks. *E. coli* biomass accumulated, to a larger extent, on the meniscus line of the flasks (see

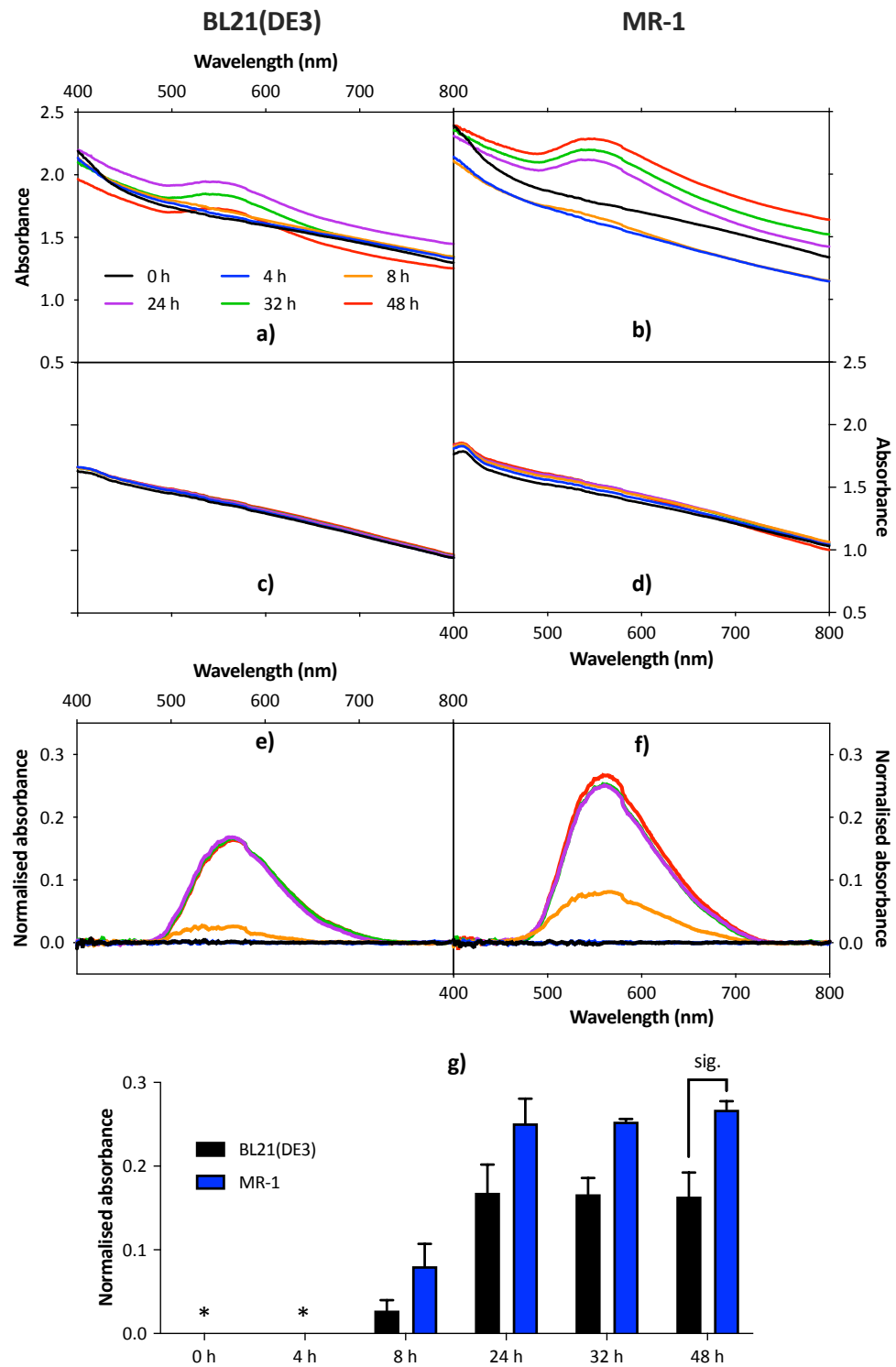


**Figure 5.2:** Visible spectra of BL21(DE3) and MR-1 monitored during the implementation of method I. Graph a) shows the spectra of BL21(DE3) during incubation in HAuCl<sub>4</sub> solution, b) has the spectra of MR-1 during incubation in HAuCl<sub>4</sub> solution, c) shows the spectra of BL21(DE3) during incubation in DI water, and d) has the spectra of MR-1 during incubation in DI water. Graph e) shows the spectra of graph a) after baseline correction

and graph f) has the spectra of graph b) after baseline correction. Graph g) shows the peaks of the curves in graphs e) and f). The asterisk symbol was used for the cases where plasmon bands were not detected, and the connection between the data shows the result of the statistical analysis (only the 48-h measurements were evaluated). Measurements are average of three independent replicates. For clarity of the graphs containing the spectra, error bars were not shown (**Figure 12.2** contains spectra with error bars for graph a), **Figure 12.3** contains spectra for graph b), **Figure 12.4** for graph c), **Figure 12.5** for graph d), **Figure 12.6** for graph e) and **Figure 12.7** for graph f)).

picture a) of **Figure 12.9**) and, to a lower extent, on a film that formed inside the flasks (pictures a) and b) of **Figure 12.9**). In fact, bacterial cells were detected in TEM analyses of the substances accumulated on the meniscus line and on the film (data not shown). Since the microbes did not multiply throughout the incubation in chloroauric acid solution (because of lack of nutrients), the accumulation of biomass on the flasks reduced bacterial concentration in the medium. Hence, because the bacterial culture provides major contribution to the extinction of light in spectrophotometry, lower biomass concentration yielded a spectrum with lower intensity.

The curves of the spectra after baseline correction are depicted in graphs e) and f). Graph g) shows the heights of the peaks of the normalised curves and reveals that the peaks for MR-1 at the 48-h measurement (the only measurement analysed statistically) are significantly higher than the peaks for BL21(DE3). It is important to clarify that although the AuNPs made by MR-1 generated plasmon bands bigger than those made by BL21(DE3), it is not possible to extract much information from these data. In other words, a comparison of plasmon bands in the present case does not allow a conclusion that MR-1 formed more, bigger or different shaped nanoparticles than BL21(DE3). That is because, as explained in section 3.4.1, LSPR is dependent on several variables, including size, shape, particle concentration and proximity towards other nanoparticles. **Figure 3.4** shows that the characteristics of the

plasmon bands can vary considerably for homogeneous particles with minor variation in size. Considering that the particles made by the cells are not homogeneous – because of the large width of the plasmon bands in graphs a) and b) of **Figure 5.2** – it can be expected that the characteristics of the bands will vary even more. Hence, determining characteristics of nanoparticles based on measurements of visible spectra is only possible in cases where the samples contain homogeneous particles with pre-determined sizes and shapes. Yet, in the present case it is possible to qualitatively define, through visible spectra, that there is a significant difference between the gold nanoparticles made by both cells. In order to determine where the differences are – either in size, shape and/or amount of AuNPs produced – the additional comparison methods were developed/applied.

The sizes and shapes of the nanoparticles, as well as TEM images of the cultures, are revealed in **Figure 5.3**. As demonstrated in graphs a) and b) of **Figure 5.3**, MR-1 synthesised smaller nanoparticles than BL21(DE3). In fact, as shown in graph c), the AuNPs made by *S. oneidensis* are significantly smaller than those made by *E. coli*. Interestingly, the majority of the particles (74 out of 300) formed by MR-1 had maximum frontal area of 100 nm<sup>2</sup> (graph b)). The number for BL21(DE3) was considerably lower, 34. On the other hand, the particles from *E. coli* presented higher frequency in all other bins of graph a). A similar trend was seen in the shapes, with MR-1 synthesising 211 round-shaped particles against 152 particles made by BL21(DE3). Yet, it should be noted that round-shaped particles were predominant in both strains. Interestingly, the number of hexagonal nanoparticles synthesised by BL21(DE3) was more than five times higher than for MR-1. Also of note, none of the strains formed pentagon-shaped particles. Altogether, the results in **Figure 5.3** show that BL21(DE3) cells synthesised particles significantly bigger than MR-1. In addition, BL21(DE3) made significantly less round-shaped and significantly more trapezoid and hexagonal-shaped particles than MR-1.

Specific productivity by each strain is revealed in **Figure 5.4**. According to this figure, both cultures presented similar results – 24.47 and 20.6 mg per

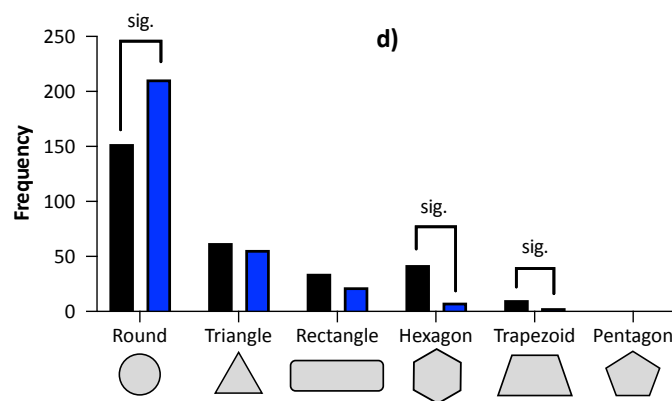
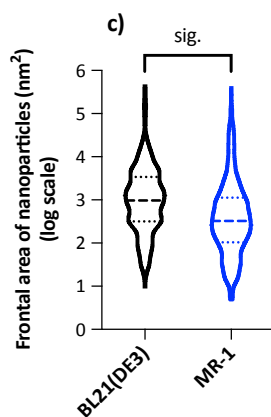
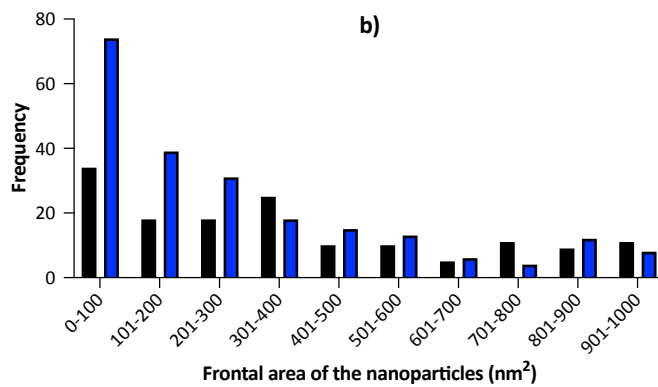
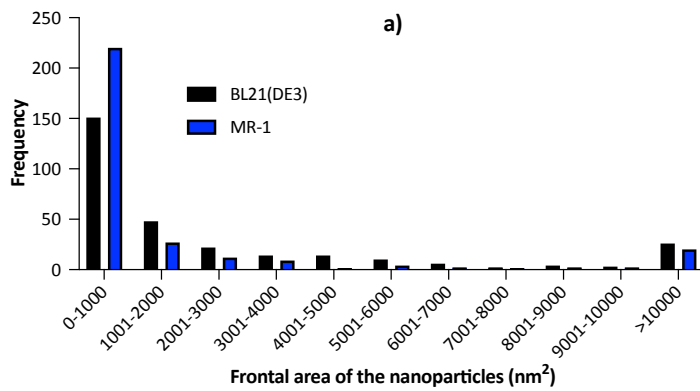
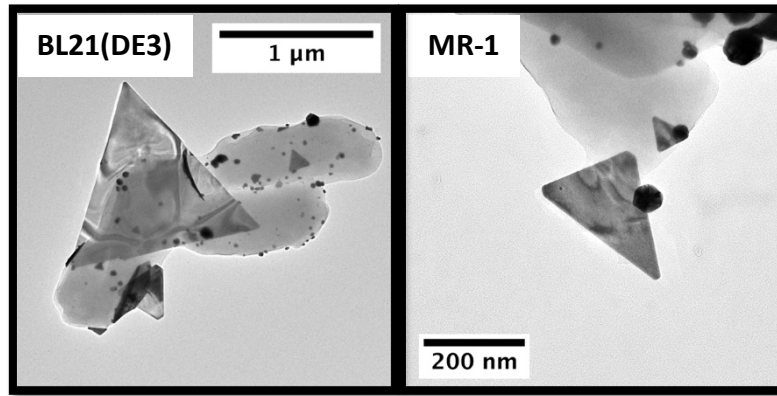


**Figure 5.3:** TEM images and determination of sizes and shapes of the gold nanoparticles synthesised by BL21(DE3) and MR-1 through method I. The



images on top correspond to TEM images of the cultures after incubation in 1 mM HAuCl<sub>4</sub>. For additional images of these cultures as well as of cells after incubation in DI water (control) see **Figure 12.10**. Graph a) contains a histogram of the frontal area of the nanoparticles synthesised by the two cultures. Graph b) contains a histogram with bin range of 0 to 1000 nm<sup>2</sup> and bin width of 100 nm<sup>2</sup>. Both graphs have the same data, but graph b) was built to provide a detailed breakdown of the first bin in graph a), which contained the majority of the particles. Graph c) shows violin plots of the frontal area of the nanoparticles synthesised by both strains. The median and the quartiles are represented by the dashed and dotted lines, respectively. Note that the y-axis is in log scale. Graph d) shows a histogram depicting the categorisation of the nanoparticles according to shape. The connections between the data show the pairs that are significantly different. The results in graphs a) to d) were determined by measuring 300 particles per strain (100 per independent replicate).

100 mg of dry cells of BL21(DE3) and MR-1, respectively. Unfortunately, it is not possible to differentiate the contribution of gold ions and gold nanoparticles to the values of productivity. However, because **Figure 5.1** showed that both strains adsorbed essentially all gold ions in solution, it can be considered that the contribution of gold ions was the same for both cultures. In that case, the amount of gold nanoparticles synthesised should be what differentiates the values of specific productivity in both strains.

## 5.4 Discussion

Method I was found to be an effective method for the synthesis of gold nanoparticles by *E. coli* and *S. oneidensis* – as revealed by the results shown in this chapter and in Chapter 14, Appendix IV. The AuNPs fabricated by both strains were mostly attached to the cells and not released into the solution. Because thin-sections of the cultures were not analysed with electron microscopy, it is not possible to confirm the precise location of the particles

within the cells. However, TEM images in **Figure 5.3** and **Figure 12.10** have shown particles on the surface of the cells and in the periplasmic space (image c) of **Figure 12.10** clearly depicts nanoparticles in the periplasm). These results are in accordance with previous reports that identified the location of biosynthesised gold nanoparticles within the cells of *E. coli* and *S. oneidensis* (Deplanche and Macaskie, 2008, De Corte et al., 2011, Torgeman, 2017). Suresh et al. (2011), whose method was used as reference for method I, intriguingly reported the presence of MR-1-made AuNPs free in solution. The relevance of identifying the location of the particles within the cells lies in the fact that some applications, as catalysis, utilise whole cells embedded with the nanoparticles, and, if the particles are located inside the organisms, they will not be accessible for the reactants.

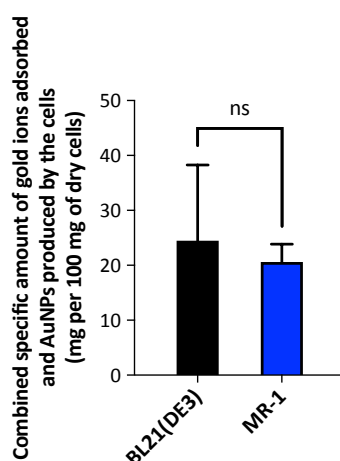


**Figure 5.4:** Specific productivity of gold nanoparticles by BL21(DE3) and MR-1 as determined from TGA measurements. Note that the values determined are a sum of gold ions adsorbed and gold nanoparticles produced. Results are average of two independent replicates. The connection between the data shows the results of the statistical analysis (ns stands for not significant).

Intriguingly, while nanoparticle formation is not a fast process – as can be observed in **Figure 5.2**, adsorption of gold ions was found to be fast (**Figure 5.1**). Although the reason for this difference in kinetics is not entirely clear, De

Corte et al. (2011) have also observed that the synthesis of AuNPs by *S. oneidensis* involved a fast adsorption and slow reduction process. A possible explanation is that the instant interaction of the metallic ions with the cell envelopes is sufficient for an immediate and permanent adsorption, whereas for the formation of nanoparticles reductive biomolecules have to be accessible for the ions – a process which may require active or passive absorption of the ions, pores to be opened on cell walls and/or the cells to lyse (Hoyle and Beveridge, 1984, Ferris and Beveridge, 1986).

A synthesis mechanism can be proposed based on these results and the explanations given in sections 3.4.1.4.1 and 3.4.1.4.3. Upon resuspension of biomass into gold solution, the metallic ions instantly interacted electrostatically with amino, carboxyl and phosphate groups of the cell envelopes. The adsorption was toxic to the cells (more details on the toxicity of gold ions is given in chapter 7) and led to a quick death, potentially caused by an uncontrolled increase in superoxide concentration. The cell walls of the deceased bacteria then allowed gold ions to access the outer layer and periplasmic space of the microbes, with some ions possibly reaching inner parts of the cells. At these locations, the ions encountered the reductive biomolecules, possibly *c*-type cytochromes, hydrogenases, nitrate reductases and/or phosphatases, and the capping agents.

Suresh et al. (2011) found that MR-1 synthesised extracellular AuNPs of spherical shape in the size range of 2 to 50 nm (ca. 3 to 2000 nm<sup>2</sup> of frontal area), with an average size of 12 nm (115 nm<sup>2</sup> of frontal area). Apart from the location of the particles outside the cells, these results share similarities with the results in **Figure 5.3**, which shows prevalence of round-shaped nanoparticles with diameter  $\leq 11$  nm. The study by Du et al. (2007), which also adopted a protocol with similarities to method I, reported that *E. coli* synthesised gold nanoparticles with average diameter of 25 nm (490 nm<sup>2</sup> of frontal area). According to the article, the nanoparticles were mostly spherical, but triangular and quasi-hexagonal particles were also found. Again, these findings are in accordance with the present study because in the case of BL21(DE3) out of 300 particles characterised more than 100 were a combination of triangular and hexagonal particles. Regarding size, graph b) of **Figure 5.3** showed a substantial

frequency of nanoparticles with frontal area in the range from 301 to 400 nm<sup>2</sup> (diameters of ca. 20 to 23 nm), not far from the average reported by Du et al. (2007). Nevertheless, what is most relevant in these comparisons is that the pattern observed in the present study of *S. oneidensis* synthesising more round-shaped and smaller particles than *E. coli* was also evident in these previous studies.

In fact, this pattern was true for other studies employing *E. coli* and *S. oneidensis* for the synthesis of gold nanoparticles. For example, De Corte et al. (2011), Ishiki et al. (2017), Wu and Ng (2017) and Huang et al. (2019) all applied *S. oneidensis* for the synthesis of gold nanoparticles. The sizes of the nanoparticles reported were 5 to 10 nm, 10 nm, 10 to 20 nm, and 15 nm, respectively; and, all studies described the formation of spherical nanoparticles. On the other hand, Deplanche and Macaskie (2008), Niide et al. (2011), Srivastava et al. (2013) and Torgeman (2017) reported the synthesis of AuNPs by *E. coli*. The respective sizes measured were 5 to 50 nm, 4 to 30 nm, 50 nm, and 20 to 80 nm. Regarding shapes, Deplanche and Macaskie (2008) described that the particles were predominantly nanospheres, but nanorods and nanoprisms were occasionally found. Altogether, these previous reports confirm that the same pattern found in the present study (*S. oneidensis* forming smaller and more round-shaped nanoparticles) is observed in the literature.

The comparison of productivity with previous works should not be too accurate, as, to our knowledge, no other study applied TGA measurements for determining productivity of biofabricated gold nanoparticles. Moreover, only a few of the aforementioned studies calculated yield. That was the case, for example, of the article by Wu and Ng (2017). The study determined a productivity of around 60 ppm AuNPs by 0.6 g/L of MR-1 – equivalent to 10 mg of gold nanoparticles per 100 mg of cells. Although the number is lower than the value found in the present study (20.6 mg per 100 mg of dry cells), it should be reinforced that the value in **Figure 5.4** considers the amount of both, adsorbed gold ions and AuNPs. Huang et al. (2019) determined productivity by MR-1 through measurements of OD<sub>530</sub>, which were then converted into yield with a standard curve made from AuNPs prepared chemically. The authors reported a

productivity of 167 ppm by 1.2 g/L of biomass – equivalent to 13.92 mg per 100 mg of cells. Finally, Suresh et al. (2011) synthesised around 174 mg AuNPs from 1 L of *S. oneidensis*. Since the authors did not provide the concentration of MR-1 in 1-L culture, it is not possible to calculate productivity per 100 mg of cells. However, it is possible to adapt the yield for the present case: in the present study 174 mg of AuNPs in 1 L of MR-1 corresponds to 5.8 mg of nanoparticles per 100 mg of dry cells.

Unexpectedly, the results of **Figure 5.4** combined with those of **Figure 5.3** do not give a direct correlation with those of **Figure 5.2**, i.e. the strain with the highest plasmon band (MR-1) produced the smallest particles and had the lowest productivity. As explained in section 3.4.1, size, shape and particle concentration are just a few of the variables capable of influencing LSPR. Therefore, it is possible that another variable – as surface ligand, dielectric constant of the surrounding material and proximity towards other nanoparticles – not measured in the present study is causing this divergence (Eustis and El-Sayed, 2006). Another possible explanation is that since BL21(DE3) synthesised higher amounts of triangular and rectangular-shaped particles, and significantly higher amounts of trapezoid and hexagonal-shaped particles, the combination of the LSPR pattern of each shape could have broadened the plasmon band of BL21(DE3) as a whole (Orendorff et al., 2006). A third, and less likely, possibility is the lower concentration of *E. coli* ( $8.30 \times 10^7$  cfu/mL) applied in the experiments in relation to *S. oneidensis* ( $1.05 \times 10^8$  cfu/mL), which, thus, yielded a smaller plasmon band.

It is important to emphasise that the variation in results by the two strains is not categorising the microbes by quality. As explained in section 3.4.1, the performance of nanoparticles in a specific application vary with changes in the characteristics of the particles. Therefore, each strain should have an application for which it is more effective. Nevertheless, one variable that can be taken as positive in all occasions is productivity. Hence, in that aspect both strains presented equal performance in the synthesis of nanoparticles.

## 5.5 Conclusion

The procedures of resuspending pre-washed aerobically-grown bacterial cells at an OD<sub>600</sub> of 2.5 in 1 mM HAuCl<sub>4</sub> solution and leave them incubating aerobically at 30 °C and 180 rpm for 48 h (a brief description of method I) was found to favour microbial synthesis of gold nanoparticles. Measurements of amount of gold ions adsorbed from solution, surface plasmon bands generated, size and shape of the particles and specific productivity allowed a comparative evaluation of the AuNPs synthesised by BL21(DE3) and MR-1. The analyses determined that *S. oneidensis* formed more round-shaped and smaller particles than *E. coli*. BL21(DE3), on the other hand, fabricated more trapezoid and hexagonal-shaped particles than MR-1. These results reveal that *S. oneidensis* is a better strain in applications where smaller and round-shaped particles are more suitable. Most importantly, this chapter presented a platform for reliably comparing biofabricated nanoparticles – the analyses performed in this study can be easily extended to other scenarios and organisms.

*2<sup>nd</sup>*  
*research*  
*chapter*

*“Why, then, do you look at the straw in your brother’s eye  
but do not notice the rafter in your own eye?”*

*Matthew 7:3*





## 6 Comparing the gold nanoparticles synthesised by *Shewanella oneidensis* wild-type and mutants containing deletions in cytochromes.

---

### 6.1 Abstract

*Shewanella oneidensis* contains a group of proteins and cytochromes, called Mtr pathway, that is specialised in transferring respiratory electrons to solid terminal electron acceptors located outside the cell. The present chapter adopted the analysis platform described in chapter 5 to compare the aerobic and anaerobic synthesis of gold nanoparticles (AuNPs) by *S. oneidensis* wild-type and mutants containing deletions in cytochromes from the Mtr pathway – mainly deletions in outer membrane cytochromes (OMCs). The study evaluated the influence that c-type cytochromes have on the synthesis of AuNPs and the potential that deletion of cytochromes have to improve controllability of the characteristics of the biofabricated particles. The results determined that AuNPs can be formed in the absence of c-type cytochromes, but they were found to be able to directly or indirectly influence the process.

Apart from SmF and DmAC, all aerobic cultures presented a good correlation between the peaks of the normalised bands and the data of size, shape and productivity. For the case of anaerobic cultures less strains were evaluated and SmA and SmC had acceptable and weak correlation, respectively. Under aerobic conditions the results of MR-1 were similar to those of mutants lacking OMCs, indicating negligible expression of OMCs by MR-1. The cytochromes MtrC and MtrF had a similar performance in the synthesis of gold nanoparticles anaerobically, however, under aerobic conditions, MtrF presented higher activity than MtrC. In addition, OmcA and MtrC demonstrated a similar performance under aerobic conditions and developed a synergistic effect when present concomitantly. Interestingly, under anaerobic conditions MtrF was the dominant OMC in the synthesis of AuNPs by SmC (a mutant containing OmcA and MtrF as OMC), but under aerobic conditions OmcA was, in principle, the

main contributor. Also noteworthy, MtrF was found to synergistically interact with OmcA or MtrC to boost productivity under aerobic conditions.

## 6.2 Introduction

Chapter 5 introduced a platform that enabled the statistical comparison of the characteristics of the gold nanoparticles synthesised by two different strains. It also allowed the comparison of relevant variables in the synthesis process, as adsorption of gold ions from solution and specific productivity. Based on the results obtained it was possible to categorise the strains according to the potential application of the bacterial-made nanoparticles. The present chapter adopts the same platform to compare the synthesis of AuNPs by *Shewanella oneidensis* wild-type (MR-1) and mutants containing deletions in cytochromes (SmA, SmC, SmF, DmAC, DmAF, DmCF, TmACF, MmOP and CcmC<sup>-</sup> – **Table 4.1** contains a schematic description of the strains).

As explained in section 3.5.1, *S. oneidensis* is capable of extracellular electron transfer for the anaerobic respiration of a wide range of electron acceptors. This is only possible because this bacterium is endowed with a group of proteins and cytochromes that are specialised in transferring electrons to substrates outside the cell. This set of cellular components, named the Mtr pathway, is composed of an inner membrane tetraheme cytochrome (CymA), periplasmic electron carriers (PECs), transmembrane porins ( $\beta$ -barrel), and outer-membrane cytochromes (OMCs). The mutants tested in this chapter contain deletions mainly in OmCs, but also in PECs.

SmA is a mutant lacking OmcA, SmC has MtrC deleted and SmF has MtrF knocked-out. The three cytochromes, OmcA, MtrC and MtrF, are paralog OMCs, which means that they have the same role and can, theoretically, replace each other (although OmcA and MtrC were found to perform the task of electron transfer concomitantly and synergistically). DmAC lacks OmcA and MtrC, DmAF has deletions of OmcA and MtrF, DmCF had MtrC and MtrF knocked-out and TmACF has the three cytochromes deleted. All these mutants were adopted in

order to test the influence of each OMC in the synthesis process and to determine if it is possible to obtain improved controllability of the process with the deletion of specific cytochromes. MmOP is a strain that lacks all OMCs and all PECs. It was used to verify if further controllability can be achieved with deletion of periplasmic electron carriers. CcmC<sup>-</sup> is a mutant deficient in *c*-type cytochromes because it has a transposon insertion in *ccmC*, which encodes a protein involved in the biogenesis of cytochrome *c*. This cell was employed to test if *c*-type cytochromes are required for making AuNPs.

The study developed in this chapter was carried out to not only categorise the strains according to the potential application of the biosynthesised nanoparticles (which translates into improving controllability of the process), but also to evaluate the influence that components of the Mtr pathway have on the reduction of gold ions (as explained in section 3.5.1, the cytochromes from the Mtr pathway have residues and redox potential favourable for a reductive interaction with gold ions). These assessments were conducted under aerobic and anaerobic conditions (methods I and II, respectively).

## 6.3 Results

The standardisation of OD<sub>600</sub> at 2.5 for the biosynthesis of gold nanoparticles was also adopted in the present chapter. Since growth curves and regression analyses were not carried out for the mutant strains of *S. oneidensis*, their exact concentration at OD<sub>600</sub> of 2.5 was not determined. However, because these strains were all derived from MR-1, it can be assumed that their growth behaviour and physical characteristics are similar to those of the wild-type.

### 6.3.1 Results from the experiments conducted under aerobic conditions (method I)

The pattern of adsorption of gold ions by the different cultures can be found in **Figure 6.1**. Just like the results displayed in **Figure 5.1**, all strains

presented fast and extensive adsorption. All cultures adsorbed more than 60 % of the gold ions in the first 15 min and virtually all gold in solution within 48 h. The bacteria that showed the weakest adsorption pattern were DmAC and DmAF, with the former adsorbing 69 % within 15 min and 98 % within 48 h and the latter adsorbing 64 % in the first measurement and 96 % in the last. Because even the strains with the lowest adsorption presented vast adsorption, it can be inferred that deletion of cytochromes does not affect cellular sorption of gold ions. That is not an unexpected result, because, as explained in section 3.4.1.4.1, the sorption process is likely the result of a passive interaction between the gold ions and molecules in the cell envelopes.

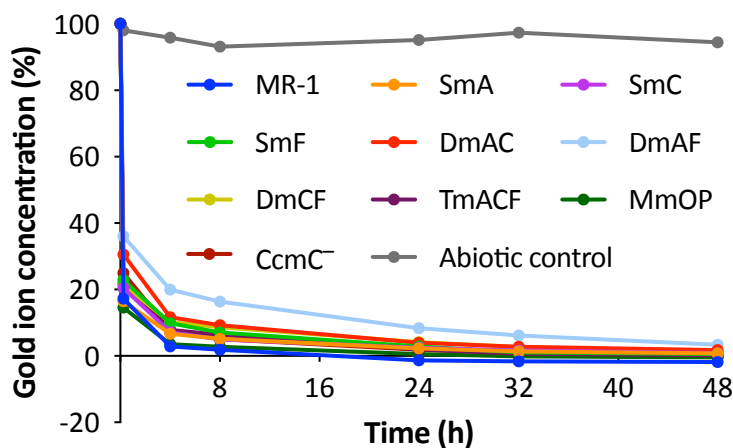


**Figure 6.1:** Bacterial adsorption of gold ions during aerobic incubation in 1 mM HAuCl<sub>4</sub> solution at 30 °C and 180 rpm for 48 h (method I). The data of abiotic control and MR-1 are the same as those of **Figure 5.1**. Results are average of three independent replicates. For clarity of the graph, error bars were not shown (**Figure 12.11** shows the curves with error bars displayed for individual strains).

Spectrophotometry data in the visible spectrum for all strains during aerobic incubation in chloroauric acid can be found in **Figure 6.2**. Spectra of the same strains during aerobic incubation in sterile DI water (controls) can be found in **Figure 12.5** (for MR-1) and **Figure 12.22** to **Figure 12.30** (for the other strains); and spectra of abiotic control are depicted in **Figure 12.8**.

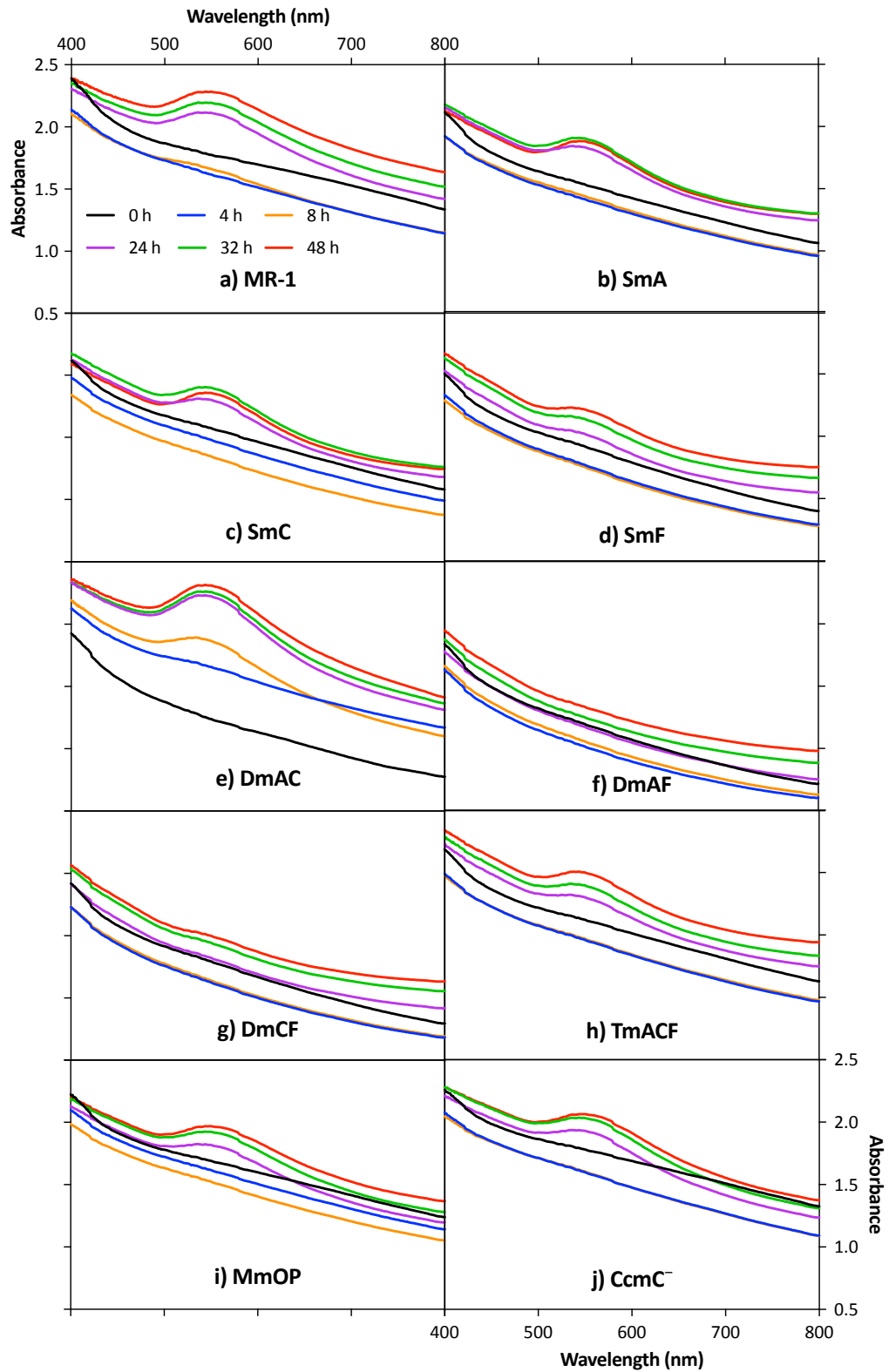


**Figure 6.2:** Visible spectra of the cultures monitored during the implementation of method I (aerobic synthesis of gold nanoparticles). The data of MR-1 are the same as those of graph b) of **Figure 5.2**. Results are average of three independent replicates. For clarity of the graphs, error

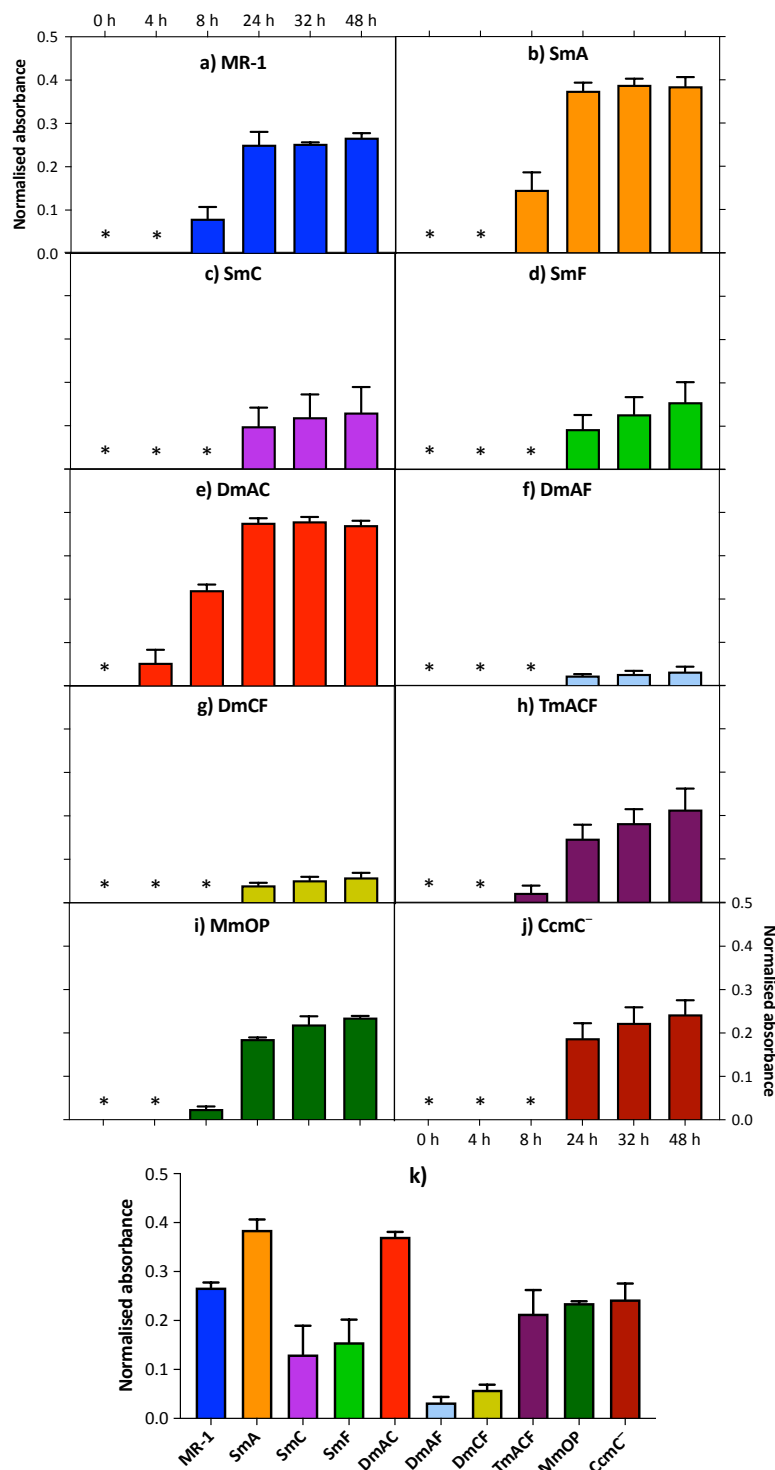
bars were not shown (**Figure 12.12** to **Figure 12.21** show the spectra with error bars).

The data in **Figure 6.2** reveal that the visible spectra presented considerable variation among strains. It means that the cytochromes under investigation influence the synthesis of gold nanoparticles. Another interesting observation was that CcmC<sup>-</sup>, a strain lacking cytochrome *c*, was capable of forming plasmon bands, indicating that cytochrome *c* is not required for the synthesis of AuNPs. It was also possible to note in **Figure 6.2** that some spectra exhibited a rise upwards in the curves as the spectra reached the longest wavelengths – a phenomenon more clearly seen in graphs b), c), d), f), g) and h). Curiously, the phenomenon – likely caused by particle aggregation – was observed more prominently in the strains lacking MtrF (Xu et al., 2018).

In order to have a statistically comparable evaluation of the plasmon bands, the baselines were corrected and the resulting curves can be found in **Figure 12.7** (for MR-1) and **Figure 12.31** to **Figure 12.39** (for the other strains). The peaks of the normalised bands were then transformed into bar graphs, which are shown in **Figure 6.3**.

A noteworthy observation from **Figure 6.3** is that DmAC (a strain containing MtrF as the sole outer membrane cytochrome) was the fastest bacterium to synthesise nanoparticles to a detectable level –it was the only one to present plasmon band at the 4-h measurement. This is an indication of high activity in the synthesis of AuNPs by this cytochrome. On the other hand, the cells expressing only MtrC (DmAF) and OmcA (DmCF) were the ones that displayed the smallest peaks, suggesting a lower activity by these cytochromes.

Overall, the peaks in graph k) can be categorised into four groups, one containing the reference strain (MR-1) and the strains that had peaks with size similar to the reference (intriguingly the three mutants with the lowest number of cytochromes – TmACF, MmOP and CcmC<sup>-</sup>), one with the cultures that presented peaks higher than the reference (SmA and DmAC), one with the strains that displayed peaks at around 0.14 (SmC and SmF) and one with the cells that generated the lowest peaks (DmAF and DmCF).



MR-1 - SmA	MR-1 - SmC	MR-1 - SmF	MR-1 - DmAC	MR-1 - DmAF
MR-1 - DmCF	SmA - SmC	SmA - SmF	SmA - DmAF	SmA - DmCF
SmA - TmACF	SmA - MmOP	SmA - CcmC <sup>-</sup>	SmC - DmAC	SmC - MmOP
SmC - CcmC <sup>-</sup>	SmF - DmAC	SmF - DmAF	SmF - DmCF	DmAC - DmAF
DmAC - DmCF	DmAC - TmACF	DmAC - MmOP	DmAC - CcmC <sup>-</sup>	DmAF - TmACF
DmAF - MmOP	DmAF - CcmC <sup>-</sup>	DmCF - TmACF	DmCF - MmOP	DmCF - CcmC <sup>-</sup>

**Figure 6.3:** Peaks of the normalised surface plasmon bands monitored during the implementation of method I (aerobic synthesis of gold

nanoparticles). The asterisk symbol was used for the cases in which plasmon bands were not detected. Results are average of three independent replicates. Graph k) shows the peaks of the 48-h measurements only. The table presents the pairs in graph k) that are significantly different.

TEM images of each culture after the incubation period in 1 mM HAuCl<sub>4</sub> are displayed in **Figure 6.4**. The images shown in this figure as well as in the figures containing additional images (**Figure 12.10** and **Figure 12.40** to **Figure 12.48**) reveal a diverse range of particles – varying from tiny circular particles, as those in image c) of **Figure 12.41**, to large rods, as the one in image b) of **Figure 12.43**. A careful visual comparison of these TEM pictures does show that differences among the overall characteristics of the particles synthesised by the various strains exist. For example, not all strains synthesised tiny circular particles (as those of image c) of **Figure 12.41**).

The TEM images of CcmC<sup>-</sup> revealed that the particles synthesised by this strain have more irregular shapes than those made the other strains. It is not entirely clear why this culture formed large quantity of particles with uneven surfaces, however it can be hypothesised that the biomolecules involved in the formation of the solid structures have affinity towards crystal face(s) different from the crystal faces that the biomolecules from the other cells have affinity to (Rawlings et al., 2015).

The histograms containing the results for frontal area measurement and shape categorisation can be found in **Figure 6.5** and **Figure 6.6**, respectively. **Figure 6.5** shows clear difference in size of nanoparticles synthesised by the strains tested. It can be observed from the violin plots that the cultures can be categorised into two groups, one which formed a vast majority of small particles, and one which had a more even distribution of sizes. The representatives of the first group are SmC, DmAF and DmCF, and the remaining strains represent the second. Interestingly, the members of the first group were the cells that synthesised the largest particles, as can be seen in the height of the violin plots.



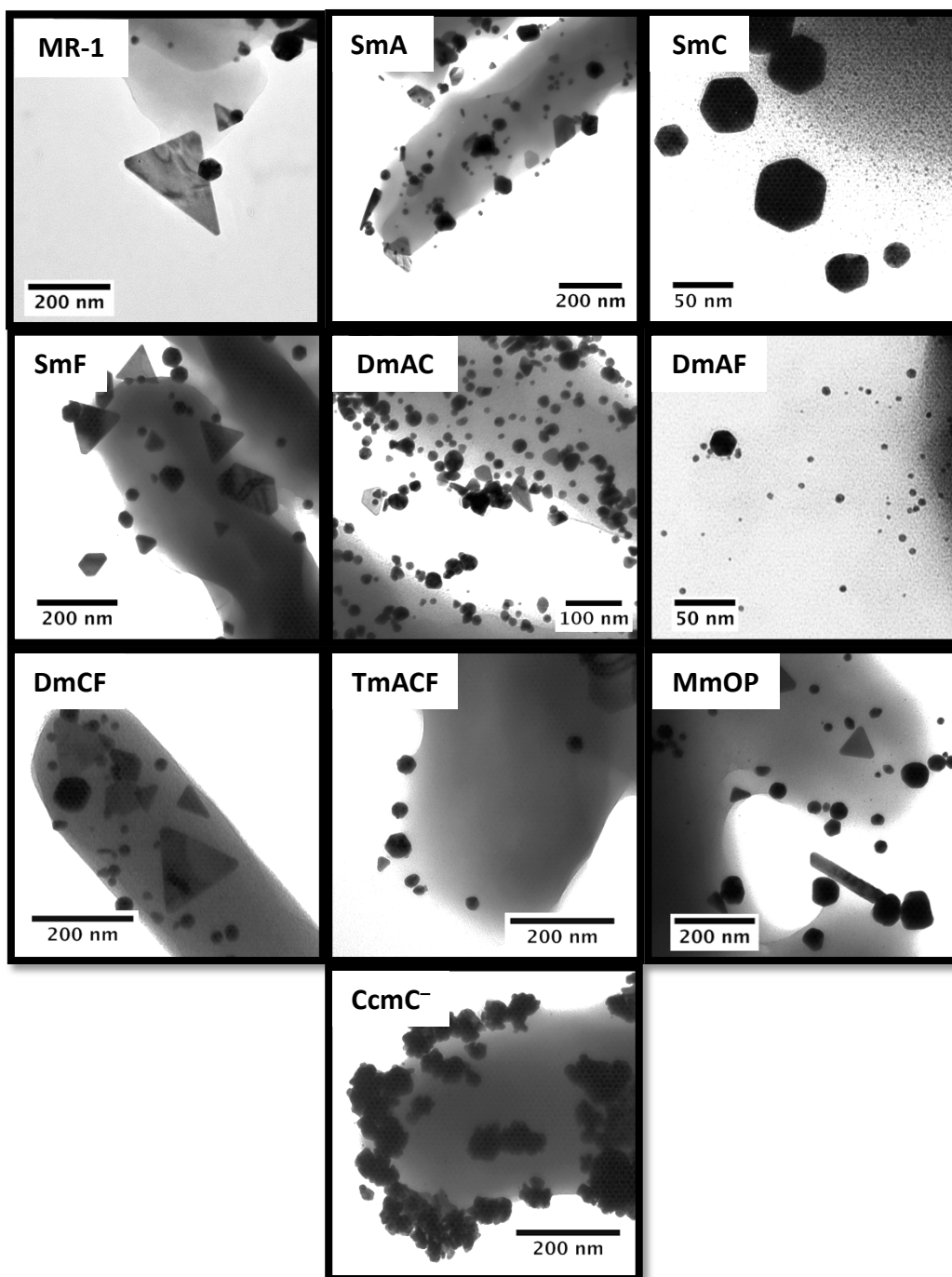
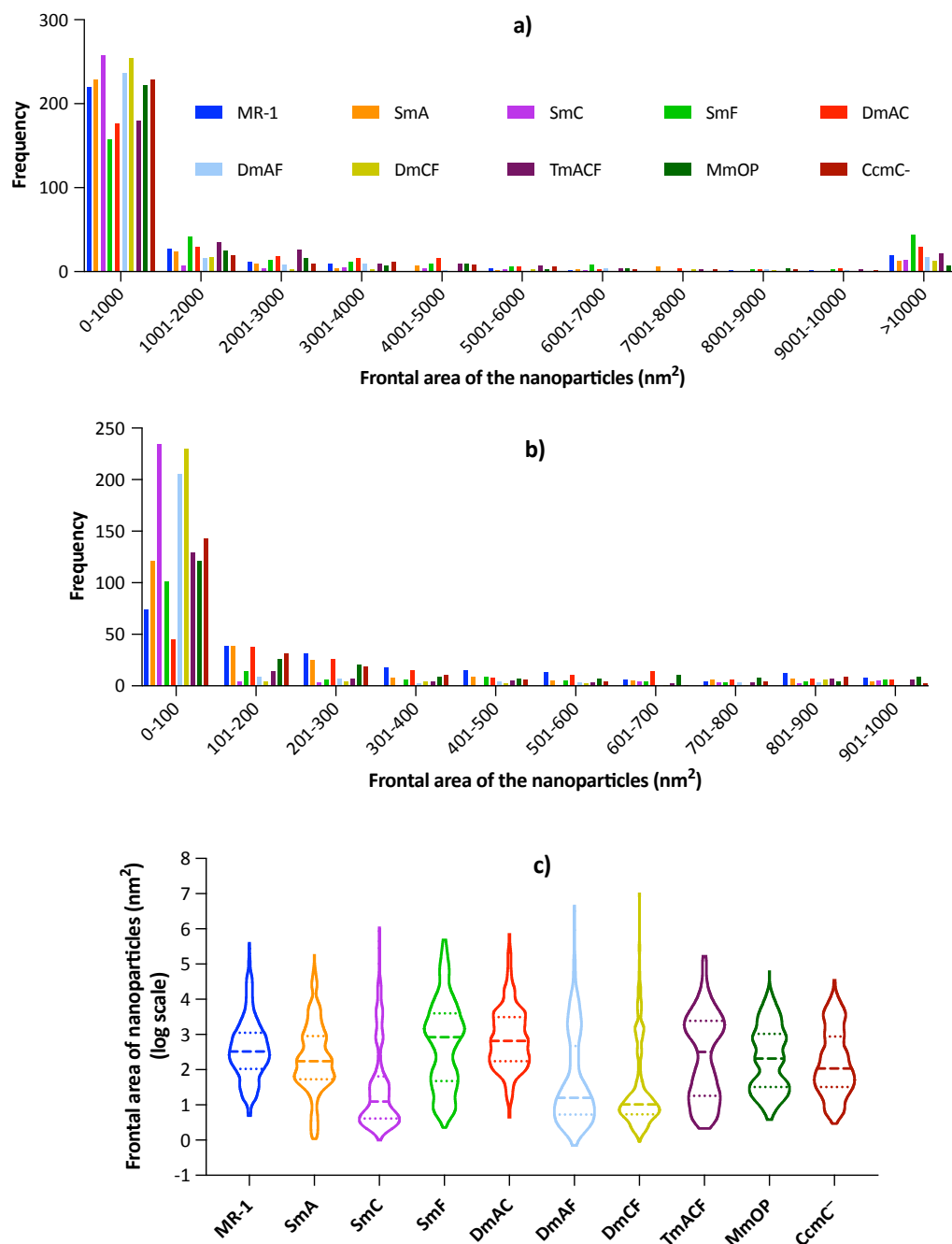


**Figure 6.4:** TEM images of the cultures after implementation of method I (aerobic synthesis of gold nanoparticles). The image of MR-1 is the same as the image in **Figure 5.3**. For additional images of MR-1 see images g), h) and i) of **Figure 12.10**, for the other strains see **Figure 12.40** to **Figure 12.48**.



MR-1 - SmC	MR-1 - DmAF	MR-1 - DmCF	MR-1 - CcmC <sup>-</sup>	SmA - SmC
SmA - SmF	SmA - DmAC	SmA - DmAF	SmA - DmCF	SmC - SmF
SmC - DmAC	SmC - TmACF	SmC - MmOP	SmC - CcmC <sup>-</sup>	SmF - DmAF
SmF - DmCF	SmF - TmACF	SmF - MmOP	SmF - CcmC <sup>-</sup>	DmAC - DmAF
DmAC - DmCF	DmAC - TmACF	DmAC - MmOP	DmAC - CcmC <sup>-</sup>	DmAF - TmACF
DmAF - MmOP	DmAF - CcmC <sup>-</sup>	DmCF - TmACF	DmCF - MmOP	DmCF - CcmC <sup>-</sup>

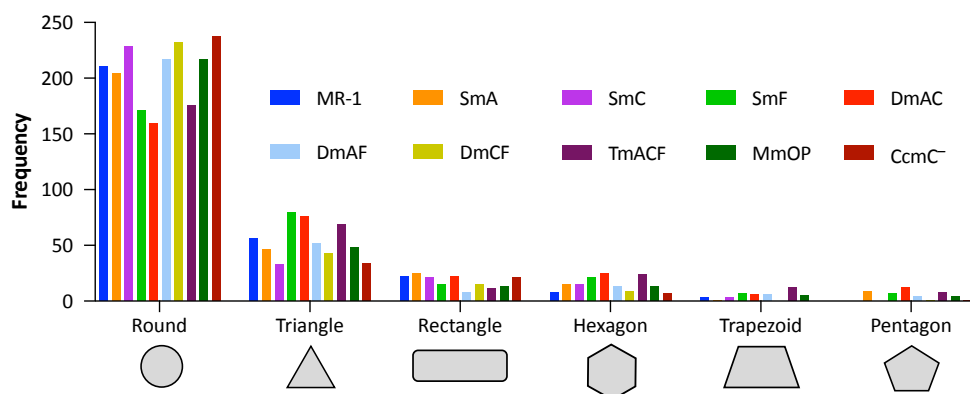
**Figure 6.5:** Frontal area of the gold nanoparticles synthesized through method I. Graph a) contains a histogram of the frontal area of the nanoparticles synthesized by the different cultures. Graph b) contains a histogram with bin range of 0 to 1000 nm<sup>2</sup> and bin width of 100 nm<sup>2</sup>. Both graphs have the same data, but graph b) was built to provide a detailed

breakdown of the first bin in graph a), which contained the majority of the particles. Graph c) shows a violin plot of the frontal area of the nanoparticles synthesised by the strains. The median and the quartiles are represented by the dashed and dotted lines, respectively. Note that the y-axis is in log scale. The data for MR-1 is the same as the data in **Figure 5.3**. The table presents the pairs in graph c) that are significantly different. Results were determined by measuring 300 particles per strain (100 per independent replicate).

It is also interesting to observe that the first bin of graph a) (0 - 1000 nm<sup>2</sup>) shows a similar frequency among MR-1, SmA, SmC, DmAF, DmCF, MmOP and CcmC<sup>-</sup>, however, when looking at bin 0 - 100 nm<sup>2</sup> in graph b) major difference among these strains can be detected, with MR-1, SmA, MmOP and CcmC<sup>-</sup> presenting a substantial reduction in frequency.

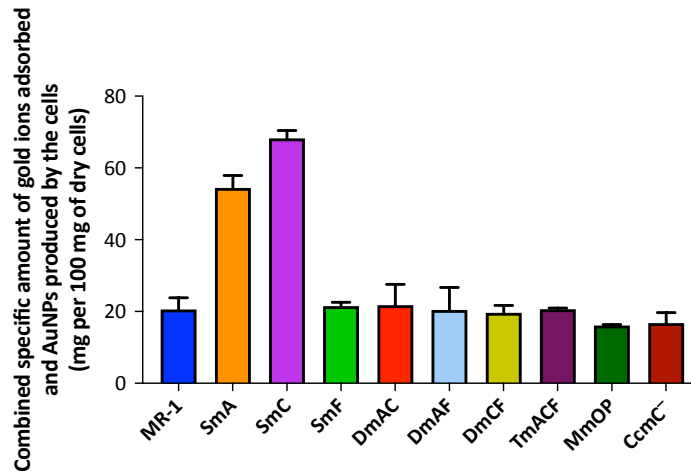
In **Figure 6.6**, although the shapes of the particles presented significant differences among strains, it can be observed that the pattern for all cultures was overall similar. In essence, all strains fabricated considerably more round-shaped particles than the other shapes. In addition, in all cases triangular AuNPs were the second most synthesised particles. The third place varied among cells, but was, essentially, either rectangular or hexagonal NPs. Likewise, fourth place was trapezoid or pentagon particles.

Specific productivity by each strain is reported in **Figure 6.7**. According to this figure, all cultures presented similar productivity in relation to the reference (MR-1), which had a result of 22.9 mg per 100 mg of dry cells – with the notable exceptions of SmA and SmC, whose results were 51.94 mg and 69.81 mg, respectively. Because the adsorption pattern for all strains was similar and all of them have adsorbed virtually all gold ions in solution by 48 h of incubation (**Figure 6.1**), it can be assumed that the contribution of gold ions into the weight was the same for all cultures. Also of note, as explained in chapter 5, productivity is the only variable that categorises the microbes by quality. Therefore, SmA and SmC can be considered as better at synthesising AuNPs than the other strains.



Round				
MR-1 - SmF	MR-1 - DmAC	MR-1 - TmACF	MR-1 - CcmC <sup>-</sup>	SmA - SmC
SmA - SmF	SmA - DmAC	SmA - DmCF	SmA - TmACF	SmA - CcmC <sup>-</sup>
SmC - SmF	SmC - DmAC	SmC - TmACF	SmF - DmAF	SmF - DmCF
SmF - MmOP	SmF - CcmC <sup>-</sup>	DmAC - DmAF	DmAC - DmCF	DmAC - MmOP
DmAC - CcmC <sup>-</sup>	DmAF - TmACF	DmCF - TmACF	TmACF - MmOP	TmACF - CcmC <sup>-</sup>
Triangle				
MR-1 - SmC	MR-1 - SmF	MR-1 - DmAC	MR-1 - CcmC <sup>-</sup>	SmA - SmF
SmA - DmAC	SmA - TmACF	SmC - SmF	SmC - DmAC	SmC - DmAF
SmC - TmACF	SmF - DmAF	SmF - DmCF	SmF - MmOP	SmF - CcmC <sup>-</sup>
DmAC - DmAF	DmAC - DmCF	DmAC - MmOP	DmAC - CcmC <sup>-</sup>	DmAF - CcmC <sup>-</sup>
DmCF - TmACF	TmACF - MmOP	TmACF - CcmC <sup>-</sup>		
Rectangle				
MR-1 - DmAF	MR-1 - TmACF	SmA - DmAF	SmA - TmACF	SmA - MmOP
SmC - DmAF	DmAC - DmAF	DmAC - TmACF	DmAF - CcmC <sup>-</sup>	
Hexagon				
MR-1 - SmF	MR-1 - DmAC	MR-1 - TmACF	SmF - DmCF	SmF - CcmC <sup>-</sup>
DmAC - DmAF	DmAC - DmCF	DmAC - MmOP	DmAC - CcmC <sup>-</sup>	DmCF - TmACF
TmACF - CcmC <sup>-</sup>				
Trapezoid				
MR-1 - TmACF	SmA - TmACF	SmC - TmACF	SmF - DmCF	SmF - CcmC <sup>-</sup>
DmAC - DmCF	DmAC - CcmC <sup>-</sup>	DmAC - DmCF	DmAF - CcmC <sup>-</sup>	DmCF - TmACF
TmACF - CcmC <sup>-</sup>				
Pentagon				
MR-1 - SmA	MR-1 - SmF	MR-1 - DmAC	MR-1 - TmACF	SmA - SmC
SmA - DmCF	SmA - CcmC <sup>-</sup>	SmC - SmF	SmC - DmAC	SmC - TmACF
DmAC - DmAF	DmAC - DmCF	DmAC - MmOP	DmAC - CcmC <sup>-</sup>	DmCF - TmACF
TmACF - CcmC <sup>-</sup>				

**Figure 6.6:** Histogram depicting the categorisation of the gold nanoparticles synthesised through method I according to shape. The data for MR-1 is the same as the data in **Figure 5.3**. The table presents the pairs that are significantly different for each shape. Results were determined by categorising 300 particles per strain (100 per independent replicate).



MR-1 - SmA	MR-1 - SmC	SmA - SmC	SmA - SmF	SmA - DmAC
SmA - DmAF	SmA - DmCF	SmA - TmACF	SmA - MmOP	SmA - CcmC
SmC - SmF	SmC - DmAC	SmC - DmAF	SmC - DmCF	SmC - TmACF
SmC - MmOP	SmC - CcmC			

**Figure 6.7:** Specific productivity of gold nanoparticles by each strain as determined from TGA measurements after the implementation of method I. Note that the values determined are a sum of gold ions adsorbed and gold nanoparticles produced. The data for MR-1 is the same as the data in **Figure 5.4**. Results are average of two independent replicates. The table presents the pairs that are significantly different.

### 6.3.2 Results from the experiments conducted under anaerobic conditions (method II)

Unfortunately, it was not possible to perform comparisons under anaerobic conditions exactly the same as the comparisons carried out under aerobic conditions. That is because, as demonstrated in Chapter 13, Appendix III, not all strains grow with ferric citrate as electron acceptor (only MR-1, SmA, SmC, SmF, DmAC and DmAF). This substrate was chosen for the anaerobic growth because it is a soluble metal that is reduced through the Mtr pathway. An insoluble metal, such as Mn(III, IV) or Fe(III) oxides, could not be adopted because it would likely interfere in the TEM and TGA measurements, as it is not possible to easily separate the cultures from the “rocks” of metal oxides. In addition, according to the results presented in the study by Coursolle and Gralnick (2010), the rate of reduction of insoluble metal oxides is slower than the

rate for soluble metals. Hence, probably less mutants would grow with a metal oxide as electron acceptor.

Also noteworthy, although it would be interesting to have all the experiments performed again under anaerobic conditions, the results from the aerobic tests led us to undertake targeted analyses under no oxygen conditions. For example, **Figure 6.1** has shown that adsorption of gold ions in solution is not influenced by cytochromes; therefore, adsorption experiments were not conducted under anaerobic conditions. In addition, the measurements of visible spectra most relevant were the ones taken at 48 h. Hence, only measurements of 0 h and 48 h were made under anaerobic conditions. Moreover, visible spectra performed with cultures incubated in DI water (controls) have proved that gold ions are mandatory for the formation of plasmon bands. Therefore, controls in DI water were not conducted anaerobically. Finally, the results of specific productivity carried out aerobically have demonstrated that all strains achieved productivity similar to MR-1, with the exception of SmA and SmC. Therefore, specific productivity under anaerobic conditions was analysed only for MR-1, SmA and SmC.

**Figure 6.8** presents the visible spectra of the cultures during implementation of method II. The figure also shows the peaks at 48 h and compares the peaks obtained aerobically with those obtained anaerobically. The spectrophotometry data of the curves after baseline correction and abiotic control can be found in **Figure 12.49** and **Figure 12.50**, respectively.

It can be seen in **Figure 6.8** that all strains generated plasmon bands, indicating that gold nanoparticles can also be fabricated under anaerobic conditions. The peaks shown in graph g) revealed two groups of cultures, one with higher peaks composed by MR-1 and SmA, and one with shorter peaks composed by the remaining strains. Controversially, SmA was the strain with the highest peak in both, aerobic and anaerobic conditions, whereas DmAC produced the second highest peak aerobically and the shortest anaerobically. This result suggests that the performance of MtrF in synthesising (or contributing to the synthesis of) AuNPs is affected by aerobicity. In the case of DmAF, the peak generated under anaerobic conditions was higher than the one determined

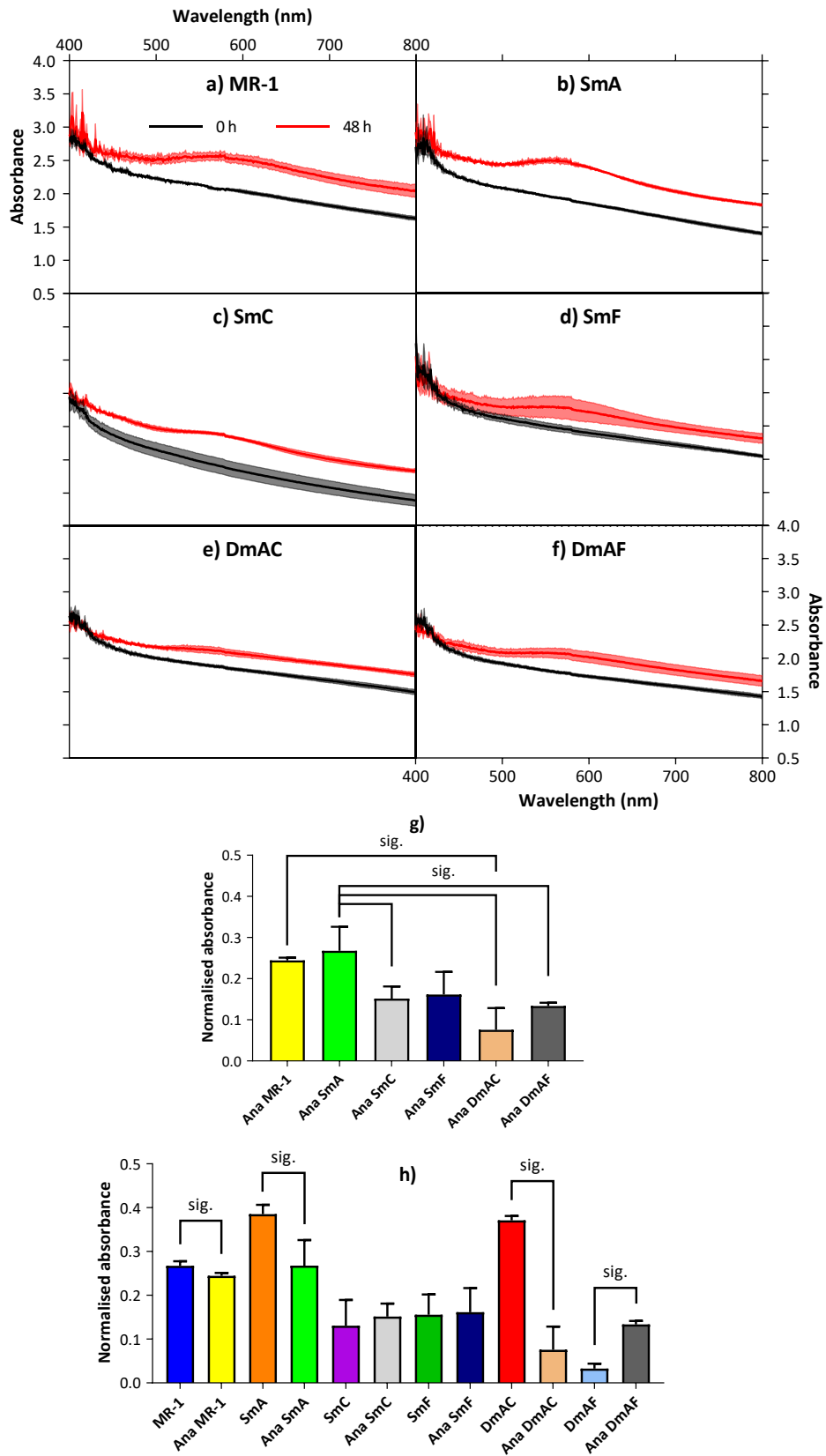


**Figure 6.8:** Visible spectra and peaks of the surface plasmon bands generated by the cultures during the implementation of method II

(anaerobic synthesis of gold nanoparticles). Graphs a) to f) show the visible spectra of the cultures. Results are average of three independent replicates. Some error bars cannot be visualised because they are smaller than the thickness of the curves. Graph g) shows peaks of the normalised plasmon bands at the 48-h measurements. Graph h) shows the peaks at the 48-h measurements comparing the results from the aerobic and anaerobic experiments. The connections between the data present the pairs that are significantly different. Statistical analyses in graph g) evaluated all strains, whereas in graph h) only the same strains (aerobically vs. anaerobically) were analysed.

aerobically, indicating that the role of MtrC in the formation of AuNPs is also influenced by aerobicity. Nevertheless, as previously explained, reliable evaluations cannot be drawn solely on results from spectrophotometry.

TEM images of the cultures after implementation of method II are depicted in **Figure 6.9**. In essence, three groups of nanoparticles stand out from the images. One composed mainly by round-shaped particles with average diameter of 5 nm – this type of particle can be better visualised in image c) of **Figure 12.51**, image a) of **Figure 12.55** and image a) of **Figure 12.56**; another composed by multi-shaped particles with size around 50 nm – representatives of this group can be seen in images a) and b) of **Figure 12.52**, image a) of **Figure 12.54** and images a) and c) of **Figure 12.56**; and, one by large triangular-shaped particles – see these in image b) of **Figure 12.51**, image c) of **Figure 12.52** and image c) of **Figure 12.54**. Interestingly, the three groups of particles were found in the six strains tested. EDS measurements of the images in **Figure 6.9** can be found in **Figure 12.57** to **Figure 12.62**. The EDS analyses confirmed the synthesis of AuNPs by all strains.

The results from the measurements of frontal area of the nanoparticles synthesised under anaerobically are depicted in **Figure 6.10**. Comparisons between the sizes of the AuNPs formed aerobically and anaerobically for each strain are also revealed in this figure. Interestingly, the results displayed in graph c) showed similar shapes of the violin plots for all strains. The shapes of the violin



plots are comparable to the shapes of the first group in **Figure 6.5** (composed by SmC, DmAF and DmCF) – a shape similar to a drop. It appears, thus, that anaerobicity led to an overall convergence of the nanoparticles' pattern in terms of size.

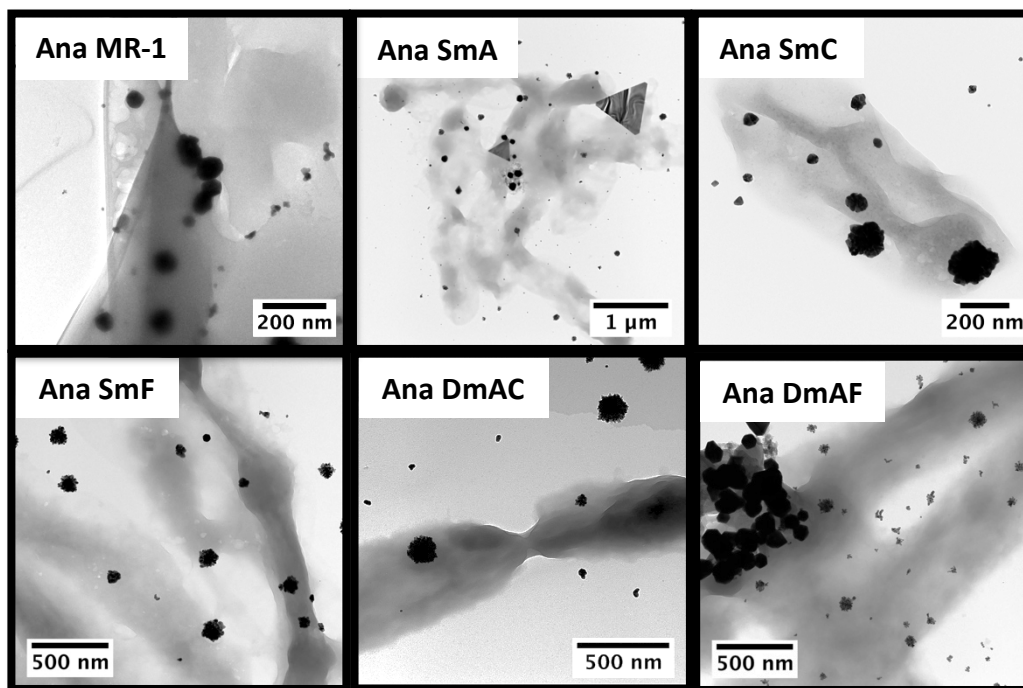
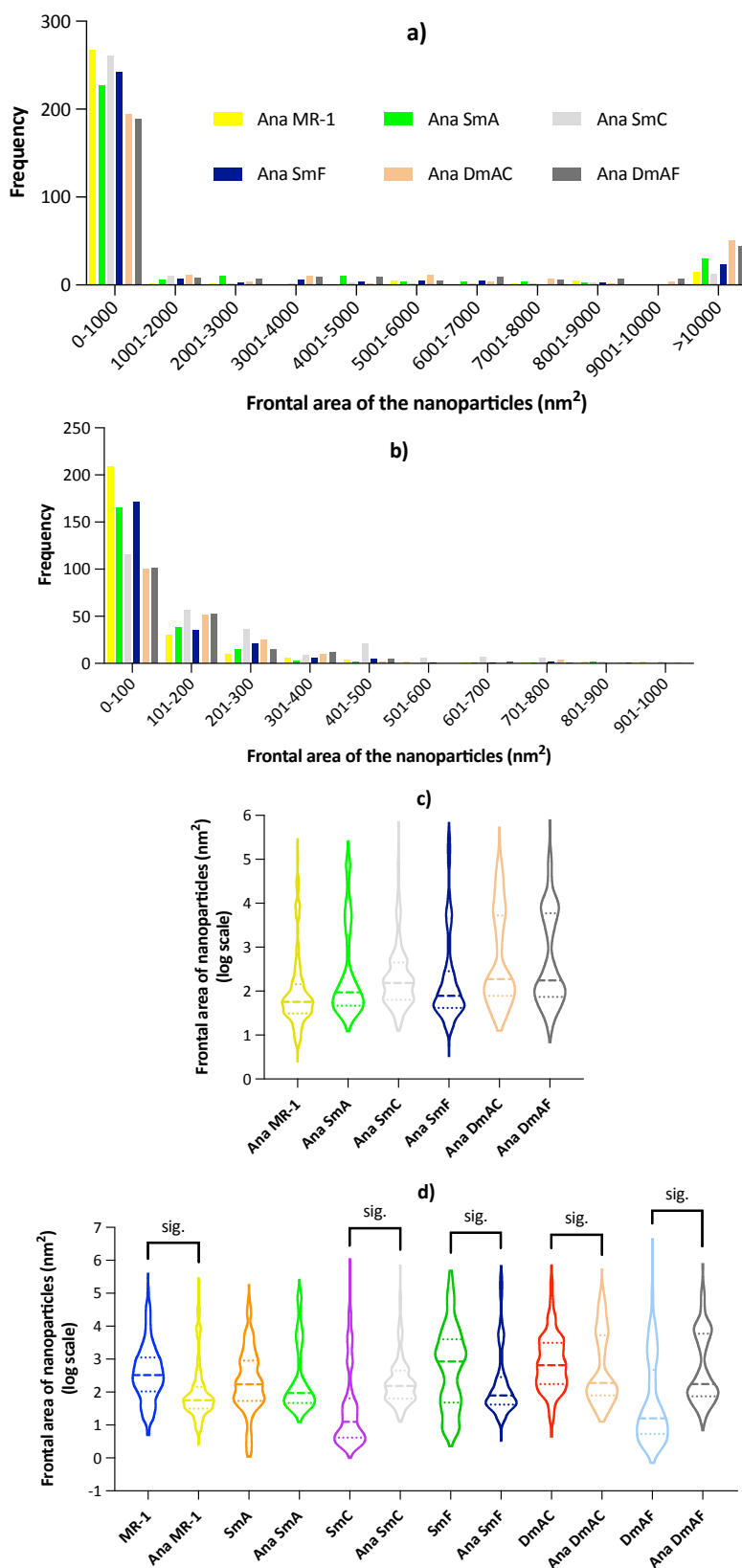


**Figure 6.9:** TEM images of the cultures after implementation of method II (anaerobic synthesis of gold nanoparticles). For additional images see **Figure 12.51** to **Figure 12.56**.

**Figure 6.10** also shows that anaerobic MR-1 fabricated AuNPs significantly smaller than all other strains. This can be better visualised in the first bin of graph b). Interestingly, the double mutants were the strains that formed the highest amount of large particles. It curiously shows that when MtrC and MtrF are the sole OMCs, the resulting AuNPs are significantly larger than the ones synthesised when both cytochromes are present (SmA). Also of note, with the exception of SmA, all cultures presented differences in the sizes of the AuNPs fabricated under aerobic and anaerobic conditions. In some cases (MR-1, SmF and DmAC), the strains formed smaller nanoparticles under anaerobic conditions, whereas in other cases (SmC and DmAF) the particles synthesised



MR-1 - SmA	MR-1 - SmC	MR-1 - SmF	MR-1 - DmAC	MR-1 - DmAF
SmA - DmAC	SmA - DmAF	SmC - SmF	SmF - DmAC	SmF - DmAF

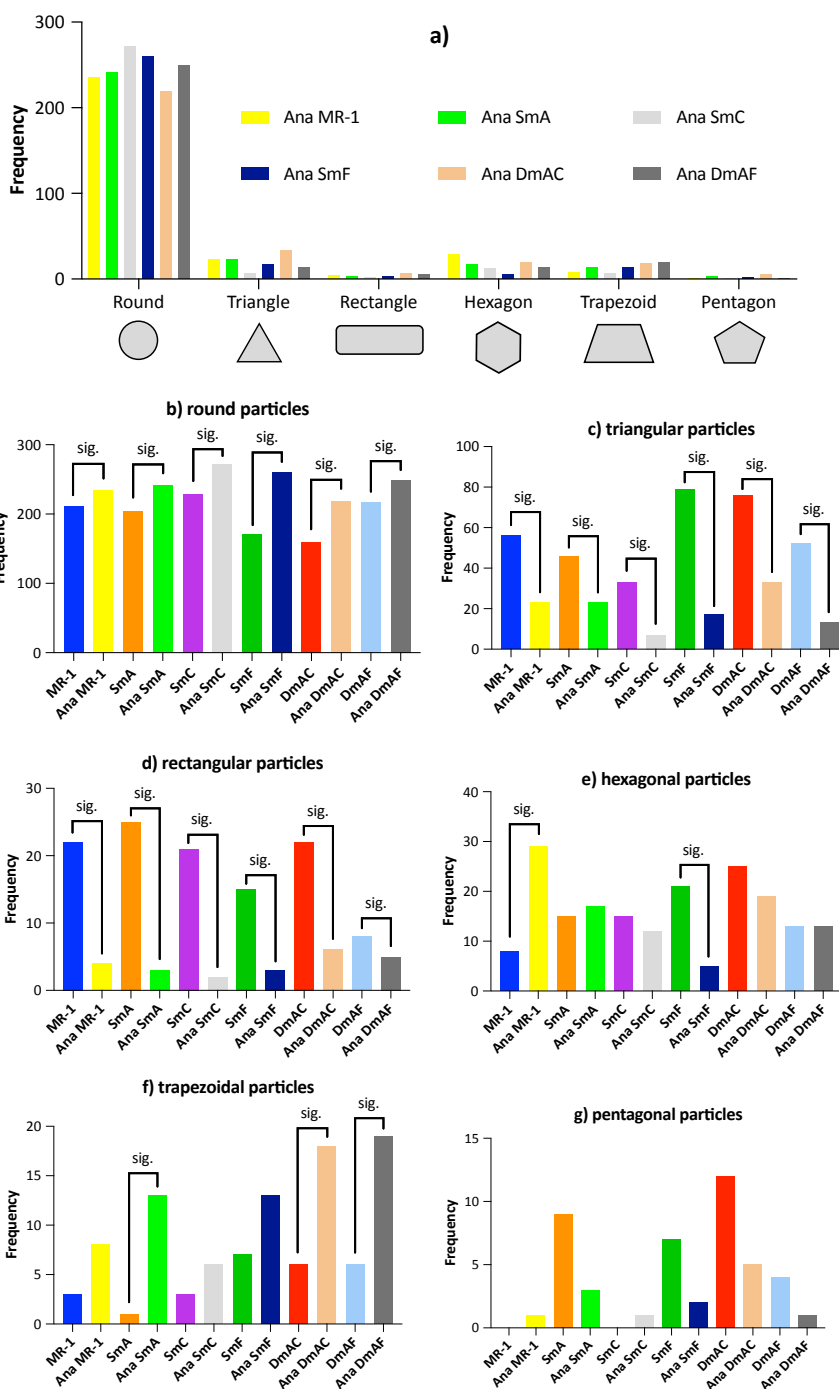
**Figure 6.10:** Frontal area of the gold nanoparticles synthesised through method II. Graph a) contains a histogram of the frontal area of the

nanoparticles synthesised anaerobically by the different cultures. Graph b) contains a histogram with bin range of 0 to 1000 nm<sup>2</sup> and bin width of 100 nm<sup>2</sup>. Both graphs have the same data, but graph b) was built to provide a detailed breakdown of the first bin in graph a), which contained the majority of the particles. Graph c) shows violin plots of the frontal area of the nanoparticles synthesised anaerobically by the strains. The median and the quartiles are represented by the dashed and dotted lines, respectively. Note that the y-axis is in log scale. The table presents the pairs in graph c) that are significantly different. Graph d) shows violin plots comparing the results from the aerobic and anaerobic experiments. The connections between the data present the pairs that are significantly different. Statistical analyses in graph c) evaluated all strains, whereas in graph d) only the same strains (aerobically vs. anaerobically) were analysed. Results were determined by measuring 300 particles per strain (100 per independent replicate).

anaerobically were larger.

**Figure 6.11** details the results of categorisation of the particles according to shape. It can be observed in this figure that round-shaped particles are also dominant in the synthesis through anaerobic conditions. As was the case in aerobic production, SmC fabricated more round-shaped particles than MR-1, SmA, SmF, DmAC and DmAF. Graphs b), c) and d) reveal an interesting pattern: under anaerobic conditions all strains formed significantly more round and significantly less triangular and rectangular particles than in the aerobic mode. It is also curious that more hexagonal particles were synthesised by MR-1 anaerobically (graph e)). Likewise, more trapezoids were made by SmA, DmAC and DmAF anaerobically (graph f)).

Specific productivity for anaerobic MR-1, SmA and SmC are shown in **Figure 6.12**. According to this figure, anaerobic conditions favour productivity of AuNPs – as all strains achieved high productivity. SmA and SmC did not synthesise more AuNPs anaerobically than aerobically, however it should be noticed that these were the two strains that outperformed the others under



Round				
MR-1 - SmC	MR-1 - SmF	SmA - SmC	SmA - SmF	SmA - DmAC
SmC - DmAC	SmC - DmAF	SmF - DmAC	DmAC - DmAF	
Triangle				
MR-1 - SmC	SmA - SmC	SmC - SmF	SmC - DmAC	SmF - DmAC
DmAC - DmAF				
Hexagon				
MR-1 - SmC	MR-1 - SmF	MR-1 - DmAF	SmF - DmCF	SmF - CcmC <sup>-</sup>
Trapezoid				
MR-1 - TmACF	SmA - TmACF	SmC - TmACF	SmF - DmCF	SmF - CcmC <sup>-</sup>

**Figure 6.11:** Histograms depicting the categorisation of the gold nanoparticles according to shape. Graph a) shows the histogram of the

nanoparticles synthesised anaerobically through method II. The table presents the pairs in graph a) that are significantly different for each shape. Graphs b) to g) compare the shapes of the particles synthesised aerobically and anaerobically. The connections between the data present the pairs that are significantly different. Statistical analyses in graph a) evaluated all strains, whereas in graphs b) to g) only the same strains (aerobically vs. anaerobically) were analysed. Results were determined by categorising 300 particles per strain (100 per independent replicate).

aerobic conditions. Nevertheless, the gain in productivity by MR-1 was substantial – from 20 to 115 mg per 100 mg of dry cells.

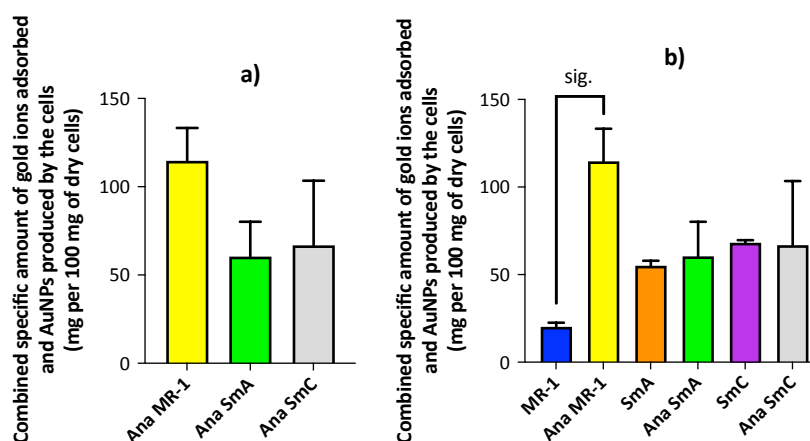


**Figure 6.12:** Specific productivity of gold nanoparticles. Graph a) shows the productivity by anaerobic strains as determined from TGA measurements after the implementation of method II. Results are average of three independent replicates. Statistical analyses determined that the pairs are not significantly different. Graph b) shows comparisons of specific productivity obtained from aerobic and anaerobic experiments. The connections between the data present the pair that is significantly different. Statistical analyses in graph a) evaluated all strains, whereas in graph b) only the same strains (aerobically vs. anaerobically) were analysed. Note that the values determined are a sum of gold ions adsorbed and gold nanoparticles produced.

## 6.4 Discussion

The results presented in this chapter confirm that *c*-type cytochromes have an influence in the aerobic and anaerobic fabrication of AuNPs. Nevertheless, the synthesis of gold nanoparticles by CcmC<sup>-</sup> shows that cytochrome *c* is not required for the formation of AuNPs. This is not an unexpected result because, as explained in section 3.4.1.4.1, a range of biomolecules (as hydrogenases, nitrate reductases, phosphatases and cytochromes) were proposed to be involved in the synthesis of metallic nanoparticles.

Although it has been demonstrated in section 3.5.1 that the cytochromes under investigation have appropriate redox potential for reduction of gold ions, it is not clear if they are actively forming the nanoparticles or if they have an indirect role in the process. It should be noted, however, that methods I and II do not sustain survival conditions for the cultures during the stage of incubation with gold ions. That is because this step takes place in a medium without nutrients, with low pH (3.17) and with lethal concentration of gold ions (the confirmation that cells are not viable while synthesising gold nanoparticles through method I is presented in chapter 7). Therefore, because the synthesis of AuNPs by methods I and II takes place through a passive reduction of gold ions, most likely the cytochromes are indirectly contributing to the process. Possibly, the electrons already inside the cytochromes are passively transferred to the gold ions upon contact between both substrates.

### 6.4.1 Correlation between surface plasmon bands and the other variables measured

Overall, there was a good correlation between the peaks of the normalised bands and the data of size and productivity. In the aerobic experiments, MR-1 (the reference strain) presented a peak with average 0.27, a median frontal area of nanoparticles of around 2.5 nm<sup>2</sup> in the log scale and a specific productivity of 20.6 mg of gold ions + AuNPs per 100 mg of dry cells. TmACF, MmOP and CcmC<sup>-</sup>, which belong to the same “group” of MR-1, all

presented similar results for frontal area of nanoparticles and specific productivity in relation to MR-1 (frontal area of MR-1 was significantly higher than that of CcmC<sup>-</sup> – p-value of 0.007 – but, it should be noted that frontal area of CcmC<sup>-</sup> was similar to those of TmACF and MmOP), and, consequently, had peaks of the normalised bands with similar size. The peaks of the bands of DmAF and DmCF were 0.03 and 0.06, respectively – smaller than the peak of MR-1. However, although specific productivity of these two cultures were the same as that of MR-1, the frontal area of the nanoparticles synthesised by the two strains were significantly smaller than the frontal area of MR-1 – justifying the smaller peaks. For the case of SmA, the peak of the normalised band was significantly higher than the peak of MR-1 (0.39 vs. 0.27), but although the frontal area of the nanoparticles did not vary among the two strains, specific productivity of SmA was more than double than productivity of MR-1 (54.4 mg vs. 20.6 mg). In a similar fashion, SmC had smaller peak of the normalised band (0.13) and smaller median frontal area of nanoparticles (around 1 nm<sup>2</sup> in the log scale) in relation to MR-1, however the peaks of the normalised bands were not as small as those of DmAF and DmCF because specific productivity of SmC was high (68.2 mg of gold ions + AuNPs per 100 mg of dry cells).

Among the aerobic experiments, SmF and DmAC were the two strains that presented poor correlation between peaks and size and productivity. In the first case (SmF), specific productivity and frontal area of the nanoparticles were similar to MR-1, however the peak of the normalised bands was smaller than that of MR-1 (0.16 vs. 0.27). In the case of DmAC, productivity and area of the nanoparticles were also similar to MR-1, but the peak was higher (0.37). It is not entirely known why this divergence took place, but the histograms of shapes (**Figure 6.6**) reveal that these two strains (SmF and DmAC) were the ones that synthesised the lowest amount of round-shaped AuNPs and the highest number of triangular-shaped particles. Although this difference in frequency of shapes can yield a different response in plasmon band, it is intriguing that the response of both strains went to opposite directions.

Evaluating the correlation for the data generated under anaerobic conditions is more limited because less strains were analysed. For the case of

MR-1, the peak of the normalised absorbance was 0.24, the median frontal area of nanoparticles was around 1.7 nm<sup>2</sup> in the log scale and specific productivity was 114.7 mg. The correlation for SmA was acceptable as this culture had a significantly larger frontal area of the nanoparticles (median of 2 nm<sup>2</sup> in the log scale), a considerably but not significantly smaller productivity (60.5 mg) and a higher (not significantly) peak of the normalised bands (0.27). In the case of SmC, the correlation was not strong. This strain presented significantly larger frontal area of the nanoparticles (median of approximately 2.3 nm<sup>2</sup> in the log scale) in relation to MR-1 and considerably but not significantly smaller productivity (66.8 mg of gold ions + AuNPs per 100 mg of dry cells) and peaks of the normalised bands (0.15). This weak correlation can be justified by the fact that SmC fabricated significantly more round-shaped AuNPs than MR-1 and SmA (graph a) of **Figure 6.11**).

#### **6.4.2 Influence of the c-type cytochromes under investigation in the synthesis of gold nanoparticles**

As the results of MR-1 are similar to those of TmACF, MmOP and CcmC<sup>-</sup>, it can be inferred that expression of OMCs by MR-1 during aerobic growth is negligible. This is not unexpected because OMCs are not involved in aerobic respiration, and, therefore, their expression is reduced when oxygen is the terminal electron acceptor (Beliaev et al., 2002, 2005). However, it is intriguing that the results of single and double mutants growing aerobically diverged from those of MR-1 – indicating that the expression of OMCs in these mutants is up-regulated.

When MR-1 grew with ferric citrate as the electron acceptor (a condition which required expression of OMCs), the nanoparticles formed diverged from those synthesised by aerobic MR-1. Graph h) of **Figure 6.8** revealed a smaller plasmon band generated by the nanoparticles made anaerobically; graph d) of **Figure 6.10** showed larger AuNPs from aerobic MR-1; graphs b), c), d) and e) of **Figure 6.11** showed that, when at anaerobic state, MR-1 makes more round and hexagonal particles and less triangular and rectangular particles; and graph b) of



**Figure 6.12** revealed that more gold nanoparticles are produced anaerobically. These results demonstrate that when the cytochromes from the Mtr pathway are at high expression levels (anaerobic conditions), major differences in the characteristics of the AuNPs occur – confirming their influence in the synthesis process.

### 6.4.3 Additional observations

Graph g) of **Figure 6.8** and graph c) of **Figure 6.10** showed that, under anaerobic conditions, the strains DmAC and DmAF, which express MtrC and MtrF as OMCs, respectively, had a similar performance in the synthesis of AuNPs. However, aerobically this pattern changes and the nanoparticles formed by DmAC and DmAF differ substantially. Under aerobic conditions MtrF was directly or indirectly responsible for fast synthesis of AuNPs (graph e) of **Figure 6.3**) and the formation of larger particles in comparison to DmAF (graph c) of **Figure 6.5**). It is not entirely known why MtrF presented such a high activity in the synthesis of AuNPs under aerobic conditions, however it should be noted that this is the cytochrome from the OMC group that has the lowest redox potential (–0.044 to –0.312 V).

Under aerobic conditions, the particles synthesised by DmAF and DmCF also shared similar characteristics, demonstrating a similar performance by OmcA and MtrC. This result matches with the study by Shi et al. (2006), which reported that purified OmcA and MtrC presented comparable reductase activities towards Fe(III)-nitrilotriacetic acid. Curiously, when both cytochromes are present concomitantly (strain SmF) the particles fabricated were significantly larger than those made by DmAF and DmCF (graph c) of **Figure 6.5**). This outcome suggests a synergistic effect between MtrC and OmcA – a hypothesis already proposed by Shi et al. (2006). In fact, Zhang et al. (2009) reported that both cytochromes form a direct interaction through intercross-linked peptides. Unfortunately, it is not possible to determine if the hypothesis of synergy between these two cytochromes is also applicable anaerobically, because DmCF was not able to grow with ferric citrate as electron donor.

The results on the frontal area of the particles synthesised by anaerobic SmC were similar to those by anaerobic DmAC (graph c) of **Figure 6.10**). This similarity is expected because most likely the expression of OmcA by the SmC mutant was low under anaerobic conditions, as it has been shown that OmcA is not capable of efficient respiration of ferric citrate (strain DmCF did not grow anaerobically) (Coursolle and Gralnick, 2010). Therefore, possibly MtrF was the main contributor in the synthesis of the nanoparticles, with OmcA potentially influencing the differences observed in the shapes of the nanoparticles (graph a) of **Figure 6.11**). Under aerobic conditions, apart from specific productivity, the results of SmC resembled more those of DmCF. These results suggest that for aerobic SmC OmcA contributed more to the characteristics of the nanoparticles (size and shape) and MtrF synergistically interacted with OmcA to boost productivity.

MtrF and MtrC also combined to boost productivity (strain SmA in **Figure 6.7**). Interestingly, SmA was the only strain in which the frontal area of the nanoparticles did not vary as a consequence of aerobicity (graph d) of **Figure 6.10**). Specific productivity also did not change according to aerobicity (graph b) of **Figure 6.12**). It is now known why the performance of both cytochromes was similar under aerobic and anaerobic conditions, but this is another matter worth of further investigation.

The results of size and shape of the nanoparticles synthesised by SmA under aerobic conditions were intermediate between DmAC and DmAF. The median frontal area of the nanoparticles made by SmA was around 2.3 nm<sup>2</sup> in the log scale and the frequency of round particles was 204, whereas the median frontal area for DmAC was ca. 3 nm<sup>2</sup> and the frequency of round particles was 159, and the median frontal area for DmAF was 1.5 nm<sup>2</sup> and the frequency of round particles was 217. These results interestingly imply that MtrC and MtrF contributed independently to the aerobic synthesis of AuNPs by SmA. The anaerobic results of SmA, DmAC and DmAF did not follow the same pattern, though. Nevertheless, the results of anaerobic SmA matched with previous studies – which tested the anaerobic reduction of U(VI) and Cr(VI) by *S. oneidensis* wild-type and mutants (including SmA) for the synthesis of

nanoparticles – in terms of the particles made by SmA not being similar to the ones synthesised by MR-1 (Marshall et al., 2006, Belchik et al., 2011).

## 6.5 Conclusion

All organisms tested in this study were capable of biofabricating gold nanoparticles, and *c*-type cytochromes, if were not directly responsible for the synthesis, at least influenced the process.

Overall, there were major differences in the nanoparticles synthesised under aerobic and anaerobic conditions. One major difference was in the shape – in all cases anaerobic cultures made significantly more round and less triangular and rectangular nanoparticles than aerobic cultures. The boost in specific productivity by MR-1 when at anaerobic conditions was also noteworthy. Therefore, in addition to deletions in outer membrane cytochromes, controllability of the particles can also be achieved through aerobicity.

The high activity of MtrF in the aerobic synthesis of gold nanoparticles is certainly worth further investigation. The strain containing MtrF as the sole OMC presented results similar to MR-1, and, most importantly, MtrF in conjunction with OmcA or MtrC had a boost in productivity.

As explained in chapter 5, it is important to emphasise that the variation in results by the different strains is not categorising the microbes by quality, since the performance of nanoparticles in a specific application vary according to the characteristics of the particles . Therefore, as exemplified in section 3.4.1, every strain should have an application for which it is more effective at. Nevertheless, specific productivity is one variable that is positive in all occasions, and, in that sense SmA, SmC and anaerobic MR-1 were the most adequate cultures for synthesising gold nanoparticles.



*3<sup>rd</sup>*  
*research*  
*chapter*

*“Come to me, all you who are toiling and loaded down,  
and I will refresh you.*

*Take my yoke upon you and learn from me,  
for I am mild-tempered and lowly in heart,  
and you will find refreshment for yourselves.*

*For my yoke is kindly, and my load is light.”*

*Matthew 11:28-30*



## **7 Tests of methods aiming to have cultures of *Escherichia coli* and *Shewanella oneidensis* actively synthesising gold nanoparticles**

---

### **7.1 Abstract**

Methods I and II have been previously determined to be successful in the synthesis of gold nanoparticles (AuNPs). Intriguingly, these methods do not provide survival conditions for the bacteria, suggesting that cultures are synthesising nanoparticles through passive mechanisms. Experiments carried out in the present chapter confirmed that cells are not viable during implementation of method I (and, most likely, during implementation of method II as well, given the similarities of the two methods). Assays of minimal inhibitory concentration carried out under aerobic conditions determined that 0.5 mM of HAuCl<sub>4</sub> in Luria Bertani medium was enough to cause major growth inhibition in MR-1, and 1 mM HAuCl<sub>4</sub> was the concentration necessary for full inhibition of BL21(DE3). Aerobic and anaerobic experiments with Au(III) at non-lethal concentration in culture medium did not reveal formation of gold nanoparticles – at least not to an extent detectable through spectrophotometry. Although not conclusive yet, these results indicate that it is not possible to have living cells of *E. coli* and *S. oneidensis* synthesising AuNPs.

### **7.2 Introduction**

The results from chapters 5, 6 and 14 (Appendix IV) have shown that *E. coli* and *S. oneidensis* successfully synthesise gold nanoparticles through method I. Method II was only tested for *S. oneidensis* (chapter 6) and was also successful. This, however, is an intriguing fact, as methods I and II do not favour bacterial survival during the step of synthesis of nanoparticles (incubation in gold solution) – the solution to which the cultures are left incubating does not have nutrients, has low pH and has gold ions at potentially toxic concentration. Therefore, the

biomass is unlikely fabricating the particles by active metabolism (for example, by utilising gold ions as terminal electron acceptors for cellular respiration). Instead, nanoparticles are being formed through unintentional interaction and reduction of gold ions.

This chapter aims to clarify if this is the case and to test if it is possible to have viable cultures fabricating AuNPs. For that, experiments of cell viability, minimal inhibitory concentration of gold ions, and attempts to have cells actively forming nanoparticles under anaerobic and aerobic conditions were carried out. The method utilised for monitoring the formation of gold nanoparticles was spectrophotometry (in the visible spectrum, 400 to 800 nm), because this has been demonstrated, in chapters 5 and 6, to be a reliable method for detecting biosynthesised AuNPs.

### 7.3 Results

The first experiments carried out tested the viability of the cells during the implementation of method I. **Figure 7.1** presents the viability tests performed with the LIVE/DEAD® *BacLight*™ bacterial viability kit. As can be seen in this figure, the results for both strains were similar. The removal of the cells from culture medium followed by the double washing steps with sterile DI water did not affect their viability (comparison of images a) and d) with b) and e)). This measurement was conducted because exposure of bacteria to DI water can cause hypo-osmotic shock and, consequently, cell lysis (Sleator and Hill, 2001). Most importantly, incubating both cultures in gold solution for the short period of 30 min was lethal to the cells (images c) and f)). Interestingly, virtually all cells in the images were found to be dead.

Since the viability analysis conducted for **Figure 7.1** presented only an illustrative and qualitative result, the quantitative test with PrestoBlue® cell viability reagent was also performed. Another reason for this second experiment was that the viability detection mechanism of *BacLight*™ differs from the one of PrestoBlue®. While the first contains SYTO® 9 and propidium iodide fluorescent



stains and evaluates membrane integrity, the second is based on a dye named resazurin and measures the reductive capability of the microorganisms. The results of the evaluation with resazurin can be found in **Figure 7.2**.

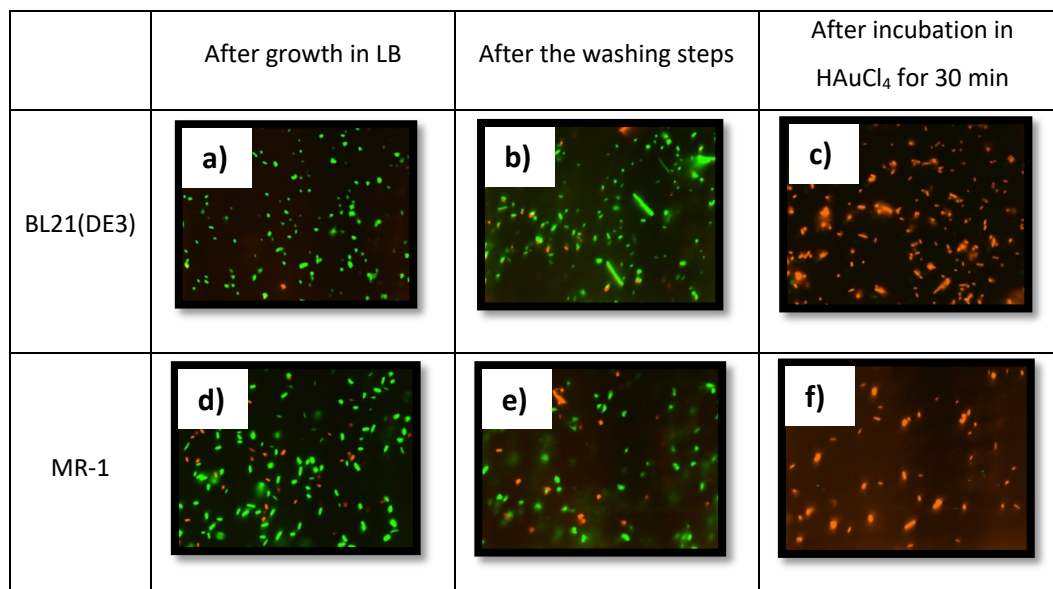


**Figure 7.1:** Images of the viability tests carried out with BacLight™ assay for BL21(DE3) (a), b) and c)) and MR-1 (d), e) and f)) at different stages of method I. a) and d) are cells after growth in LB; b) and e) are cells after the washing steps with sterile DI water; and c) and f) are cells after incubation in 1 mM HAuCl<sub>4</sub> solution for 30 min. The green and red fluorescence dots correspond to living and dead cells, respectively.

The results of **Figure 7.2** presented a similar outcome to those of **Figure 7.1**. The washing steps did not pose major influence in the viability of the cultures (BL21(DE3) was not affected and MR-1 had a reduction of ca. 18 %) and incubation in gold(III) chloride solution for 30 min was sufficient to eliminate the entire population of both cultures. In order to rule out the hypothesis that the initial contact with gold ions caused an instant shock and affected the metabolism of the cells only temporarily, extra measurements after 24 h and 48 h of incubation in gold(III) chloride solution were performed. Again, the populations did not show any signs of viability.

The experiments of resuspending and incubating the cultures in sterile DI water with pH lowered to 3.17 revealed a major resistance of *E. coli* towards

acidic environment – the cultures remained viable even after 48 h of incubation in DI water with low pH. *S. oneidensis* remained partially viable after 30 min (33 % of the initial relative fluorescence units) and even after 24 h (10 % of the initial relative fluorescence units), but did not resist incubation for 48 h in the harsh solution.

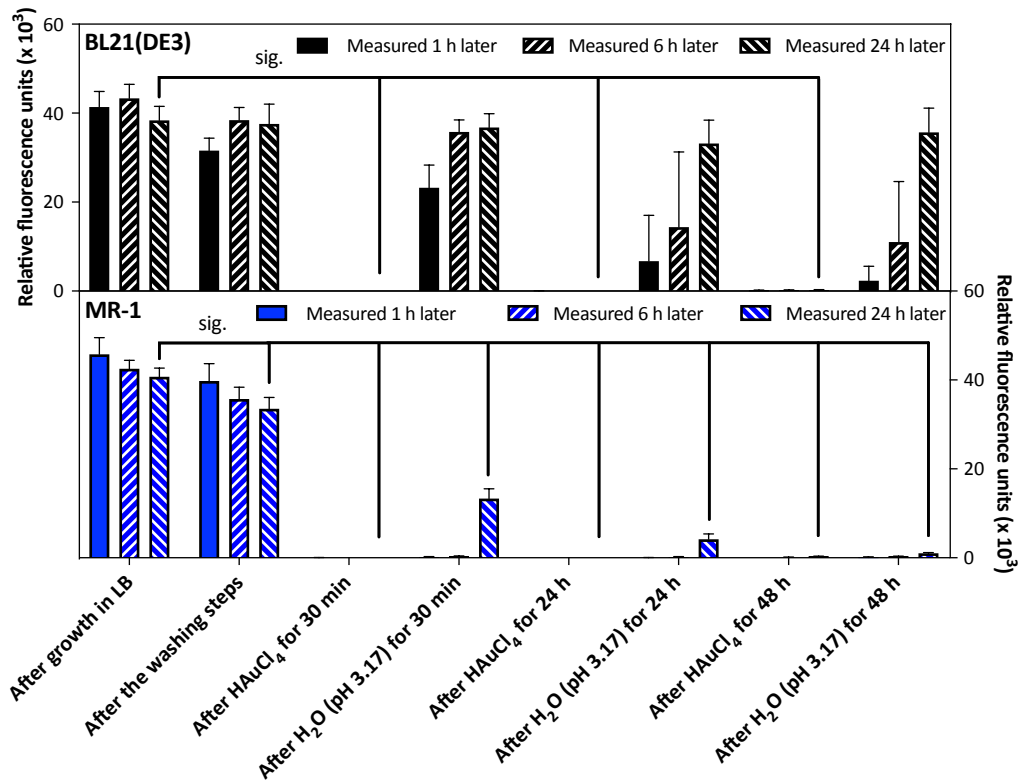


**Figure 7.2:** Viability tests carried out with PrestoBlue®. The upper panel shows results for BL21(DE3) and the lower panel shows results for MR-1. Samples were collected at five different stages of method I: after overnight growth in LB, after the washing steps with sterile DI water, and after 30 min, 24 h and 48 h of incubation in 1 mM H<sub>2</sub>AuCl<sub>4</sub>. The same procedures were conducted in cultures that were resuspended and incubated in sterile DI water with pH 3.17. The samples were added on top of the viability reagent on a 96-well plate and the plate was left incubating at 30 °C and 180 rpm for 24 h. After 1 h, 6 h and 24 h of incubation, fluorescence readings were taken. Error bars indicate the standard deviation of three independent replicates. The connections between the data present the

pairs that are significantly different. Note that only the 24-h measurements were evaluated statistically.

These results show that gold nanoparticles are synthesised by dead cells when method I – and, most likely, method II too – is implemented; and, gold ions were found to be the main agents responsible for killing the bacteria. In order to evaluate if cells that have been killed before the resuspension and incubation in 1 mM HAuCl<sub>4</sub> solution are capable of synthesising AuNPs, method I was implemented with autoclaved cells. The results, which can be found in **Figure 7.3**, reveal that autoclaved cultures can indeed fabricate nanoparticles.

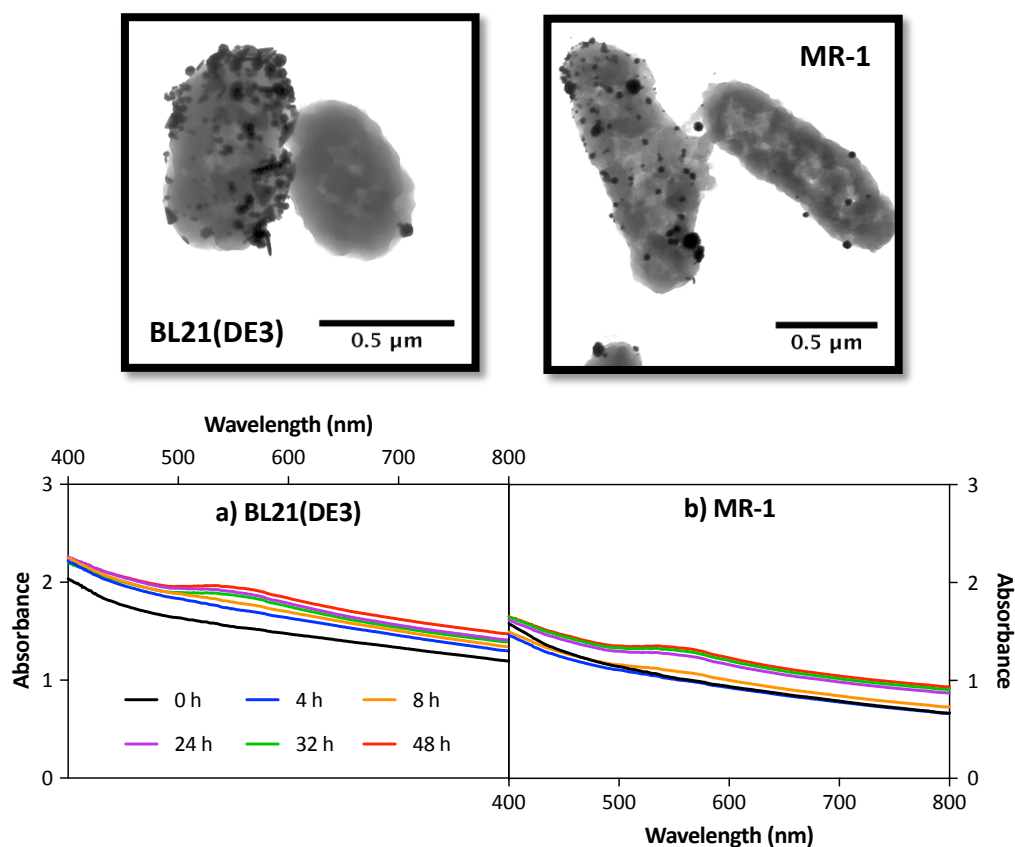


**Figure 7.3:** TEM images and visible spectra of autoclaved BL21(DE3) and MR-1 measured during the implementation of method I. The images were taken after incubation of the cultures in 1 mM HAuCl<sub>4</sub> solution. Results of the visible spectra are average of three independent replicates. For clarity of the graphs containing the spectra, error bars were not shown (**Figure 12.63** contains additional TEM images of BL21(DE3) and spectra with error

bars from graph a) and **Figure 12.64** contains additional TEM images of MR-1 and spectra with error bars from graph b)).

The next round of experiments was carried out to determine the minimum concentration of gold ions needed to inhibit aerobic growth of BL21(DE3) and MR-1 in LB. The results are depicted in **Figure 7.4**. The MIC assay ended up reinforcing the viability tests in the sense that both strains were not capable of surviving in medium with  $\text{HAuCl}_4$  at a concentration of 1 mM. In the case of *S. oneidensis*, a significant (but not major) inhibition started when gold ions were at a concentration of 0.05 mM and full growth impediment happened at 0.5 mM. *E. coli* has been shown to be more resistant, since it grew normally in medium with gold ions at concentration of 0.5 mM. At 1 mM, BL21(DE3) experienced minimal growth as a result of major inhibition.

One thing that should be taken into consideration regarding the MIC experiments is that if the cells are making AuNPs while growing, the nanoparticles would possibly interfere in the absorbance measured at 595 nm. That is because the surface plasmon band shifts the whole curve upwards, which can cause an inaccurate reading of absorbance (further explanation on this phenomenon can be found in section 5.3). In addition, gold nanoparticles have a peak of extinction at around 550 nm, but it still covers a range of ca. 100 nm (see **Figure 7.3** for example). In order to check if nanoparticles, and, consequently, plasmon bands, were formed during the MIC experiments, visible spectra of the samples were measured at the end of the assay. The samples measured were the controls (cultures growing only in LB), BL21(DE3) incubated in LB with 0.5 mM and 1 mM  $\text{HAuCl}_4$ , and MR-1 incubated in LB with 0.1 mM and 0.5 mM  $\text{HAuCl}_4$ . The results (graphs b) and c) of **Figure 7.4**) do not show plasmon bands and the spectra of the samples containing chloroauric acid were found to be similar to those of the controls. Therefore, it can be assumed that no interference took place during the  $\text{OD}_{595}$  measurements, but, most importantly, the results are indicating that no AuNPs were made by the bacteria.

These results indicate that while it is possible to have BL21(DE3) and MR-1 growing in the presence of chloroauric acid, the cells were not able to

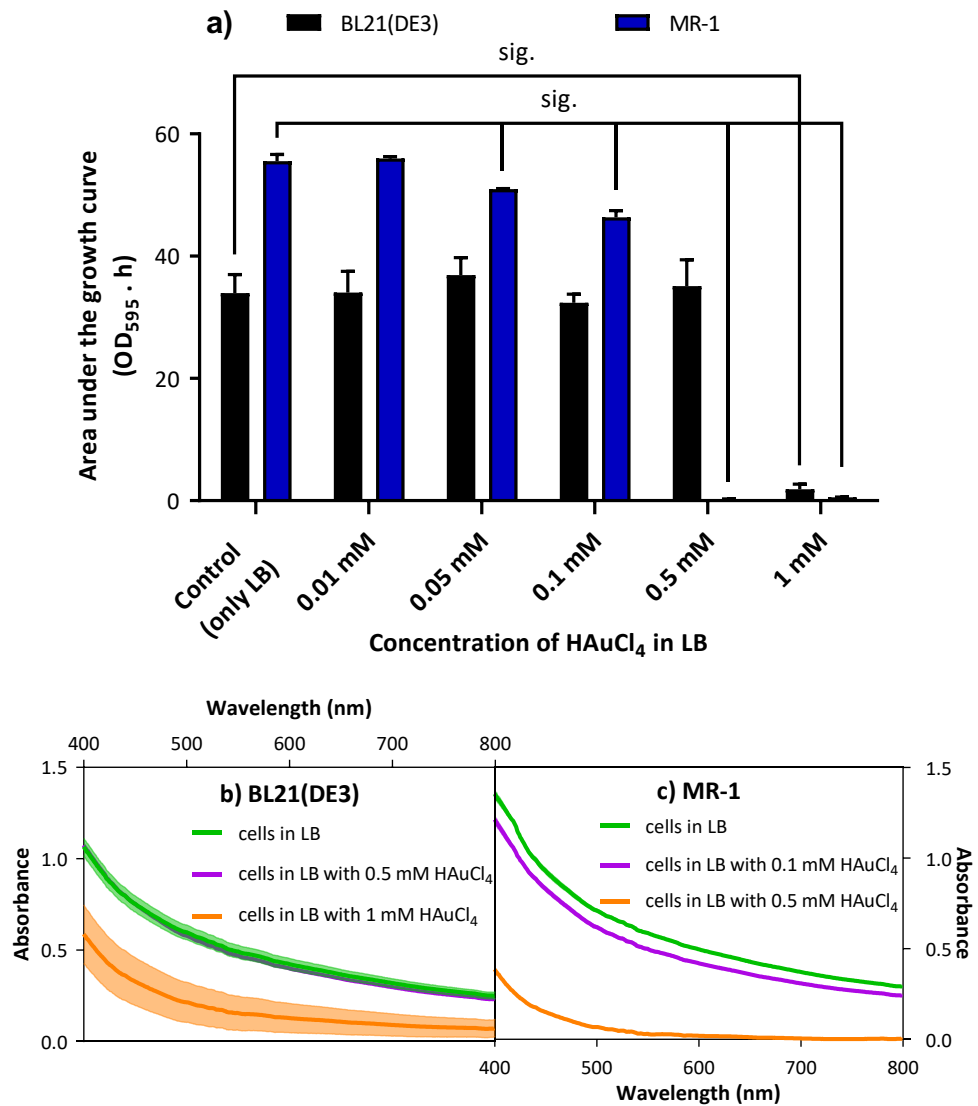


**Figure 7.4:** Experiments on minimum inhibitory concentration (MIC) of gold ions. Graph a) shows MIC results for BL21(DE3) and MR-1 cultures growing in LB added with H<sub>Au</sub>Cl<sub>4</sub> at different concentrations. Error bars indicate the standard deviation of three independent replicates. The connections between the data present the pairs that are significantly different. Graphs b) and c) show measurements of visible spectra of samples collected after the MIC assays. The samples analysed were the controls (only LB) of both strains, the cases of BL21(DE3) growing in 0.5 mM H<sub>Au</sub>Cl<sub>4</sub> and MR-1 growing in 0.1 mM H<sub>Au</sub>Cl<sub>4</sub>, and the cases in which BL21(DE3) and MR-1 did not grow – 1 mM and 0.5 mM H<sub>Au</sub>Cl<sub>4</sub>, respectively. Results are average of two independent replicates. Some error bars

cannot be visualised because they are smaller than the thickness of the curves.

synthesise gold nanoparticles (at least not to an extent detectable through LSPR). Similar experiments were thus carried out to check if a similar outcome is obtained under anaerobic conditions. For that, cells in exponential aerobic growth had their concentrations standardised and were resuspended in anaerobic LB containing non-lethal concentrations of gold(III) chloride (method III). The results are depicted in **Figure 7.5**. It is clear from the graphs that  $\text{HAuCl}_4$  at concentrations of 0.1 mM and 0.01 mM in anaerobic LB is not toxic to the bacteria tested, as the cells were capable of growing – at least to a small extent. The results also showed that, as in the aerobic tests, no gold nanoparticles were formed (at least not detected through plasmon band).

Method IV was developed to check if the nanoparticles that are potentially being synthesised by living cultures are not being detected through spectrophotometry because plasmon bands are being masked by the medium. For that, aerobic cells at  $\text{OD}_{600}$  of 2.5 were resuspended in anaerobic LB and left incubating anaerobically for 24 h before the addition of  $\text{HAuCl}_4$  to a concentration of 1 mM (the same concentration of methods I and II, which are successful in fabricating AuNPs). **Figure 7.6** shows the results of the implementation of method IV, which confirmed that it is possible to have gold nanoparticles generated by bacteria in LB that is detectable in the visible spectrum. Interestingly, abiotic controls also had formation of plasmon bands (see **Figure 12.75** for better clarity) – although the bands were considerably smaller than the ones from the cultures,

## 7.4 Discussion

The experiments performed in the present chapter have revealed that method I, and, most likely, method II, do not sustain survival conditions for the bacteria. Therefore, as intriguing as it may appear, in methods I and II gold

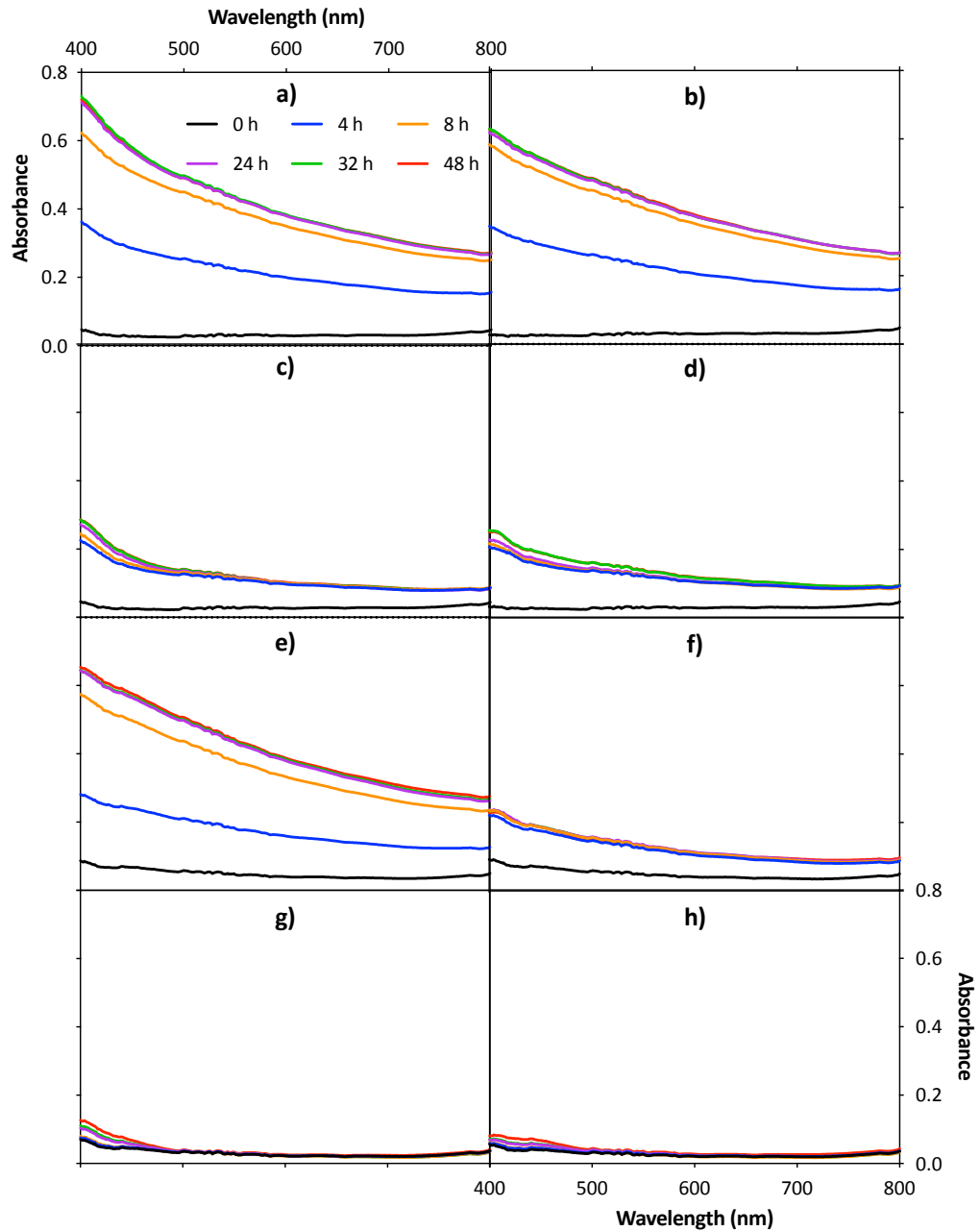


**Figure 7.5:** Visible spectra of cultures during implementation of method III (aerobic cultures at  $OD_{600}$  of 1.25 resuspended in anaerobic LB containing  $HAuCl_4$  at non-lethal concentrations). a) BL21(DE3) in LB with 0.1 mM  $HAuCl_4$ ; b) BL21(DE3) in LB with 0.01 mM  $HAuCl_4$ ; c) MR-1 in LB with 0.1 mM  $HAuCl_4$ ; d) MR-1 in LB with 0.01 mM  $HAuCl_4$ ; e) BL21(DE3) in LB; f) MR-1 in LB; g) LB with 0.1 mM  $HAuCl_4$  (abiotic control); h) LB with 0.01 mM  $HAuCl_4$  (abiotic control). Measurements are average of three independent

replicates. For clarity of the graphs, error bars were not shown (**Figure 12.65 to Figure 12.72** show the spectra with error bars).

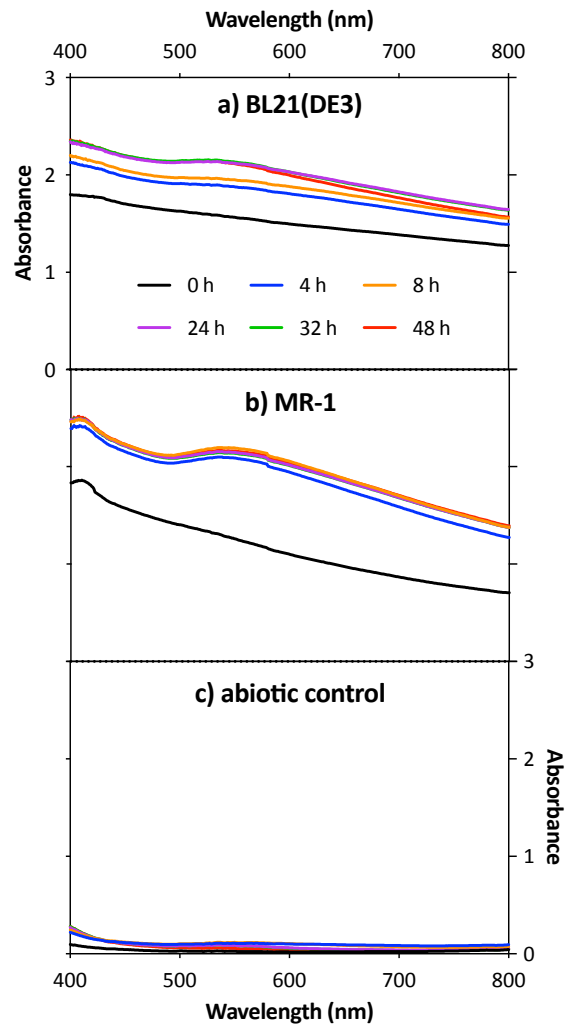


**Figure 7.6:** Visible spectra of cultures during implementation of method IV (aerobic cultures at  $OD_{600}$  of 2.5 left incubating in anaerobic LB for 24 h before addition of  $H AuCl_4$ ; measurements were taken after the incorporation of gold ions). Graph a) shows results for BL21(DE3), graph b) shows results for MR-1 and graph c) shows results for abiotic control. Measurements are average of three independent replicates. For clarity of the graphs, error bars were not shown (**Figure 12.73 to Figure 12.75** show the spectra with error bars).



nanoparticles are being synthesised by deceased cells. This was further reinforced by the results in **Figure 7.3**, which determined that cultures of BL21(DE3) and MR-1 that had been previously autoclaved were capable of forming AuNPs. The same outcome was observed by De Corte et al (2011), which found that heat-killed cells of *S. oneidensis* reduced gold ions in solution. Torgeman (2017) on the other hand, observed that *E. coli* K12 cultures that had been previously killed through the insertion of cell suspensions (in microcentrifuge tubes) in a heated water bath at 80 °C for 15 min were not capable of forming AuNPs. It is not known why this divergence took place, however it should be noted that Torgeman (2017) noticed that heat-killed cells ended up synthesising gold nanoparticles after 3 days of reaction.

The results in **Figure 7.2** notably show two different responses to the pH shock treatments. While *S. oneidensis* cells totally lost their reductive capability at the initial measurements, followed by partial recovery observed at the measurements taken 24 h later, *E. coli* presented considerable loss in the first measurements, but was capable of full recovery in all assessments taken 24 h later. This divergence in response by both strains is not unexpected because *E. coli* is endowed with extreme acid resistance mechanisms (Lund et al., 2014). Most importantly, both bacteria did not resist incubation in solution with 1 mM HAuCl<sub>4</sub> for as low as 30 min – a result that matches to the findings by Torgeman (2017), which reported the concentration of 1 mM Au(III) to be lethal to bacteria.

The attempts to have cells fabricating gold nanoparticles while growing under aerobic and anaerobic conditions in LB did not result in the formation of AuNPs – at least not to a level detectable through visible spectra assays. These are intriguing results because they are contradictory to the study by Torgeman (2017), which reported the synthesis of gold nanoparticles by living cultures of *E. coli* K12. Although the study did not show experiments confirming that cells were indeed alive while nanoparticles were made, the fact that the cultures were incubated in buffer containing non-lethal concentration of Au(III) can be considered an indication that cells were in fact alive. Nevertheless, it should be noted that even though the study claims to have proved “conclusively that the bioconversion of Au(III) solutions into AuNPs is a biological process that happens

only in the presence of metabolically active biomass”, the data presented in figure 55 of the thesis show obvious synthesis of nanoparticles by cultures that were incubated in buffer solution containing gold ions at lethal concentration (2 mM).

One possible explanation for the lack of synthesis of gold nanoparticles by growing cells is the unfavourable pH of the medium (neutral pH). The low pH of the gold solution (pH 3.17) favours the formation of AuNPs, because, as demonstrated in section 3.4.1.4.3, at this pH  $\text{AuCl}_4^-$  is the dominant Au(III) species in solution and the functional groups on the surface of bacteria are protonated. These characteristics facilitate sorption of Au(III) by the cells (Srivastava et al., 2013). At neutral pH, on the other hand, the dominance of  $\text{AuCl}_4^-$  is reduced (graph a) of **Figure 3.6**) and functional groups in bacteria are less protonated. However, in an experiment performed implementing method I with a variation of MR-1 cells being resuspended and incubated in gold solution which had the pH corrected to 7 (with NaOH) resulted in synthesis of AuNPs (**Figure 12.76**). The bands formed in the spectra shown in **Figure 12.76** are clearly smaller than the bands obtained by MR-1 through implementation of method I (graph b) of **Figure 5.2**), possibly because neutral pH is less favourable for the synthesis process. Nevertheless, the most important observation for **Figure 12.76** is that although to a lower extent, pH 7 does allow formation of AuNPs.

It is relevant to clarify that, although the experiments reported in the present chapter were not successful in having living cells synthesising nanoparticles, additional experiments could be carried out for more conclusive results. Section 6.4.1 has shown that there is an overall good correlation between the aerobic and anaerobic biosynthesis of AuNPs and the surface plasmon bands generated, however it is always interesting to conduct TEM and EDS analyses to further confirm presence or absence of nanoparticles.

Curiously, the visible spectra of the cases in which BL21(DE3) and MR-1 did not grow in the MIC experiments (LB with 1 mM and 0.5 mM  $\text{HAuCl}_4$ , respectively – graphs b) and c) of **Figure 7.4**) did not show presence of surface plasmon bands, whereas the spectra in the abiotic control (graph c)) of **Figure 7.6** revealed formation of small plasmon bands. Synthesis of AuNPs by the

abiotic control in **Figure 7.6** most likely took place through reduction of gold ions by components of the medium. As explained in section 3.4.1.4.3, Au(III) can form stable complexes with C, N, P, S, and O-donor ligands, with strong interaction taking place with thiols. Therefore, it is likely that components of LB (especially yeast extract) have such ligands available for interaction with gold ions. It is not clear, however, why AuNPs (or, at least plasmon bands) were not formed by LB with 1 mM and 0.5 mM H<sub>2</sub>AuCl<sub>4</sub> under aerobic conditions. It might be the case that oxygen is interacting with one or more molecules of LB medium and that interaction is somehow hampering gold ions to be reduced or plasmon bands to be formed.

Testing if oxygen is interacting with molecules in culture medium and preventing AuNPs to be formed/detected is also a valuable set of experiments to be carried out, since, if that is the case, then additional attempts to have gold nanoparticles being synthesised aerobically (this time without the interfering molecules) can be carried out.

Regarding the growth of cells in LB under anaerobic conditions (graphs e) and f) of **Figure 7.5**), it can be seen in that *E. coli* developed considerably more and for longer period than *S. oneidensis*. MR-1 was able to develop only for a short period of time after resuspension in anaerobic LB because when the small amount of oxygen present in anaerobic LB depleted, the medium lacked suitable terminal electron acceptors. In fact, this is an indication that *S. oneidensis* cannot utilise gold ions for respiration (especially because the development of MR-1 in graphs c) and d) were similar to the development in graph f), which did not contain Au(III)). In the case of *E. coli*, after depletion of oxygen in the medium, the cultures grew through anaerobic mixed acid fermentation of endogenous organic compounds, a metabolic activity MR-1 is capable of performing only for cell survival – not for growth (as explained in sections 3.5.1 and 3.5.2).

## 7.5 Conclusion

The experiments carried out in this chapter attempting to have living cultures synthesising gold nanoparticles did not reveal formation of AuNPs. The finding was not conclusive, though, as it could have been the case that nanoparticles were formed, but were not detected through spectrophotometry. TEM and EDS analyses could potentially cast a light into this. Additional attempts with other culture media could also yield a different outcome. Nevertheless, it should be noted that living cells not synthesising gold nanoparticles is not an unexpected result, because gold is not an element essential for the cultures; and, if Au(III) is present in the medium at non-toxic concentration, there is no advantage for the bacteria to uptake the ions and reduce them inside the cell.

# *Future studies*

*Martha, on the other hand, was distracted with attending to many duties.*

*So she came to Him and said:*

*“Lord, does it not matter to you that my sister has left me alone to attend to things?*

*Tell her to come and help me.”*

*In answer the Lord said to her:*

*“Martha, Martha, you are anxious and disturbed about many things.*

*A few things, though, are needed, or just one.*

*For her part, Mary chose the good portion,*

*and it will not be taken away from her.”*

*Luke 10:40-42*



## 8 Future studies

---

Several new research avenues were, hopefully, opened from the experimental work carried out in the present study. In fact, every intriguing result reported here is worth further investigation. Unfortunately, because of high volume of cases, it is not possible to list here all outcomes that had unpredictable results in the thesis; nevertheless, some suggestions for future work are pointed out below.

The comparison platform developed in chapter 5 can also be applied for testing the influence that other gene products have on the synthesis of nanoparticles. For example, the NiFe hydrogenase HyaB of *S. oneidensis* was already found to play a role in the reduction of Pd(II) and Tc(VII) (Marshall et al., 2008, Ng et al., 2013b). The findings from these extra experiments could then, hopefully, help solving the puzzle on the biomolecules and mechanisms involved in the adsorption and bioreduction of gold ions by *E. coli* and *S. oneidensis*. Obviously, the same platform could be extended to other metallic ions and organisms.

Determining expression levels of the cytochromes under investigation in chapter 6 should provide additional data that could explain some of the interesting results observed – as the high activity of MtrF under aerobic conditions. In fact, finding the cause for the high activity of MtrF in the aerobic synthesis of gold nanoparticles is certainly worth further investigation, as it can provide additional tools for fine tuning microbial synthesis of metallic nanoparticles.

The intriguing findings that SmA and SmC had improved productivity of AuNPs under aerobic conditions (**Figure 6.7**) are results that certainly worth further investigation. This research avenue would improve our understanding of *S. oneidensis* and could potentially identify currently unknown synergistic effects among cytochromes. That discovery could thus find applications in biotechnological systems involving *S. oneidensis*, such as microbial fuel cells.

Performing catalytic tests with the gold nanoparticles generated by the strains in chapters 5 and 6 is a useful manner to confirm the controllability of the synthesis of AuNPs according to specific applications. For example, two reactions can be carried out, one in which smaller particles are known to be most efficient and another where bigger particles are better. If the strains that synthesised more of the small particles (such as aerobic DmAF and DmCF) perform better in the first reaction in relation to the other cultures, and vice-versa, it means that higher controllability has been achieved.

The results of the experiments on minimum inhibitory concentration were interesting and are also worth further investigation. More specifically, *E. coli* was found to be more resistant towards gold ions than *S. oneidensis*. Discovering the machinery responsible for the increased resistance of BL21(DE3) could provide valuable information that can be applied in the construction of cell lines with improved resistance towards Au(III).

The additional tests suggested in chapter 7 are also relevant for improving the understanding of the aspects involved in microbial synthesis of gold nanoparticles. These include TEM and EDS analyses of the samples that did not present formation of AuNPs detectable through spectrophotometry and testing if oxygen is interacting with molecules in culture medium and preventing AuNPs to be formed/detected. Testing the synthesis with other culture media, apart from LB, should also provide interesting information to the subject. The results from these experiments could potentially provide a satisfactory answer on whether living cells of *S. oneidensis* and *E. coli* are able to synthesise AuNPs.

Finally, it is certainly important to extend this research to the application of microorganisms for the bioremediation of toxic compounds. As previously reported, and further reinforced in the present study, microbes have an outstanding capability to adsorb/absorb metallic ions in solution at a surprisingly high rate and amount. Most interestingly, the findings of the present study have shown that cells do not have to be alive in order to reduce the ions. In bioremediation applications this is a valuable feature, as using deceased organisms for cleaning processes prevent a potentially harmful destabilisation of environmental microbiota.



# Conclusion

*“For this perfume oil could have been sold for more than 300 denarii  
and the money given to the poor!”  
And they were greatly annoyed with her.  
But Jesus said: “Let her alone. Why do you try to make trouble for her?  
She did a fine deed toward me.  
For you always have the poor with you,  
and you can do them good whenever you want to,  
but you will not always have me.  
She did what she could;  
she poured perfumed oil on my body beforehand,  
in view of the burial”  
Mark 14:5-8*



## 9 Conclusion

---

The present thesis has revealed interesting discoveries. The first research chapter confirmed that method I allows synthesis of gold nanoparticles by cultures of BL21(DE3) and MR-1. The chapter also introduced a methodology for comparing the nanoparticles fabricated by different organisms. The organisms compared in the chapter were *E. coli* and *S. oneidensis*, and the variables considered for comparison were amount of gold ions adsorbed from solution, size and shape of the nanoparticles, heights of peaks of surface plasmon bands and specific productivity. The results demonstrated that adsorption of Au(III) from solution by both cells was similarly extensive; MR-1 formed more round-shaped and smaller particles than BL21(DE3), which, on the other hand, fabricated more trapezoid and hexagonal particles; *S. oneidensis* generated a significantly higher plasmon band; and, both organisms presented similar specific productivity. The most relevant achievement of this chapter was that the comparison methodology adopted allowed the qualification of the strains according to the application to which the biosynthesised nanoparticles are more suitable for.

In the second research chapter the same comparative methodology was applied for comparing the nanoparticles made, under aerobic and anaerobic conditions, by MR-1 and mutants of MR-1 lacking different *c*-type cytochromes. Several interesting results were obtained. It has been found that cytochrome *c* is not required for the synthesis of gold nanoparticles, but they influence the process. It has also been determined that aerobicity influences the biosynthesis of AuNPs, with anaerobic conditions favouring the fabrication of round nanoparticles and improving specific productivity. Curiously, under aerobic conditions, MR-1 presented results similar to the ones of mutants lacking OMCs, which can be an indication that MR-1 is expressing negligible levels of OMCs aerobically. Some interesting results were observed in terms of the performance and contribution of specific cytochromes to the characteristics of the AuNPs. For example, OmcA and MtrC, when at aerobic conditions, presented similar

performance individually and revealed synergistic effect when combined. Moreover, MtrC and MtrF performed similarly under anaerobic conditions, but, aerobically, MtrF was more active than MtrC. In fact, MtrF under aerobic conditions was the cytochrome that stood out, especially because it boosted productivity by SmA and SmC. The results revealed in this chapter were valuable because they confirmed that the assessed cytochromes influence the characteristics of the AuNPs and because they qualified all the strains tested according to the most suitable applications of the nanoparticles.

The third research chapter confirmed that method I and, most likely, method II do not sustain survival conditions for the cells. This is an intriguing finding that suggests that AuNPs are synthesised passively. Multiple experiments then were carried out to attempt to have living cells making nanoparticles, based on the results obtained from assays on minimum inhibitory concentration of gold ions. All of them were not successful – if nanoparticles were synthesised, they were not detected through spectrophotometry. Most interestingly, the experiments of the third research chapter related to the fabrication of metallic nanoparticles by metabolically active bacteria yielded several intriguing results that are worth further investigation.

# *References*

*He said: "Come!"*

*So Peter got out of the boat and walked over the waters and went toward Jesus.*

*But looking at the windstorm, he became afraid.*

*And when he started to sink, he cried out: "Lord, save me!"*

*Immediately stretching out his hand, Jesus caught hold of him and said to him:*

*"You with little faith, why did you give way to doubt?"*

*Matthew 14:29-31*



## 10 References

---

- ADSCHIRI, T., HAKUTA, Y., SUE, K. & ARAI, K. 2001. Hydrothermal synthesis of metal oxide nanoparticles at supercritical conditions. *Journal of Nanoparticle Research*, 3, 227-235.
- AHMAD, A., MUKHERJEE, P., SENAPATI, S., MANDAL, D., ISLAM KHAN, M., KUMAR, R. & SASTRY, M. 2003. Extracellular biosynthesis of silver nanoparticles using the fungus *Fusarium oxysporum*. *Colloids and Surfaces B: Biointerfaces*, 28, 313-318.
- AKBARI, B., TAVANDASHTI, M. P. & ZANDRAHIMI, M. 2011. Particle size characterization of nanoparticles - A practical approach. *Iranian Journal of Materials Science & Engineering*, 8, 48-56.
- AMENDOLA, V. & MENEGHETTI, M. 2009. Laser ablation synthesis in solution and size manipulation of noble metal nanoparticles. *Physical Chemistry Chemical Physics*, 11, 3805-3821.
- AMENDOLA, V., PILOT, R., FRASCONI, M., MARAGÒ, O. M. & IATÌ, M. A. 2017. Surface plasmon resonance in gold nanoparticles: a review. *Journal of Physics: Condensed Matter*, 29, 203002.
- ANNAMALAI, J. & NALLAMUTHU, T. 2015. Characterization of biosynthesized gold nanoparticles from aqueous extract of *Chlorella vulgaris* and their anti-pathogenic properties. *Applied Nanoscience*, 5, 603-607.
- ANSARI, A. A., KHAN, M. N., ALHOSHAN, M., ALDWAYYAN, A. S. & ALSALHI, M. S. 2010. Nanostructured materials: classification, properties, fabrication, characterization and their applications in biomedical sciences. In: KESTELL, A. E. & DELOREY, G. T. (eds.) *Nanoparticles: properties, classification, characterization, and fabrication*. New York, NY: Nova Science Publishers, Inc.
- ANSHUP, VENKATARAMAN, J. S., SUBRAMANIAM, C., KUMAR, R. R., PRIYA, S., KUMAR, T. R. S., OMKUMAR, R. V., JOHN, A. & PRADEEP, T. 2005. Growth of gold nanoparticles in human cells. *Langmuir*, 21, 11562-11567.
- ARORA, M. P. 2007. *Biotechnology*, Mumbai, India, Himalaya Publishing House.

- ARRUEBO, M., VALLADARES, M. & GONZÁLEZ-FERNÁNDEZ, A. 2009. Antibody-conjugated nanoparticles for biomedical applications. *Journal of Nanomaterials*, 439389.
- ASADABAD, M. A. & ESKANDARI, M. J. 2016. Electron diffraction. In: JANECEK, M. & KRAL, R. (eds.) *Modern electron microscopy in physical and life sciences*. Rijeka, Croatia: InTech.
- AYDOGAN, B., LI, J., RAJH, T., CHAUDHARY, A., CHMURA, S. J., PELIZZARI, C., WIETHOLT, C., KURTOGLU, M. & REDMOND, P. 2010. AuNP-DG: Deoxyglucose-labeled gold nanoparticles as X-ray computed tomography contrast agents for cancer imaging. *Molecular Imaging and Biology*, 12, 463-467.
- BABA, T., ARA, T., HASEGAWA, M., TAKAI, Y., OKUMURA, Y., BABA, M., DATSENKO, K. A., TOMITA, M., WANNER, B. L. & MORI, H. 2006. Construction of *Escherichia coli* K-12 in-frame, single-gene knockout mutants: the Keio collection. *Molecular Systems Biology*, 2.
- BAYER, M. E. & BAYER, M. H. 1991. Lanthanide accumulation in the periplasmic space of *Escherichia coli* B. *Journal of Bacteriology*, 173, 141-149.
- BAYFORD, R., RADEMACHER, T., ROITT, I. & WANG, S. X. 2017. Emerging applications of nanotechnology for diagnosis and therapy of disease: a review. *Physiological Measurement*, 38, R183-R203.
- BAZYLINSKI, D. A. & FRANKEL, R. B. 2004. Magnetosome formation in prokaryotes. *Nature Reviews Microbiology*, 2, 217-230.
- BELCHIK, S. M., KENNEDY, D. W., DOHNALKOVA, A. C., WANG, Y., SEVINC, P. C., WU, H., LIN, Y., LU, H. P., FREDRICKSON, J. K. & SHI, L. 2011. Extracellular reduction of hexavalent chromium by cytochromes MtrC and OmcA of *Shewanella oneidensis* MR-1. *Applied and Environmental Microbiology*, 77, 4035-4041.
- BELIAEV, A. S., KLINGEMAN, D. M., KLAPPENBACH, J. A., WU, L., ROMINE, M. F., TIEDJE, J. M., NEALSON, K. H., FREDRICKSON, J. K. & ZHOU, J. 2005. Global transcriptome analysis of *Shewanella oneidensis* MR-1 exposed to different terminal electron acceptors. *Journal of Bacteriology*, 187, 7138-7145.



- BELIAEV, A. S., SAFFARINI, D. A., MCLAUGHLIN, J. L. & HUNNICUTT, D. 2001. MtrC, an outer membrane decahaem c cytochrome required for metal reduction in *Shewanella putrefaciens* MR-1. *Molecular Microbiology*, 39, 722-730.
- BELIAEV, A. S., THOMPSON, D. K., KHARE, T., LIM, H., BRANDT, C. C., LI, G., MURRAY, A. E., HEIDELBERG, J. F., GIOMETTI, C. S., YATES III, J., NEALSON, K. H., TIEDJE, J. M. & ZHOU, J. 2002. Gene and protein expression profiles of *Shewanella oneidensis* during anaerobic growth with different electron acceptors. *OMICS: A Journal of Integrative Biology*, 6.
- BERTHIAUME, F., MAGUIRE, T. J. & YARMUSH, M. L. 2011. Tissue engineering and regenerative medicine: History, progress, and challenges. *Annual Review of Chemical and Biomolecular Engineering*, 2, 403-430.
- BEVERIDGE, T. J. & KOVAL, S. F. 1981. Binding of metals to cell envelopes of *Escherichia coli* K-12. *Applied and Environmental Microbiology*, 42, 325-335.
- BHADWAL, A. S., TRIPATHI, R. M., GUPTA, R. K., KUMAR, N., SINGH, R. P. & SHRIVASTAV, A. 2014. Biogenic synthesis and photocatalytic activity of CdS nanoparticles. *RSC Advances*, 4, 9484-9490.
- BHAGAT, S. M. 1986. Ferromagnetic resonance. In: WHAN, R. E. (ed.) *ASM handbook archive: materials characterization*. United States of America: ASM International.
- BHATIA, S. & GOLI, D. 2018. *Introduction to pharmaceutical biotechnology - basic techniques and concepts*, Bristol, UK, IOP Publishing Ltd.
- BHATTACHARJEE, S. 2016. DLS and zeta potential - What they are and what they are not? *Journal of Controlled Release*, 235, 337-351.
- BINNS, C. 2010. *Introduction to nanoscience and nanotechnology*, Hoboken, NJ, John Wiley & Sons, Inc.
- BISWAS, A., BAYER, I. S., BIRIS, A. S., WANG, T., DERVISHI, E. & FAUPEL, F. 2012. Advances in top-down and bottom-up surface nanofabrication: Techniques, applications & future prospects. *Advances in Colloid and Interface Science*, 170, 2-27.

- BLAKEMORE, R. P. 1982. Magnetotactic bacteria. *Annual Review of Microbiology*, 36, 217-238.
- BOUHENNI, R., GEHRKE, A. & SAFFARINI, D. 2005. Identification of genes involved in cytochrome *c* biogenesis in *Shewanella oneidensis*, using a modified *mariner* transposon. *Applied and Environmental Microbiology*, 71, 4935-4937.
- BRENNAN, C. M., KEANE, M. L., HUNT, T. M., GOULET, M. T., MAZZUCCA, N. Q., SEXTON, Z., MEZOIAN, T., DOUGLAS, K. E., OSBORN, J. M. & PELLOCK, B. J. 2013. *Shewanella oneidensis* Hfq promotes exponential phase growth, stationary phase culture density, and cell survival. *BMC Microbiology*, 13.
- BREUER, M., ROSSO, K. M., BLUMBERGER, J. & BUTT, J. N. 2015. Multi-haem cytochromes in *Shewanella oneidensis* MR-1: structures, functions and opportunities. *Journal of the Royal Society Interface*, 12, 20141117.
- BROWN, C. M., CAMPBELL, I. & PRIEST, F. G. 1987. *Introduction to biotechnology*, Oxford, UK, Blackwell Scientific Publications.
- BRYDSON, R. 2007. Electron energy-loss spectroscopy and energy dispersive X-ray analysis. *In*: KIRKLAND, A. I. & HUTCHISON, J. L. (eds.) *Nanocharacterisation*. Cambridge, UK: The Royal Society of Chemistry.
- BU'LOCK, J. D. 1987. Introduction to basic biotechnology. *In*: BU'LOCK, J. D. & KRISTIANSEN, B. (eds.) *Basic biotechnology*. London, UK: Academic Press Inc.
- BUCKING, C., PIEPENBROCK, A., KAPPLER, A. & GESCHER, J. 2012. Outer-membrane cytochrome-independent reduction of extracellular electron acceptors in *Shewanella oneidensis*. *Microbiology*, 158, 2144-2157.
- BURDA, C., CHEN, X., NARAYANAN, R. & EL-SAYED, M. A. 2005. Chemistry and properties of nanocrystals of different shapes. *Chemical Reviews*, 105, 1025-1102.
- BUSZEWSKI, B., RAILEAN-PLUGARU, V., POMASTOWSKI, P., RAFINSKA, K., SZULTKA-MLYNSKA, M., GOLINSKA, P., WYPIJ, M., LASKOWSKI, D. & DAHM, H. 2018. Antimicrobial activity of biosilver nanoparticles produced by a novel *Streptacidiphilus durhamensis* strain. *Journal of Microbiology, Immunology and Infection*, 51, 45-54.

- CANU, G. & BUSCAGLIA, V. 2017. Hydrothermal synthesis of strontium titanate: thermodynamic considerations, morphology control and crystallisation mechanisms. *CrystEngComm*, 19, 3867-3891.
- CAO, S., TAO, F., TANG, Y., LI, Y. & YU, J. 2016. Size- and shape-dependent catalytic performances of oxidation and reduction reactions on nanocatalysts. *Chemical Society Reviews*, 45, 4747-4765.
- CARVALHO, P. M., FELÍCIO, M. R., SANTOS, N. C., GONÇALVES, S. & DOMINGUES, M. M. 2018. Application of light scattering techniques to nanoparticle characterization and development. *Frontiers in Chemistry*, 6, 237.
- CASTRO-LONGORIA, E., MORENO-VELÁSQUEZ, S. D., VILCHIS-NESTOR, A. R., ARENAS-BERUMEN, E. & AVALOS-BORJA, M. 2012. Production of platinum nanoparticles and nanoaggregates using *Neurospora crassa*. *Journal of Microbiology and Biotechnology*, 22, 1000-1004.
- CASTRO-LONGORIA, E., VILCHIS-NESTOR, A. R. & AVALOS-BORJA, M. 2011. Biosynthesis of silver, gold and bimetallic nanoparticles using the filamentous fungus *Neurospora crassa*. *Colloids and Surfaces B: Biointerfaces*, 83, 42-48.
- CHAKRABORTY, N., BANERJEE, A., LAHIRI, S., PANDA, A., GHOSH, A. N. & PAL, R. 2009. Biorecovery of gold using cyanobacteria and an eukaryotic alga with special reference to nanogold formation - a novel phenomenon. *Journal of Applied Phycology*, 21, 145-152.
- CHE MAN, Y. B., SYAHARIZA, Z. A. & ROHMAN, A. 2010. Fourier transform infrared (FTIR) spectroscopy: development, techniques, and application in the analyses of fats and oils. In: REES, O. J. (ed.) *Fourier transform infrared spectroscopy: developments, techniques and applications*. New York, NY: Nova Science Publishers, Inc.
- CHEN, P.-Y., DANG, X., KLUG, M. T., COURCHESNE, N.-M. D., QI, J., HYDER, M. N., BELCHER, A. M. & HAMMOND, P. T. 2015. M13 virus-enabled synthesis of titanium dioxide nanowires for tunable mesoporous semiconducting networks. *Chemistry of Materials*, 27, 1531-1540.

- CHENG, Y., KE, Z., BIAN, X., ZHANG, J., HUANG, Z., LV, Y. & LIU, M. 2019. Selective mineralization and recovery of Au(III) from multi-ionic aqueous systems by *Bacillus licheniformis* FZUL-63. *Minerals*, 9, 392.
- CHOI, Y., PARK, T. J., LEE, D. C. & LEE, S. Y. 2018. Recombinant *Escherichia coli* as a biofactory for various single- and multi-element nanomaterials. *Proceedings of the National Academy of Sciences of the United States of America*, 115, 5944-5949.
- CLARKE, T. A., EDWARDS, M. J., GATES, A. J., HALL, A., WHITE, G. F., BRADLEY, J., REARDON, C. L., SHI, L., BELIAEV, A. S., MARSHALL, M. J., WANG, Z., WATMOUGH, N. J., FREDRICKSON, J. K., ZACHARA, J. M., BUTT, J. N. & RICHARDSON, D. J. 2011. Structure of a bacterial cell surface decaheme electron conduit. *Proceedings of the National Academy of Sciences of the United States of America*, 108, 9384-9389.
- CLARKE, T. A., HOLLEY, T., HARTSHORNE, R. S., FREDRICKSON, J. K., ZACHARA, J. M., SHI, L. & RICHARDSON, D. J. 2008. The role of multihaem cytochromes in the respiration of nitrite in *Escherichia coli* and Fe(III) in *Shewanella oneidensis*. *Biochemical Society Transactions*, 36, 1005-1010.
- COURSOLLE, D. & GRALNICK, J. A. 2010. Modularity of the Mtr respiratory pathway of *Shewanella oneidensis* strain MR-1. *Molecular Microbiology*, 77, 995-1008.
- COURSOLLE, D. & GRALNICK, J. A. 2012. Reconstruction of extracellular respiratory pathways for iron(III) reduction in *Shewanella oneidensis* strain MR-1. *Frontiers in Microbiology*, 3, 1-11.
- COURTNEY, J., DEPLANCHE, K., REES, N. V. & MACASKIE, L. E. 2016. Biomanufacture of nano-Pd(0) by *Escherichia coli* and electrochemical activity of bio-Pd(0) made at the expense of H<sub>2</sub> and formate as electron donors. *Biotechnology Letters*, 38, 1903-1910.
- DA SILVA FERREIRA, V., CONZFERREIRA, M. E., LIMA, L. M. T. R., FRASÉS, S., DE SOUZA, W. & SANT'ANNA, C. 2017. Green production of microalgae-based silver chloride nanoparticles with antimicrobial activity against pathogenic bacteria. *Enzyme and Microbial Technology*, 97, 114-121.

- DANIEL, M.-C. & ASTRUC, D. 2004. Gold nanoparticles: Assembly, supramolecular chemistry, quantum-size-related properties, and applications toward biology, catalysis, and nanotechnology. *Chemical Reviews*, 104, 293-346.
- DE CORTE, S., HENNEBEL, T., VERSCHUERE, S., CUVELIER, C., VERSTRAETE, W. & BOON, N. 2011. Gold nanoparticle formation using *Shewanella oneidensis*: a fast biosorption and slow reduction process. *Journal of Chemical Technology and Biotechnology*, 86, 547-553.
- DE WINDT, W., AELTERMAN, P. & VERSTRAETE, W. 2005. Bioreductive deposition of palladium (0) nanoparticles on *Shewanella oneidensis* with catalytic activity towards reductive dechlorination of polychlorinated biphenyls. *Environmental Microbiology*, 7, 314-325.
- DE WINDT, W., BOON, N., VAN DEN BULCKE, J., RUBBERECHT, L., PRATA, F., MAST, J., HENNEBEL, T. & VERSTRAETE, W. 2006. Biological control of the size and reactivity of catalytic Pd(0) produced by *Shewanella oneidensis*. *Antonie van Leeuwenhoek*, 90, 377-389.
- DEL RÍO, E., GAONA, D., HERNÁNDEZ-GARRIDO, J. C., CALVINO, J. J., BASALLOTE, M. G., FERNÁNDEZ-TRUJILLO, M. J., PÉREZ-OMIL, J. A. & GATICA, J. M. 2014. Speciation-controlled incipient wetness impregnation: A rational synthetic approach to prepare sub-nanosized and highly active ceria-zirconia supported gold catalysts. *Journal of Catalysis*, 318, 119-127.
- DEPLANCHE, K., CALDELARI, I., MIKHEENKO, I. P., SARGENT, F. & MACASKIE, L. E. 2010. Involvement of hydrogenases in the formation of highly catalytic Pd(0) nanoparticles by bioreduction of Pd(II) using *Escherichia coli* mutant strains. *Microbiology*, 156, 2630-2640.
- DEPLANCHE, K. & MACASKIE, L. E. 2008. Biorecovery of gold by *Escherichia coli* and *Desulfovibrio desulfuricans*. *Biotechnology and Bioengineering*, 99, 1055-1064.
- DHAND, C., DWIVEDI, N., LOH, X. J., YING, A. N. J., VERMA, N. K., BEUERMAN, R. W., LAKSHMINARAYANAN, R. & RAMAKRISHNA, S. 2015. Methods and strategies for the synthesis of diverse nanoparticles and their applications: a comprehensive overview. *RSC Advances*, 5, 105003-105037.

- DONNELLY, C. W. 2014. From Pasteur to probiotics: A historical overview of cheese and microbes. *In: DONNELLY, C. W. (ed.) Cheese and microbes.* Washington, DC: ASM Press.
- DREXLER, K. E. 1986. *Engines of creation: the coming era of nanotechnology,* Garden City, NY, Anchor Press / Doubleday.
- DU, L., JIANG, H., LIU, X. & WANG, E. 2007. Biosynthesis of gold nanoparticles assisted by *Escherichia coli* DH5alpha and its application on direct electrochemistry of hemoglobin. *Electrochemistry Communications*, 9, 1165-1170.
- DUNBAR, C. E., HIGH, K. A., JOUNG, J. K., KOHN, D. B., OZAWA, K. & SADELAIN, M. 2018. Gene therapy comes of age. *Science*, 359, eaan4672.
- DURAND, G. A., RAOULT, D. & DUBOURG, G. 2019. Antibiotic discovery: history, methods and perspectives. *International Journal of Antimicrobial Agents*, 53, 371-382.
- DURKAN, C. 2019. *Size really does matter: the nanotechnology revolution,* London, UK, World Scientific Publishing Europe Ltd.
- DURÁN, N., MARCATO, P. D., ALVES, O. L., DE SOUZA, G. I. H. & ESPOSITO, E. 2005. Mechanistic aspects of biosynthesis of silver nanoparticles by several *Fusarium oxysporum* strains. *Journal of Nanobiotechnology*, 3.
- DYKMAN, L. A. & KHLEBTSOV, N. G. 2011. Gold nanoparticles in biology and medicine: Recent advances and prospects. *Acta Naturae*, 3, 34-55.
- EALIAS, A. M. & SARAVANAKUMAR, M. P. 2017. A review on the classification, characterisation, synthesis of nanoparticles and their application. *IOP Conference Series: Materials Science and Engineering*, 263, 032019.
- EDWARDS, M. J., BAIDEN, N. A., JOHS, A., TOMANICEK, S. J., LIANG, L., SHI, L., FREDRICKSON, J. K., ZACHARA, J. M., GATES, A. J., BUTT, J. N., RICHARDSON, D. J. & CLARKE, T. A. 2014. The X-ray crystal structure of *Shewanella oneidensis* OmcA reveals new insight at the microbe-mineral interface. *FEBS Letters*, 588, 1886-1890.
- EIGLER, D. M. & SCHWEIZER, E. K. 1990. Positioning single atoms with a scanning tunnelling microscope. *Nature*, 344, 524-526.

- EL-SAYED, I. H., HUANG, X. & EL-SAYED, M. A. 2005. Surface plasmon resonance scattering and absorption of anti-EGFR antibody conjugated gold nanoparticles in cancer diagnostics: applications in oral cancer. *Nano Letters*, 5, 829-834.
- EUGENIO, M., MÜLLER, N., FRASÉS, S., ALMEIDA-PAES, R., LIMA, L. M. T. R., LEMGRUBER, L., FARINA, M., DE SOUZA, W. & SANT'ANNA, C. 2016. Yeast-derived biosynthesis of silver/silver chloride nanoparticles and their antiproliferative activity against bacteria. *RSC Advances*, 6, 9893-9904.
- EUSTIS, S. & EL-SAYED, M. A. 2006. Why gold nanoparticles are more precious than pretty gold: Noble metal surface plasmon resonance and its enhancement of the radiative and nonradiative properties of nanocrystals of different shapes. *Chemical Society Reviews*, 35, 209-217.
- FANG, X., WANG, Y., WANG, Z., JIANG, Z. & DONG, M. 2019. Microorganism assisted synthesized nanoparticles for catalytic applications. *Energies*, 12, 190.
- FARADAY, M. 1857. X. The Bakerian Lecture - Experimental relations of gold (and other metals) to light. *Philosophical Transactions of the Royal Society of London*, 147.
- FERRIS, F. G. & BEVERIDGE, T. J. 1986. Site specificity of metallic ion binding in *Escherichia coli* K-12 lipopolysaccharide. *Canadian Journal of Microbiology*, 32, 52-55.
- FEYNMAN, R. P. 1960. There's plenty of room at the bottom. *Engineering and Science*, 23, 22-36.
- FIELD, S. J., DOBBIN, P. S., CHEESMAN, M. R., WATMOUGH, N. J., THOMSON, A. J. & RICHARDSON, D. J. 2000. Purification and magneto-optical spectroscopic characterization of cytoplasmic membrane and outer membrane multiheme c-type cytochromes from *Shewanella frigidimarina* NCIMB400. *The Journal of Biological Chemistry*, 275, 8515-8522.
- FIRER-SHERWOOD, M., PULCU, G. S. & ELLIOTT, S. J. 2008. Electrochemical interrogations of the Mtr cytochromes from *Shewanella*: opening a potential window. *Journal of Biological Inorganic Chemistry*, 13, 849-854.

- FLEMMING, C. A., FERRIS, F. G., BEVERIDGE, T. J. & BAILEY, G. W. 1990. Remobilization of toxic heavy metals adsorbed to bacterial wall-clay composites. *Applied and Environmental Microbiology*, 56, 3191-3203.
- FREESTONE, I., MEEKS, N., SAX, M. & HIGGITT, C. 2007. The Lycurgus cup - A Roman nanotechnology. *Gold Bulletin*, 40, 270-277.
- GAHLAWAT, G. & CHOUDHURY, A. R. 2019. A review on the biosynthesis of metal and metal salt nanoparticles by microbes. *RSC Advances*, 9, 12944-12967.
- GANACHARI, S. V., BHAT, R., DESHPANDE, R. & VENKATARAMAN, A. 2012. Extracellular biosynthesis of silver nanoparticles using fungi *Penicillium diversum* and their antimicrobial activity studies. *BioNanoScience*, 2, 316-321.
- GAO, H., BARUA, S., LIANG, Y., WU, L., DONG, Y., REED, S., CHEN, J., CULLEY, D., KENNEDY, D., YANG, Y., HE, Z., NEALSON, K. H., FREDRICKSON, J. K., TIEDJE, J. M., ROMINE, M. & ZHOU, J. 2010. Impacts of *Shewanella oneidensis* c-type cytochromes on aerobic and anaerobic respiration. *Microbial Biotechnology*, 3, 455-466.
- GARDEA-TORRESDEY, J. L., PARSONS, J. G., GOMEZ, E., PERALTA-VIDEA, J., TROIANI, H. E., SANTIAGO, P. & YACAMAN, M. J. 2002. Formation and growth of Au nanoparticles inside live alfalfa plants. *Nano Letters*, 2, 397-401.
- GERICKE, M. & PINCHES, A. 2006. Biological synthesis of metal nanoparticles. *Hydrometallurgy*, 83, 132-140.
- GERRARD, T. L., TELFORD, J. N. & WILLIAMS, H. H. 1974. Detection of selenium deposits in *Escherichia coli* by electron microscopy. *Journal of Bacteriology*, 119, 1057-1060.
- GESCHER, J. S., CORDOVA, C. D. & SPORMANN, A. M. 2008. Dissimilatory iron reduction in *Escherichia coli*: identification of CymA of *Shewanella oneidensis* and NapC of *E. coli* as ferric reductases. *Molecular Microbiology*, 68, 706-719.
- GIMENO, M. C. 2008. The chemistry of gold. In: LAGUNA, A. (ed.) *Modern supramolecular gold chemistry: gold-metal interactions and applications*. Weinheim, Germany: WILEY-VCH Verlag GmbH & Co. KGaA.



- GODALE, C. H. & SHARON, M. 2019. Contemporary history of nanotechnology. In: SHARON, M. (ed.) *History of nanotechnology: from prehistoric to modern times*. Beverly, MA: Scrivener Publishing.
- GOEL, A. 2006. *Colloidal chemistry*, New Delhi, India, Discovery Publishing House.
- GOMEZ-BOLIVAR, J., MIKHEENKO, I. P., OROZCO, R. L., SHARMA, S., BANERJEE, D., WALKER, M., HAND, R. A., MERROUN, M. L. & MACASKIE, L. E. 2019. Synthesis of Pd/Ru bimetallic nanoparticles by *Escherichia coli* and potential as a catalyst for upgrading 5-hydroxymethyl furfural into liquid fuel precursors. *Frontiers in Microbiology*, 10, 1276.
- GOODHEW, P. J., HUMPHREYS, J. & BEANLAND, R. 2001. *Electron microscopy and analysis*, Boca Raton, FL, CRC Press.
- GORBY, Y. A., YANINA, S., MCLEAN, J. S., ROSSO, K. M., MOYLES, D., DOHNALKOVA, A., BEVERIDGE, T. J., CHANG, I. S., KIM, B. H., KIM, K. S., CULLEY, D. E., REED, S. B., ROMINE, M. F., SAFFARINI, D. A., HILL, E. A., SHI, L., ELIAS, D. A., KENNEDY, D. W., PINCHUK, G., WATANABE, K., ISHII, S., LOGAN, B., NEALSON, K. H. & FREDRICKSON, J. K. 2006. Electrically conductive bacterial nanowires produced by *Shewanella oneidensis* strain MR-1 and other microorganisms. *Proceedings of the National Academy of Sciences of the United States of America*, 103, 11358-11363.
- GREQUE DE MORAIS, M., GUIMARÃES MARTINS, V., STEFFENS, D., PRANKE, P. & VIEIRA DA COSTA, J. A. 2014. Biological applications of nanobiotechnology. *Journal of Nanoscience and Nanotechnology*, 14, 1007-1017.
- GUO, D., XIE, G. & LUO, J. 2014. Mechanical properties of nanoparticles: basics and applications. *Journal of Physics D: Applied Physics*, 47, 013001.
- GURUNATHAN, S., KALISHWARALAL, K., VAIDYANATHAN, R., DEEPAK, V., PANDIAN, S. R. K., MUNIYANDI, J., HARIHARAN, N. & EOM, S. H. 2009. Biosynthesis, purification and characterization of silver nanoparticles using *Escherichia coli*. *Colloids and Surfaces B: Biointerfaces*, 74, 328-335.
- HAISS, W., THANH, N. T. K., AVEYARD, J. & FERNIG, D. G. 2007. Determination of size and concentration of gold nanoparticles from UV-Vis spectra. *Analytical Chemistry*, 79, 4215-4221.

- HARDEN, D. B. & TOYNBEE, J. M. C. 1959. The Rothschild Lycurgus Cup. *Archaeologia*, 97, 179-212.
- HARGITTAI, M., SCHULZ, A., RÉFFY, B. & KOLONITS, M. 2001. Molecular structure, bonding, and Jahn-Teller effect in gold chlorides: Quantum chemical study of AuCl<sub>3</sub>, Au<sub>2</sub>Cl<sub>6</sub>, AuCl<sub>4</sub><sup>-</sup>, AuCl, and Au<sub>2</sub>Cl<sub>2</sub> and electron diffraction study of Au<sub>2</sub>Cl<sub>6</sub>. *Journal of the American Chemical Society*, 123, 1449-1458.
- HARTSHORNE, R. S., JEPSON, B. N., CLARKE, T. A., FIELD, S. J., FREDRICKSON, J., ZACHARA, J., SHI, L., BUTT, J. N. & RICHARDSON, D. J. 2007. Characterization of *Shewanella oneidensis* MtrC: a cell-surface decaheme cytochrome involved in respiratory electron transport to extracellular electron acceptors. *Journal of Biological Inorganic Chemistry*, 12, 1083-1094.
- HARTSHORNE, R. S., REARDON, C. L., ROSS, D., NUESTER, J., CLARKE, T. A., GATES, A. J., MILLS, P. C., FREDRICKSON, J. K., ZACHARA, J. M., SHI, L., BELIAEV, A. S., MARSHALL, M. J., TIEN, M., BRANTLEY, S., BUTT, J. N. & RICHARDSON, D. J. 2009. Characterization of an electron conduit between bacteria and the extracellular environment. *Proceedings of the National Academy of Sciences of the United States of America*, 106, 22169-22174.
- HE, S., GUO, Z., ZHANG, Y., ZHANG, S., WANG, J. & GU, N. 2007. Biosynthesis of gold nanoparticles using the bacteria *Rhodospseudomonas capsulata*. *Materials Letters*, 61, 3984-3987.
- HEIDELBERG, J. F., PAULSEN, I. T., NELSON, K. E., GAIDOS, E. J., NELSON, W. C., READ, T. D., EISEN, J. A., SESHADRI, R., WARD, N., METHE, B., CLAYTON, R. A., MEYER, T., TSAPIN, A., SCOTT, J., BEANAN, M., BRINKAC, L., DAUGHERTY, S., DEBOY, R. T., DODSON, R. J., DURKIN, A. S., HAFT, D. H., KOLONAY, J. F., MADUPU, R., PETERSON, J. D., UMayAM, L. A., WHITE, O., WOLF, A. M., VAMATHEVAN, J., WEIDMAN, J., IMPRAIM, M., LEE, K., BERRY, K., LEE, C., MUELLER, J., KHOURI, H., GILL, J., UTTERBACK, T. R., MCDONALD, L. A., FELDBLYUM, T. V., SMITH, H. O., VENTER, J. C., NEALSON, K. H. & FRASER, C. M. 2002. Genome sequence of the

- dissimilatory metal ion-reducing bacterium *Shewanella oneidensis*.  
*Nature Biotechnology*, 20, 1118-1123.
- HEINZ, H., PRAMANIK, C., HEINZ, O., DING, Y., MISHRA, R. K., MARCHON, D.,  
FLATT, R. J., ESTRELA-LOPIS, I., LLOP, J., MOYA, S. & ZIOLO, R. F. 2017.  
Nanoparticle decoration with surfactants: Molecular interactions,  
assembly, and applications. *Surface Science Reports*, 72, 1-58.
- HENCH, L. L. & WEST, J. K. 1990. The Sol-Gel process. *Chemical Reviews*, 90, 33-  
72.
- HOMBERGER, M. & SIMON, U. 2010. On the application potential of gold  
nanoparticles in nanoelectronics and biomedicine. *Philosophical  
Transactions of the Royal Society A*, 368, 1405-1453.
- HONDOU, N., BRYDSON, R., WANG, P., HOLTON, M. D., BROWN, M. R., REES, P.,  
SUMMERS, H. D. & BROWN, A. 2012. Quantitative characterization of  
nanoparticle agglomeration within biological media. *Journal of  
Nanoparticle Research*, 14, 977.
- HORNSEY, I. S. 2003. *History of beer and brewing*, Cambridge, UK, The Royal  
Society of Chemistry.
- HORVATH, H. 2009. Gustav Mie and the scattering and absorption of light by  
particles: Historic developments and basics. *Journal of Quantitative  
Spectroscopy & Radiative Transfer*, 110, 787-799.
- HOYLE, B. & BEVERIDGE, T. J. 1983. Binding of metallic ions to the outer  
membrane of *Escherichia coli*. *Applied and Environmental Microbiology*,  
46, 749-752.
- HOYLE, B. D. & BEVERIDGE, T. J. 1984. Metal binding by the peptidoglycan  
sacculus of *Escherichia coli* K-12. *Canadian Journal of Microbiology*, 30,  
204-211.
- HUANG, B. C., YI, Y.-C., CHANG, J.-S. & NG, I.-S. 2019. Mechanism study of photo-  
induced gold nanoparticles formation by *Shewanella oneidensis* MR-1.  
*Scientific Reports*, 9, 7589.
- HULLA, J. E., SAHU, S. C. & HAYES, A. W. 2015. Nanotechnology: history and  
future. *Human and Experimental Toxicology*, 34, 1318-1321.

- IDA, T. 2007. Characterization methods for nanostructure of materials. *In:* HOSOKAWA, M., NOGI, K., NAITO, M. & YOKOYAMA, T. (eds.) *Nanoparticle technology handbook*. Amsterdam, The Netherlands: Elsevier B.V.
- IRAVANI, S., KORBKANDI, H., MIRMOHAMMADI, S. V. & ZOLFAGHARI, B. 2014. Synthesis of silver nanoparticles: chemical, physical and biological methods. *Research in Pharmaceutical Sciences*, 9, 385-406.
- ISHIKI, K., OKADA, K., LE, D. Q., SHIIGI, H. & NAGAOKA, T. 2017. Investigation concerning the formation process of gold nanoparticles by *Shewanella oneidensis* MR-1. *Analytical Sciences*, 33, 129-131.
- JAIN, K. K. 2007. Applications of nanobiotechnology in clinical diagnostics. *Clinical Chemistry*, 53, 2002-2009.
- JAMES, L. K. 1993. *Nobel laureates in chemistry, 1901-1992*, Washington, DC, American Chemical Society and Chemical Heritage Foundation.
- JENA, J., PRADHAN, N., NAYAK, R. R., DASH, B. P., SUKLA, L. B., PANDA, P. K. & MISHRA, B. K. 2014. Microalga *Scenedesmus* sp.: A potential low-cost green machine for silver nanoparticle synthesis. *Journal of Microbiology and Biotechnology*, 24, 522-533.
- JENSEN, H. M., ALBERS, A. E., MALLEY, K. R., LONDER, Y. Y., COHEN, B. E., HELMS, B. A., WEIGELE, P., GROVES, J. T. & AJO-FRANKLIN, C. M. 2010. Engineering of a synthetic electron conduit in living cells. *Proceedings of the National Academy of Sciences of the United States of America*, 107, 19213-19218.
- JEONG, H., BARBE, V., LEE, C. H., VALLENET, D., YU, D. S., CHOI, S.-H., COULOUX, A., LEE, S.-W., YOON, S. H., CATTOLICO, L., HUR, C.-G., PARK, H.-S., SÉGURENS, B., KIM, S. C., OH, T. K., LENSKI, R. E., STUDIER, F. W., DAEGELEN, P. & KIM, J. F. 2009. Genome sequences of *Escherichia coli* B strains REL606 and BL21(DE3). *Journal of Molecular Biology*, 394, 644-652.
- JIANG, W., SAXENA, A., SONG, B., WARD, B. B., BEVERIDGE, T. J. & MYNENI, S. C. B. 2004. Elucidation of functional groups on Gram-positive and Gram-

- negative bacterial surfaces using infrared spectroscopy. *Langmuir*, 20, 11433-11442.
- JOGLER, C. & SCHULER, D. 2009. Genomics, genetics, and cell biology of magnetosome formation. *Annual Review of Microbiology*, 63, 501-521.
- KALIMUTHU, K., BABU, R. S., VENKATARAMAN, D., BILAL, M. & GURUNATHAN, S. 2008. Biosynthesis of silver nanocrystals by *Bacillus licheniformis*. *Colloids and Surfaces B: Biointerfaces*, 65, 150-153.
- KALISHWARALAL, K., DEEPAK, V., RAMKUMARPANDIAN, S., NELLAIAH, H. & SANGILIYANDI, G. 2008. Extracellular biosynthesis of silver nanoparticles by the culture supernatant of *Bacillus licheniformis*. *Materials Letters*, 62, 4411-4413.
- KANG, S. H., BOZHILOV, K. N., MYUNG, N. V., MULCHANDANI, A. & CHEN, W. 2008. Microbial synthesis of CdS nanocrystals in genetically engineered *E. coli*. *Angewandte Chemie-International Edition*, 47, 5186-5189.
- KARTHIKEYAN, S. & BEVERIDGE, T. J. 2002. *Pseudomonas aeruginosa* biofilms react with and precipitate toxic soluble gold. *Environmental Microbiology*, 4, 667-675.
- KAUL, R. K., KUMAR, P., BURMAN, U., JOSHI, P., AGRAWAL, A., RALIYA, R. & TARAFDAR, J. C. 2012. Magnesium and iron nanoparticles production using microorganisms and various salts. *Materials Science-Poland*, 30, 254-258.
- KHAN, I., SAEED, K. & KHAN, I. 2017. Nanoparticles: Properties, applications and toxicities. *Arabian Journal of Chemistry*.
- KHLEBTSOV, B. N. & KHLEBTSOV, N. G. 2011. On the measurement of gold nanoparticle sizes by the dynamic light scattering method. *Colloid Journal*, 73, 118-127.
- KHOT, L. R., SANKARAN, S., MAJA, J. M., EHSANI, R. & SCHUSTER, E. W. 2012. Applications of nanomaterials in agricultural production and crop protection: A review. *Crop Protection*, 35, 64-70.
- KIM, K. D., HAN, D. N. & KIM, H. T. 2004. Optimization of experimental conditions based on the Taguchi robust design for the formation of nano-sized silver

- particles by chemical reduction method. *Chemical Engineering Journal*, 104, 55-61.
- KIM, M., OSONE, S., KIM, T., HIGASHI, H. & SETO, T. 2017. Synthesis of nanoparticles by laser ablation: a review. *KONA Powder and Particle Journal*, 34, 80-90.
- KITAGAWA, M., ARA, T., ARIFUZZAMAN, M., IOKA-NAKAMICHI, T., INAMOTO, E., TOYONAGA, H. & MORI, H. 2005. Complete set of ORF clones of *Escherichia coli* ASKA library (a complete set of *E. coli* K-12 ORF archive): Unique resources for biological research. *DNA Research*, 12, 291-299.
- KOBAYASHI, M., TOMITA, S., SAWADA, K., SHIBA, K., YANAGI, H., YAMASHITA, I. & URAOKA, Y. 2012. Chiral meta-molecules consisting of gold nanoparticles and genetically engineered tobacco mosaic virus. *Optics Express*, 20, 24856-24863.
- KONG, F.-Y., ZHANG, J.-W., LI, R.-F., WANG, Z.-X., WANG, W.-J. & WANG, W. 2017. Unique roles of gold nanoparticles in drug delivery, targeting and imaging applications. *Molecules*, 22.
- KOROBUSHKINA, E. D., KARAVAIKO, G. I. & KOROBUSHKIN, I. M. 1983. Biochemistry of gold. *Ecological Bulletins*, 35, 325-333.
- KOUZUMA, A., KASAI, T., HIROSE, A. & WATANABE, K. 2015. Catabolic and regulatory systems in *Shewanella oneidensis* MR-1 involved in electricity generation in microbial fuel cells. *Frontiers in Microbiology*, 6.
- KRACKE, F., VASSILEV, I. & KROMER, J. O. 2015. Microbial electron transport and energy conservation - the foundation for optimizing bioelectrochemical systems. *Frontiers in Microbiology*, 6.
- KUDR, J., HADDAD, Y., RICHTER, L., HEGER, Z., CERNAK, M., ADAM, V. & ZITKA, O. 2017. Magnetic nanoparticles: From design and synthesis to real world applications. *Nanomaterials*, 7.
- KULKARNI, R. R., SHAIWALE, N. S., DEOBAGKAR, D. N. & DEOBAGKAR, D. D. 2015. Synthesis and extracellular accumulation of silver nanoparticles by employing radiation-resistant *Deinococcus radiodurans*, their characterization, and determination of bioactivity. *International Journal of Nanomedicine*, 10, 963-974.

- KUMAR, N. & KUMBHAT, S. 2016. *Essentials in nanoscience & nanotechnology*, Hoboken, NJ, John Wiley & Sons, Inc.
- KUMAR, S. A., ABYANEH, M. K., GOSAVI, S. W., KULKARNI, S. K., PASRICHA, R., AHMAD, A. & KHAN, M. I. 2007. Nitrate reductase-mediated synthesis of silver nanoparticles from AgNO<sub>3</sub>. *Biotechnology Letters*, 29, 439-445.
- KWON, K. C., JO, E., KWON, Y.-W., LEE, B., RYU, J. H., LEE, E. J., KIM, K. & LEE, J. 2017. Superparamagnetic gold nanoparticles synthesized on protein particle scaffolds for cancer theragnosis. *Advanced Materials*, 29.
- LEARMAN, D. R., YI, H., BROWN, S. D., MARTIN, S. L., GEESEY, G. G., STEVENS, A. M. & HOCELLA JR., M. F. 2009. Involvement of *Shewanella oneidensis* MR-1 LuxS in biofilm development and sulfur metabolism. *Applied and Environmental Microbiology*, 75, 1301-1307.
- LEE, J., MAHENDRA, S. & ALVAREZ, P. J. J. 2010. Nanomaterials in the construction industry: A review of their applications and environmental health and safety considerations. *ACS Nano*, 4, 3580-3590.
- LEE, K., CONBOY, M., PARK, H. M., JIANG, F., KIM, H. J., DEWITT, M. A., MACKLEY, V. A., CHANG, K., RAO, A., SKINNER, C., SHOBHA, T., MEHDIPOUR, M., LIU, H., HUANG, W.-C., LAN, F., BRAY, N. L., LI, S., CORN, J. E., KATAOKA, K., DOUDNA, J. A., CONBOY, I. & MURTHY, N. 2017. Nanoparticle delivery of Cas9 ribonucleoprotein and donor DNA in vivo induces homology-directed DNA repair. *Nature Biomedical Engineering*, 1, 889-901.
- LEE, N.-Y., KO, W.-C. & HSUEH, P.-R. 2019. Nanoparticles in the treatment of infections caused by multidrug-resistant organisms. *Frontiers in Pharmacology*, 10, 1153.
- LEE, S. Y. 1996. High cell-density culture of *Escherichia coli*. *Trends in Biotechnology*, 14, 98-105.
- LEMIRE, J. A., HARRISON, J. J. & TURNER, R. J. 2013. Antimicrobial activity of metals: mechanisms, molecular targets and applications. *Nature Reviews Microbiology*, 11, 371-384.
- LEONG, S. S., YEAP, S. P. & LIM, J. K. 2016. Working principle and application of magnetic separation for biomedical diagnostic at high- and low-field gradients. *Interface Focus*, 6, 20160048.

- LEVSKAYA, A., CHEVALIER, A. A., TABOR, J. J., SIMPSON, Z. B., LAVERY, L. A., LEVY, M., DAVIDSON, E. A., SCOURAS, A., ELLINGTON, A. D., MARCOTTE, E. M. & VOIGT, C. A. 2005. Engineering *Escherichia coli* to see light. *Nature*, 438, 441-442.
- LI, D.-B., CHENG, Y.-Y., WU, C., LI, W.-W., LI, N., YANG, Z.-C., TONG, Z.-H. & YU, H.-Q. 2014. Selenite reduction by *Shewanella oneidensis* MR-1 is mediated by fumarate reductase in periplasm. *Scientific Reports*, 4.
- LI, J., WU, Q. & WU, J. 2016. Synthesis of nanoparticles via solvothermal and hydrothermal methods. In: ALIOFKHAZRAEI, M. (ed.) *Handbook of nanoparticles*. Cham, Switzerland: Springer International Publishing AG Switzerland.
- LI, V. L. 2014. *Advancing silver nanostructures towards antibacterial applications*. Doctor of Philosophy, RMIT University.
- LI, X., XU, H., CHEN, Z.-S. & CHEN, G. 2011. Biosynthesis of nanoparticles by microorganisms and their applications. *Journal of Nanomaterials*, 1-16.
- LIDE, D. R. 1993. *CRC handbook of chemistry and physics*, Boca Raton, FL, CRC Press, Inc.
- LIN, Z., YE, Y., LI, Q., XU, Z. & WANG, M. 2011. A further insight into the biosorption mechanism of Au(III) by infrared spectrometry. *BMC Biotechnology*, 11, 98.
- LIU, C., GORBY, Y. A., ZACHARA, J. M., FREDRICKSON, J. K. & BROWN, C. F. 2002. Reduction kinetics of Fe(III), Co(III), U(VI), Cr(VI), and Tc(VII) in cultures of dissimilatory metal-reducing bacteria. *Biotechnology and Bioengineering*, 80, 637-649.
- LLOYD, J. R., BYRNE, J. M. & COKER, V. S. 2011. Biotechnological synthesis of functional nanomaterials. *Current Opinion in Biotechnology*, 22, 509-515.
- LLOYD, J. R., COLE, J. A. & MACASKIE, L. E. 1997. Reduction and removal of heptavalent technetium from solution by *Escherichia coli*. *Journal of Bacteriology*, 179, 2014-2021.
- LOHSE, A., ULLRICH, S., KATZMANN, E., BORG, S., WANNER, G., RICHTER, M., VOIGT, B., SCHWEDER, T. & SCHULER, D. 2011. Functional analysis of the



- magnetosome island in *Magnetospirillum gryphiswaldense*: The *mamAB* operon is sufficient for magnetite biomineralization. *PLoS ONE*, 6.
- LOWER, B. H. & BAZYLINSKI, D. A. 2013. The bacterial magnetosome: A unique prokaryotic organelle. *Journal of Molecular Microbiology and Biotechnology*, 23, 63-80.
- LU, A.-H., SALABAS, E. L. & SCHUTH, F. 2007. Magnetic nanoparticles: Synthesis, protection, functionalization, and application. *Angewandte Chemie International Edition*, 46, 1222-1244.
- LUND, P., TRAMONTI, A. & DE BIASE, D. 2014. Coping with low pH: molecular strategies in neutrophilic bacteria. *FEMS Microbiology Reviews*, 38, 1091-1125.
- LUTZ, S. & IAMURRI, S. M. 2018. Protein engineering: Past, present, and future. *In: BORNSCHEUER, U. T. & HÖHNE, M. (eds.) Protein engineering: Methods and protocols*. New York, NY: Humana Press.
- MABBETT, A. N., SANYAHUMBI, D., YONG, P. & MACASKIE, L. E. 2006. Biorecovered precious metals from industrial wastes: Single-step conversion of a mixed metal liquid waste to a bioinorganic catalyst with environmental application. *Environmental Science & Technology*, 40, 1015-1021.
- MACDONELL, M. T. & COLWELL, R. R. 1985. Phylogeny of the vibronaceae, and recommendation for two new genera, *Listonella* and *Shewanella*. *Systematic and Applied Microbiology*, 6, 171-182.
- MADIGAN, M. T., MARTINKO, J. M., STAHL, D. A. & CLARK, D. P. 2012. *Brock biology of microorganisms*, San Francisco, CA, Benjamin Cummings.
- MAIER, S. A. 2007. *Plasmonics: fundamentals and applications*, New York, NY, Springer Science+Business Media LLC.
- MAINE, E., THOMAS, V. J., BLIEMEL, M., MURIRA, A. & UTTERBACK, J. 2014. The emergence of the nanobiotechnology industry. *Nature Nanotechnology*, 9, 2-5.
- MANZONI, C., KIA, D. A., VANDROVCOVA, J., HARDY, J., WOOD, N. W., LEWIS, P. A. & FERRARI, R. 2018. Genome, transcriptome and proteome: The rise of

- omics data and their integration in biomedical sciences. *Briefings in Bioinformatics*, 19, 286-302.
- MARRITT, S. J., LOWE, T. G., BYE, J., MCMILLAN, D. G. G., SHI, L., FREDRICKSON, J., ZACHARA, J., RICHARDSON, D. J., CHEESMAN, M. R., JEUKEN, L. J. C. & BUTT, J. N. 2012. A functional description of CymA, an electron-transfer hub supporting anaerobic respiratory flexibility in *Shewanella*. *Biochemical Journal*, 444, 465-474.
- MARSHALL, M. J., BELIAEV, A. S., DOHNALKOVA, A. C., KENNEDY, D. W., SHI, L., WANG, Z., BOYANOV, M. I., LAI, B., KEMNER, K. M., MCLEAN, J. S., REED, S. B., CULLEY, D. E., BAILEY, V. L., SIMONSON, C. J., SAFFARINI, D. A., ROMINE, M. F., ZACHARA, J. M. & FREDRICKSON, J. K. 2006. c-Type cytochrome-dependent formation of U(IV) nanoparticles by *Shewanella oneidensis*. *Plos Biology*, 4, 1324-1333.
- MARSHALL, M. J., PLYMALE, A. E., KENNEDY, D. W., SHI, L., WANG, Z., REED, S. B., DOHNALKOVA, A. C., SIMONSON, C. J., LIU, C., SAFFARINI, D. A., ROMINE, M. F., ZACHARA, J. M., BELIAEV, A. S. & FREDRICKSON, J. K. 2008. Hydrogenase- and outer membrane c-type cytochrome-facilitated reduction of technetium(VII) by *Shewanella oneidensis* MR-1. *Environmental Microbiology*, 10, 125-136.
- MARSHALL, M. R. 2010. Ash analysis. In: NIELSEN, S. S. (ed.) *Food analysis*. Fourth ed. New York, NY: Springer Science+Business Media, LLC.
- MARSILI, E., BARON, D. B., SHIKHARE, I. D., COURSOLE, D., GRALNICK, J. A. & BOND, D. R. 2008. *Shewanella* secretes flavins that mediate extracellular electron transfer. *Proceedings of the National Academy of Sciences of the United States of America*, 105, 3968-3973.
- MATHEW, J., JOY, J. & GEORGE, S. C. 2018. Potential applications of nanotechnology in transportation: A review. *Journal of King Saud University - Science*.
- MAYER, F. 1993. Cell structure. In: REHM, H.-J., REED, G., PUHLER, A. & STADLER, P. (eds.) *Biotechnology*. Second ed. Weinheim, Federal Republic of Germany: VCH Verlagsgesellschaft mbH.

- MCGOVERN, P. E., GLUSKER, D. L., EXNER, L. J. & VOIGT, M. M. 1996. Neolithic resinated wine. *Nature*, 381, 480-481.
- MCGOVERN, P. E. & MONDAVI, R. G. 2007. *Ancient wine: The search for the origins of viniculture*, Princeton, NJ, Princeton University Press.
- MIE, G. 1908. Beiträge zur optik trüber medien, speziell kolloidaler metallösungen. *Annalen der Physik*, 330, 377-445.
- MIKHEENKO, I. P., ROUSSET, M., DEMENTIN, S. & MACASKIE, L. E. 2008. Bioaccumulation of palladium by *Desulfovibrio fructosivorans* wild-type and hydrogenase-deficient strains. *Applied and Environmental Microbiology*, 74, 6144-6146.
- MODY, V. V., SIWALE, R., SINGH, A. & MODY, H. R. 2010. Introduction to metallic nanoparticles. *Journal of Pharmacy & BioAllied Sciences*, 2, 282-289.
- MOEINZADEH, S. & JABBARI, E. 2017. Nanoparticles and their applications. In: BHUSHAN, B. (ed.) *Springer handbook of nanotechnology*. Fourth ed. Berlin, Germany: Springer-Verlag GmbH.
- MOMA, J. A., NTHO, T. A. & SCURRELL, M. 2016. Gold-catalysed reactions. In: MISHRA, N. K. (ed.) *Catalytic application of nano-gold catalysts*. Rijeka, Croatia: InTech.
- MOURDIKODIS, S., PALLARES, R. M. & THANH, N. T. K. 2018. Characterization techniques for nanoparticles: comparison and complementarity upon studying nanoparticle properties. *Nanoscale*, 10, 12871-12934.
- MUKHERJEE, P., AHMAD, A., MANDAL, D., SENAPATI, S., SAINKAR, S. R., KHAN, M. I., RAMANI, R., PARISCHA, R., AJAYAKUMAR, P. V., ALAM, M., SASTRY, M. & KUMAR, R. 2001. Bioreduction of AuCl<sub>4</sub><sup>-</sup> ions by the fungus, *Verticillium sp.* and surface trapping of the gold nanoparticles formed. *Angewandte Chemie - International Edition*, 40, 3585-3588.
- MULLEN, M. D., WOLF, D. C., FERRIS, F. G., BEVERIDGE, T. J., FLEMMING, C. A. & BAILEY, G. W. 1989. Bacterial sorption of heavy metals. *Applied and Environmental Microbiology*, 55, 3143-3149.
- MULVANEY, P. 1996. Surface plasmon spectroscopy of nanosized metal particles. *Langmuir*, 12, 788-800.

- MURAT, D., QUINLAN, A., VALI, H. & KOMEILI, A. 2010. Comprehensive genetic dissection of the magnetosome gene island reveals the step-wise assembly of a prokaryotic organelle. *Proceedings of the National Academy of Sciences of the United States of America*, 107, 5593-5598.
- MUÑOZ-VILLAGRÁN, C., CONTRERAS, F., CORNEJO, F., FIGUEROA, M., VALENZUELA-BEZANILLA, D., LURASCHI, R., REINOSO, C., RIVAS-PARDO, J., VÁSQUEZ, C., CASTRO, M. & ARENAS, F. 2020. Understanding gold toxicity in aerobically-grown *Escherichia coli*. *Biological Research*, 53, 26.
- MYERS, C. R. & MYERS, J. M. 1997. Cloning and sequence of *cymA*, a gene encoding a tetraheme cytochrome *c* required for reduction of iron(III), fumarate, and nitrate by *Shewanella putrefaciens* MR-1. *Journal of Bacteriology*, 179, 1143-1152.
- MYERS, C. R. & NEALSON, K. H. 1988. Bacterial manganese reduction and growth with manganese oxide as the sole electron acceptor. *Science*, 240, 1319-1321.
- MYERS, J. M. & MYERS, C. R. 1998. Isolation and sequence of *omcA*, a gene encoding a decaheme outer membrane cytochrome *c* of *Shewanella putrefaciens* MR-1, and detection of *omcA* homologs in other strains of *S. putrefaciens*. *Biochimica et Biophysica Acta*, 1373, 237-251.
- MYERS, J. M. & MYERS, C. R. 2003. Overlapping role of the outer membrane cytochromes of *Shewanella oneidensis* MR-1 in the reduction of manganese(IV) oxide. *Letters in Applied Microbiology*, 37, 21-25.
- NARAYANAN, R. & EL-SAYED, M. A. 2008. Some aspects of colloidal nanoparticle stability, catalytic activity, and recycling potential. *Topics in Catalysis*, 47, 15-21.
- NASROLLAHZADEH, M., SAJADI, S. M., SAJJADI, M. & ISSAABADI, Z. 2019. An introduction to nanotechnology. In: NASROLLAHZADEH, M., SAJADI, S. M., SAJJADI, M., ISSAABADI, Z. & ATAROD, M. (eds.) *An introduction to green nanotechnology*. London, UK: Academic Press.
- NAURÚ IDALIA, V.-M. & BERNARDO, F. 2017. *Escherichia coli* as a model organism and its application in biotechnology. In: SAMIE, A. (ed.)

*Escherichia coli: Recent advances on physiology, pathogenesis and biotechnological applications*. Rijeka, Croatia: InTech.

- NEWMAN, T. H., WILLIAMS, K. E. & PEASE, R. F. W. 1987. High resolution patterning system with a single bore objective lens. *Journal of Vacuum Science & Technology B: Microelectronics Processing and Phenomena*, 5, 88-91.
- NEWSOME, L., MORRIS, K. & LLOYD, J. R. 2014. The biogeochemistry and bioremediation of uranium and other priority radionuclides. *Chemical Geology*, 363, 164-184.
- NG, C. K., SIVAKUMAR, K., LIU, X., MADHAIYAN, M., JI, L., YANG, L., TANG, C., SONG, H., KJELLEBERG, S. & CAO, B. 2013a. Influence of outer membrane c-type cytochromes on particle size and activity of extracellular nanoparticles produced by *Shewanella oneidensis*. *Biotechnology and Bioengineering*, 110, 1831-1837.
- NG, C. K., TAN, T. K. C., SONG, H. & CAO, B. 2013b. Reductive formation of palladium nanoparticles by *Shewanella oneidensis*: role of outer membrane cytochromes and hydrogenases. *RSC Advances*, 3, 22498-22503.
- NIEMEYER, C. M. & MIRKIN, C. A. 2004. Preface. In: NIEMEYER, C. M. & MIRKIN, C. A. (eds.) *Nanobiotechnology: concepts, applications and perspectives*. Weinheim, Germany: WILEY-VCH Verlag GmbH & Co. KGaA.
- NIES, D. H. 1999. Microbial heavy-metal resistance. *Applied Microbiology and Biotechnology*, 51, 730-750.
- NIIDE, T., GOTO, M. & KAMIYA, N. 2011. Biocatalytic synthesis of gold nanoparticles with cofactor regeneration in recombinant *Escherichia coli* cells. *Chemical Communications*, 47, 7350-7352.
- NIKAM, A. V., PRASAD, B. L. V. & KULKARNI, A. A. 2018. Wet chemical synthesis of metal oxide nanoparticles: a review. *CrystEngComm*, 20, 5091-5107.
- ORENDORFF, C. J., SAU, T. K. & MURPHY, C. J. 2006. Shape-dependent plasmon-resonant gold nanoparticles. *Small*, 2, 636-639.

- PAN, P. & WOOD, S. A. 1991. Gold-chloride complexes in very acidic aqueous solutions and at temperatures 25-300 °C: A laser Raman spectroscopic study. *Geochimica et Cosmochimica Acta*, 55, 2365-2371.
- PANTIDOS, N. & HORSFALL, L. E. 2014. Biological synthesis of metallic nanoparticles by bacteria, fungi and plants. *Journal of Nanomedicine & Nanotechnology*, 5, 233.
- PARASHAR, M., SHUKLA, V. K. & SINGH, R. 2020. Metal oxides nanoparticles via sol-gel method: a review on synthesis, characterization and applications. *Journal of Materials Science: Materials in Electronics*, 31, 3729-3749.
- PARK, T. J., LEE, K. G. & LEE, S. Y. 2016. Advances in microbial biosynthesis of metal nanoparticles. *Applied Microbiology and Biotechnology*, 100, 521-534.
- PARK, T. J., LEE, S. Y., HEO, N. S. & SEO, T. S. 2010. In vivo synthesis of diverse metal nanoparticles by recombinant *Escherichia coli*. *Angewandte Chemie-International Edition*, 49, 7019-7024.
- PATEL, A. K., SINGHANIA, R. R. & PANDEY, A. 2017. Production, purification, and application of microbial enzymes. In: BRAHMACHARI, G., DEMAIN, A. L. & ADRIANO, J. L. (eds.) *Biotechnology of microbial enzymes: Production, biocatalysts and industrial applications*. London, UK: Academic Press.
- PETIT, S. & MADEJOVA, J. 2013. Fourier transform infrared spectroscopy. In: BERGAYA, F. & LAGALY, G. (eds.) *Handbook of clay science - part B: techniques and applications*. Second ed. Amsterdam, The Netherlands: Elsevier Ltd.
- PINCHUK, G. E., GEYDEBREKHT, O. V., HILL, E. A., REED, J. L., KONOPKA, A. E., BELIAEV, A. S. & FREDRICKSON, J. K. 2011. Pyruvate and lactate metabolism by *Shewanella oneidensis* MR-1 under fermentation, oxygen limitation, and fumarate respiration conditions. *Applied and Environmental Microbiology*, 77, 8234-8240.
- PIRBADIAN, S., BARCHINGER, S. E., LEUNG, K. M., BYUN, H. S., JANGIR, Y., BOUHENNI, R. A., REED, S. B., ROMINE, M. F., SAFFARINI, D. A., SHI, L., GORBY, Y. A., GOLBECK, J. H. & EL-NAGGAR, M. Y. 2014. *Shewanella oneidensis* MR-1 nanowires are outer membrane and periplasmic

extensions of the extracellular electron transport components.

*Proceedings of the National Academy of Sciences of the United States of America*, 111, 12883-12888.

- PITTS, K. E., DOBBIN, P. S., REYES-RAMIREZ, F., THOMSON, A. J., RICHARDSON, D. J. & SEWARD, H. E. 2003. Characterization of the *Shewanella oneidensis* MR-1 decaheme cytochrome MtrA. *The Journal of Biological Chemistry*, 278, 27758-27765.
- POOLE JR., C. P. & OWENS, F. J. 2003. *Introduction to nanotechnology*, Hoboken, NJ, John Wiley & Sons, Inc.
- PRIESTLEY, R. E., MANSFIELD, A., BYE, J., DEPLANCHE, K., JORGE, A. B., BRETT, D., MACASKIE, L. E. & SHARMA, S. 2015. Pd nanoparticles supported on reduced graphene-*E. coli* hybrid with enhanced crystallinity in bacterial biomass. *RSC Advances*, 5, 84093-84103.
- QU, Y., YOU, S., ZHANG, X., PEI, X., SHEN, W., LI, Z., LI, S. & ZHANG, Z. 2018. Biosynthesis of gold nanoparticles using cell-free extracts of *Magnusiomyces ingens* LH-F1 for nitrophenols reduction. *Bioprocess and Biosystems Engineering*, 41, 359-367.
- RAFFI, M., RUMAIZ, A. K., HASAN, M. M. & ISMAT SHAH, S. 2007. Studies of the growth parameters for silver nanoparticle synthesis by inert gas condensation. *Journal of Materials Research*, 22, 3378-3384.
- RAI, M., INGLE, A. P., GUPTA, I. R., BIRLA, S. S., YADAV, A. P. & ABD-ELSALAM, K. A. 2013. Potential role of biological systems in formation of nanoparticles: mechanism of synthesis and biomedical applications. *Current Nanoscience*, 9, 576-587.
- RAJ, R., DALEI, K., CHAKRABORTY, J. & DAS, S. 2016. Extracellular polymeric substances of a marine bacterium mediated synthesis of CdS nanoparticles for removal of cadmium from aqueous solution. *Journal of Colloid and Interface Science*, 462, 166-175.
- RAJPUT, S., WEREZUK, R., LANGE, R. M. & MCDERMOTT, M. T. 2016. Fungal isolate optimized for biogenesis of silver nanoparticles with enhanced colloidal stability. *Langmuir*, 32, 8688-8697.

- RAMSTEDT, M., LEONE, L., PERSSON, P. & SHCHUKAREV, A. 2014. Cell wall composition of *Bacillus subtilis* changes as a function of pH and Zn<sup>2+</sup> exposure: insights from Cryo-XPS measurements. *Langmuir*, 30, 4367-4374.
- RANJITHA, V. R. & RAI, V. R. 2017. Actinomycetes mediated synthesis of gold nanoparticles from the culture supernatant of *Streptomyces griseoruber* with special reference to catalytic activity. *3 Biotech*, 7, 299.
- RAWLINGS, A. E., BRAMBLE, J. P., TANG, A. A. S., SOMNER, L. A., MONNINGTON, A. E., COOKE, D. J., MCPHERSON, M. J., TOMLINSON, D. C. & STANILAND, S. S. 2015. Phage display selected magnetite interacting Adhirons for shape controlled nanoparticle synthesis. *Chemical Science*, 6, 5586-5594.
- REHM, H.-J. & PRAVE, P. 1987. Biotechnology - History, Processes, and Products. In: PRAVE, P., FAUST, U., SITTIG, W. & SUKATSCH, D. A. (eds.) *Basic Biotechnology*. Weinheim, Federal Republic of Germany: VCH Verlagsgesellschaft mbH.
- REZA GHORBANI, H., AKBAR SAFEKORDI, A., ATTAR, H. & REZAYAT SORKHABADI, S. M. 2011. Biological and non-biological methods for silver nanoparticles synthesis. *Chemical and Biochemical Engineering Quarterly*, 25, 317-326.
- RICHARDSON, D. J., BUTT, J. N., FREDRICKSON, J. K., ZACHARA, J. M., SHI, L., EDWARDS, M. J., WHITE, G., BAIDEN, N., GATES, A. J., MARRITT, S. J. & CLARKE, T. A. 2012. The 'porin-cytochrome' model for microbe-to-mineral electron transfer. *Molecular Microbiology*, 85, 201-212.
- ROSHMI, T., SOUMYA, K. R., JYOTHIS, M. & RADHAKRISHNAN, E. K. 2015. Effect of biofabricated gold nanoparticle-based antibiotic conjugates on minimum inhibitory concentration of bacterial isolates of clinical origin. *Gold Bulletin*, 48, 63-71.
- SADLER, P. J. 1976. The biological chemistry of gold: advances in understanding with modern techniques. *Gold Bulletin*, 9, 110-118.
- SALTIEL, C., CHEN, Q., MANICKAVASAGAM, S., SCHADLER, L. S., SIEGEL, R. W. & MENGUC, M. P. 2004. Identification of the dispersion behavior of surface treated nanoscale powders. *Journal of Nanoparticle Research*, 6, 35-46.



- SAMBROOK, J. & RUSSELL, D. W. 2001. *Molecular cloning - a laboratory manual*, Cold Spring Harbor, Cold Spring Harbor Laboratory Press.
- SANZ-MEDEL, A. & PEREIRO, R. 2014. *Atomic absorption spectrometry: an introduction*, New York, NY, Momentum Press, LLC.
- SARDAR, M., MISHRA, A. & AHMAD, R. 2014. Biosynthesis of metal nanoparticles and their applications. *In: TIWARI, A. & TURNER, A. P. F. (eds.) Biosensors nanotechnology*. Salem, MA: Scrivener Publishing LLC.
- SAVVAIDIS, I., KARAMUSHKA, V. I., LEE, H. & TREVORS, J. T. 1998. Micro-organism-gold interactions. *BioMetals*, 11, 69-78.
- SAWERS, R. G. & CLARK, D. P. 2004. Fermentative pyruvate and acetyl-Coenzyme A metabolism. *EcoSal Plus*.
- SCHAMING, D. & REMITA, H. 2015. Nanotechnology: from the ancient time to nowadays. *Foundations of Chemistry*, 17, 187-205.
- SCHRÖFEL, A., KRATOSOVA, G., SAFARIK, I., SAFARIKOVA, M., RASKA, I. & SHOR, L. M. 2014. Applications of biosynthesized metallic nanoparticles - A review. *Acta Biomaterialia*, 10, 4023-4042.
- SCIMECA, M., BISCHETTI, S., LAMSIRA, H. K., BONFIGLIO, R. & BONANNO, E. 2018. Energy dispersive X-ray (EDX) microanalysis: A powerful tool in biomedical research and diagnosis. *European Journal of Histochemistry*, 62, 2841.
- SCOTT, G. D. 1995. A study of the Lycurgus Cup. *Journal of Glass Studies*, 37, 51-64.
- SCRAGG, A. H. 1988. Biotechnology. *In: SCRAGG, A. H. (ed.) Biotechnology for engineers - biological systems in technological processes*. Chichester, UK: Ellis Horwood Limited.
- SCUDINO, S., SAKALIYSKA, M., SURREDDI, K. B. & ECKERT, J. 2009. Mechanical alloying and milling of Al-Mg alloys. *Journal of Alloys and Compounds*, 483, 2-7.
- SENAPATI, S., SYED, A., MOEEZ, S., KUMAR, A. & AHMAD, A. 2012. Intracellular synthesis of gold nanoparticles using alga *Tetraselmis kochinensis*. *Materials Letters*, 79, 116-118.

- SEVIN, D. C., FUHRER, T., ZAMBONI, N. & SAUER, U. 2017. Nontargeted *in vitro* metabolomics for high-throughput identification of novel enzymes in *Escherichia coli*. *Nature Methods*, 14, 187-194.
- SHAKIBAIE, M., FOROOTANFAR, H., MOLLAZADEH-MOGHADDAM, K., BAGHERZADEH, Z., NAFISSI-VARCHEH, N., SHAHVERDI, A. R. & FARAMARZI, M. A. 2010. Green synthesis of gold nanoparticles by the marine microalga *Tetraselmis suecica*. *Biotechnology and Applied Biochemistry*, 57, 71-75.
- SHANKAR, S. S., AHMAD, A., PASRICHA, R. & SASTRY, M. 2003. Bioreduction of chloroaurate ions by geranium leaves and its endophytic fungus yields gold nanoparticles of different shapes. *Journal of Materials Chemistry*, 13, 1822-1826.
- SHANKAR, S. S., RAI, A., ANKAMWAR, B., SINGH, A., AHMAD, A. & SASTRY, M. 2004. Biological synthesis of triangular gold nanoprisms. *Nature Materials*, 3, 482-488.
- SHI, L., CHEN, B., WANG, Z., ELIAS, D. A., MAYER, M. U., GORBY, Y. A., NI, S., LOWER, B. H., KENNEDY, D. W., WUNSCHER, D. S., MOTTAZ, H. M., MARSHALL, M. J., HILL, E. A., BELIAEV, A. S., ZACHARA, J. M., FREDRICKSON, J. K. & SQUIER, T. C. 2006. Isolation of a high-affinity functional protein complex between OmcA and MtrC: Two outer membrane decaheme c-type cytochromes of *Shewanella oneidensis* MR-1. *Journal of Bacteriology*, 188, 4705-4714.
- SHI, L., ROSSO, K. M., CLARKE, T. A., RICHARDSON, D. J., ZACHARA, J. M. & FREDRICKSON, J. K. 2012. Molecular underpinnings of Fe(III) oxide reduction by *Shewanella oneidensis* MR-1. *Frontiers in Microbiology*, 3, 50.
- SHI, L., SQUIER, T. C., ZACHARA, J. M. & FREDRICKSON, J. K. 2007. Respiration of metal (hydr)oxides by *Shewanella* and *Geobacter*: a key role for multiheme c-type cytochromes. *Molecular Microbiology*, 65, 12-20.
- SI, R. & FLYTZANI-STEPHANOPOULOS, M. 2008. Shape and crystal-plane effects of nanoscale ceria on the activity of Au-CeO<sub>2</sub> catalysts for the water-gas shift reaction. *Angewandte Chemie-International Edition*, 47, 2884-2887.

- SIH, B. C. & WOLF, M. O. 2005. Metal nanoparticle-conjugated polymer nanocomposites. *Chemical Communications*, 0, 3375-3384.
- SIMCHI, A., AHMADI, R., SEYED REIHANI, S. M. & MAHDAVI, A. 2007. Kinetics and mechanisms of nanoparticle formation and growth in vapor phase condensation process. *Materials and Design*, 28, 850-856.
- SLEATOR, R. D. & HILL, C. 2001. Bacterial osmoadaptation: the role of osmolytes in bacterial stress and virulence. *FEMS Microbiology Reviews*, 26, 49-71.
- SMITH, J. E. 2009. *Biotechnology*, Cambridge, UK, Cambridge University Press.
- SRIRAMULU, M. & SUMATHI, S. 2018. Biosynthesis of palladium nanoparticles using *Saccharomyces cerevisiae* extract and its photocatalytic degradation behaviour. *Advances in Natural Sciences: Nanoscience and Nanotechnology*, 9, 025018.
- SRIVASTAVA, S. K., YAMADA, R., OGINO, C. & KONDO, A. 2013. Biogenic synthesis and characterization of gold nanoparticles by *Escherichia coli* K12 and its heterogeneous catalysis in degradation of 4-nitrophenol. *Nanoscale Research Letters*, 8.
- STANILAND, S. S. & RAWLINGS, A. E. 2016. Crystallizing the function of the magnetosome membrane mineralization protein Mms6. *Biochemical Society Transactions*, 44, 883-890.
- STOCKWELL, S. 2017. *Modern biotechnology : Defining and solving human problems*, New York, NY, Momentum Press, LLC.
- STUDIER, F. W. & MOFFATT, B. A. 1986. Use of bacteriophage T7 RNA polymerase to direct selective high-level expression of cloned genes. *Journal of Molecular Biology*, 189, 113-130.
- SUNKAR, S. & NACHIYAR, C. V. 2012. Biogenesis of antibacterial silver nanoparticles using the endophytic bacterium *Bacillus cereus* isolated from *Garcinia xanthochymus*. *Asian Pacific Journal of Tropical Biomedicine*, 2, 953-959.
- SURESH, A. K., PELLETIER, D. A., WANG, W., BROICH, M. L., MOON, J.-W., GU, B., ALLISON, D. P., JOY, D. C., PHELPS, T. J. & DOKTYCZ, M. J. 2011. Biofabrication of discrete spherical gold nanoparticles using the metal-

- reducing bacterium *Shewanella oneidensis*. *Acta Biomaterialia*, 7, 2148-2152.
- SURESH, A. K., PELLETIER, D. A., WANG, W., MOON, J.-W., GU, B., MORTENSEN, N. P., ALLISON, D. P., JOY, D. C., PHELPS, T. J. & DOKTYCZ, M. J. 2010. Silver nanocrystallites: biofabrication using *Shewanella oneidensis*, and an evaluation of their comparative toxicity on Gram-negative and Gram-positive bacteria. *Environmental Science & Technology*, 44, 5210-5215.
- SUZUKI, H. 2013. Microbial production of amino acids and their derivatives for use in foods, nutraceuticals and medications. *In*: MCNEIL, B., ARCHER, D., GIAVASIS, I. & HARVEY, L. (eds.) *Microbial production of food ingredients, enzymes and nutraceuticals*. Cambridge, UK: Woodhead Publishing Limited.
- SYCH, J. M., LACROIX, C. & STEVENS, M. J. A. 2016. Vitamin B<sub>12</sub> - Physiology, production and application. *In*: VANDAMME, E. J. & REVUELTA, J. L. (eds.) *Industrial biotechnology of vitamins, biopigments and antioxidants*. Weinheim, Germany: Wiley-VCH Verlag GmbH & Co. KGaA.
- TADROS, T. F. 2015. *Interfacial phenomena and colloid stability - basic principles*, Berlin, Germany, Walter De Gruyter GmbH.
- TANAKA, M., ARAKAKI, A. & MATSUNAGA, T. 2010. Identification and functional characterization of liposome tubulation protein from magnetotactic bacteria. *Molecular Microbiology*, 76, 480-488.
- TANIGUCHI, N. On the basic concept of "nano-technology". Proceedings of the international conference on production engineering (part II), 1974 Tokyo. The Japan Society of Precision Engineering and International Institution for Production Engineering Research, 18-23.
- TAVAKOLI, A., SOHRABI, M. & KARGARI, A. 2007. A review of methods for synthesis of nanostructured metals with emphasis on iron compounds. *Chemical Papers*, 61, 151-170.
- TCHERNIAK, A., HA, J. W., DOMINGUEZ-MEDINA, S., SLAUGHTER, L. S. & LINK, S. 2010. Probing a century old prediction one plasmonic particle at a time. *Nano Letters*, 10, 1398-1404.

- TEO, B. K. & SUN, X. H. 2006. From top-down to bottom-up to hybrid nanotechnologies: Road to nanodevices. *Journal of Cluster Science*, 17, 529-540.
- THOMPSON, D. 2007. Michael Faraday's recognition of ruby gold: the birth of modern nanotechnology. *Gold Bulletin*, 40, 267-269.
- TIKHONOVA, T. V. & POPOV, V. O. 2014. Structural and functional studies of multiheme cytochromes c involved in extracellular electron transport in bacterial dissimilatory metal reduction. *Biochemistry (Moscow)*, 79, 1584-1601.
- TORGEMAN, E. 2017. *Biosynthesis of gold and palladium nanoparticles via bacteria*. Master in Chemistry, University of Oslo.
- TOSHIMA, N. 2004. Metal nanoparticles for catalysis. In: LIZ-MARZÁN, L. M. & KAMAT, P. V. (eds.) *Nanoscale materials*. Dordrecht, The Netherlands: Kluwer Academic Publishers.
- UNDEN, G., STEINMETZ, P. A. & DEGREIF-DUNNWALD, P. 2014. The aerobic and anaerobic respiratory chain of *Escherichia coli* and *Salmonella enterica*: enzymes and energetics. *EcoSal Plus*.
- VALDEN, M., LAI, X. & GOODMAN, D. W. 1998. Onset of catalytic activity of gold clusters on titania with the appearance of nonmetallic properties. *Science*, 281, 1647-1650.
- VENKATESWARAN, K., MOSER, D. P., DOLLHOPF, M. E., LIES, D. P., SAFFARINI, D. A., MACGREGOR, B. J., RINGELBERG, D. B., WHITE, D. C., NISHIJIMA, M., SANO, H., BURGHARDT, J., STACKEBRANDT, E. & NEALSON, K. H. 1999. Polyphasic taxonomy of the genus *Shewanella* and description of *Shewanella oneidensis* sp. nov. *International Journal of Systematic Bacteriology*, 49, 705-724.
- VOLLATH, D. 2013. *Nanomaterials - an introduction to synthesis, properties, and applications*, Weinheim, Germany, Wiley-VCH Verlag GmbH & Co. KGaA.
- VON CANSTEIN, H., OGAWA, J., SHIMIZU, S. & LLOYD, J. R. 2008. Secretion of flavins by *Shewanella* species and their role in extracellular electron transfer. *Applied and Environmental Microbiology*, 74, 615-623.

- WALKER, S. G., FLEMMING, C. A., FERRIS, F. G., BEVERIDGE, T. J. & BAILEY, G. W. 1989. Physicochemical interaction of *Escherichia coli* cell envelopes and *Bacillus subtilis* cell walls with two clays and ability of the composite to immobilize heavy metals from solution. *Applied and Environmental Microbiology*, 55, 2976-2984.
- WALTER, P., WELCOMME, E., HALLÉGOT, P., ZALUZEC, N. J., DEEB, C., CASTAING, J., VEYSSIÈRE, P., BRÉLIAUX, R., LÉVEQUE, J.-L. & TSOUCARIS, G. 2006. Early use of PbS nanotechnology for an ancient hair dyeing formula. *Nano Letters*, 6, 2215-2219.
- WANG, L., HU, C. & SHAO, L. 2017. The antimicrobial activity of nanoparticles: present situation and prospects for the future. *International Journal of Nanomedicine*, 12, 1227-1249.
- WAUTELET, M. 2009. *Nanotechnologies*, London, UK, The Institution of Engineering and Technology.
- WEN, Y. & XIA, D. 2018. A thermodynamics model for morphology prediction of aluminum nano crystals fabricated by the inert gas condensation method. *Nanotechnology*, 29, 125301.
- WHITE, G. F., SHI, Z., SHI, L., WANG, Z., DOHNALKOVA, A. C., MARSHALL, M. J., FREDRICKSON, J. K., ZACHARA, J. M., BUTT, J. N., RICHARDSON, D. J. & CLARKE, T. A. 2013. Rapid electron exchange between surface-exposed bacterial cytochromes and Fe(III) minerals. *Proceedings of the National Academy of Sciences of the United States of America*, 110, 6346-6351.
- WILKS, J. C., KITKO, R. D., CLEETON, S. H., LEE, G. E., UGWU, C. S., JONES, B. D., BONDURANT, S. S. & SLONCZEWSKI, J. L. 2009. Acid and base stress and transcriptomic responses in *Bacillus subtilis*. *Applied and Environmental Microbiology*, 75, 981-990.
- WILLIAMS, J. M. & PETERSON, S. W. 1969. A novel example of the  $[H_5O_2]^+$  ion. A neutron diffraction study of  $HAuCl_4 \cdot 4H_2O$ . *Journal of the American Chemical Society*, 91, 776-777.
- WOODRUFF, H. B. 2014. Selman A. Waksman, winner of the 1952 Nobel Prize for Physiology or Medicine. *Applied and Environmental Microbiology*, 80, 2-8.

- WREN, A. W., LAFFIR, F. R., MELLOTT, N. P. & TOWLER, M. R. 2011. X-ray photoelectron spectroscopy: studies from industrial & bioactive glass to biomaterials. In: WAGNER, J. M. (ed.) *X-ray photoelectron spectroscopy*. New York, NY: Nova Science Publishers, Inc.
- WU, J. & IZPISUA BELMONTE, J. C. 2016. Stem cells: A renaissance in human biology research. *Cell*, 165, 1572-1585.
- WU, J.-W. & NG, I.-S. 2017. Biofabrication of gold nanoparticles by *Shewanella* species. *Bioresources and Bioprocessing*, 4, 50.
- WU, R., CUI, L., CHEN, L., WANG, C., CAO, C., SHENG, G., YU, H. & ZHAO, F. 2013. Effects of bio-Au nanoparticles on electrochemical activity of *Shewanella oneidensis* wild type and  $\Delta omcA/mtrC$  mutant. *Scientific Reports*, 3.
- XIA, Y. N., XIONG, Y. J., LIM, B. & SKRABALAK, S. E. 2009. Shape-controlled synthesis of metal nanocrystals: Simple chemistry meets complex physics? *Angewandte Chemie International Edition*, 48, 60-103.
- XU, J. X., SIRIWARDANA, K., ZHOU, Y., ZOU, S. & ZHANG, D. 2018. Quantification of gold nanoparticle ultraviolet-visible extinction, absorption, and scattering cross-section spectra and scattering depolarization spectra: the effects of nanoparticle geometry, solvent composition, ligand functionalization, and nanoparticle aggregation. *Analytical Chemistry*, 90, 785-793.
- XUE, Y., LI, X., LI, H. & ZHANG, W. 2014. Quantifying thiol-gold interactions towards the efficient strength control. *Nature Communications*, 5, 4348.
- YANG, J., LI, S., HUANG, X., LI, J., LI, L., PAN, Y. & LI, Y. 2013. MamX encoded by the *mamXY* operon is involved in control of magnetosome maturation in *Magnetospirillum gryphiswaldense* MSR-1. *BMC Microbiology*, 13.
- YANG, X., SU, L.-J., LA ROSA, F. G., SMITH, E. E., SCHLAEPFER, I. R., CHO, S. K., KAVANAGH, B., PARK, W. & FLAIG, T. W. 2017. The antineoplastic activity of photothermal ablative therapy with targeted gold nanorods in an orthotopic urinary bladder cancer model. *Bladder Cancer*, 3, 201-210.
- YANG, Y., MATSUBARA, S., XIONG, L., HAYAKAWA, T. & NOGAMI, M. 2007. Solvothermal synthesis of multiple shapes of silver nanoparticles and their SERS properties. *Journal of Physical Chemistry C*, 111, 9095-9104.

- YE, N., YAN, T., JIANG, Z., WU, W. & FANG, T. 2018. A review: Conventional and supercritical hydro/solvothermal synthesis of ultrafine particles as cathode in lithium battery. *Ceramics International*, 44, 4521-4537.
- YEH, Y.-C., CRERAN, B. & ROTELLO, V. M. 2012. Gold nanoparticles: preparation, properties, and applications in bionanotechnology. *Nanoscale*, 4, 1871-1880.
- ZHANG, H., TANG, X., MUNSKE, G. R., TOLIC, N., ANDERSON, G. A. & BRUCE, J. E. 2009. Identification of protein-protein interactions and topologies in living cells with chemical cross-linking and mass spectrometry. *Molecular & Cellular Proteomics*, 8, 409-420.



# *A p p e n d i c e s*

*If, then, your hand or your foot makes you stumble,  
cut it off and throw it away from you.*

*It is better for you to enter into life maimed or lame  
than to be thrown with two hands or two feet into the everlasting fire.*

*Also, if your eye makes you stumble,  
tear it out and throw it away from you.*

*It is better for you to enter one-eyed into life  
than to be thrown with two eyes into the fiery Gehenna*

*Matthew 18:8-9*



## 11 Appendix I

---

This appendix section discusses the tests made to check the gene deletions performed by the research group led by Prof. Jeffrey Gralnick from the University of Minnesota to create mutants of *S. oneidensis* MR-1 lacking specific proteins and cytochromes. These mutants were kindly sent to us by Gralnick's group and were applied in our studies. The strain BG148, kindly provided by Dr. Matthew J. Marshall from Pacific Northwest National Laboratory, was not tested for deletion because this bacterium does not contain gene deletion, instead it has a transposon insertion.

All strains provided by Prof. Gralnick had their gene removals checked and confirmed, however for mutant JG1176 not all cytochromes removed had deletions confirmed. These are OmcA, MtrC, MtrF, MtrA and CctA. In the case of the first four cytochromes listed, two attempts were made, but the amount of base pairs sequenced were too small to reach a definition on the exact parts that were deleted. For the case of CctA the deletion was not checked, because it was considered that the presence or absence of this cytochrome was irrelevant for this study. It should be noted, however, that all strains and cytochromes checked had their deletions confirmed. Therefore, it can be expected that the cytochromes that were not checked are indeed absent from the cells.

The procedures for testing the deletions took essentially four steps. First, a region of interest within the genome was PCR (polymerase chain reaction) amplified, the amplification was then confirmed with an agarose gel, the PCR product was purified from the gel and sent for sequencing. These procedures were all conducted following standard molecular biology techniques. DNA sequencing took place at the Core Genomic Facility of The University of Sheffield, which utilises Applied Biosystems' 3730 DNA Analyser.

**Table 11.1** contains the sequence of the primers used for checking the deletions and **Table 11.2** has a description of the PCR reactions conducted. The results for each reaction are then detailed afterwards.

**Table 11.1:** Primers used for checking deletions in the mutant strains of *Shewanella oneidensis* MR-1.

Primer n.	Sequence
P1	CGACGTACTIONCAAAGTCCATCCAATAAAC
P2	CGTAAAATCTTCTAAGCCTTTGCTAATGTGTGACT
P3	TAGAAAGATCCAAGTCACACATTAGCAAAGGC
P4	TTGCTCTGGCGTCATTTTCTCATCCC
P5	TCGTTACGGTTCGATTGGCTATTTGAGAAATATCA
P6	GATATTTCCCTGCAATAGTTTTAATCATCATTAAACACATATCAAATAAG
P7	TTTTTTCCCTGCATAGTTTGGCATTG
P8	AGTTCAACAAGCTTTAAACAATGTCATTTCAAATTAATAATTTGACA
P9	TACCTTGACGCCCTGTTTGGGG
P10	ATCGATAATTCAATTCCTTATGGTGTTTTTGAGAATGATTTTCTTT
P11	GCTCACCTTGGTAGCGCTTCT
P12	GCTGTAACCGGTCAAACACCTAACC
P13	TATGGGCAACACCAACTTGCATATTGCC

**Table 11.2:** Polymerase chain reactions carried out for checking the deletions in the mutant strains of *Shewanella oneidensis* MR-1.

Strain checked for deletion	ORF checked for deletion	Primers used	Results*
JG719	<i>omcA</i>	P1 and P2	1
JG731	<i>mtrC</i>	P3 and P4	2
JG635	<i>mtrF</i>	P5 and P6	3
JG749	<i>omcA</i> and <i>mtrC</i>	P4 and P1	4
JG641	<i>omcA</i> and <i>mtrF</i>	P5 and P7	5
JG636	<i>mtrC</i>	P3 and P4	6
JG636	<i>mtrF</i>	P5 and P6	Same as 3
JG596	<i>omcA</i> , <i>mtrC</i> and <i>mtrF</i>	P4 and P5	7
JG1176	<i>mtrD</i>	P8 and P9	8
JG1176	<i>dmsE</i>	P10 and P11	9
JG1176	<i>so4360</i>	P12 and P13	10

\* Explanation of the numbered results is given below.

## Result 1

The full sequence of *omcA* is presented below. The sequence underlined is the part of *omcA* that has been deleted. The sequence of the scar is described afterwards.

5' – ATGATGAAACGGTTCAATTTCAATACCGCAACAAAAGCGATGTTGGGTGCCGGTTT  
ACTTTCACCTCCTTCTCACTGGCTGCGGTGGCAGTGATGGTAAAGATGGTGAAGACGGT  
AAACCAGGCGTTGTTGGAGTTAATATCAACTCAACCTCAACCTTAAAAGCAAAATTCAC  
TAATGCCACTGTTGATGCAGGTAAAGTCACTGTCAACTTCACCCTAGAAAATGCCAATG  
GTGTAGCAGTATTAGGCTTAACCAAAGATCACGATTTGCGATTTGGTATTGCGCAATTA  
ACTCCC GTTAAAGAAAAAGTGGGAGAAACAGAAGCTGACCGCGGTTATCAATGGCAA  
GCTTATATCAATGCCAAGAAAGAACCCGGTACCGTTCATCAGGCGTTGATAACCTCAA  
TCCATCGACCCAGTTTCAAGCGAACGTTGAGTCTGCCAATAAATGCGACACTTGTTTAG  
TAGACCATGGCGATGGTAGCTACAGTTATACATACCAAGTTAACGTTGCCAATGTGACT  
GAGCCGGTAAAAGTCACTTACAGTGCAGATGCCACTCAACGTGCGACCATGGAACCTTG  
AGTACCGCAACTTGCGGCGAATGCGCATTTCGATTGGCAACCTTCAACAGGTAAAACA  
GAAGGCATTCAAACCTCGCAATGTCGTCTCTATTCAAGCATGTTATACCTGTCACCAACCA  
GAAAGCTTAGCGCTGCATGGTGGCCGTCGTATCGATATTGAAAACGTGCATCTTGCCA  
CACTGCAACCTCTGGTGATCCAGAATCAGGCAATAGCATTGAATTTACTTATATGATCCA  
TGCTATCCATAAAGGTGGCGAGCGTCATACCTTCGATGCTACCGGTGCACAAGTGCCTG  
CCCCATATAAAATTATTGGCTATGGCGGTAAGGTAATCGATTATGGCAAAGTGCATTAC  
CCCCAAAACCCAGCCGCAGATTGTGCAGCCTGTCACGTTGAAGGCGCTGGCGCACCTG  
CTAATGCCGATCTGTTCAAAGCAGATTTAAGCAATCAAGCATGTATTGGCTGTCACACT  
GAAAAACCATCTGCTCACCATAGCAGCACTGATTGTATGGCTTGCCACAATGCAACCAA  
GCCTTACGGCGGTACGGGAAGTGCAGCTAACGTCATGGCGATGTAATGAAAGCTTAT  
AACGATAGCCTTGGTTATAAAGCGAAATTCAGCAACATTGGTATTA AAAATAATGCCCT  
AACATTCGATGTACAAATTCTTGATAATAAAGATCAACCTATCGGCAAGGAATTTATTTT  
GGATCCGAGTGCATACACTAAATCGAGTATCTATTTCTCATGGGGAATAGATAAAGATT  
ACCCTGCTTATACCGCAGGTAGCAGATATAGTGATCGTGGCTTTGCATTATCAAATTCG  
AAGGTTTTCAACTTACAACGAAGCAACTAAAACCTTCACTATTGACAGTACAAATAGCAA  
CTTAAAGCTGCCAGCTGATCTAACTGGTATGAATGTTGAGTTGTATGCTGGTGTAGCAA  
CCTGTTTTAACAAGGTGGATACGGCGTTGAAGATGTTGTAGCGACCCCATGTTCTACC  
GATACTCGCTACGCTTACATCCAAGACCAACCATTCCGTTTCAAATGGAATGGAACGGGA

TACCAATTCTGCCGCTGAAAAACGTAGAGCGATTATCGATACAGCTAAGTGTTTCAGGTT  
GCCATAACAAGGAAATTGTTTCATTATGACAACGGCGTTAACTGTCAAGCTTGTCATACT  
CCTGATAAGGGTTTAAAAACTGACAACACTTACCCAGGAACTAAAGTTCCAACGAGCTT  
TGCGTGGAAGCCCACGAAAGTGAAGGCCATTATCTGAAATATGCAGGCGTACAATCT  
GGCACTGTACTAAAAACCGATTGTGCAACATGTCATACTGCTGATAAATCCAACGTAGT  
AACGGGTATCGCTTTAGGCAGATCGCCAGAGCGCGCATGGCTTTACGGCGATATTAAG  
AACAATGGTGCCGTAATTTGGGTATCTTCCGATGCTGGCGCATGCTTAAGTTGCCACCA  
GAAGTATCTGTCTGATGCAGCCAAGTCTCATATTGAAACTAACGGCGGTATCTTAAATG  
GTA TAGTGCTGCAGATGTTCAA ACTCGTGCATCTGAAAGCTGTGCAACGTGCCATACT  
CCATCGCAATTGATGGAAGCACACGGTAACTAA – 3'

Scar: 5' – GGGCCC – 3'

## Result 2

The full sequence of *mtrC* is presented below. The sequence underlined is the part of *mtrC* that has been deleted. The sequence of the scar is described afterwards.

5' – ATGATGAACGCACAAAATCAAAAATCGCACTGCTGCTCGCAGCAAGTGCCGTCAC  
CAATGGCCTTAACCGGCTGTGGTGGAAAGCGATGGTAATAACGGCAATGATGGTAGTGA  
TGGTGGTGAGCCAGCAGGTAGCATCCAGACGTTAAACCTAGATATCACTAAAGTAAGC  
TATGAAAATGGTGACCTATGGTCACTGTTTTCGCCACTAACGAAGCCGACATGCCAGT  
GATTGGTCTCGCAAATTTAGAAATCAAAAAGCACTGCAATTAATACCGGAAGGGGCG  
ACAGGCCCAGGTAATAGCGCTAACTGGCAAGGCTTAGGCTCATCAAAGAGCTATGTGCG  
ATAATAAAAACGGTAGCTATACCTTTAAATTCGACGCCTTCGATAGTAATAAGGTCTTTA  
ATGCTCAATTAACGCAACGCTTTAACGTTGTTTCTGCTGCGGGTAAATTAGCAGACGGA  
ACGACCGTTCCCGTTGCCGAAATGGTTGAAGATTTTCGACGGCCAAGGTAATGCGCCGC  
AATATACAAAAATATCGTTAGCCACGAAGTATGTGCTTCTTGCCACGTAGAAGGTGAA  
AAGATTTATACCAAGCTACTGAAGTCGAACTTGTATTTCTTGCCCACTCAAGAGTTT  
GCGGATGGTCGCGGCAAACCCCATGTCGCCTTTAGTCACTTAATTCACAATGTGCATAA  
TGCCAACAAAGCTTGGGGCAAAGACAATAAAATCCCTACAGTTGCACAAAATATTGTCC  
AAGATAATTGCCAAGTTTGTACGTTGAATCCGACATGCTACCGAGGCAAAAACTGG  
TCACGTATTCCAACAATGGAAGTCTGTTCTAGCTGTCACGTAGACATCGATTTTGCTGCG  
GGTAAAGGCCACTCTCAACA ACTCGATAACTCCA ACTGTATCGCCTGCCATAACAGCGA

CTGGACTGCTGAGTTACACACAGCCAAAACCACCGCAACTAAGAACTTGATTAATCAAT  
ACGGTATCGAGACTACCTCGACAATTAATACCGAAACTAAAGCAGCCACAATTAGTGTT  
CAAGTTGTAGATGCGAACGGTACTGCTGTTGATCTCAAGACCATCCTGCCTAAAGTGCA  
ACGCTTAGAGATCATCACCAACGTTGGTCCTAATAATGCAACCTTAGGTTATAGTGGA  
AAGATTCAATATTTGCAATCAAAAATGGAGCTCTTGATCCAAAAGCTACTATCAATGAT  
GCTGGCAAACCTGGTTTATACCACTACTAAAGACCTCAAACCTTGCCAAAACGGCGCAGA  
CAGCGACACAGCATTAGCTTTGTAGGTTGGTCAATGTGTTCTAGCGAAGGTAAGTTTG  
TAGACTGTGCAGACCCTGCATTTGATGGTGTGATGTAACCTAAGTATACCGGCATGAAA  
GCGGATTTAGCCTTTGCTACTTTGTCAGGTAAAGCACCAAGTACTCGCCACGTTGATTCT  
GTAAACATGACAGCCTGTGCCAATTGCCACACTGCTGAGTTCGAAATTCACAAAGGCAA  
ACAACATGCAGGCTTTGTGATGACAGAGCAACTATCACACACCCAAGATGCTAACGGT  
AAAGCGATTGTAGGCCTTGACGCATGTGTGACTTGTACTACTCCTGATGGCACCTATAG  
CTTTGCCAACCGTGGTGCCTAGAGCTAAACTACACAAAAAACACGTTGAAGATGCCT  
ACGGCCTCATTGGTGGCAATTGTGCCTCTTGTCACTCAGACTTCAACCTTGAGTCTTTCA  
AGAAGAAAGGCGCATTGAATACTGCCGCTGCAGCAGATAAAACAGGTCTATATTCTAC  
GCCGATCACTGCAACTTGTACTACCTGTCACACAGTTGGCAGCCAGTACATGGTCCATA  
CGAAAGAAACCCTGGAGTCTTTCGGTGCAGTTGTTGATGGCACAAAAGATGATGCTAC  
CAGTGCGGCACAGTCAGAAACCTGTTTCTACTGCCATACCCCAACAGTTGCAGATCACA  
CTAAAGTGAAAATGTAA – 3'

Scar: 5' – GCCC – 3'

### Result 3

The full sequence of *mtrF* is presented below. The sequence underlined is the part of *mtrF* that has been deleted. No scar was detected.

5' – ATGAATAAGTTTGAAGCTTTACCACGCAATACAGTCTGATGCTGCTCATTGCCAC  
GCTACTCTCTGCCTGTGGAGGCAGTGATGGTGTGATGATGGCTCACCCGGCGAGCCAGGT  
AAACCTCCGGCAATGACAATCAGCAGCCTAAATATCAGTGTAGATAAAGTCGCCATCAG  
CGATGGTATTGCCAAGTTGATTATCAAGTCAGCAACCAAGAAAACCAAGCCGTAGTG  
GGTATTCTTCCGCCACCTTTATCGCTGCGCAATTAAGTGCCTCAAGGCGCTACAGGCGCT  
GGCAATAGTAGTGAGTGGCAGCATTTTACCTCAGAAACCTGCGCCGCTTCATGTCCCGG  
CACTTTCGTCGATCATAAAAACGGCCATTATAGTTATCGCTTTAGTGCGACATTCAACGG  
CATGAATGGGGTGACATTTCTAAGTGTGATGCCACCCAACGCTTAGTGATAAAAATCGGTG

GTGATGCGCTCGCCGATGGCACTGTA~~CTCCCTATAACCAACCAACATTATGATTGGCAG~~  
TCCTCAGGCAATATGCTGGCCTATACCCGTA~~ACTTAGTCTCGATCGACACTTGTAATAGT~~  
TGCCATAGTAATTTGGCTTTCCATGGAGGACGTTATAATCAAGTTGAAACCTGTGTGAC  
CTGCCATAACAGTAAAAAAGTCAGCAATGCCGCGGATATTTTCCCGCAAATGATCCACA  
GTAAACATTTAACCGGATTCCCTCAATCCATCAGTAATTGCCAGACTTGCCATGCTGATA  
ACCCTGATTTGGCCGATCGTCAAAATTGGTACCGAGTACCGACCATGGAAGCCTGCGGT  
GCATGTCATACTCAAATCAATTTCCCTGCGGGTCAAGGCCACCCAGCGCAAACGGATAA  
TAGCAATTGCGTTGCCTGTCACAATGCAGATTGGACGGCAAACGTGCACAGTAATGCA  
GCTCAAACCTCTGCCTTGGCTCAGTTTAATGCAAGCATCAGCAGTGCCAGTATGGATGC  
CAATGGCACAATCACGGTCGCGGTGAGCCTAACCAACCCAACCACAGGAACCGCTTAT  
GCTGATAGCGCCGATAAATTTAAATTTATTAGTGA~~CTTAAGGATTTATGCTAACTGGGG~~  
AACCAGCTTCGACTACAGCAGCCGTTCTGCTCGCTCGATTAGACTTCCGGAATCAACCC  
CCATAGCAGGAAGCAATGGAACATACAGCTACAATATTTCAAGTCTCACAGTACCCGCA  
GGTACTGAGTCCGACCGTGCGGATTGGCCATTCAAGGTCGAGTGTGCGCAAAAGATA  
GTGTCTTAGTGGATTGCAGCACCGAACTGGCAGAAGTGCTTGTGATCAAATCAAGTCAC  
AGTTACTTCAATATGTCTGCATTAACCACCACAGGCAGACGCGAAGTCATCAGTAATGC  
AAAATGTGCTAGCTGCCATGGCGATCAGCAATTAACATCCATGGCGCCCGCAACGATT  
TAGCGGGTCAATGTCAGCTCTGCCACAATCCGAATATGCTCGCCGACGCCACAGCAACC  
AACCCATCGATGACATCTTTTGATTTTAAACAGTTAATCCACGGGCTCCATAGCAGCCAA  
TTTGCAGGTTTTGAAGACCTCAATTACCCTGGGAATATCGGTAATTGCGCCCAATGCCA  
CATCAACGATTCGACAGGTATCTCTACTGTAGCCCTCCCCTTAAATGCGGCCGTTCAACC  
TCTCGCGCTTAACAATGGCACCTTCACCAGTCCAATTGCCGCTGTATGTAGCAATTGTCA  
CTCAAGTGATGCAACTCAAATCATATGAGGCAACAAGGTGCAGTGTTTGCCGGAACC  
AAAGCCGATGCAACCGCAGGCACTGAAACCTGTGCATTTTGCCACGGACAAGGCACTG  
TCGCCGACGTACTCAAAGTCCATCCAATAAACTAA – 3'

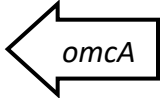
#### **Result 4**

The result for the deletion of *omcA* was the same as result 1. For the case of *mtrC*, the result was also the same as result 2, but the scar was different: 5' – ATCC – 3'.



### Result 5

The result for the deletion of *mtrF* was the same as result 3. For the case of *omcA*, the whole open reading frame was deleted and parts of the noncoding regions before the stop and after the start codons were also removed, as shown below:

5' – TATCGAC  GATATTTCCCTGCAATAGTTTTAATCATCATTAAACACAT  
ATCAAATAAGAACAAATCTCATTA – 3'

### Result 6

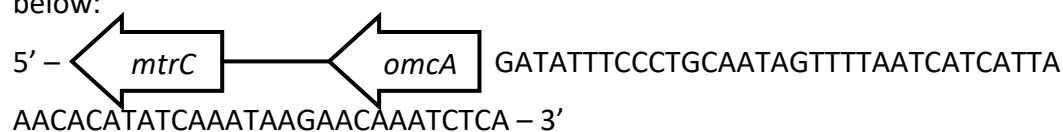
The result for the deletion of *mtrC* was different than result 2 and is presented below. The sequence underlined is the part of *mtrC* that has been deleted. No scar was detected.

5' – ATGATGAACGCACAAAAATCAAAAATCGCACTGCTGCTCGCAGCAAGTGCCGTCA  
CAATGGCCTTAACCGGCTGTGGTGGAAGCGATGGTAATAACGGCAATGATGGTAGTGA  
TGGTGGTGAGCCAGCAGGTAGCATCCAGACGTTAAACCTAGATATCACTAAAGTAAGC  
TATGAAAATGGTGACCTATGGTCACTGTTTTCGCCACTAACGAAGCCGACATGCCAGT  
GATTGGTCTCGCAAATTTAGAAATCAAAAAGCACTGCAATTAATACCGGAAGGGGCG  
ACAGGCCAGGTAATAGCGCTAACTGGCAAGGCTTAGGCTCATCAAAGAGCTATGTGC  
ATAATAAAAACGGTAGCTATACCTTTAAATTCGACGCCTTCGATAGTAATAAGGTCTTTA  
ATGCTCAATTAACGCAACGCTTTAACGTTGTTTCTGCTGCGGGTAAATTAGCAGACGGA  
ACGACCGTCCCGTTGCCGAAATGGTTGAAGATTTTCGACGGCCAAGGTAATGCGCCGC  
AATATACAAAAATATCGTTAGCCACGAAGTATGTGCTTCTTGCCACGTAGAAGGTGAA  
AAGATTTATCACCAAGCTACTGAAGTCGAACTTGTATTTCTTGCCCACTCAAGAGTTT  
GCGGATGGTCGCGGCAAACCCCATGTGCGCTTTAGTCACTTAATTCACAATGTGCATAA  
TGCCAACAAAGCTTGGGGCAAAGACAATAAAATCCCTACAGTTGCACAAAATATTGTCC  
AAGATAATTGCCAAGTTTGTACGTTGAATCCGACATGCTCACCGAGGCCAAAAACTGG  
TCACGTATTCCAACAATGGAAGTCTGTTCTAGCTGTCACGTAGACATCGATTTTGCTGCG  
GGTAAAGGCCACTCTCAACAACTCGATAACTCCAAGTATCGCCTGCCATAACAGCGA  
CTGGACTGCTGAGTTACACACAGCCAAAACCACCGCAACTAAGAAGTTGATTAATCAAT  
ACGGTATCGAGACTACCTCGACAATTAATACCGAACTAAAGCAGCCACAATTAGTGT  
CAAGTTGTAGATGCGAACGGTACTGCTGTTGATCTCAAGACCATCCTGCCTAAAGTGCA  
ACGCTTAGAGATCATACCAACGTTGGTCCTAATAATGCAACCTTAGGTTATAGTGGCA

AAGATTCAATATTTGCAATCAAAAATGGAGCTCTTGATCCAAAAGCTACTATCAATGAT  
GCTGGCAAACCTGGTTTATAACCACTACTAAAGACCTCAAACCTGGCCAAAACGGCGCAGA  
CAGCGACACAGCATTAGCTTTGTAGGTTGGTCAATGTGTTCTAGCGAAGGTAAGTTTG  
TAGACTGTGCAGACCCTGCATTTGATGGTGTGATGTAACCTAAGTATACCGGCATGAAA  
GCGGATTTAGCCTTTGCTACTTTGTCAGGTAAAGCACCAAGTACTCGCCACGTTGATTCT  
GTTAACATGACAGCCTGTGCCAATTGCCACACTGCTGAGTTCGAAATTCACAAAGGCAA  
ACAACATGCAGGCTTTGTGATGACAGAGCAACTATCACACACCCAAGATGCTAACGGT  
AAAGCGATTGTAGGCCTTGACGCATGTGTGACTTGTGATACTCCTGATGGCACCTATAG  
CTTTGCCAACCGTGGTGCCTAGAGCTAAACTACACAAAAACACGTTGAAGATGCCT  
ACGGCCTCATTGGTGGCAATTGTGCCTCTTGCTACTCAGACTTCAACCTTGAGTCTTTCA  
AGAAGAAAGGCGCATTGAATACTGCCGCTGCAGCAGATAAAACAGGTCTATATTCTAC  
GCCGATCACTGCAACTTGTACTACCTGTCACACAGTTGGCAGCCAGTACATGGTCCATA  
CGAAAGAAACCCTGGAGTCTTTCCGGTGCAGTTGTTGATGGCACAAAAGATGATGCTAC  
CAGTGCGGCACAGTCAGAAACCTGTTTCTACTGCCATACCCCAACAGTTGCAGATCACA  
CTAAAGTGAAAATGTAA – 3'

### Result 7

The result for the deletion of *mtrF* was the same as result 3. For the cases of *omcA* and *mtrC*, the whole open reading frames were deleted and part of the noncoding region after the start codon of *omcA* has been removed (nothing of the noncoding region before the stop codon of *mtrC* was deleted), as shown below:



### Result 8

The full sequence of *mtrD* is presented below. The sequence underlined is the part of *mtrD* that has been deleted. No scar was detected.

5' – ATGGACATGGATATTGGTTTAAAGTTCAACAGCATAACTCAAATTATGCTTACATTA  
ATGTTATCGATTCTCAGCCTTTCAACCTTAGCAACGCCTTGGGATGATAAGAGCTCTGA  
GGAAGTCGTAGCAACGTTAGATAAGAAGTTTGCCGAAGGTAATACTCGGCCAAAGGC  
GCTGACACTTGCTTGATGTGCCATAAGAAAAGTGCAGTTGTCATGGCTATATTTCGATGG

CGTTCATGGCAATCCCAACATCAAAGATTCCCCATGGCTGACTTACAATGTGAGGCCT  
GCCACGGCCCCGCTGGGTAATCATAACAAAGGTGGGAAAGAGCCGATGATCACCTTTGG  
CCAGAACTCCCCTGTCCCCGCACAAAAGCAAAATAGTGTCTGCATGAGCTGCCATAACG  
ACGATCAACGTATCGCTTGGAAAGGCAACCACCATGATAATGCCGATATTCCTTGCAGT  
AGCTGTCACCAAGTGCATGTCGCAAAAGATCCCATCAGCGACAAAGCCAACGAAGTCG  
CGATTTGTACCCAATGCCATAGTCAACAAAAGCCGATATGCACAAACGCTCATCGCAC  
CCTTTGCAATGGCAACAAATGGTCTGTAGTGATTGCCACAATCCCCATGGCAGTTTGAA  
TGATGCGAGTTTGAAACAAATGACCGTCAATGAAAAGTCTACAGCTGCCATGCCGAA  
AAACGTGGCCCTAAACTCTGGGAACATGCCCTGTTACGGATAATTGTGCCAACTGTCA  
TAACCCCCACGGCAGTGTGAATGAGTCAATGTTAATCAGCAAACCACCTCAATTATGCC  
AGCAGTGCCATGCCTCCGATGGCCATAGTAGTAATGCCTACTTTGGTAATCAAACCAAC  
GCCTTACCTCGGGTAATTCCTGTATGAATTGCATGGTCAAGTGCATGGTTCAAATCAC  
CCATCCGGCAAGTTGCTGCAGAGATAA – 3'

### **Result 9**

The full sequence of *dmsE* is presented below. The sequence underlined is the part of *dmsE* that has been deleted. The sequence of the scar is described afterwards.

5' – ATGAGATGGCGTAAAATTTAAACTCTGATAATGGGGGCGAGCCTGTTCCCTTATATT  
ATCTCCATCTGTTAAAGCTCAAGAAATTCATCAACTCACGAAACGGGAGAACAAATAG  
AAAAATACTCACAGATAAGTTTGCTGAAGGAAAATACTCTACTAAAGGTGCTGATAGT  
TGTTAATGTGCCATCGTAAAATAACACCGTTATGGCTATTTTTGATGGAGTACATGG  
CGATATCAATAATAGCAAATCTCCAATGGCTGGATTGCAATGTGAGGCATGTCATGGGC  
CGCTTGGACAGCATAATAAAGGAGGTAAGGAGCCAATGATTAGCTTTGGTTCTGACAG  
TCCATTGTCAGCACCGAGCCAAAATACCGTTTGTTTAGGTTGCCATCAAAAACTGAGC  
AAAGTGGCTGGCATAGCAGCTTACATAACATGGAAGAAATTGCCTGTGCTGATTGCCAT  
AAAGTCCATGCAGCTAAAGATCCGTTCTACAAAAGCAGCAGGTGAGCCAAGTGTGTA  
CTTCTTGTCATACTCGGCAGAAATCCGATATGAATAAGCGTTCATCTCATCCATTAAAGT  
GGAATGACATGACCTGCATCGATTGTCATAACCCCCACGGTTCATTTAACGAGAGCGCC  
TTAAAAAGACCTCGGTCAATGACACTTGCTATAGCTGTCATGCGGAAAAACGCGTCC  
TTTCCTGTGGGAACATGCCCTGTGACCGAAAAGTCTCCACTTGCCACAATCCCCACG  
GTAGCGTGAATGACGCCCTCGTCAAGCAGCGAGTCCCTCAGCTTTGTCAACAATGTCAT

GCCGATGATGGACATGCCAGTCGGGTAGTCACTCCGCCGGGTGCTGACGCGTTTGGTG  
CTGGTATGGGGTGTCTTAATTGTCATAGCCAAATCCATGGCTCCAACCACCTAGCGGC  
AGCAATTTTGCCCGTTGA – 3'

Scar: 5' – GGATTCGCCAAGGGCGAATTCGCCCTTTATGAATCC – 3'

### Result 10

The full sequence of *so4360* is presented below. The sequence underlined is the part of *so4360* that has been deleted. No scar was detected.

5' – ATGAAAAAATACTTTTATTTAAGCTAATTTTATTAGCGCTTTTTGCCTGTCATCGC  
TTACCATTGCTGCAGAAAATCTAGAGTCATTATTAATTAAGAAGTTTGAAGAGAAGCAA  
TATTCTAAGAGTGGTGCAGATACCTGCCTCACCTGCCATAAAAAAGATGAAAAGGTTAG  
CAGTTTTTTTAATTCAGCCATGGCATATCCAATCAAAAAGGGCCGATGGCAGGTTTAC  
AATGTGAAACCTGTCACGGGCCACAGGGTAAGCATCGTGGAAAAAATGAACCAATGAT  
CACCTTTGGTGAGCAAGGAAATATTGATATCAATAAACAAAATGGTATTTGTTTATCTTG  
CCATAAAAAATGAGATGCAAAGTGATTGGCATAATGCAGCCCATCAGCAACAAGCTTGC  
AGTAGTTGCCATAATTCACGCAGAGGTGGATCCTATATTGGCAAACGCAGTAAGCCA  
AAATAAAGTGTGTGCCGATTGCCACCAAGCAGAAAGTCATCAGACATTAATGCGTTCAT  
CACACCCGCTAACAAATGGGCAGATGACATGTA CTGTCATGGAGCACATGGCAC  
AATTAATGATGTTGATTGATAAAAAATAATATTAACCAAACCTGTTATACCTGCCATGC  
GGATAAAAGAGGGCCACTGCTTTGGGAGCATGCCCCCGTCGTTGATGATTGCACCCAT  
TGCCATAATGCTCACGGAAGTGTGAATGACAATTTATTAAGACCAGAGCGCCATTGTT  
ATGTCAGCAATGCCATAACGGTAATCCCCATGCTGCTGTGGATCAAGGCATTGCCGGCA  
CGAATGTATTTAATAGTTCAGGTAGTTGTTTAAATTGCCACAATCAAATACACGGTTCAA  
ATCATCCTTCTGGCAATAAGTTACTGAAGTAA – 3'

## 12 Appendix II

---

This appendix section presents supplementary information and figures that are relevant for the thesis but are not part of the core explanation.

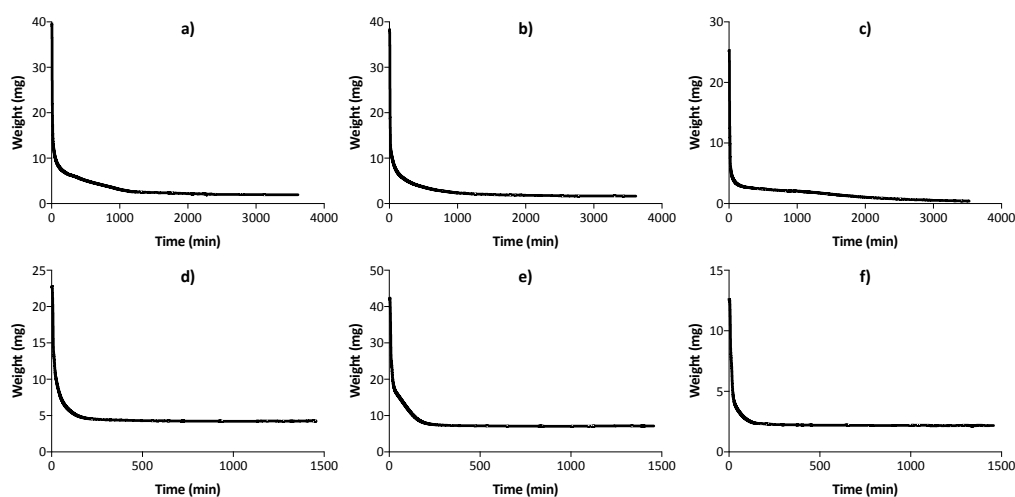


**Figure 12.1:** Examples of real TGA measurements. These examples demonstrate the reason for adopting different time in the burning step at 600 °C for the cases of samples with (24 h) and without (60 h) gold nanoparticles. Graphs a), b) and c) are the cases without nanoparticles; and graphs d), e) and f) are the cases with nanoparticles. Time zero corresponds to the moment the TGA starts raising the temperature from 105 °C to 600 °C. Therefore, at time zero samples were already dry. After reaching 600 °C, the temperature was then kept constant for 24 h or 60 h, depending on the sample. For cases a), b) and c) it took ca. 2000, 1700 and 3200 minutes for the samples to reach a constant weight, respectively; for cases d), e) and f) it took ca. 300, 350 and 250 minutes for the samples to reach a constant weight, respectively. Hence, it can be seen that for the cases of samples containing gold nanoparticles the burning process reach weight stabilisation much faster than for the cases without nanoparticles. The substantial contribution of the nanoparticles to the final weight of the ashes is hypothesised to be the cause of this difference.

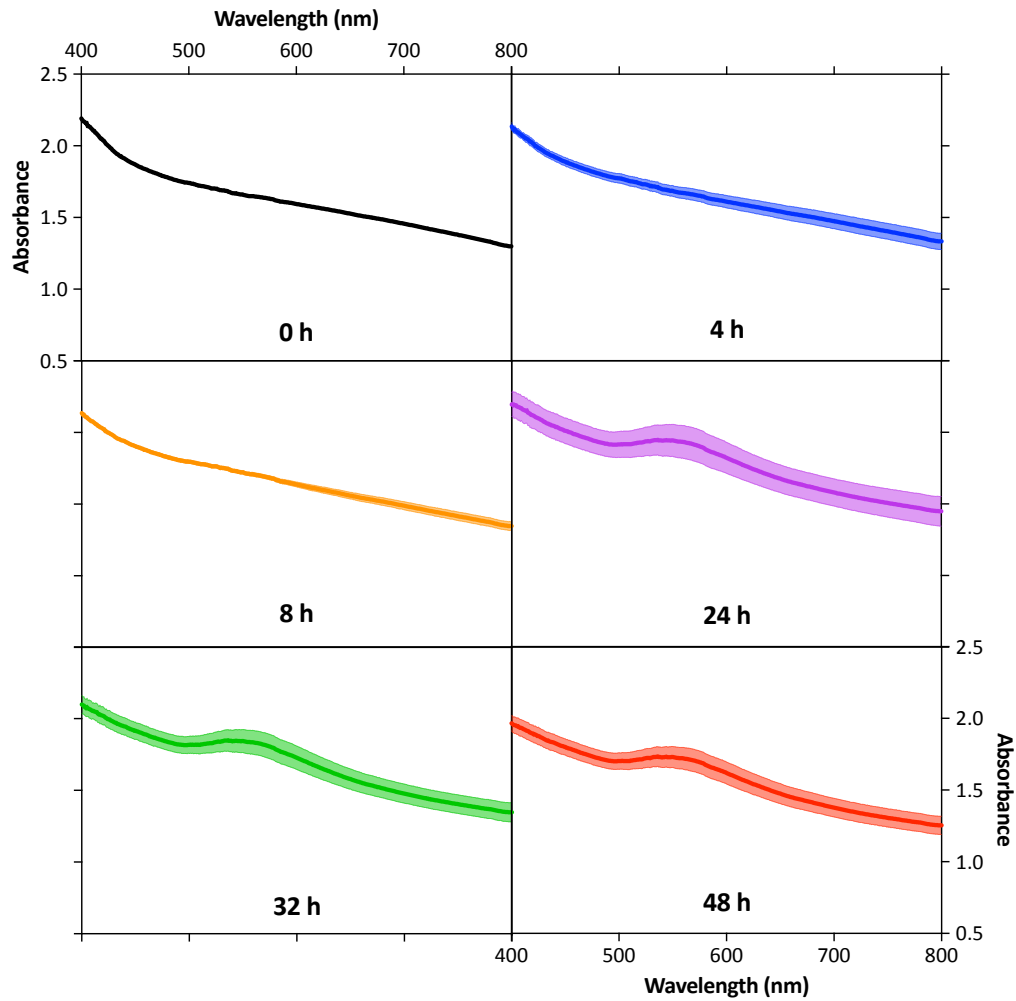


**Figure 12.2:** Visible spectra from graph a) of **Figure 5.2** divided into individual measurements. Results are average of three independent replicates. Some error bars cannot be visualised because they are smaller than the thickness of the curves.

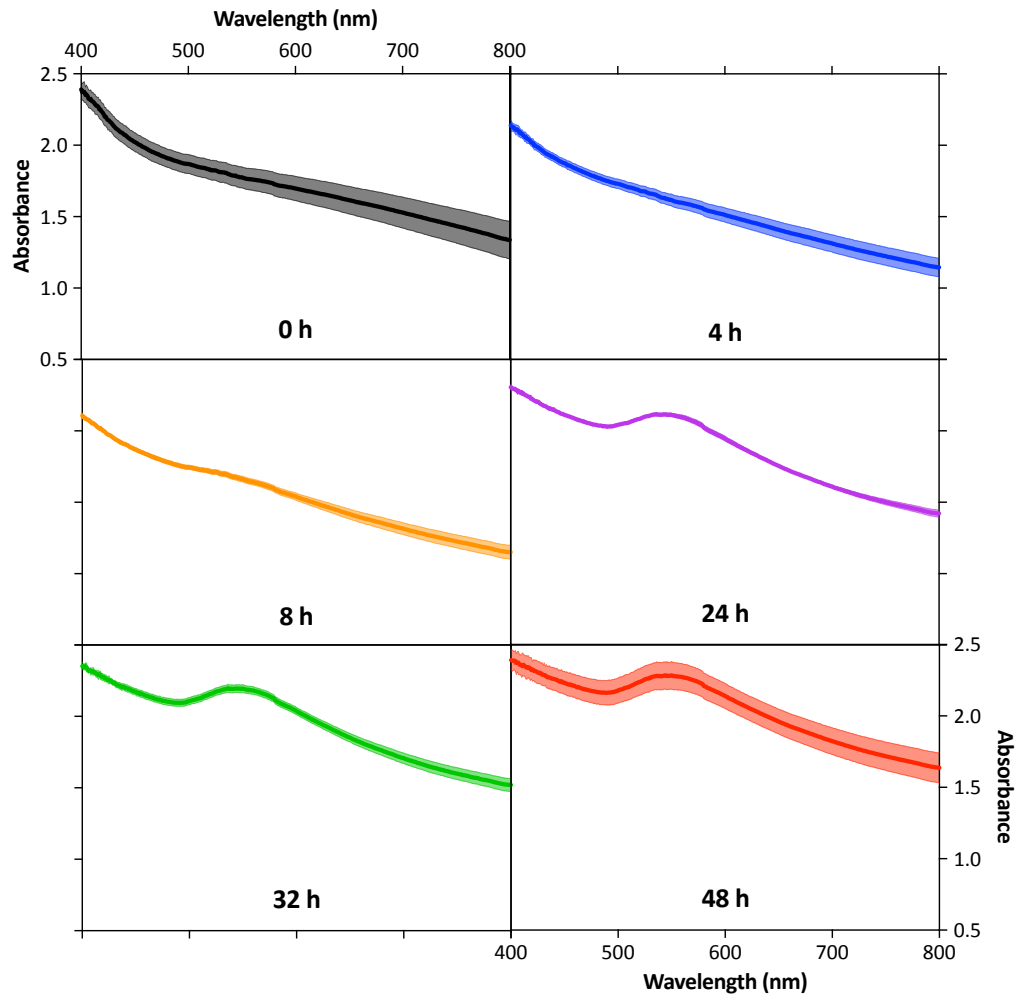


**Figure 12.3:** Visible spectra from graph b) of **Figure 5.2** divided into individual measurements. Results are average of three independent replicates. Some error bars cannot be visualised because they are smaller than the thickness of the curves.

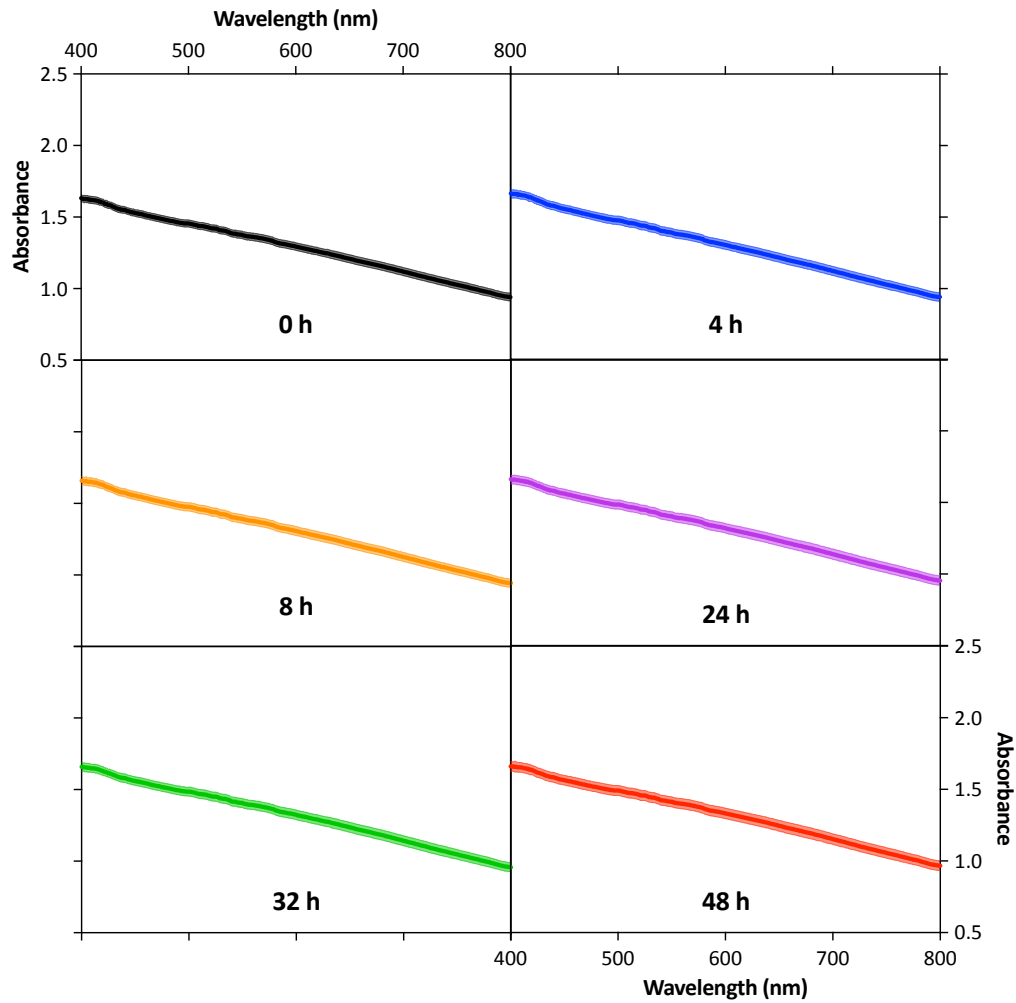


**Figure 12.4:** Visible spectra from graph c) of **Figure 5.2** divided into individual measurements. Results are average of three independent replicates. Error bars cannot be visualised because they are smaller than the thickness of the curves.



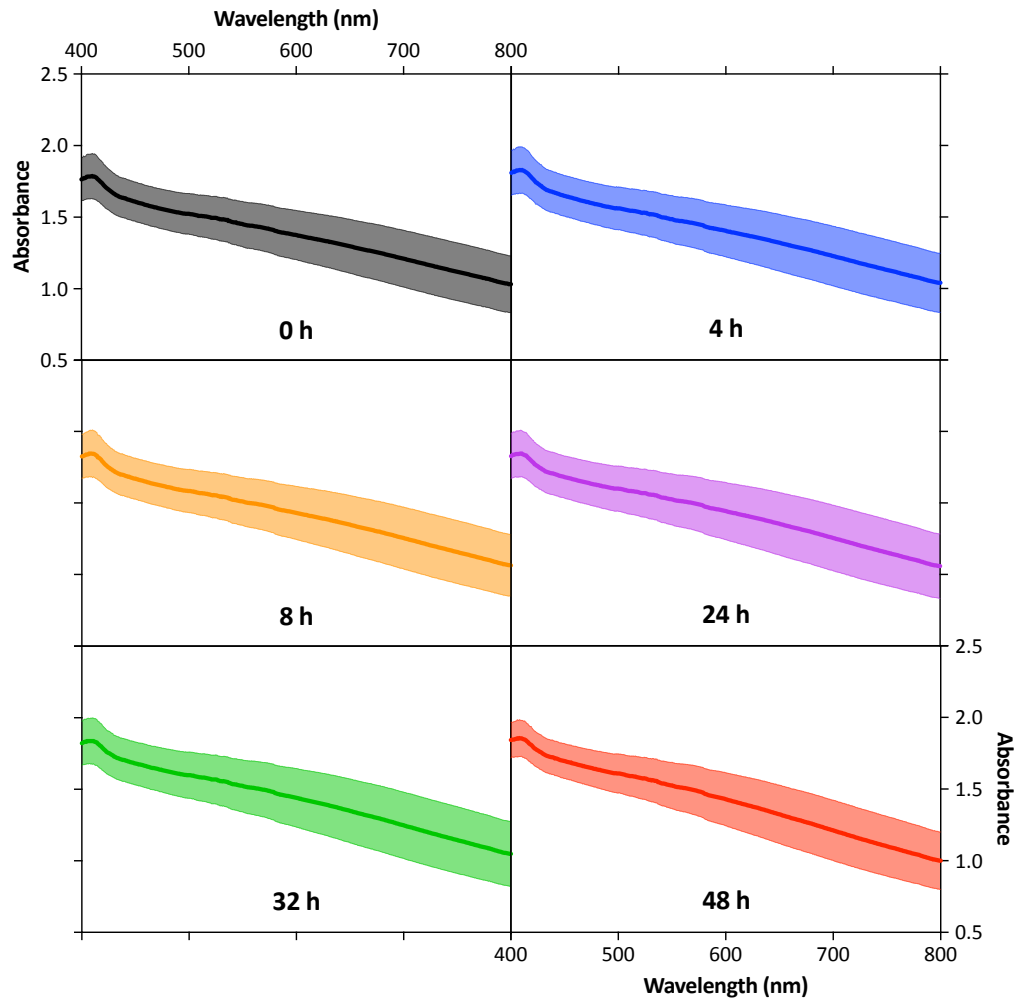


**Figure 12.5:** Visible spectra from graph d) of **Figure 5.2** divided into individual measurements. Error bars indicate the standard deviation of three independent replicates.

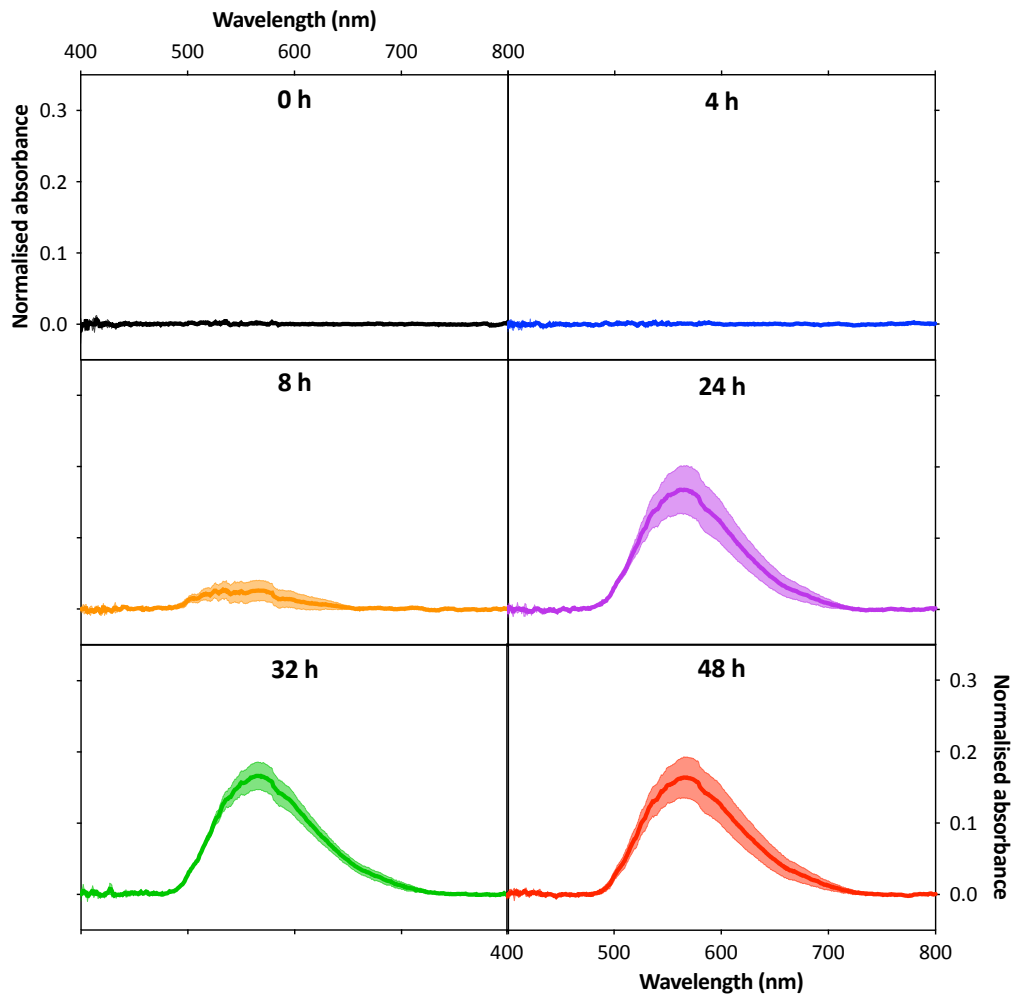


**Figure 12.6:** Spectra from graph e) of **Figure 5.2** divided into individual measurements. Results are average of three independent replicates. Some error bars cannot be visualised because they are smaller than the thickness of the curves.

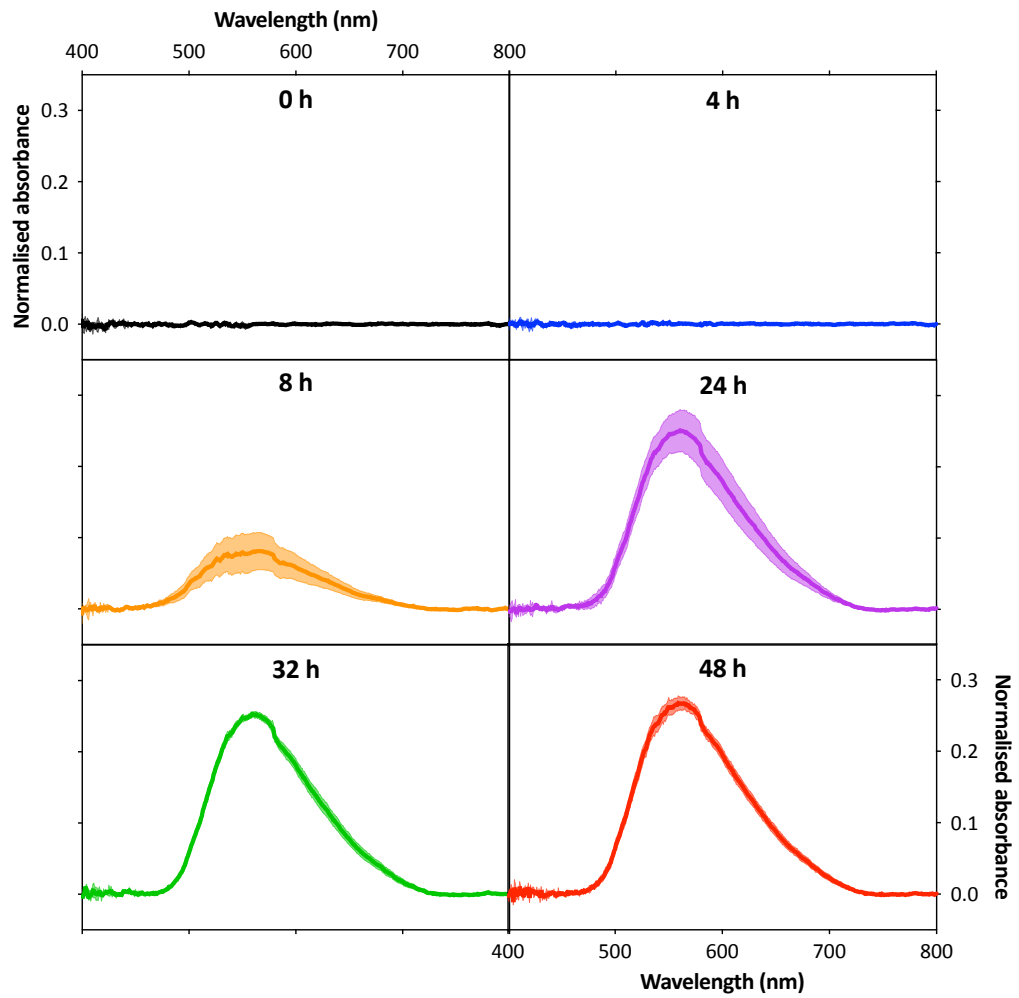


**Figure 12.7:** Spectra from graph f) of **Figure 5.2** divided into individual measurements. Results are average of three independent replicates. Some error bars cannot be visualised because they are smaller than the thickness of the curves.

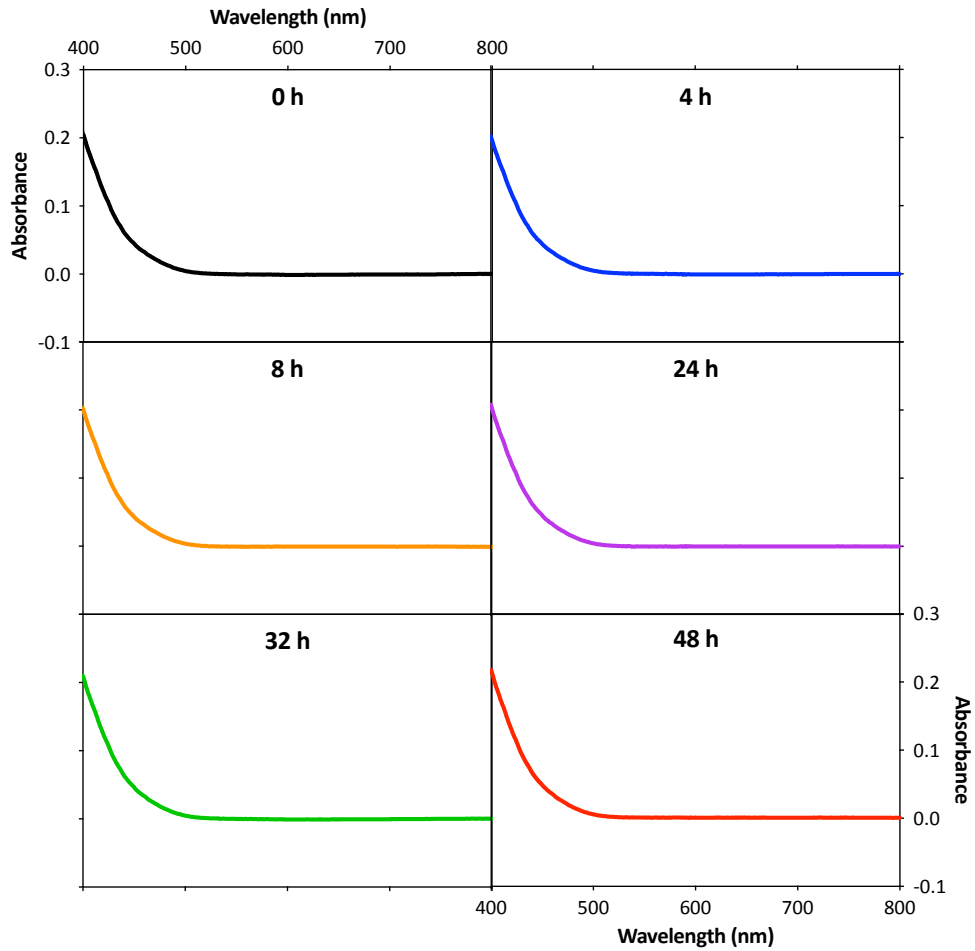


**Figure 12.8:** Visible spectra of 1 mM HAuCl<sub>4</sub> solution incubated under aerobic conditions at 30 °C and 180 rpm for 48 h – abiotic control of method I. Results are average of three independent replicates. Error bars cannot be visualised because they are smaller than the thickness of the curves.

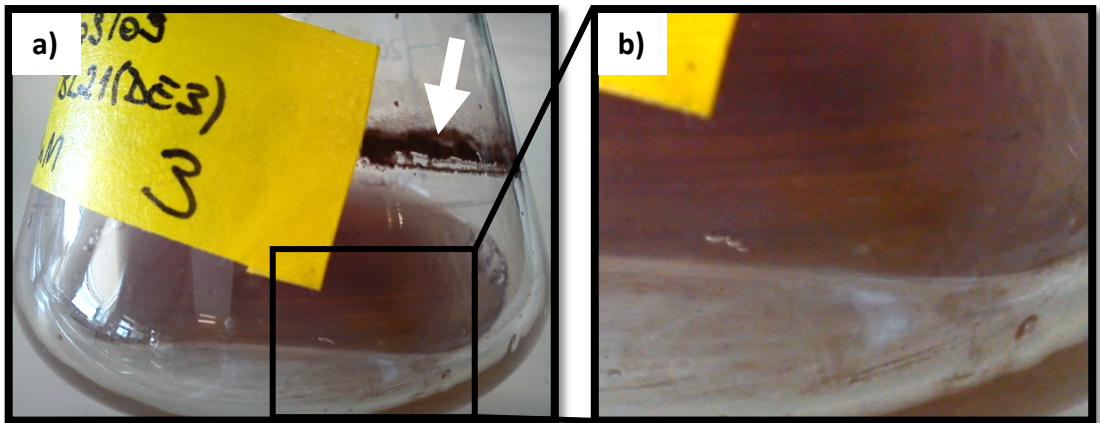


**Figure 12.9:** Picture of a shake flask with BL21(DE3) culture after incubation in 1 mM H<sub>AuCl</sub><sub>4</sub> solution for 48 h. Cell accumulation on the meniscus line is indicated by the white arrow. Picture b) shows a zoom of the film formed inside the flask, also containing accumulated cells.

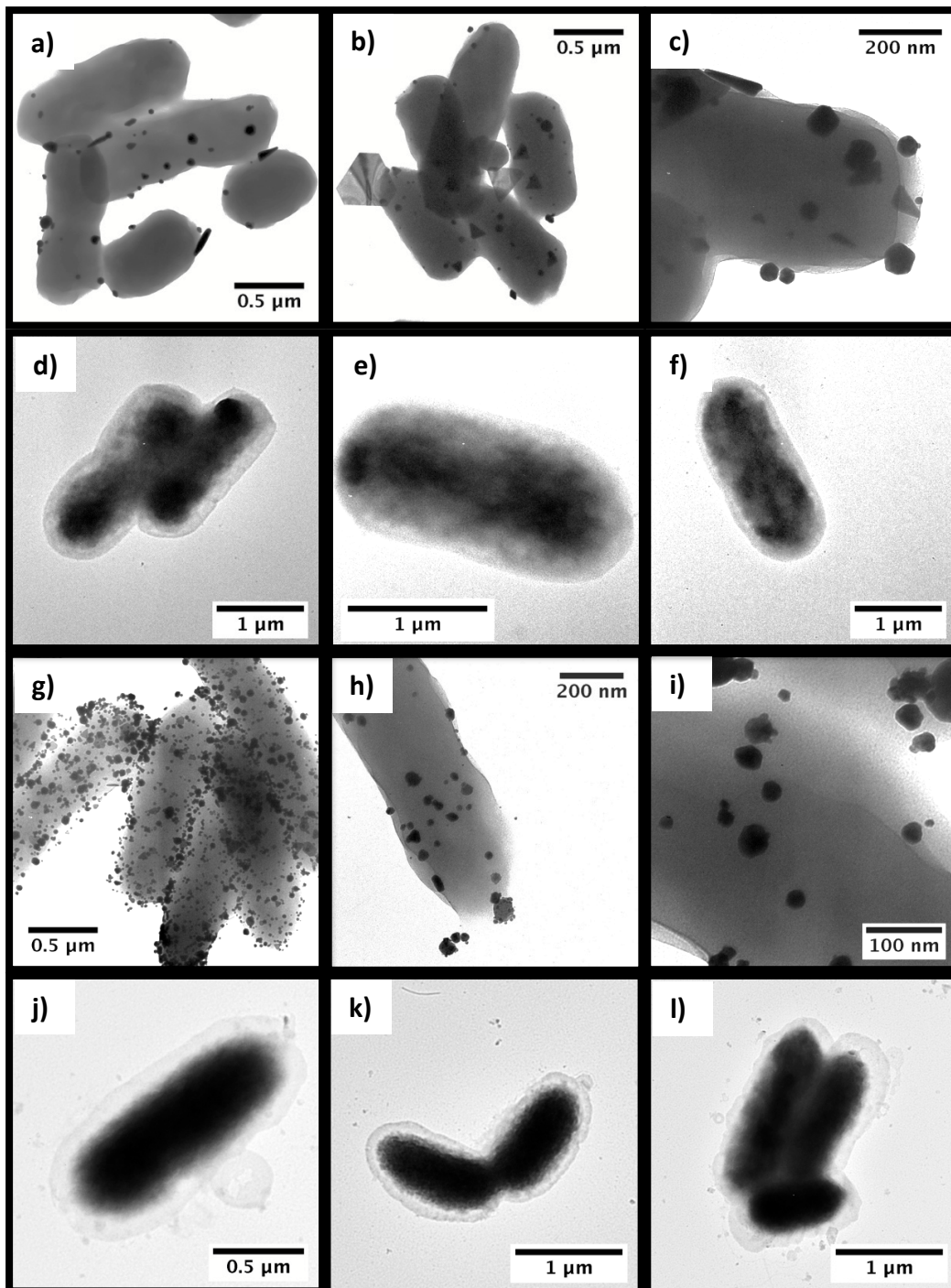


**Figure 12.10:** TEM images of BL21(DE3) and MR-1 after implementation of method I. Images a), b) and c) show BL21(DE3) cultures after incubation in 1 mM HAuCl<sub>4</sub> solution; images d), e) and f) show BL21(DE3) cultures after incubation in sterile DI water (control); images g), h) and i) show MR-1 cultures after incubation in 1 mM HAuCl<sub>4</sub> solution; and images j), k) and l) show MR-1 cultures after incubation in sterile DI water (control).

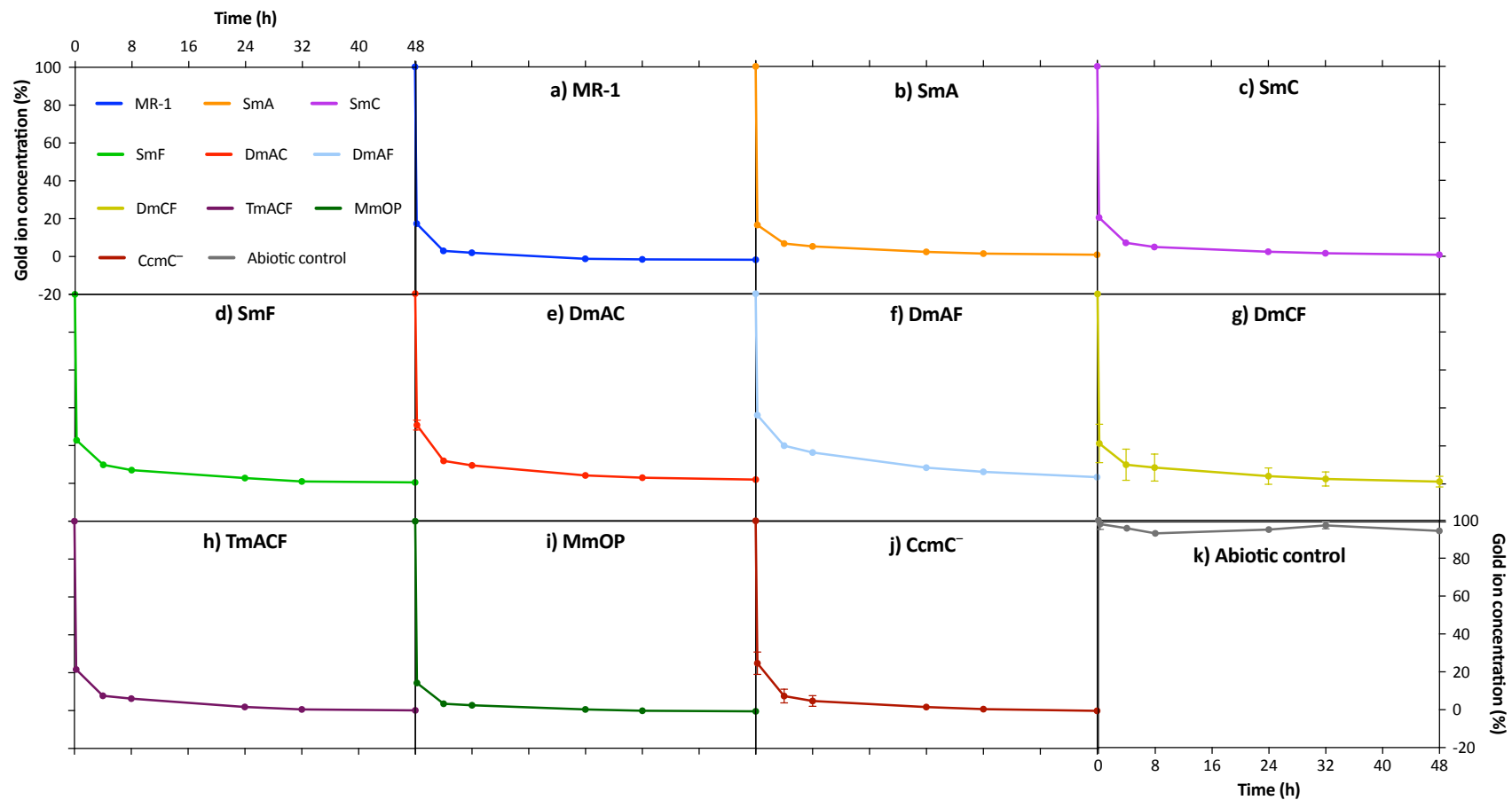


**Figure 12.11:** Adsorption curves from **Figure 6.1** divided into individual cultures. Error bars indicate the standard deviation of three independent replicates. Some error bars cannot be visualised because they are smaller than the symbols.

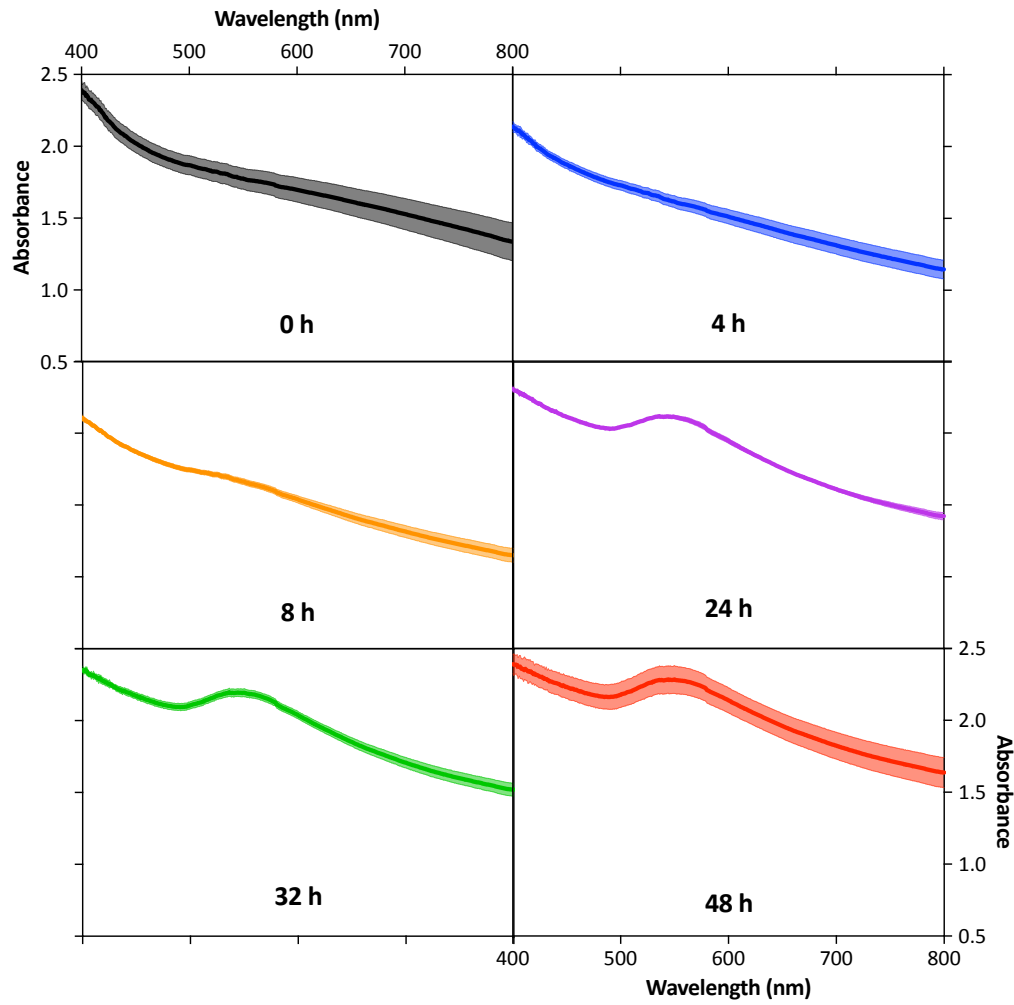


**Figure 12.12:** Visible spectra from graph a) of **Figure 6.2** divided into individual measurements. Error bars indicate the standard deviation of three independent replicates.



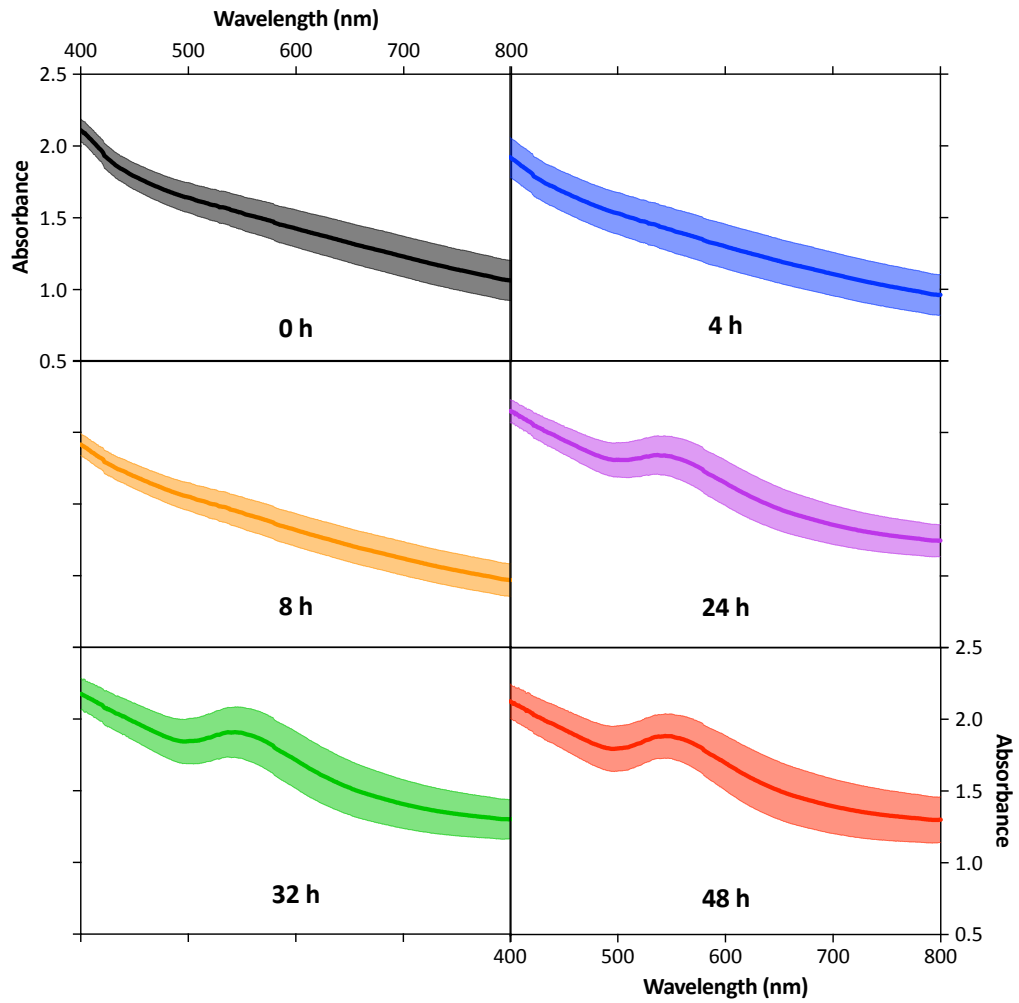


**Figure 12.13:** Visible spectra from graph b) of **Figure 6.2** divided into individual measurements. Error bars indicate the standard deviation of three independent replicates.

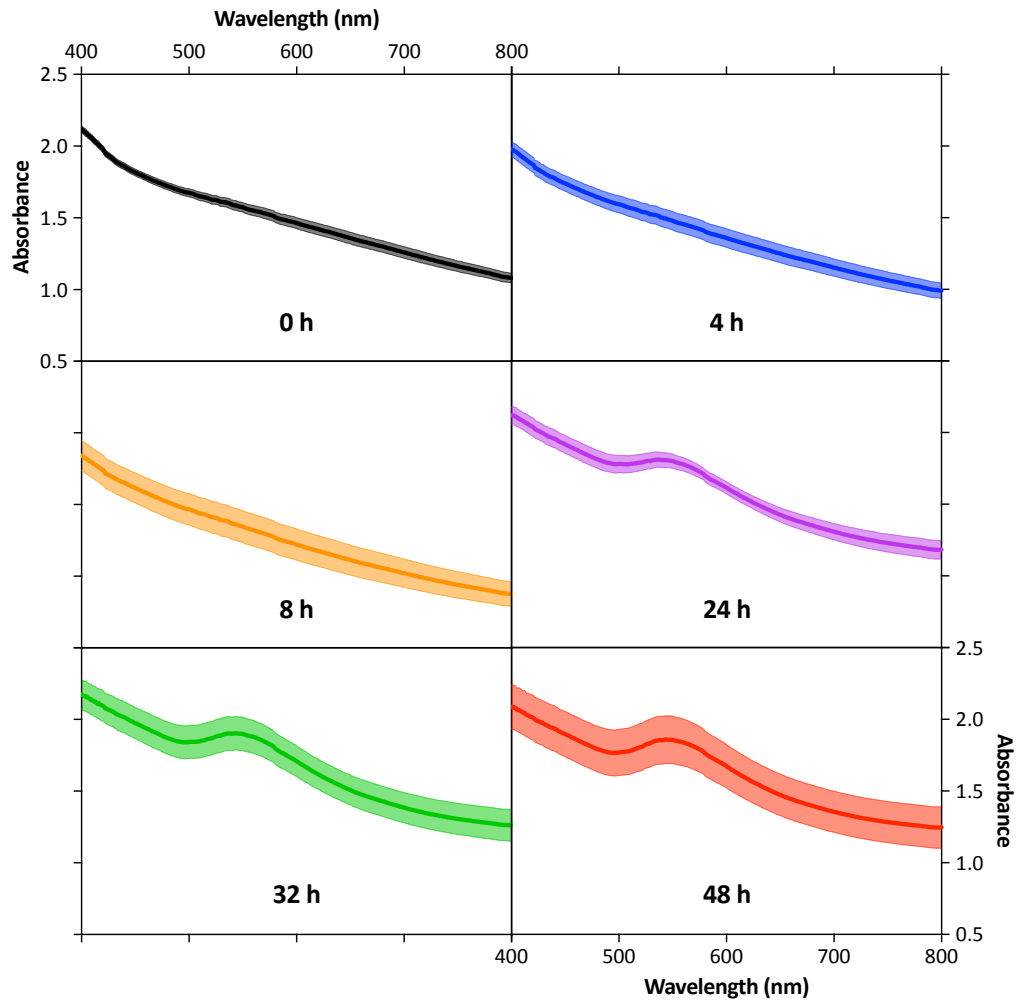


**Figure 12.14:** Visible spectra from graph c) of **Figure 6.2** divided into individual measurements. Error bars indicate the standard deviation of three independent replicates.

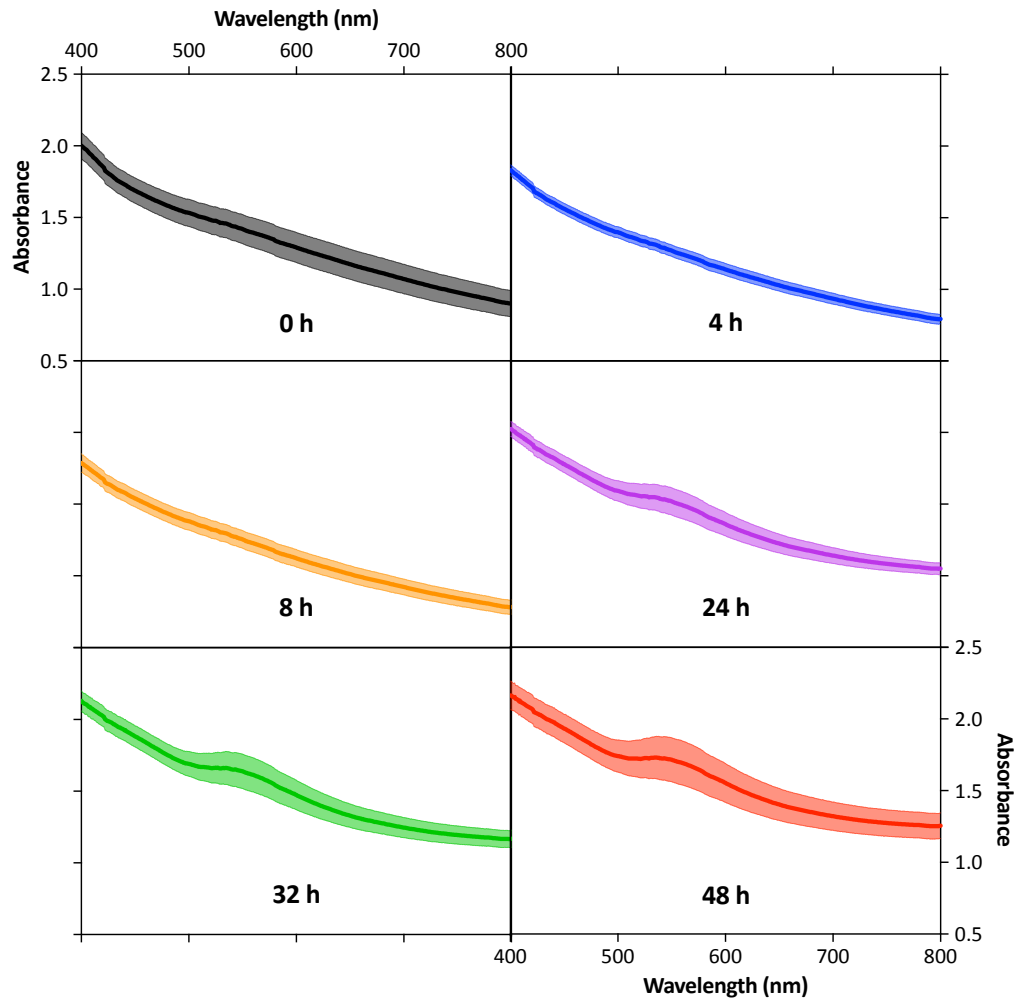


**Figure 12.15:** Visible spectra from graph d) of **Figure 6.2** divided into individual measurements. Error bars indicate the standard deviation of three independent replicates.

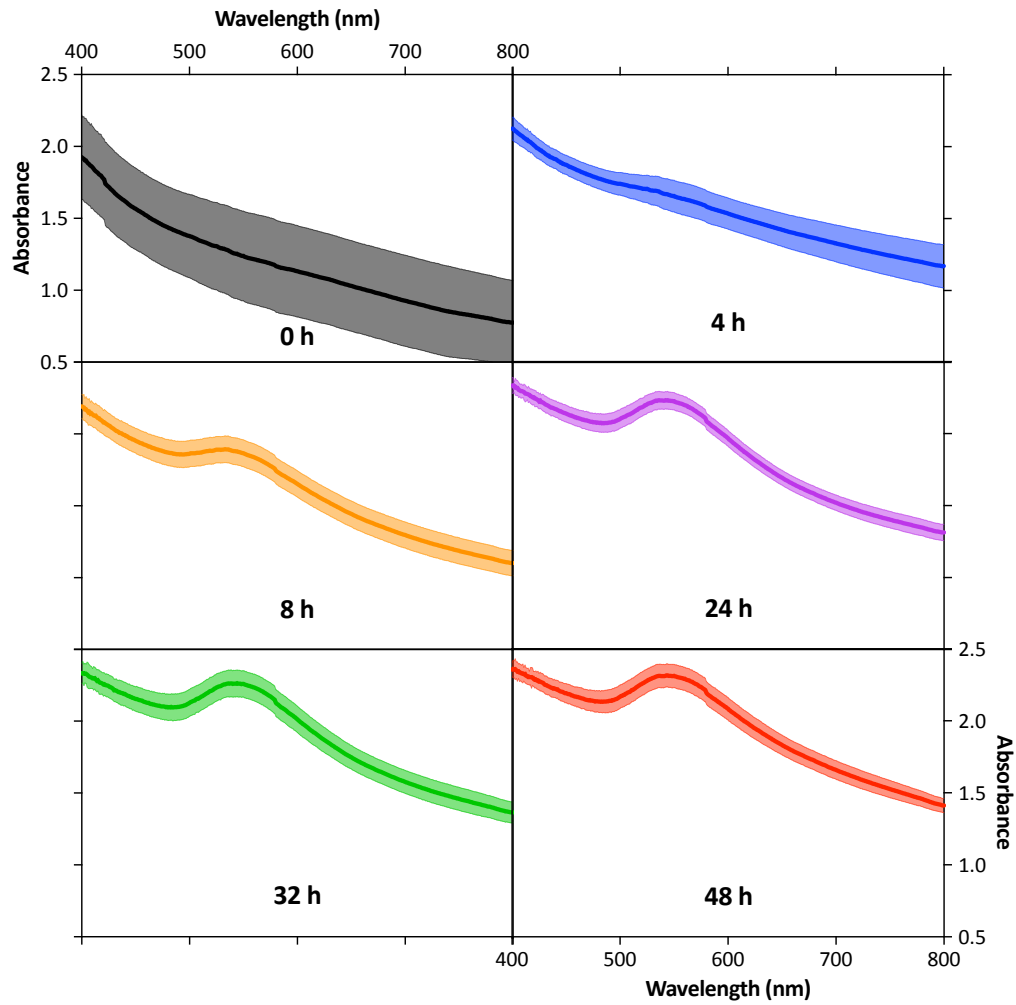


**Figure 12.16:** Visible spectra from graph e) of **Figure 6.2** divided into individual measurements. Error bars indicate the standard deviation of three independent replicates.

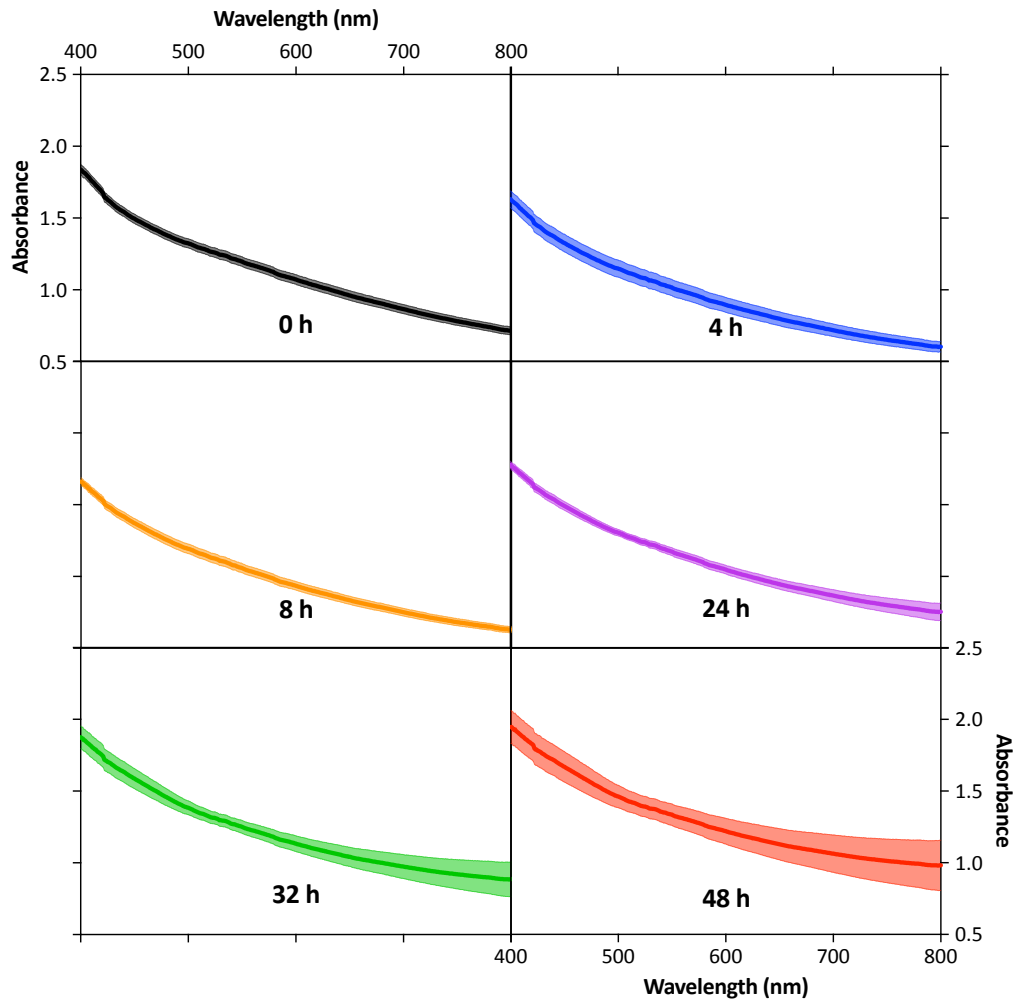


**Figure 12.17:** Visible spectra from graph f) of **Figure 6.2** divided into individual measurements. Error bars indicate the standard deviation of three independent replicates.

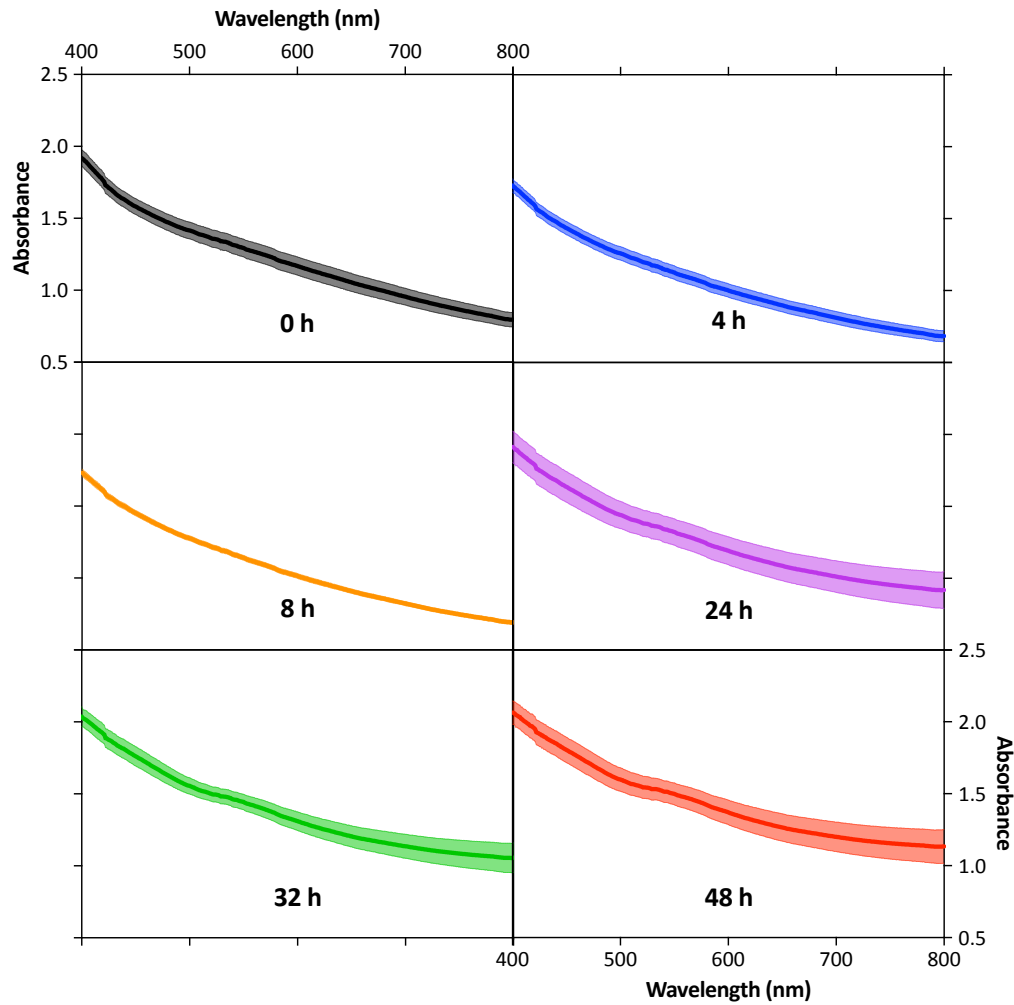


**Figure 12.18:** Visible spectra from graph g) of **Figure 6.2** divided into individual measurements. Results are average of three independent replicates. Some error bars cannot be visualised because they are smaller than the thickness of the curves.

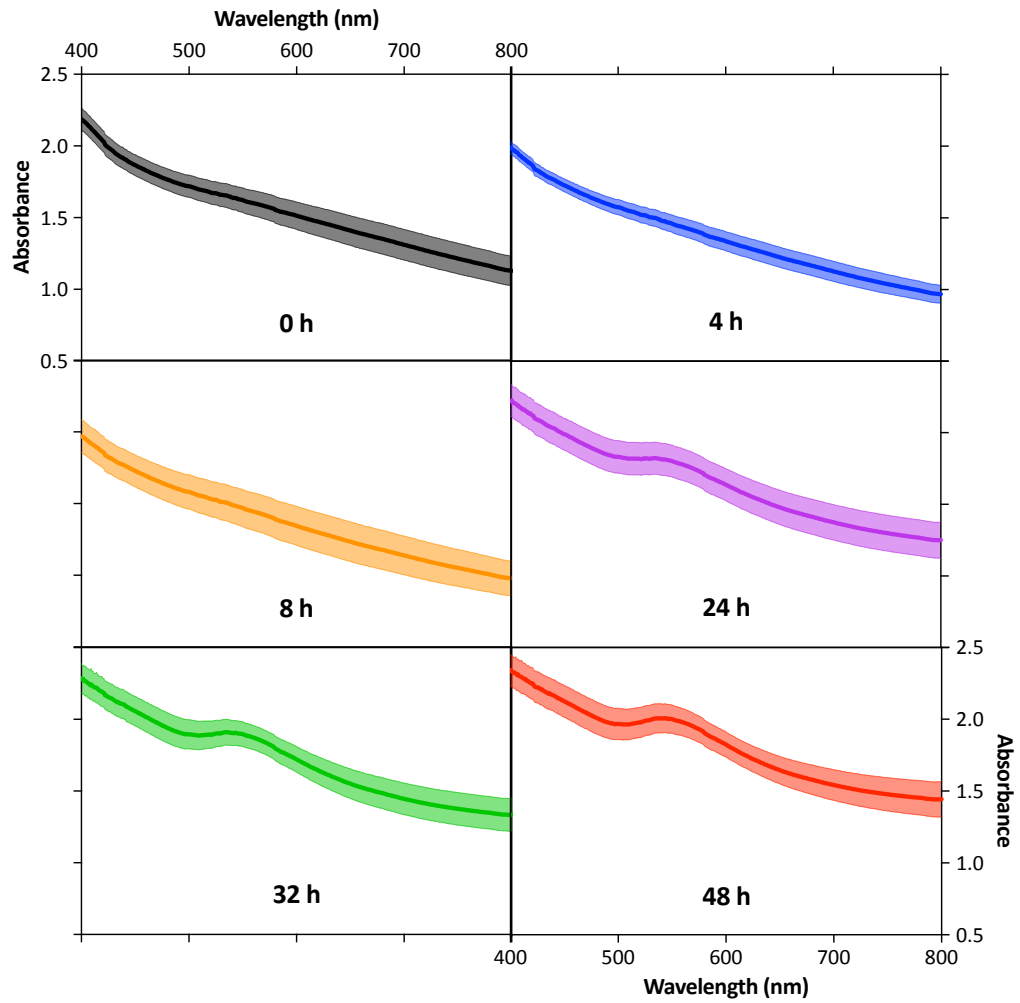


**Figure 12.19:** Visible spectra from graph h) of **Figure 6.2** divided into individual measurements. Error bars indicate the standard deviation of three independent replicates.

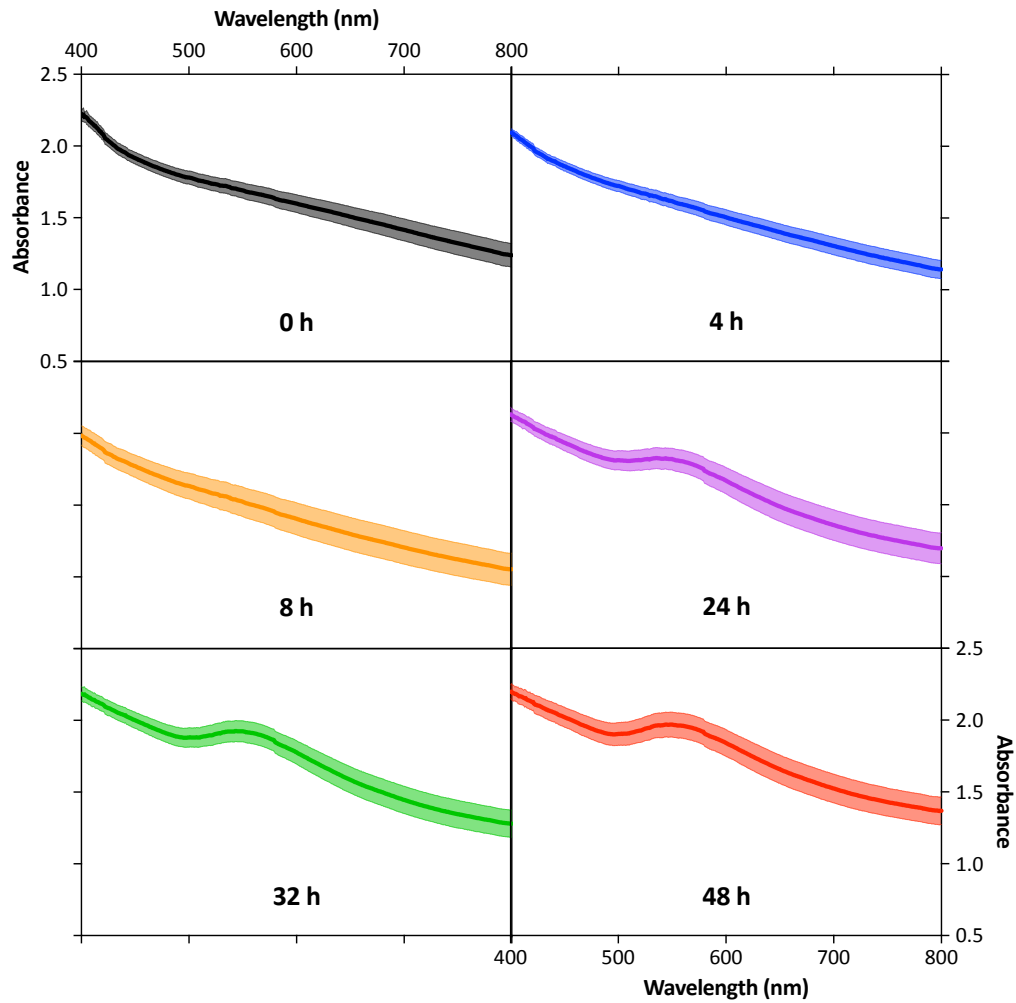


**Figure 12.20:** Visible spectra from graph i) of **Figure 6.2** divided into individual measurements. Error bars indicate the standard deviation of three independent replicates.



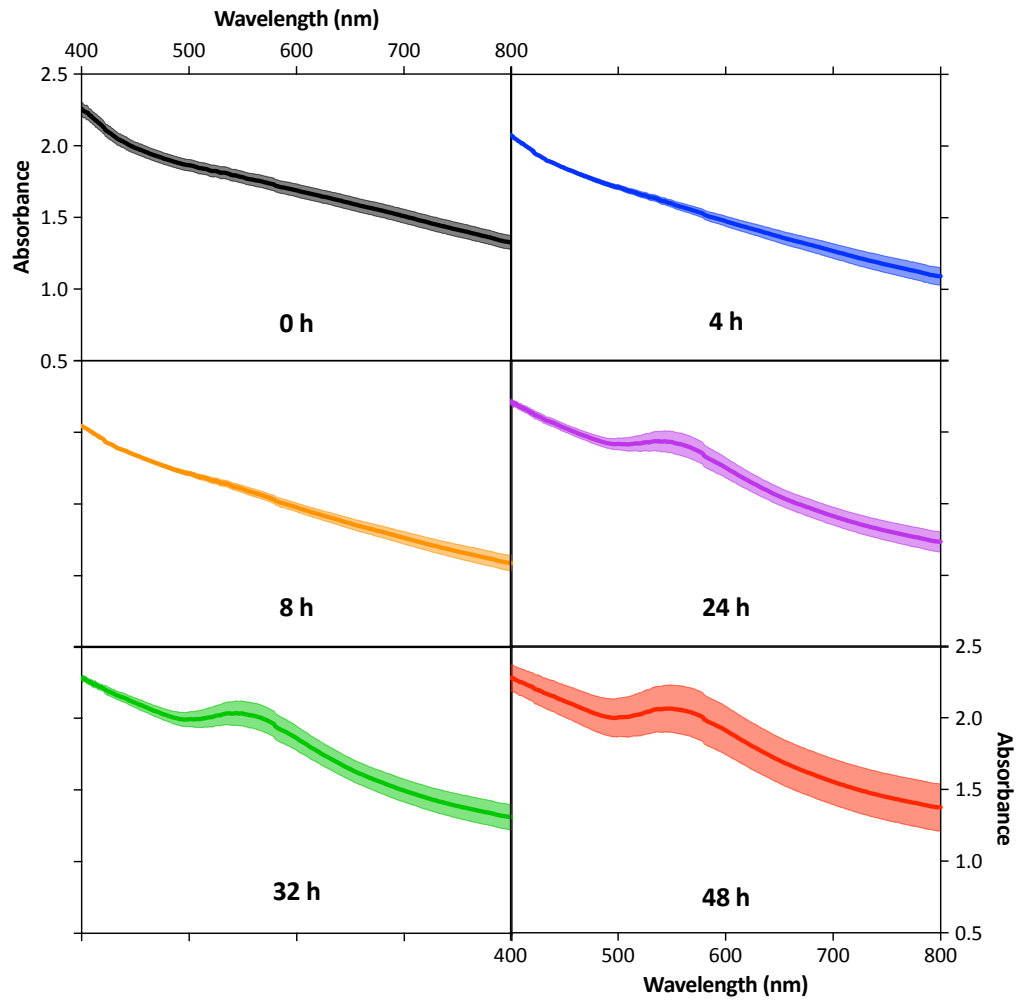


**Figure 12.21:** Visible spectra from graph j) of **Figure 6.2** divided into individual measurements. Error bars indicate the standard deviation of three independent replicates.

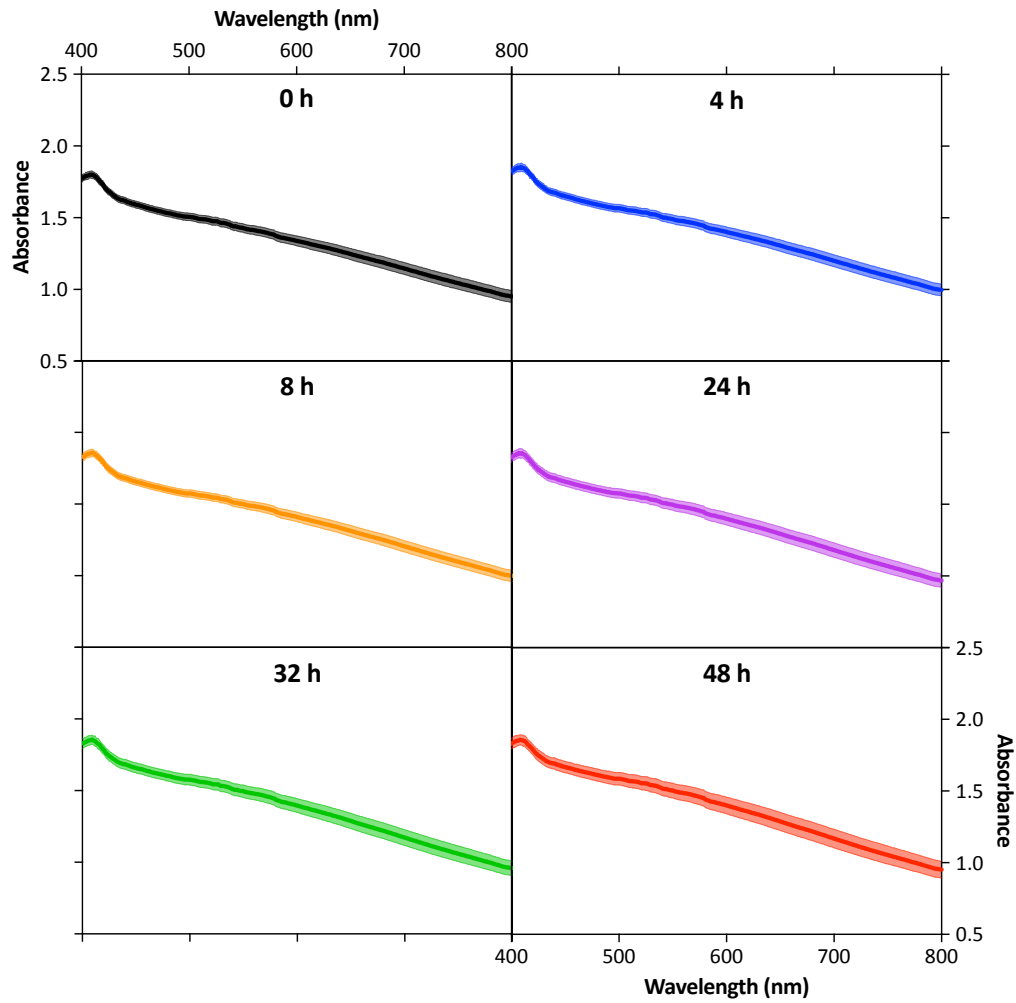


**Figure 12.22:** Visible spectra of SmA monitored during aerobic incubation in DI water (control of method I). Error bars indicate the standard deviation of three independent replicates.

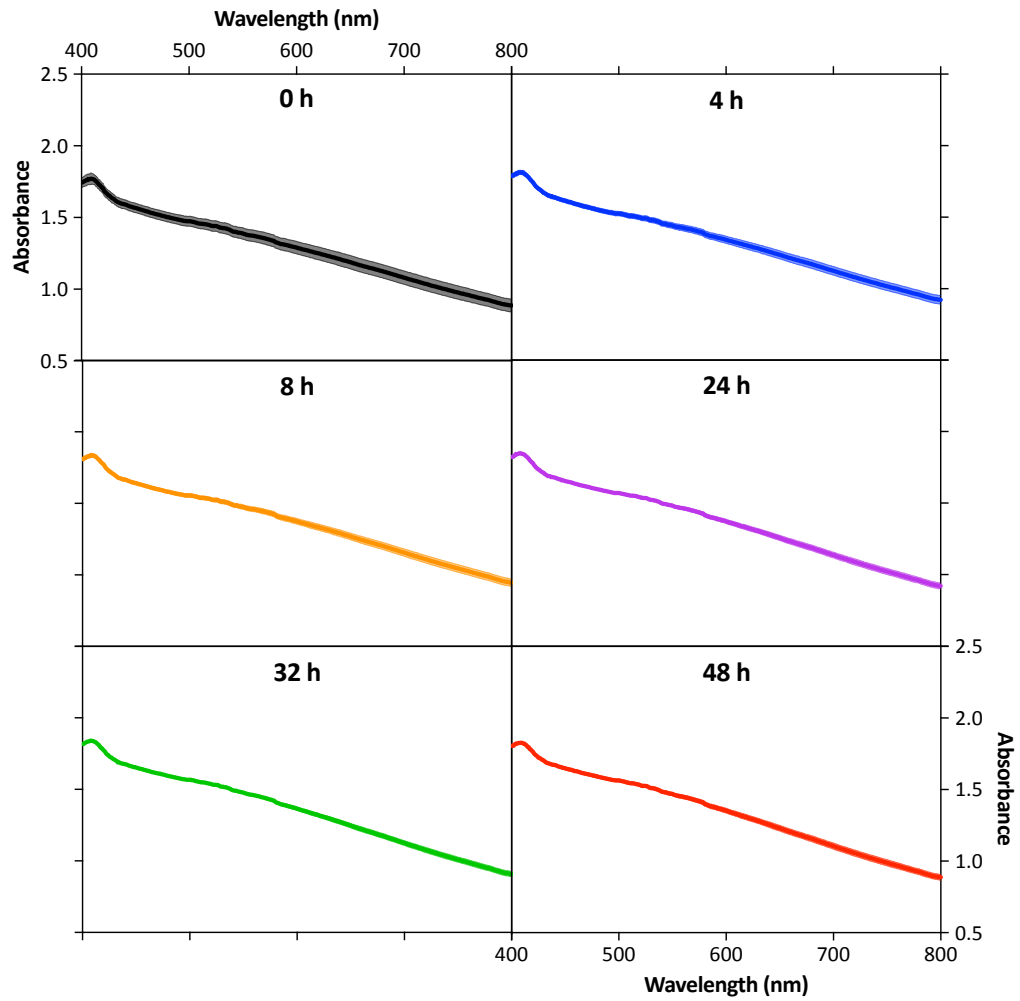


**Figure 12.23:** Visible spectra of SmC monitored during aerobic incubation in DI water (control of method I). Results are average of three independent replicates. Some error bars cannot be visualised because they are smaller than the thickness of the curves.

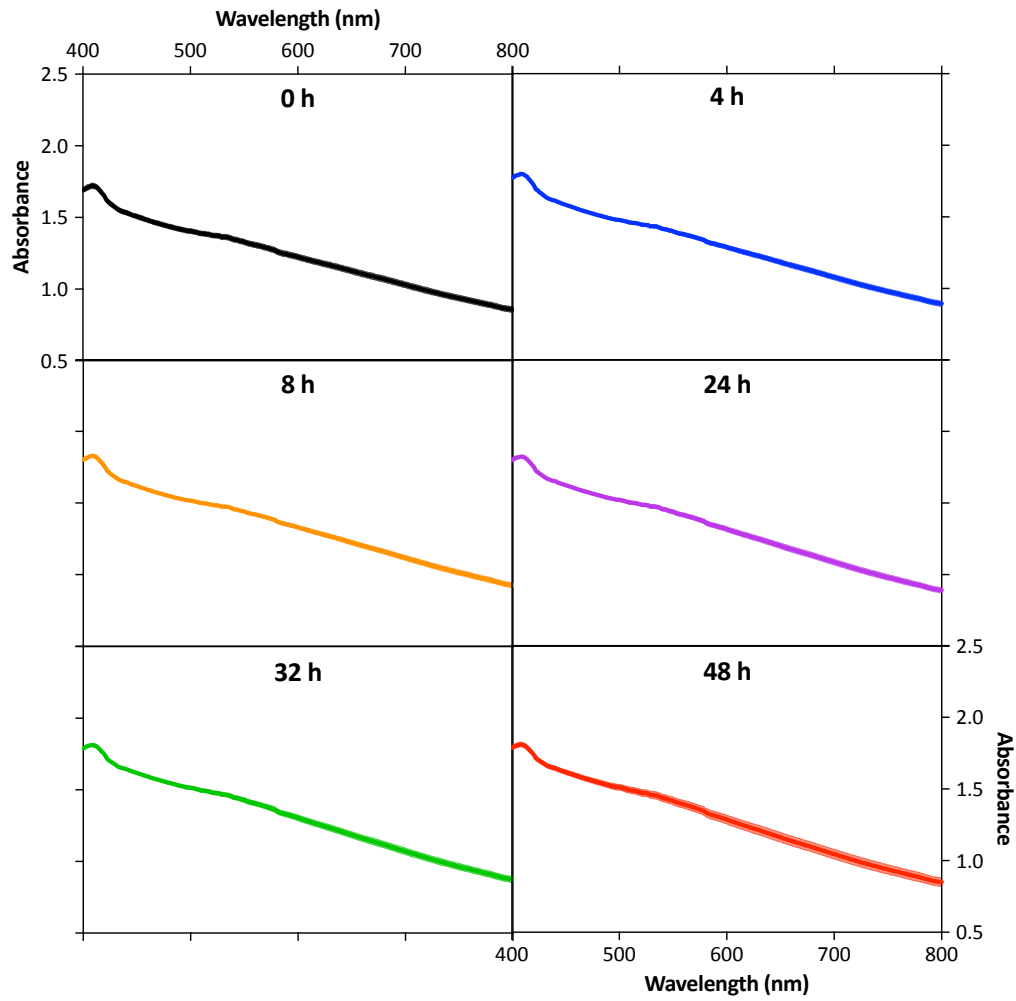


**Figure 12.24:** Visible spectra of SmF monitored during aerobic incubation in DI water (control of method I). Results are average of three independent replicates. Some error bars cannot be visualised because they are smaller than the thickness of the curves.

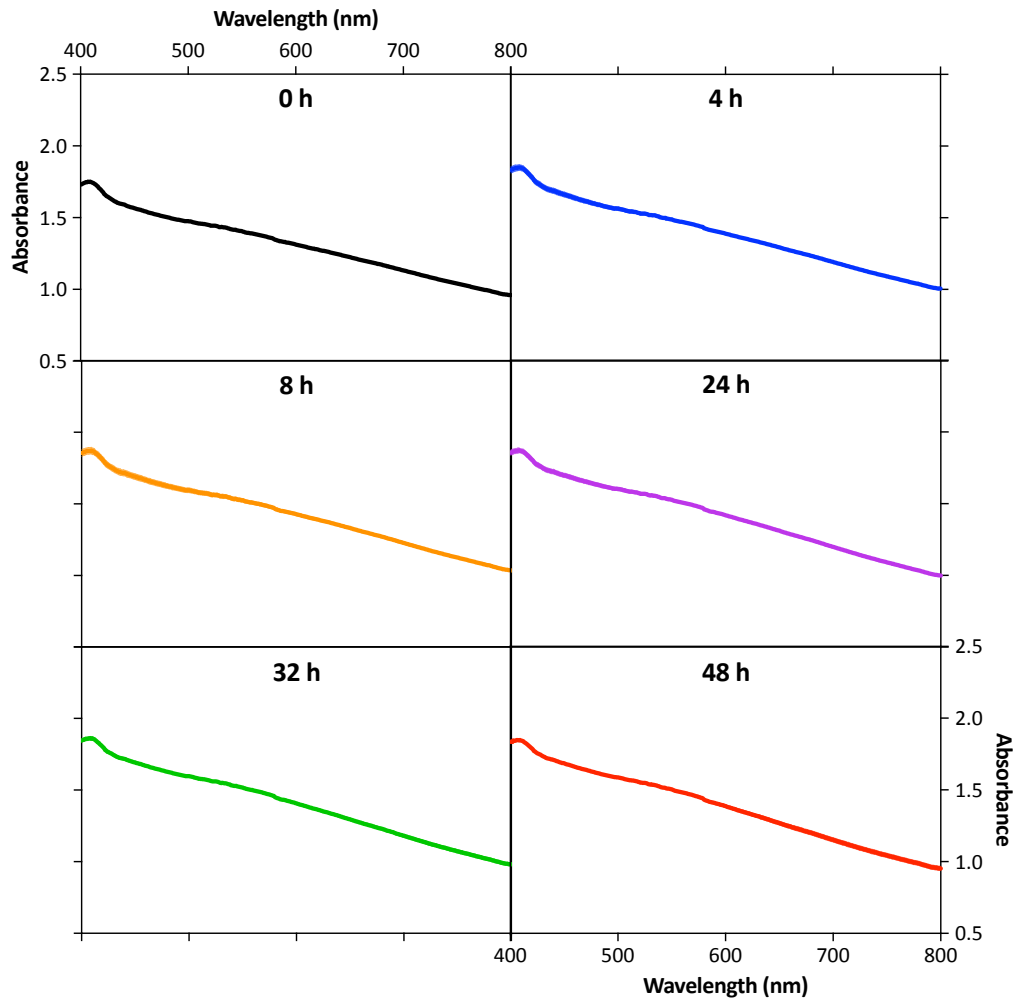


**Figure 12.25:** Visible spectra of DmAC monitored during aerobic incubation in DI water (control of method I). Results are average of three independent replicates. Error bars cannot be visualised because they are smaller than the thickness of the curves.

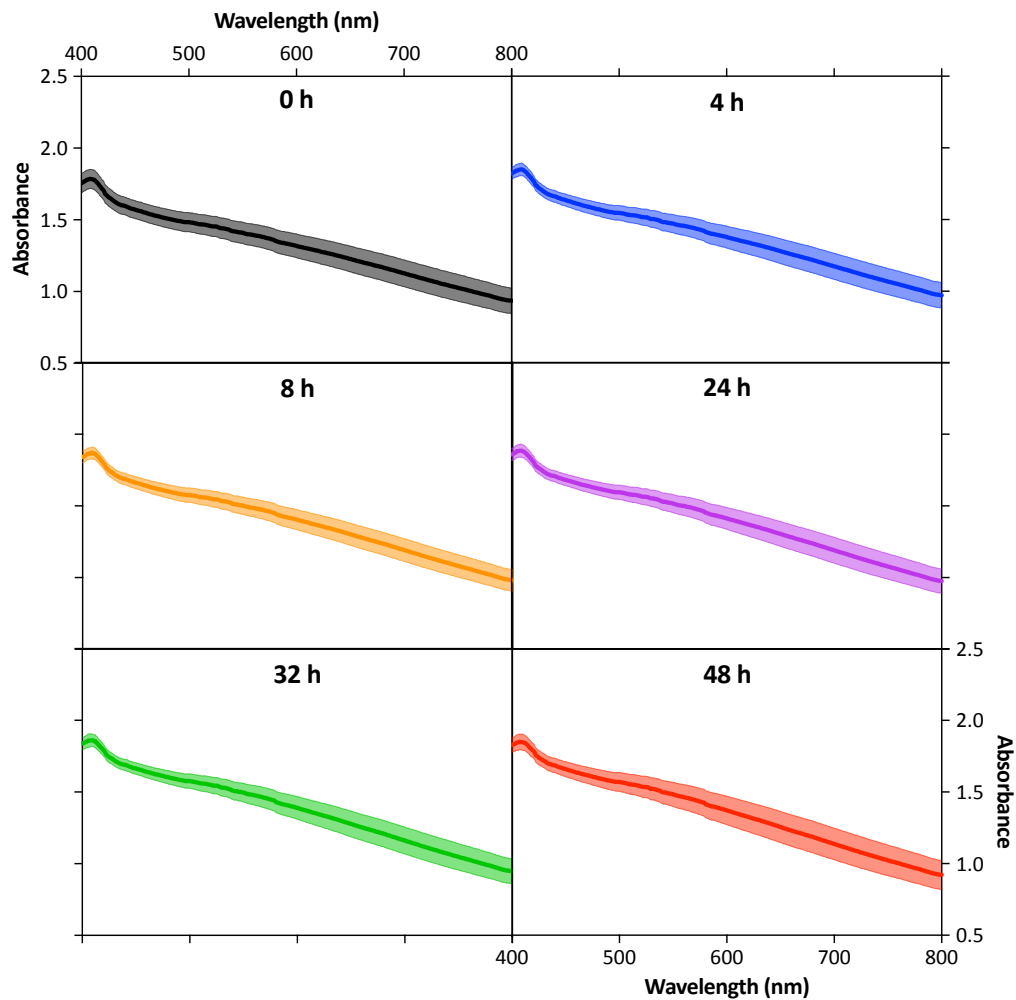


**Figure 12.26:** Visible spectra of DmAF monitored during aerobic incubation in DI water (control of method I). Error bars indicate the standard deviation of three independent replicates.

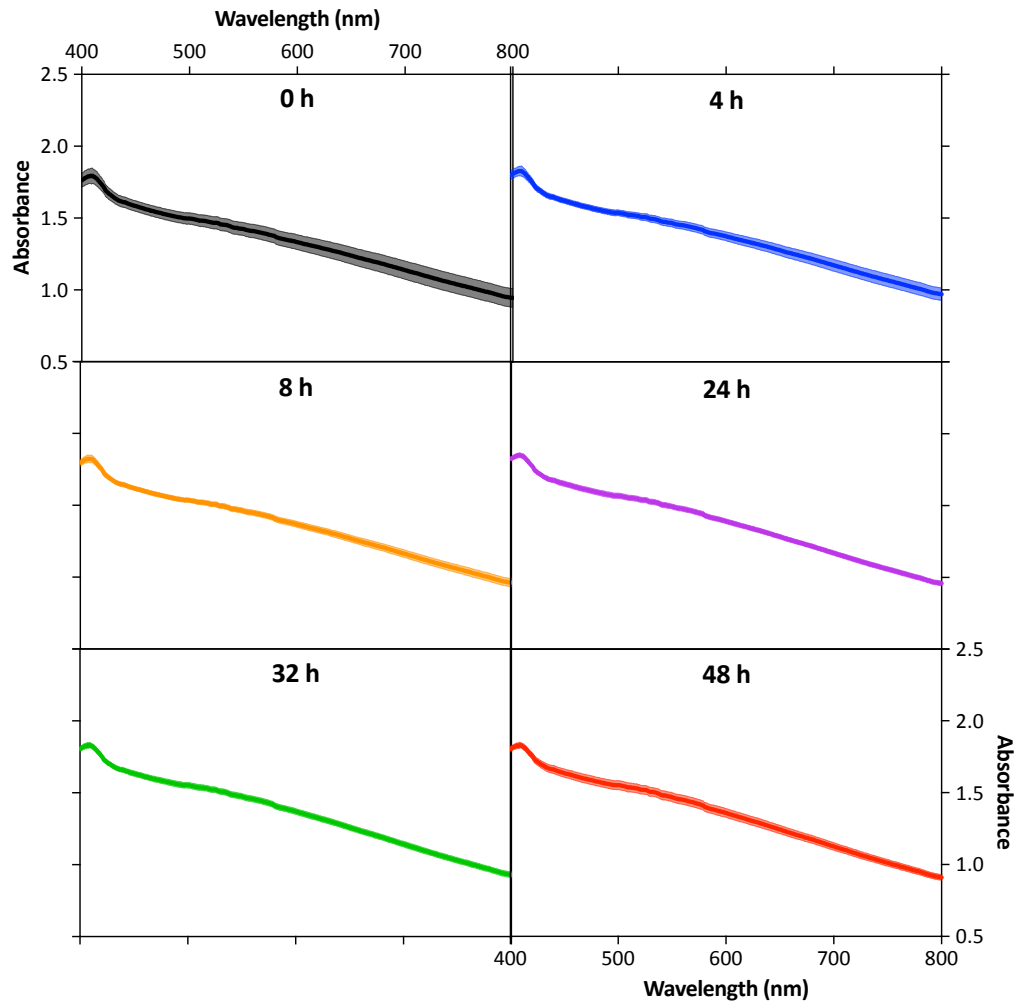


**Figure 12.27:** Visible spectra of DmCF monitored during aerobic incubation in DI water (control of method I). Results are average of three independent replicates. Some error bars cannot be visualised because they are smaller than the thickness of the curves.

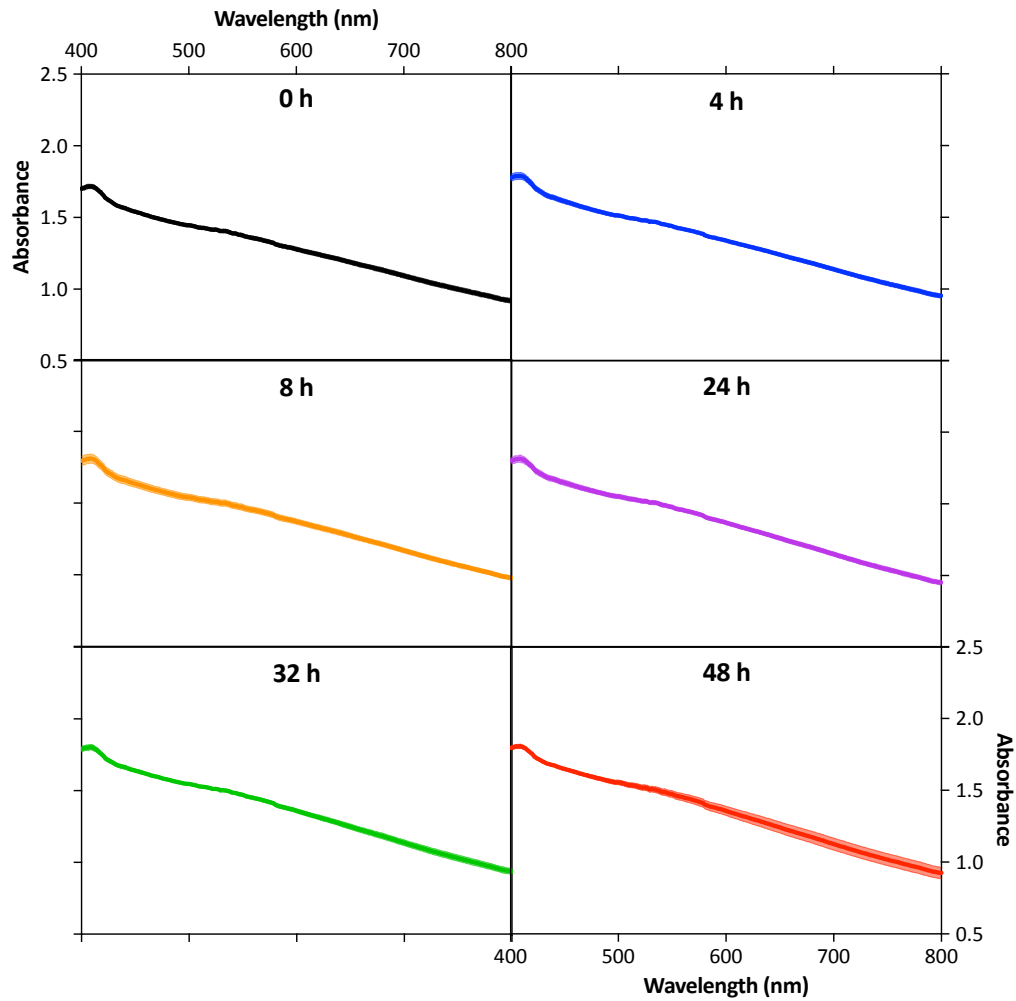


**Figure 12.28:** Visible spectra of TmACF monitored during aerobic incubation in DI water (control of method I). Results are average of three independent replicates. Some error bars cannot be visualised because they are smaller than the thickness of the curves.



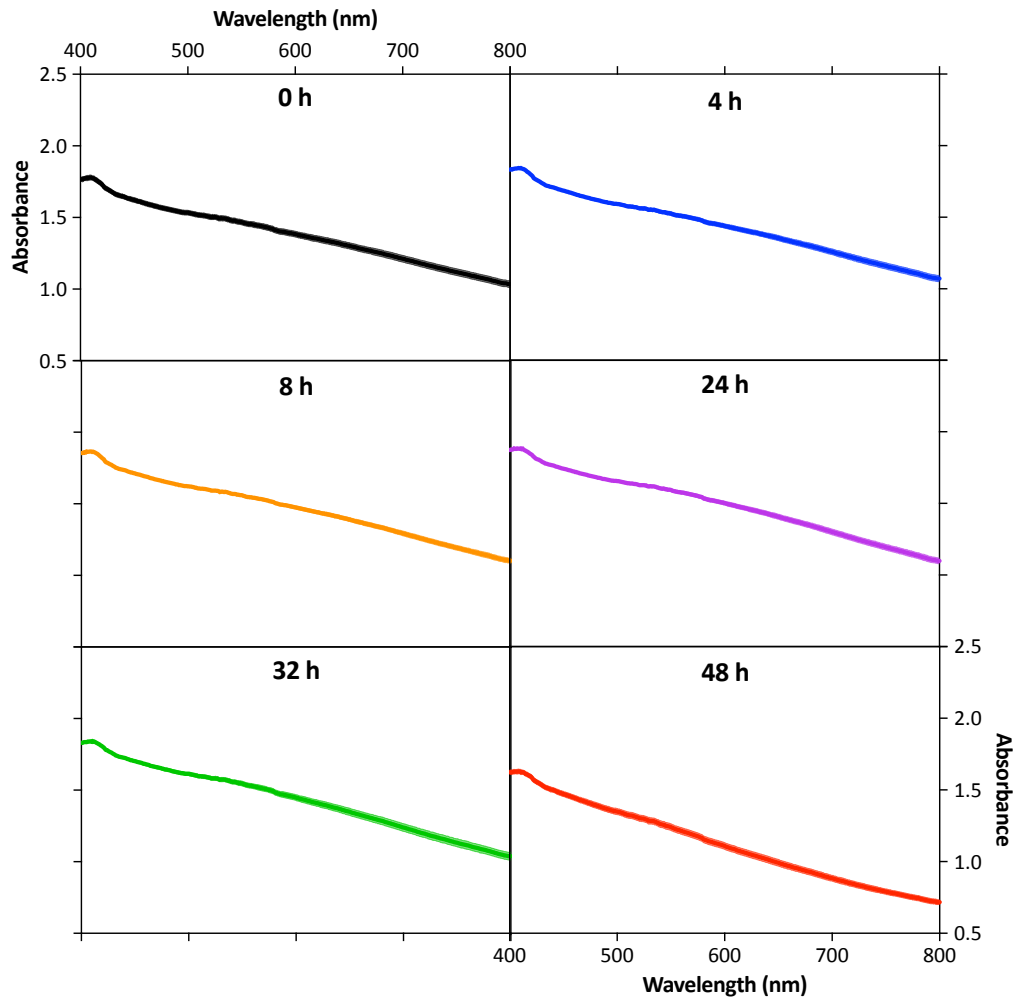


**Figure 12.29:** Visible spectra of MmOP monitored during aerobic incubation in DI water (control of method I). Results are average of three independent replicates. Error bars cannot be visualised because they are smaller than the thickness of the curves.

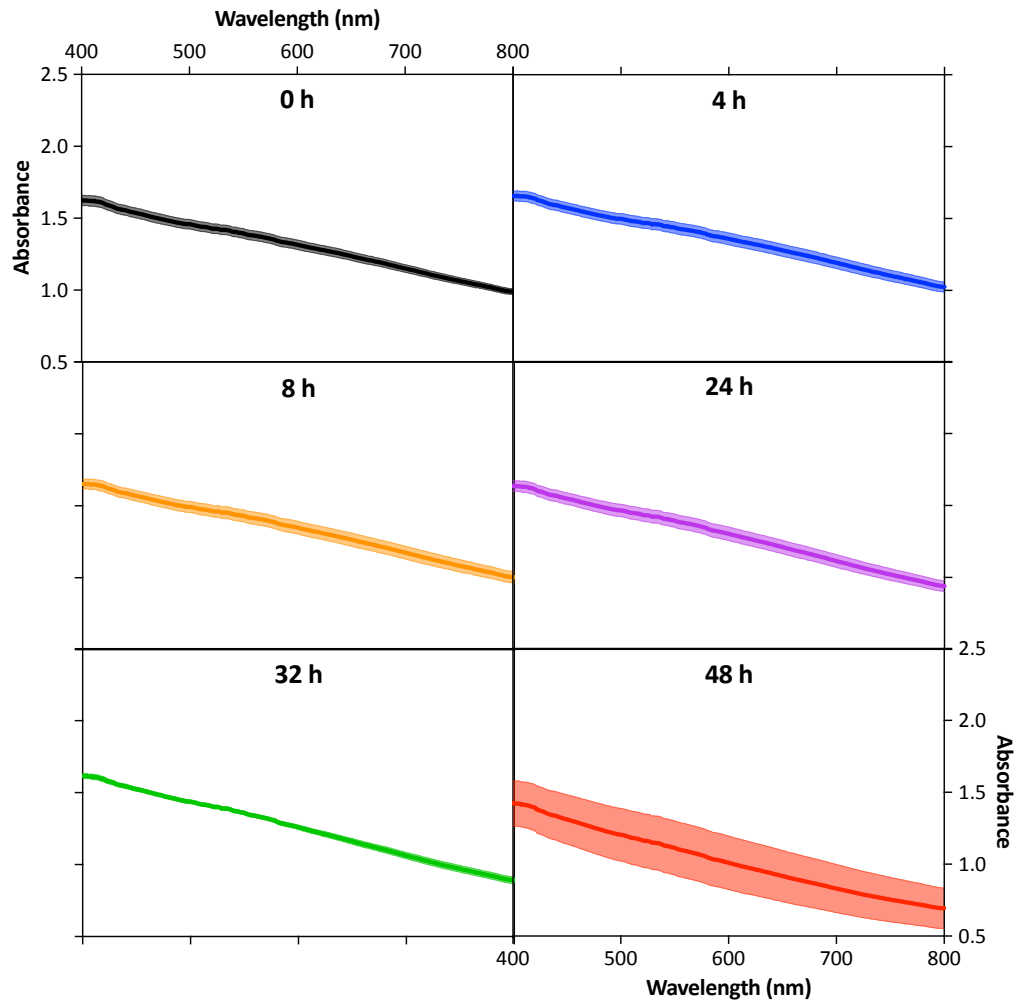


**Figure 12.30:** Visible spectra of  $CcmC^-$  monitored during aerobic incubation in DI water (control of method I). Results are average of three independent replicates. Some error bars cannot be visualised because they are smaller than the thickness of the curves.

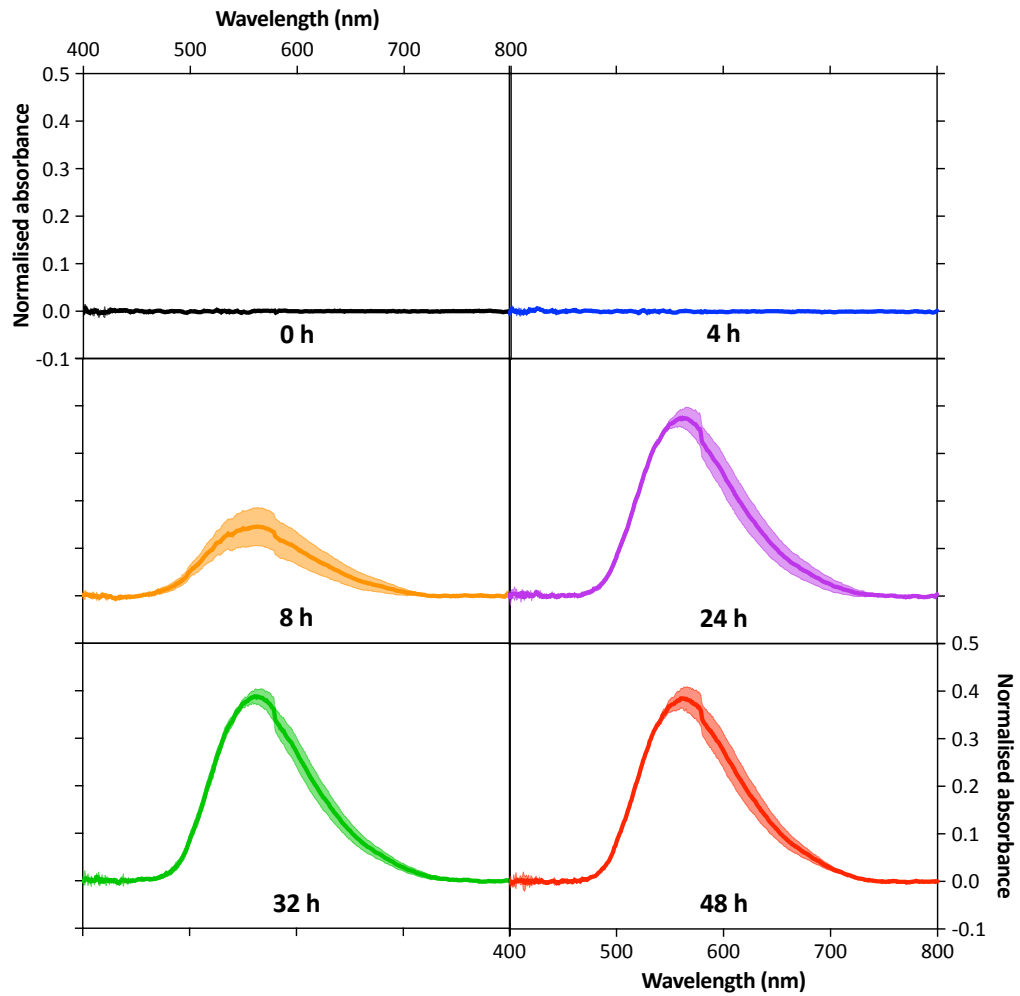


**Figure 12.31:** Spectra of SmA after baseline correction. The original visible spectra are shown in graph b) of **Figure 6.2**. Results are average of three independent replicates. Some error bars cannot be visualised because they are smaller than the thickness of the curves.

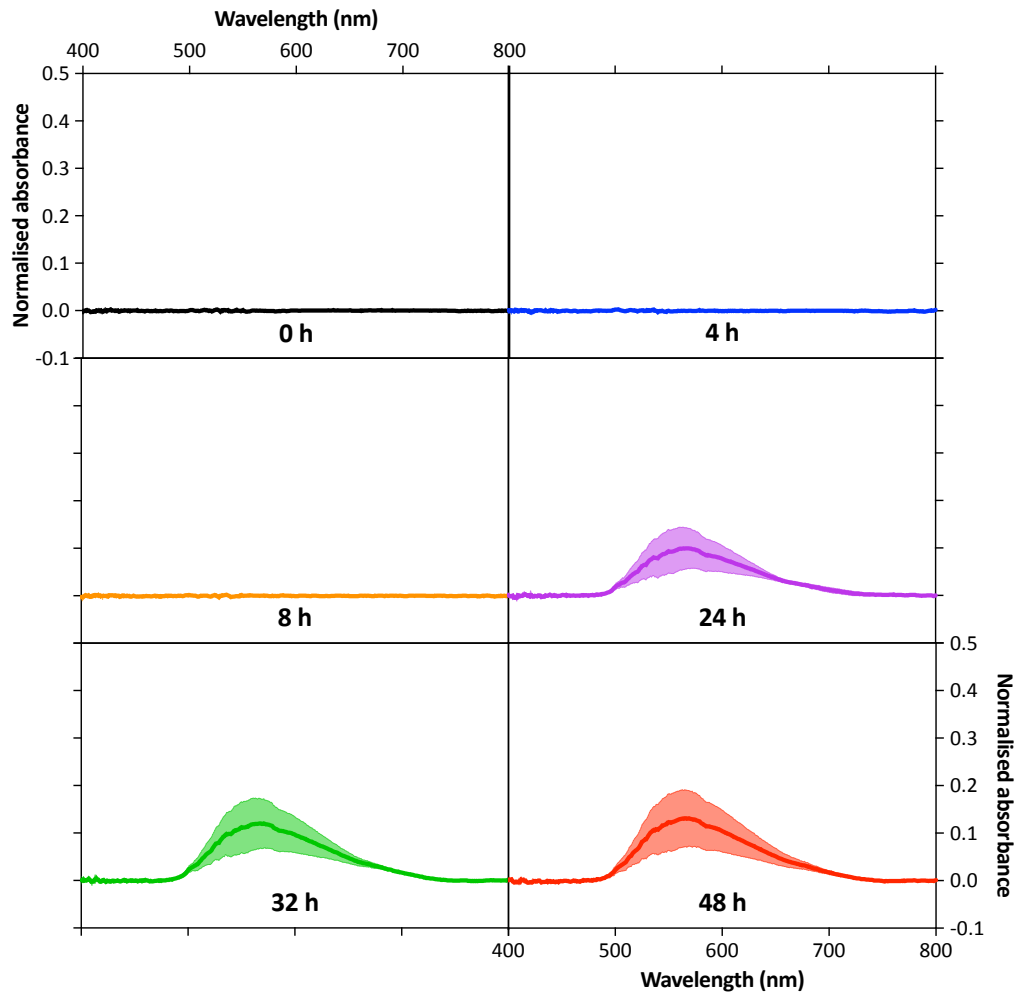


**Figure 12.32:** Spectra of SmC after baseline correction. The original visible spectra are shown in graph c) of **Figure 6.2**. Results are average of three independent replicates. Some error bars cannot be visualised because they are smaller than the thickness of the curves.

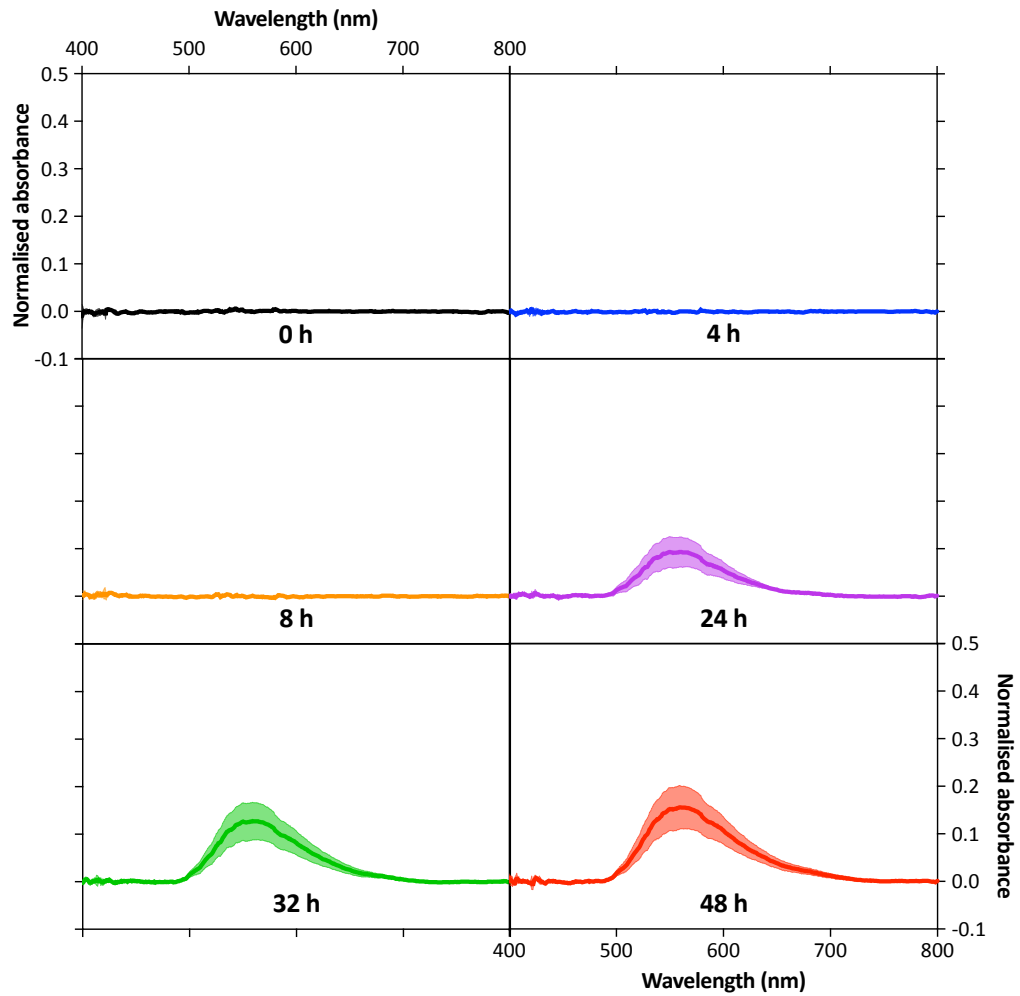


**Figure 12.33:** Spectra of SmF after baseline correction. The original visible spectra are shown in graph d) of **Figure 6.2**. Results are average of three independent replicates. Some error bars cannot be visualised because they are smaller than the thickness of the curves.

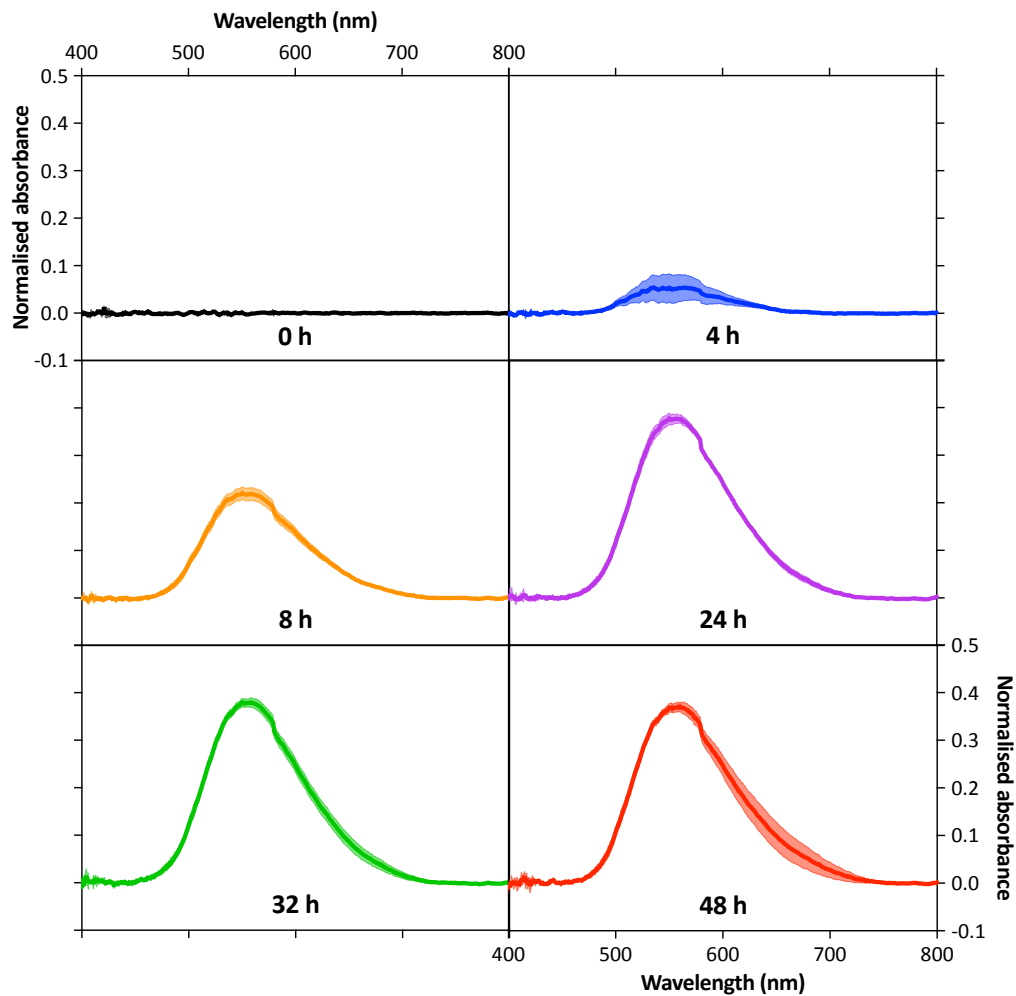


**Figure 12.34:** Spectra of DmAC after baseline correction. The original visible spectra are shown in graph e) of **Figure 6.2**. Results are average of three independent replicates. Some error bars cannot be visualised because they are smaller than the thickness of the curves.

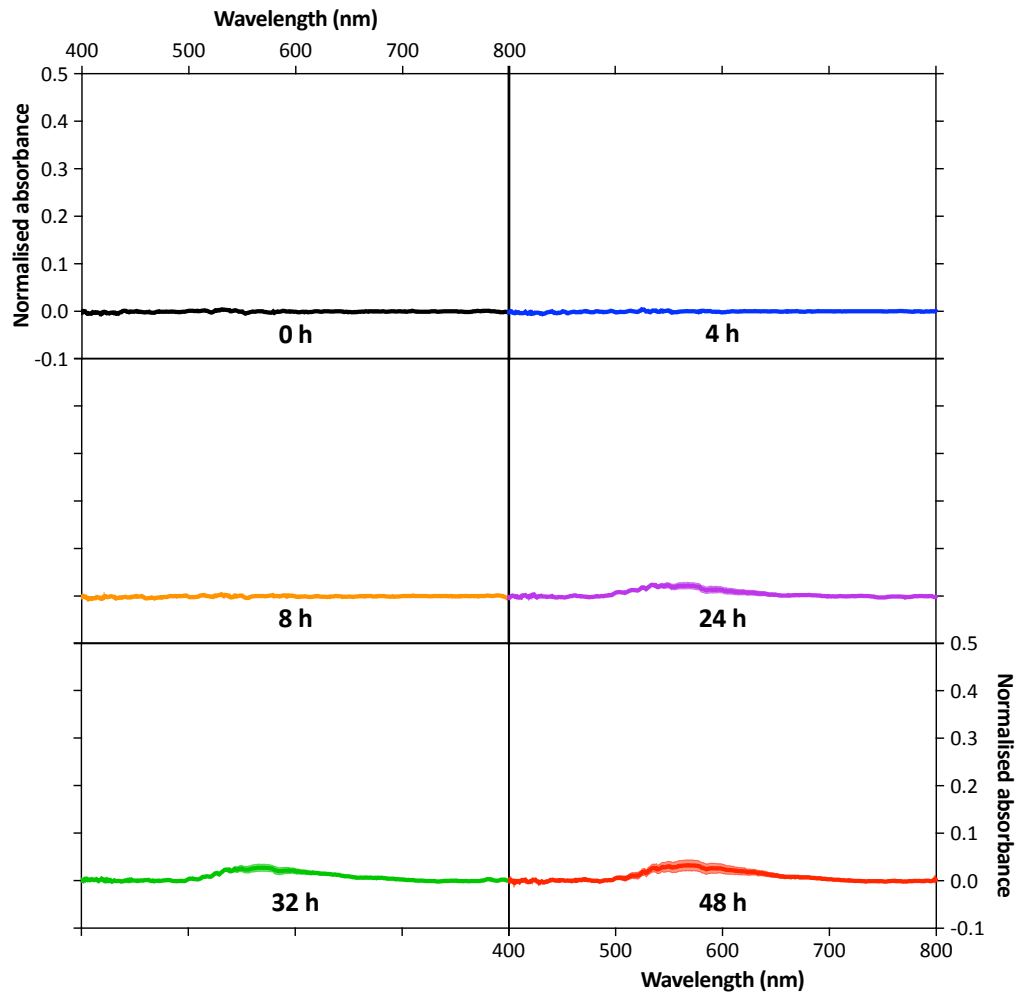


**Figure 12.35:** Spectra of DmAF after baseline correction. The original visible spectra are shown in graph f) of **Figure 6.2**. Results are average of three independent replicates. Some error bars cannot be visualised because they are smaller than the thickness of the curves.

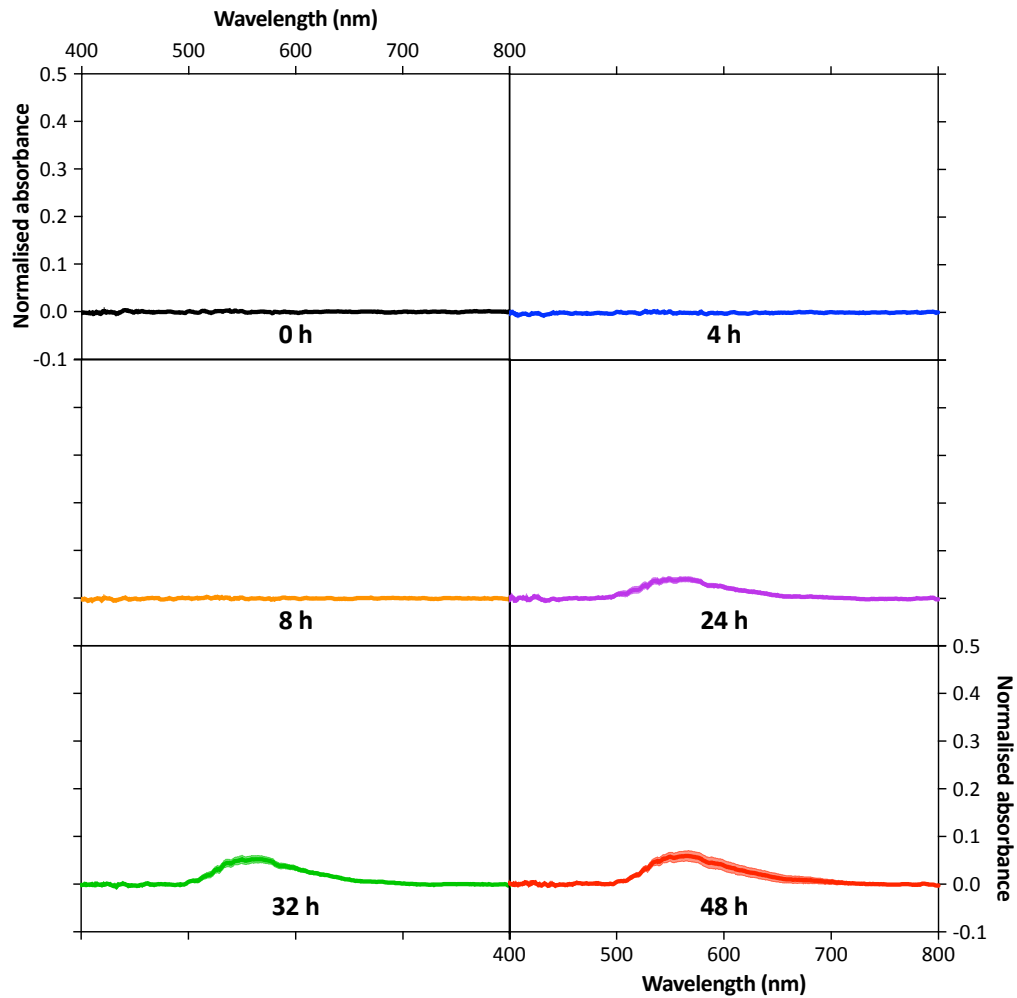


**Figure 12.36:** Spectra of DmCF after baseline correction. The original visible spectra are shown in graph g) of **Figure 6.2**. Results are average of three independent replicates. Some error bars cannot be visualised because they are smaller than the thickness of the curves.



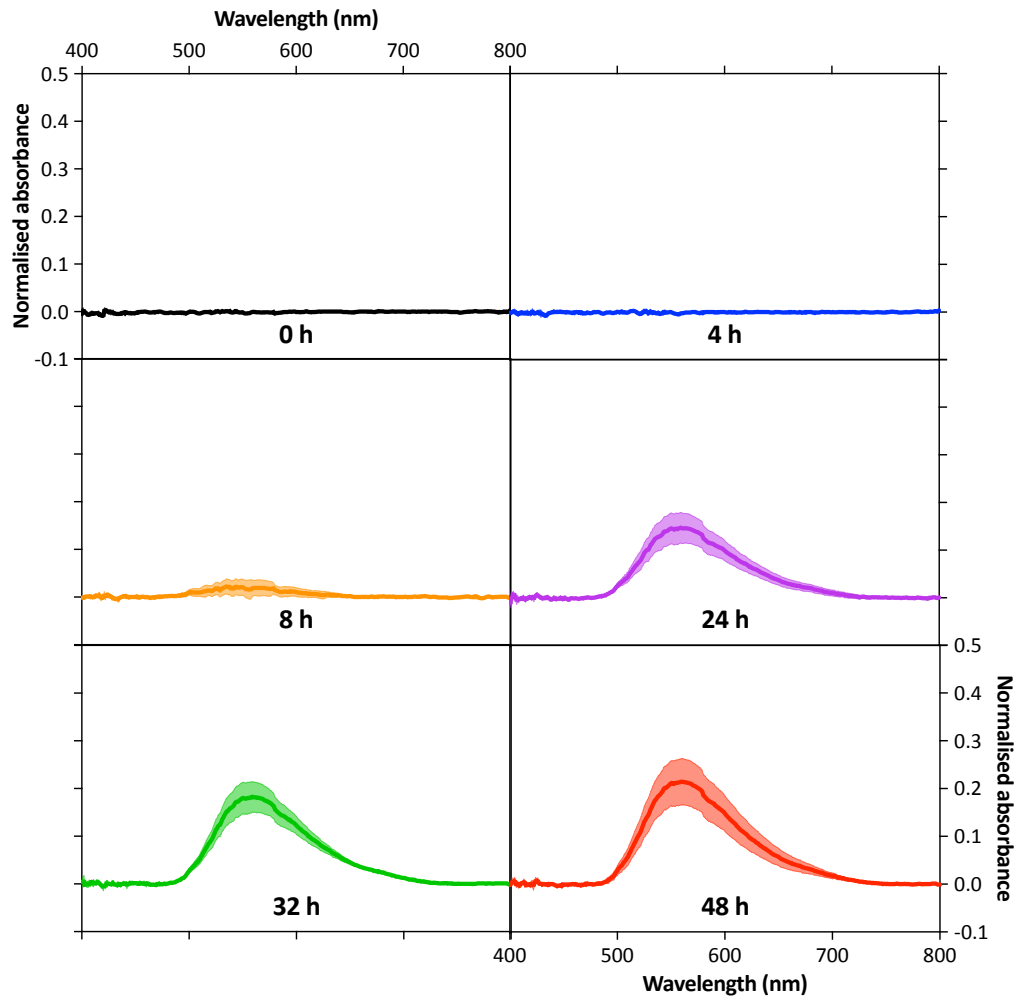


**Figure 12.37:** Spectra of TmACF after baseline correction. The original visible spectra are shown in graph h) of **Figure 6.2**. Results are average of three independent replicates. Some error bars cannot be visualised because they are smaller than the thickness of the curves.

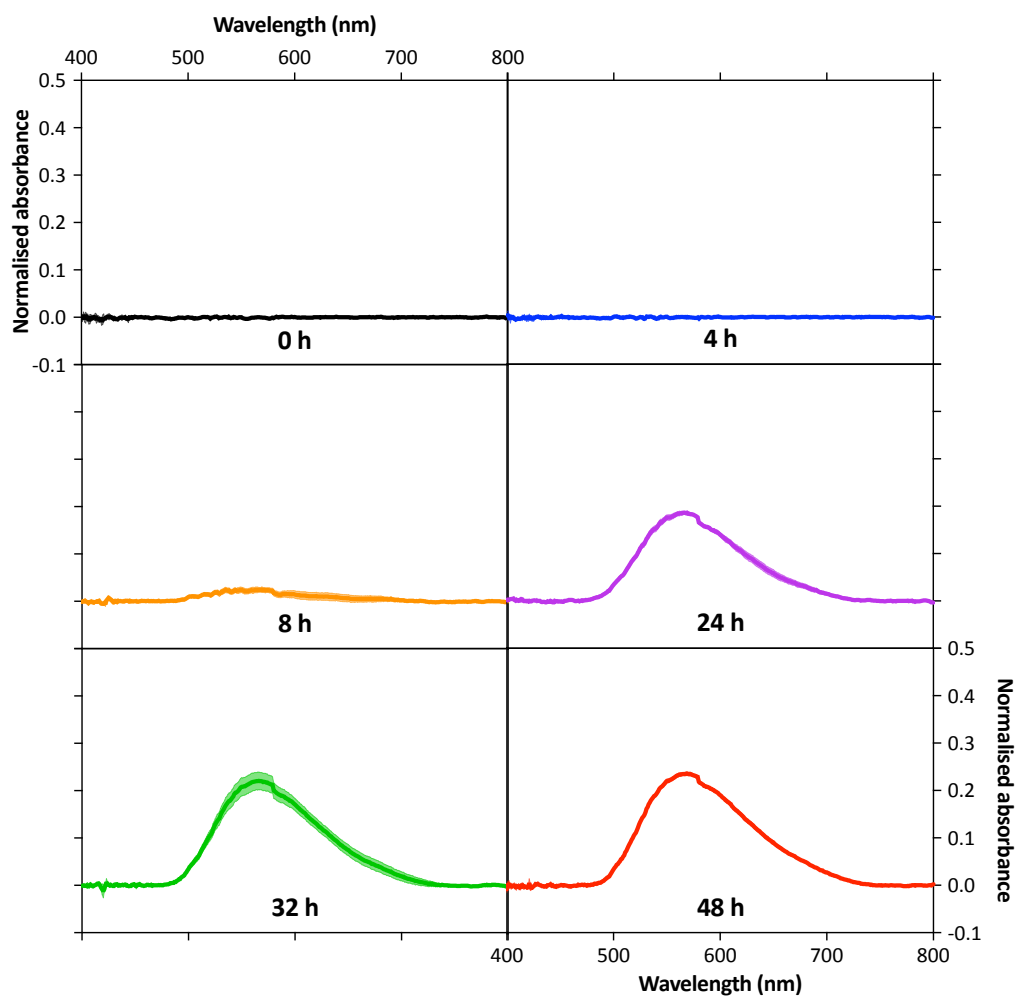


**Figure 12.38:** Spectra of MmOP after baseline correction. The original visible spectra are shown in graph i) of **Figure 6.2**. Results are average of three independent replicates. Some error bars cannot be visualised because they are smaller than the thickness of the curves.

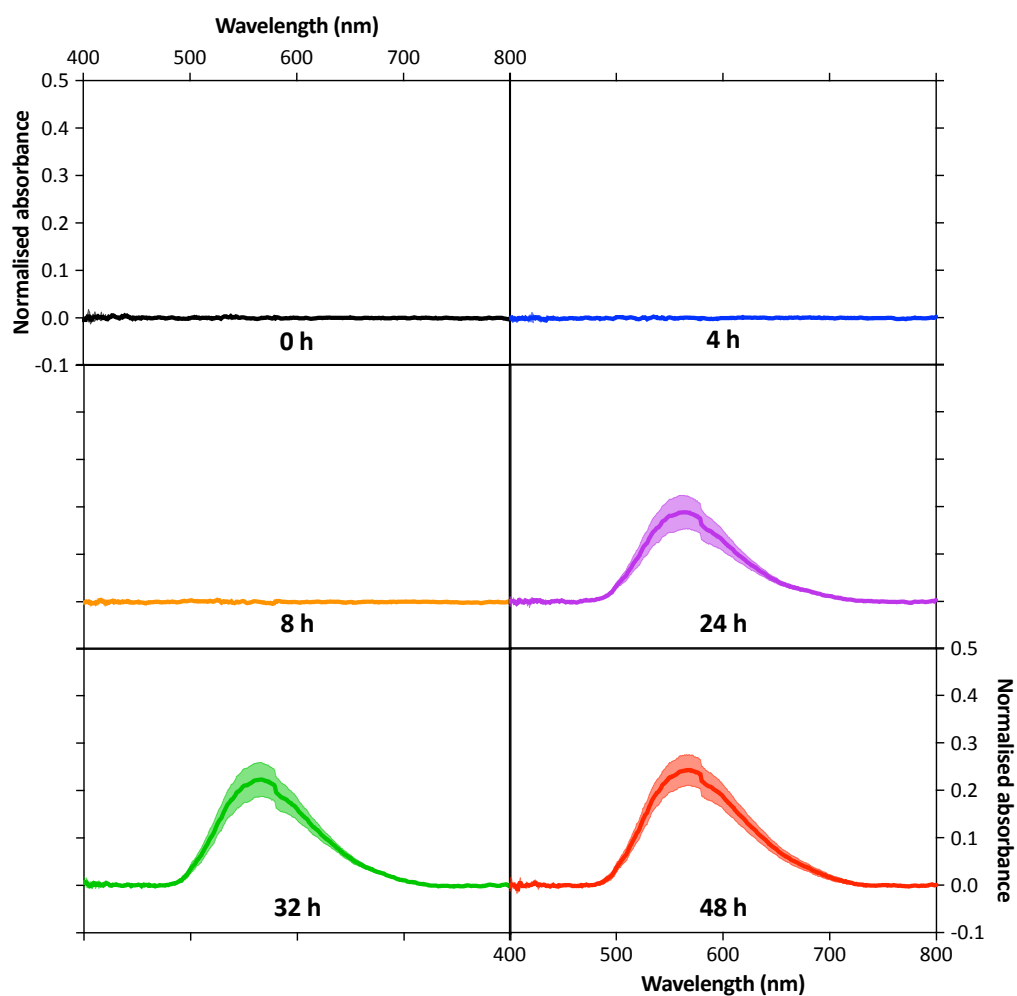


**Figure 12.39:** Spectra of  $CcmC^-$  after baseline correction. The original visible spectra are shown in graph j) of **Figure 6.2**. Results are average of three independent replicates. Some error bars cannot be visualised because they are smaller than the thickness of the curves.

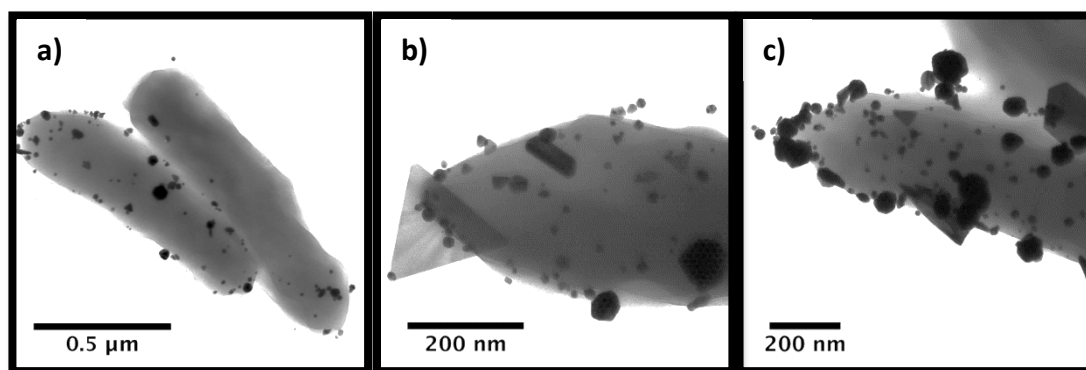


**Figure 12.40:** Additional TEM images of SmA after implementation of method I (aerobic synthesis of gold nanoparticles).

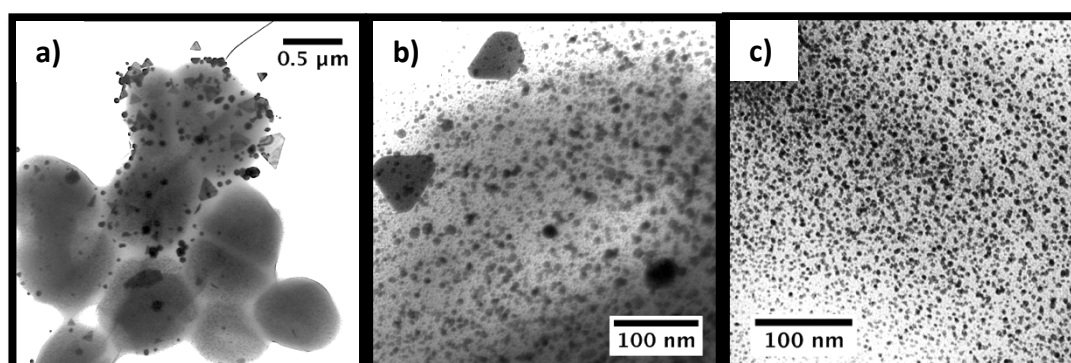


**Figure 12.41:** Additional TEM images of SmC after implementation of method I (aerobic synthesis of gold nanoparticles).

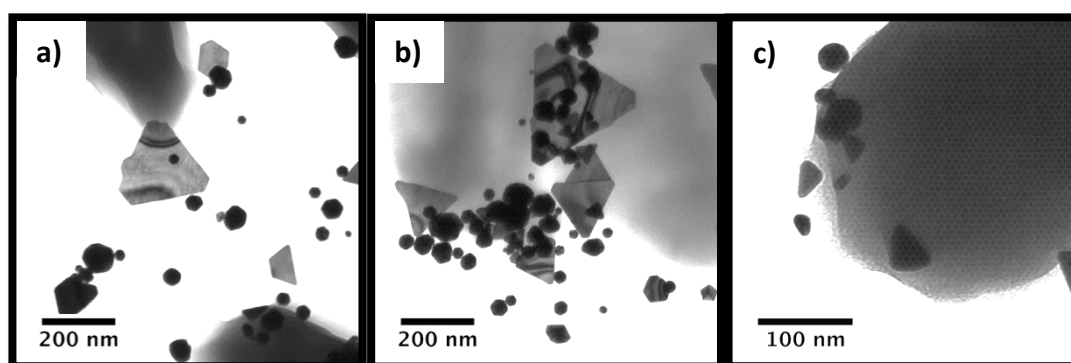


**Figure 12.42:** Additional TEM images of SmF after implementation of method I (aerobic synthesis of gold nanoparticles).

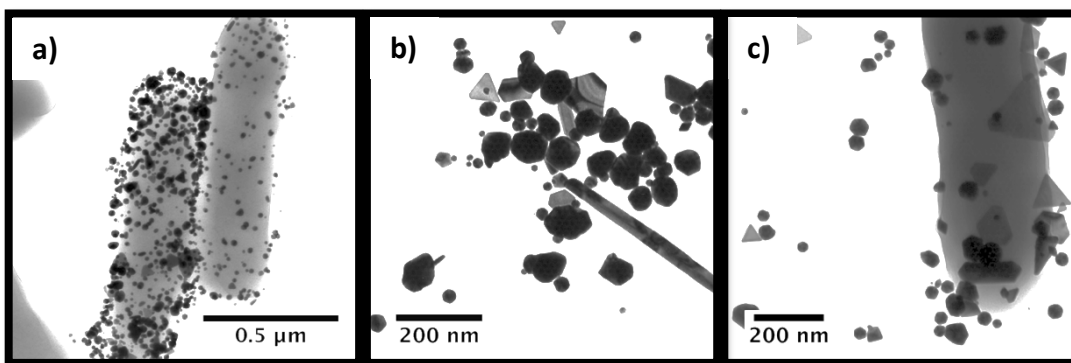


**Figure 12.43:** Additional TEM images of DmAC after implementation of method I (aerobic synthesis of gold nanoparticles).

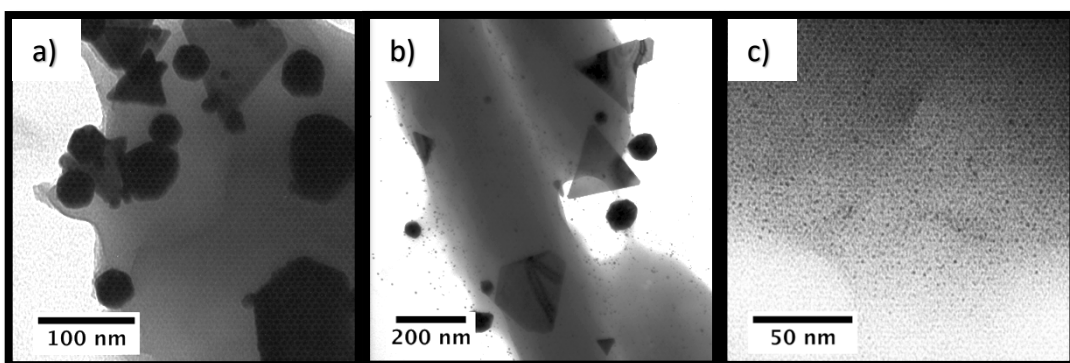


**Figure 12.44:** Additional TEM images of DmAF after implementation of method I (aerobic synthesis of gold nanoparticles).

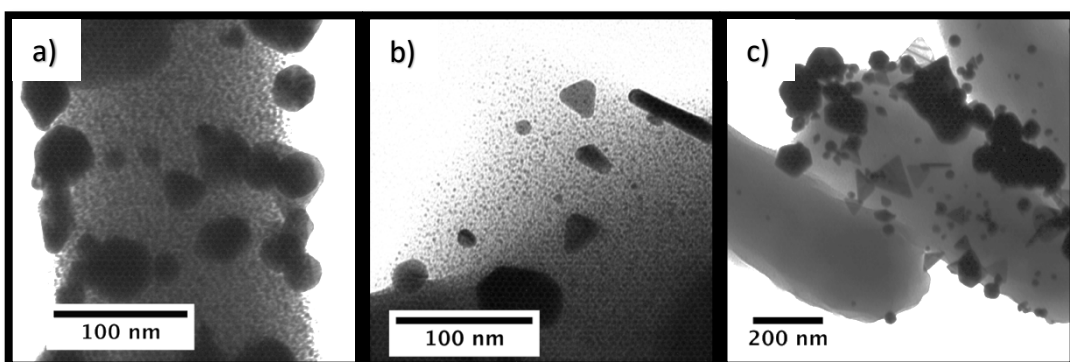


**Figure 12.45:** Additional TEM images of DmCF after implementation of method I (aerobic synthesis of gold nanoparticles).

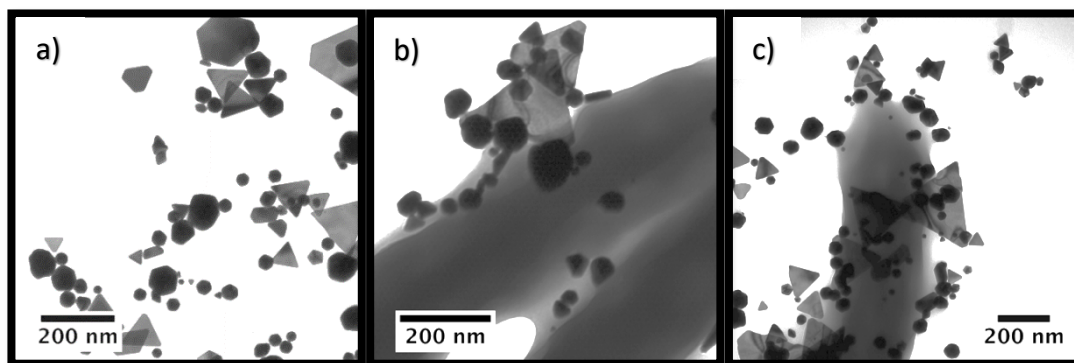


**Figure 12.46:** Additional TEM images of TmACF after implementation of method I (aerobic synthesis of gold nanoparticles).

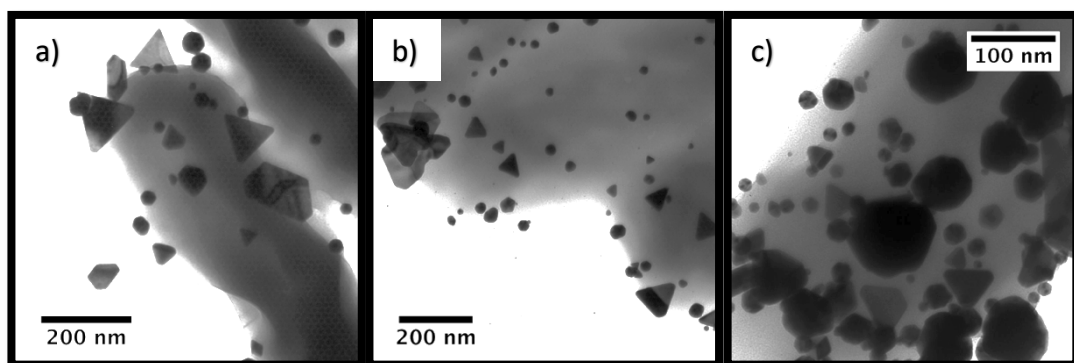


**Figure 12.47:** Additional TEM images of MmOP after implementation of method I (aerobic synthesis of gold nanoparticles).

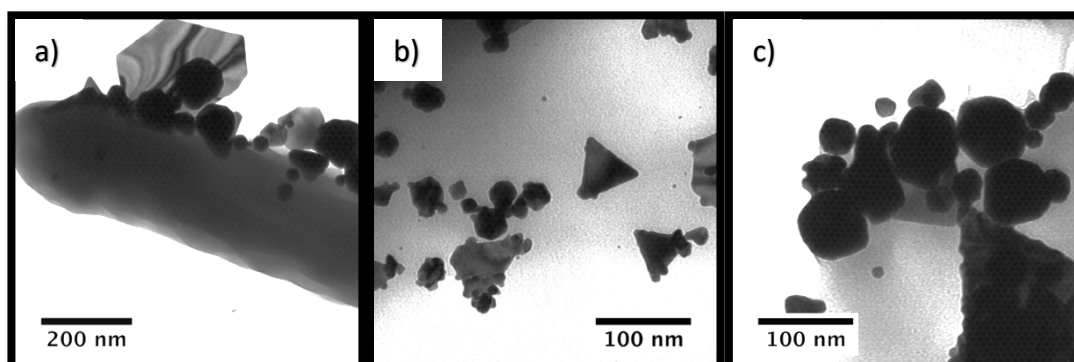


**Figure 12.48:** Additional TEM images of CcmC<sup>-</sup> after implementation of method I (aerobic synthesis of gold nanoparticles).

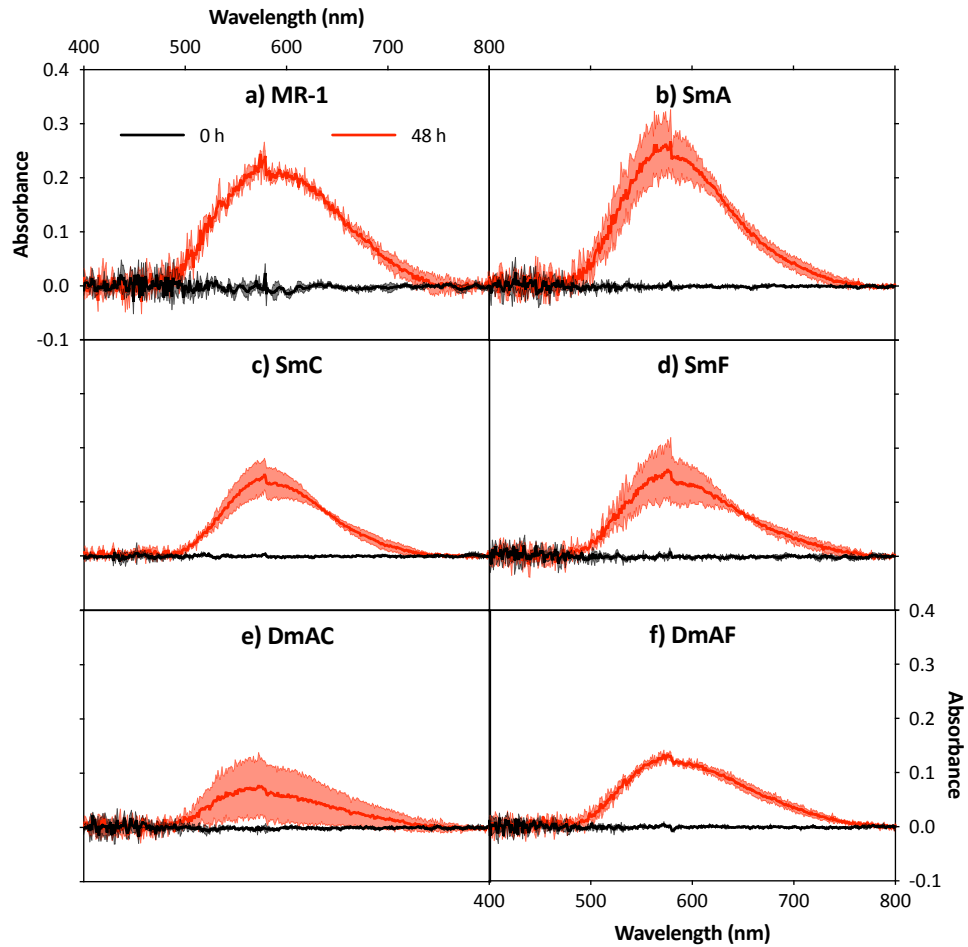


**Figure 12.49:** Spectra of the anaerobic cultures after baseline correction. The original visible spectra are shown in graphs a) to f) of **Figure 6.8**. Results are average of three independent replicates. Some error bars cannot be visualised because they are smaller than the thickness of the curves.

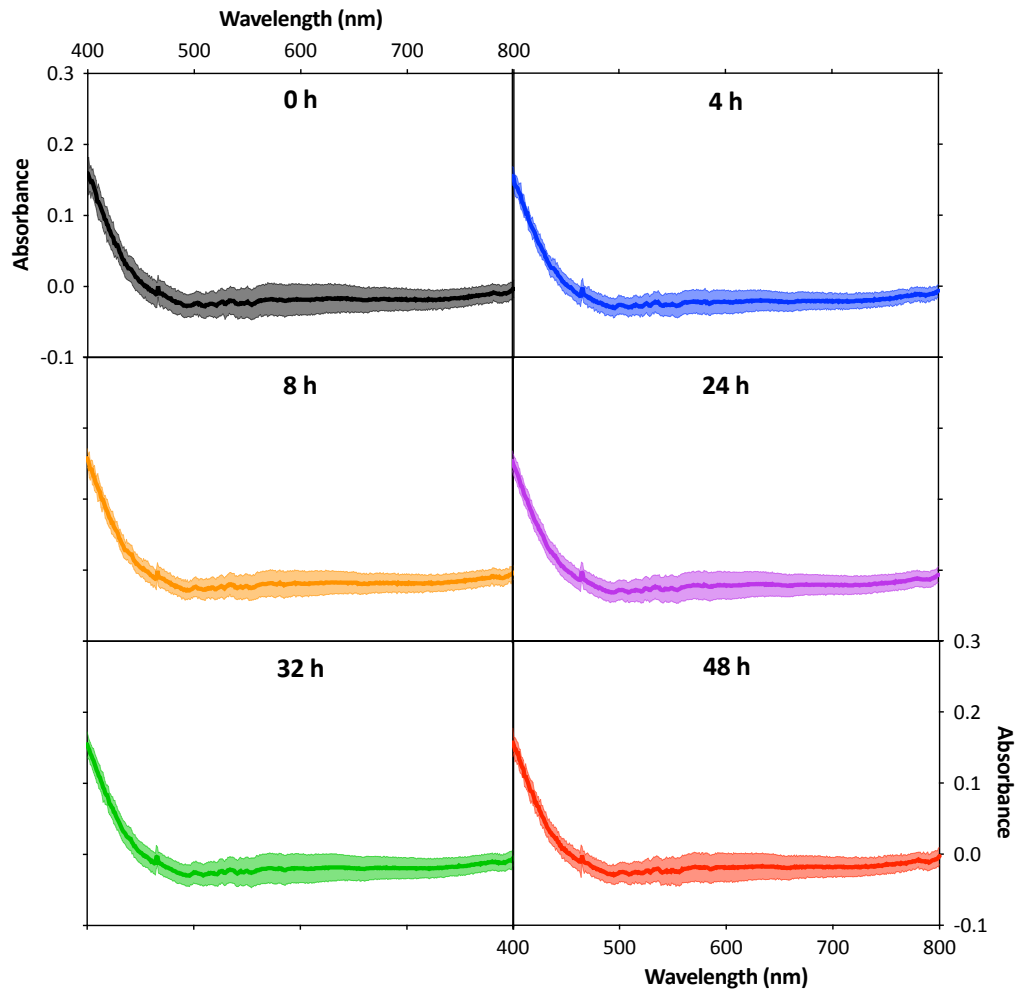


**Figure 12.50:** Visible spectra of anaerobic 1 mM  $\text{HAuCl}_4$  solution incubated under anaerobic conditions at 30 °C and 180 rpm for 48 h – abiotic control of method II. Error bars indicate the standard deviation of three independent replicates.



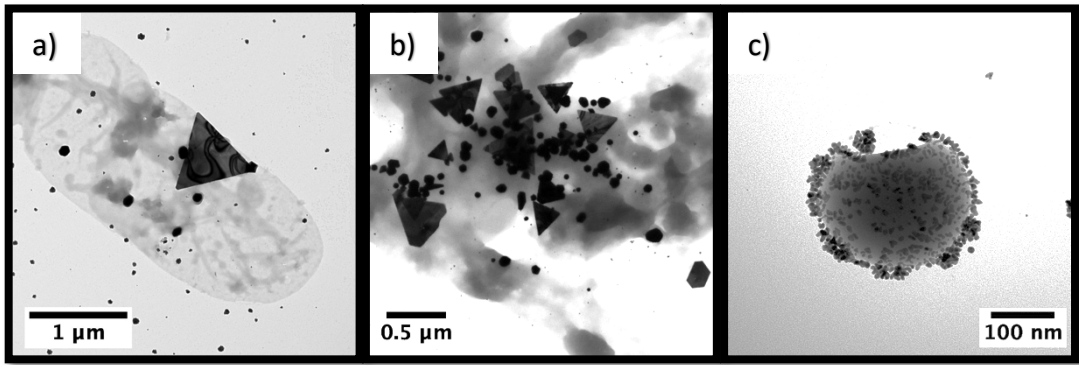


**Figure 12.51:** Additional TEM images of MR-1 after implementation of method II (anaerobic synthesis of gold nanoparticles).

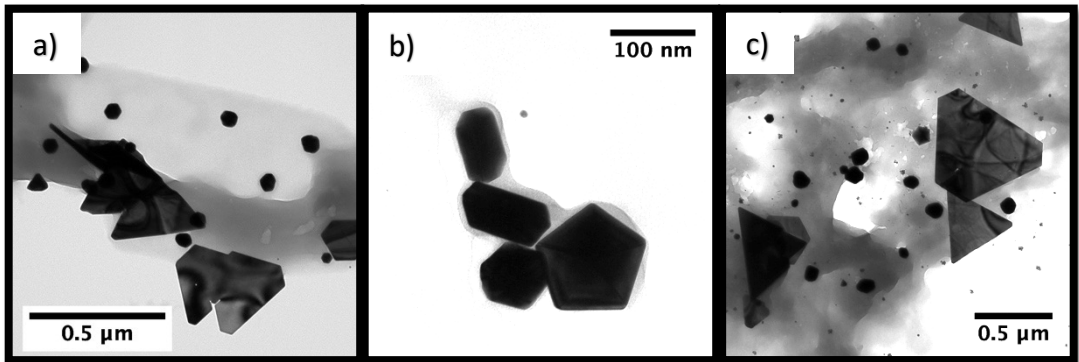


**Figure 12.52:** Additional TEM images of SmA after implementation of method II (anaerobic synthesis of gold nanoparticles).

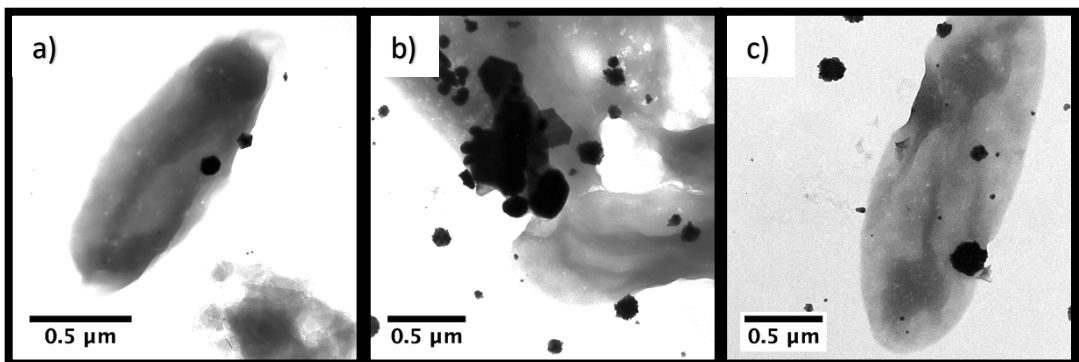


**Figure 12.53:** Additional TEM images of SmC after implementation of method II (anaerobic synthesis of gold nanoparticles).

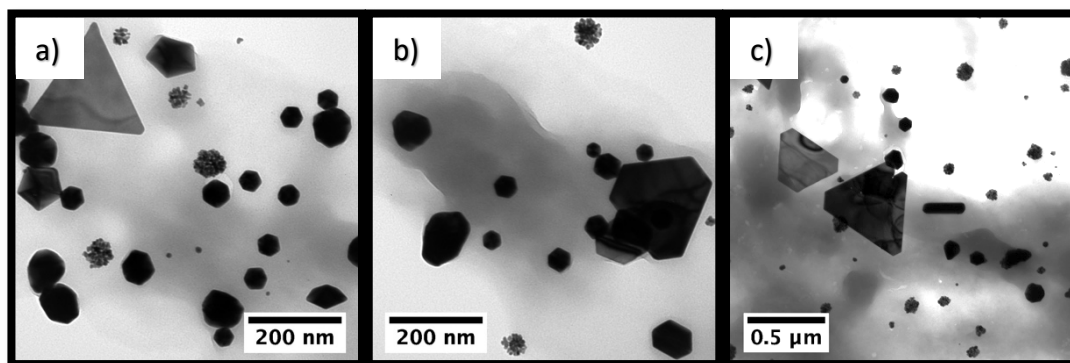


**Figure 12.54:** Additional TEM images of SmF after implementation of method II (anaerobic synthesis of gold nanoparticles).

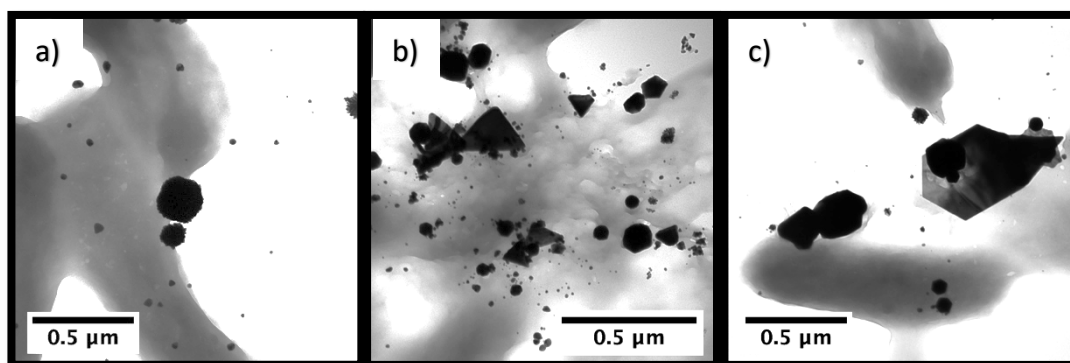


**Figure 12.55:** Additional TEM images of DmAC after implementation of method II (anaerobic synthesis of gold nanoparticles).

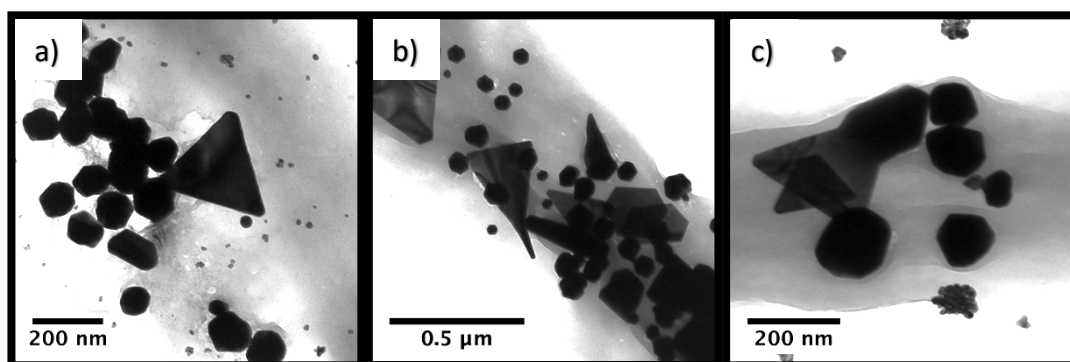


**Figure 12.56:** Additional TEM images of DmAF after implementation of method II (anaerobic synthesis of gold nanoparticles).

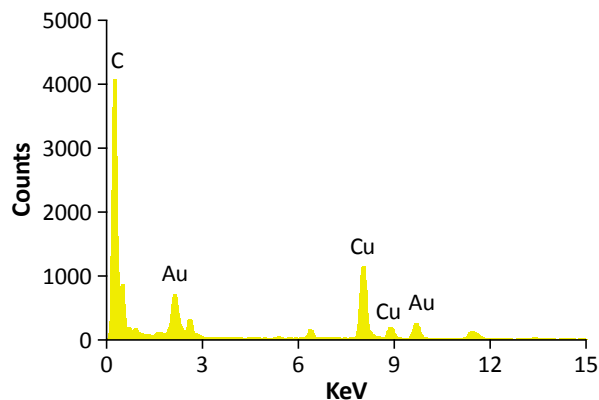


**Figure 12.57:** EDS measurement of nanoparticles made anaerobically by MR-1 through method II (anaerobic synthesis of gold nanoparticles).

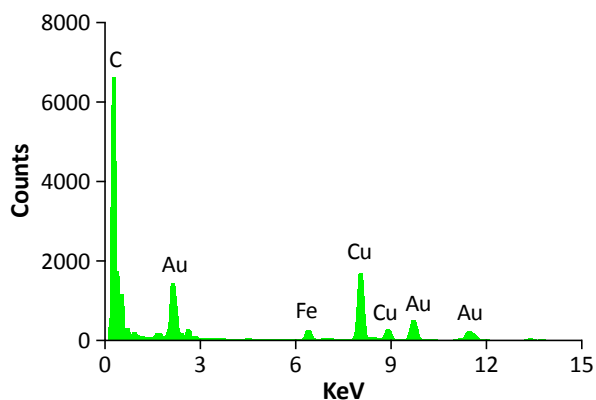


**Figure 12.58:** EDS measurement of nanoparticles made anaerobically by SmA through method II (anaerobic synthesis of gold nanoparticles).

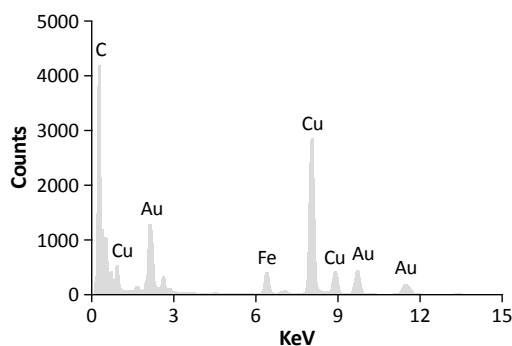


**Figure 12.59:** EDS measurement of nanoparticles made anaerobically by SmC through method II (anaerobic synthesis of gold nanoparticles).

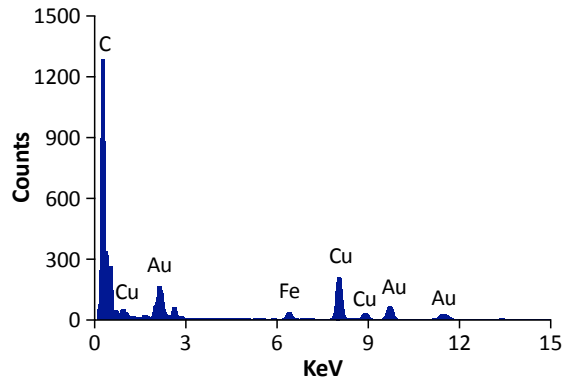


**Figure 12.60:** EDS measurement of nanoparticles made anaerobically by SmF through method II (anaerobic synthesis of gold nanoparticles).

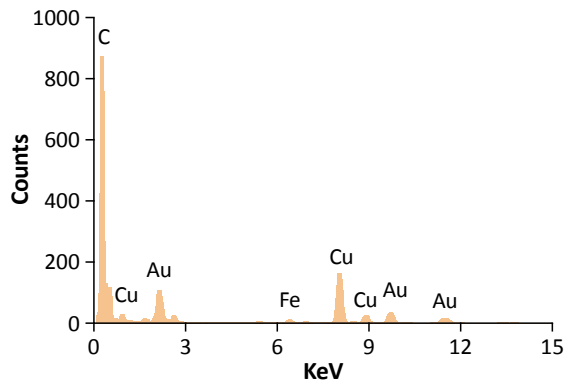


**Figure 12.61:** EDS measurement of nanoparticles made anaerobically by DmAC through method II (anaerobic synthesis of gold nanoparticles).

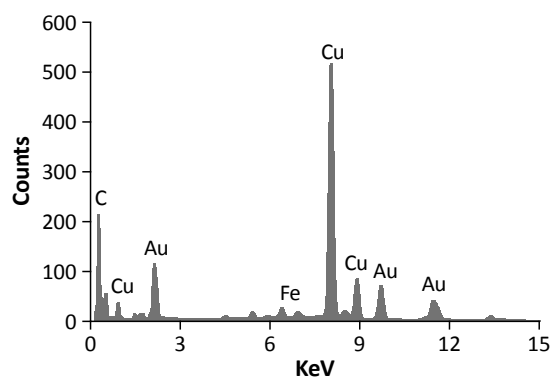


**Figure 12.62:** EDS measurement of nanoparticles made anaerobically by DmAF through method II (anaerobic synthesis of gold nanoparticles).

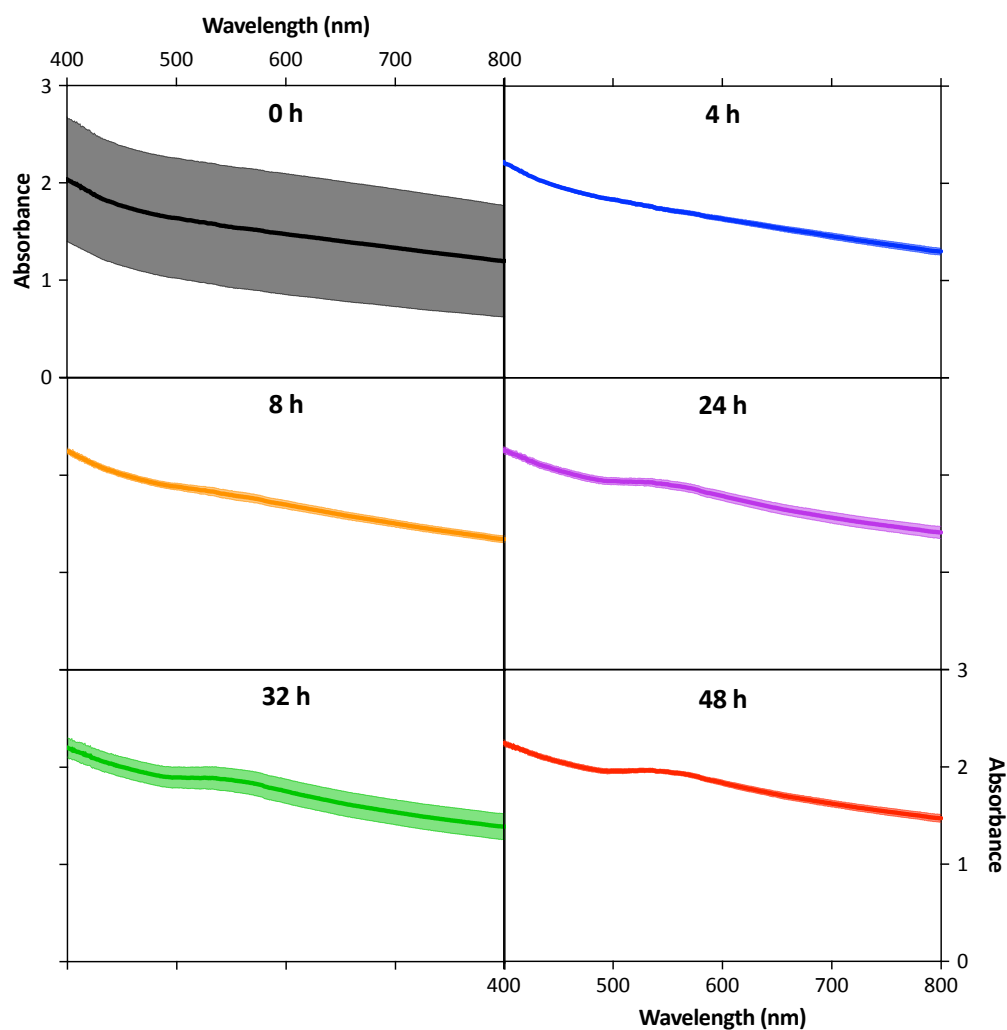
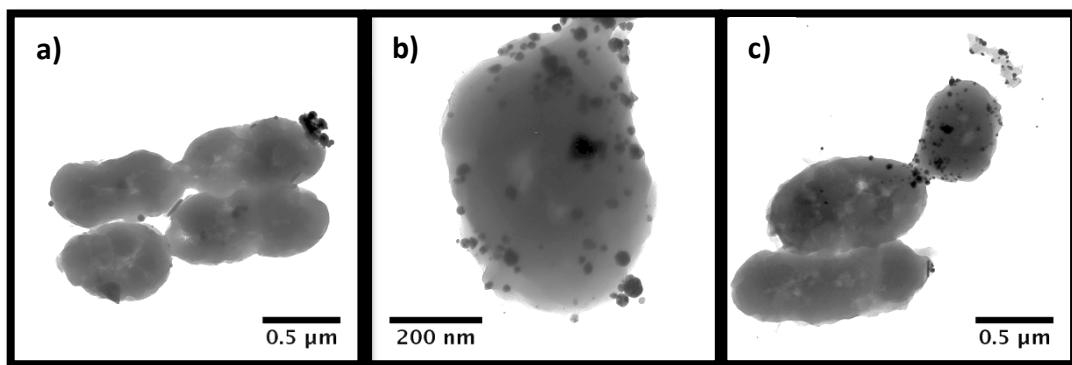


**Figure 12.63:** Additional TEM images of autoclaved BL21(DE3) after implementation of method I and visible spectra from graph a) of **Figure 7.3** divided into individual measurements. Results are average of three independent replicates. Some error bars cannot be visualised because they are smaller than the thickness of the curves.

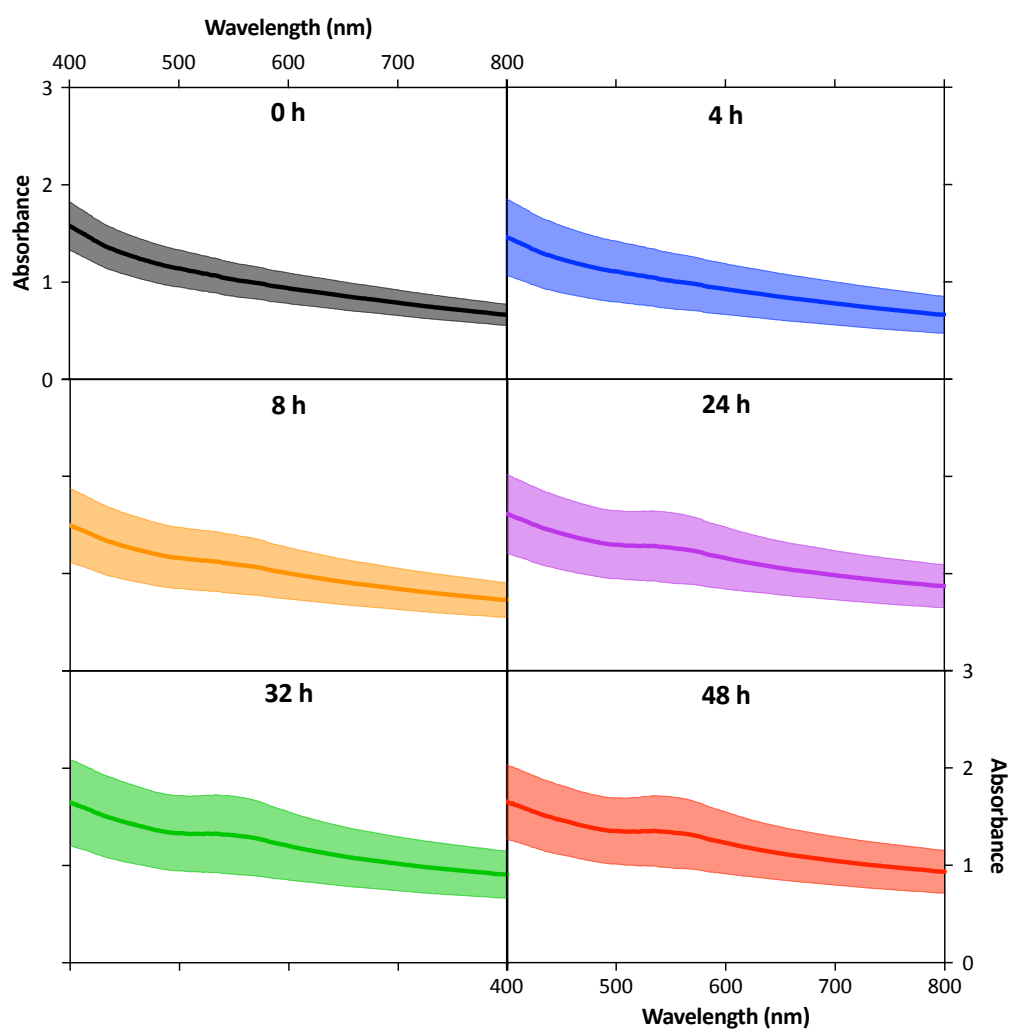
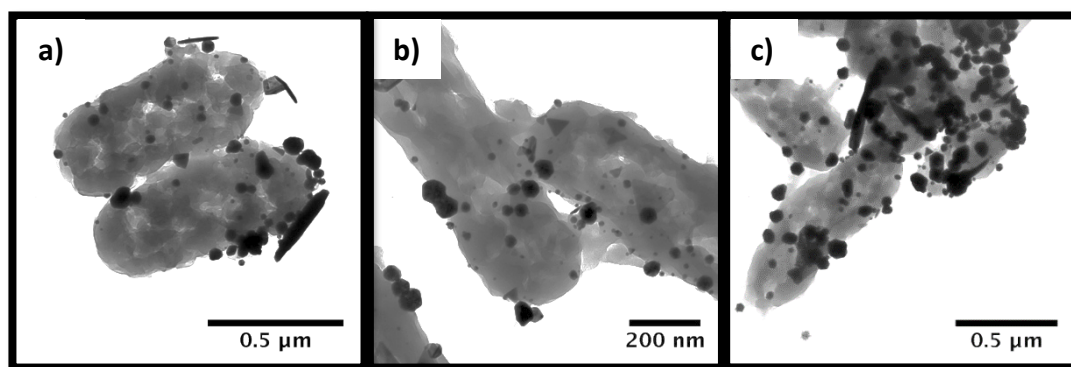


**Figure 12.64:** Additional TEM images of autoclaved MR-1 after implementation of method I and visible spectra from graph b) of **Figure 7.3** divided into individual measurements. Error bars indicate the standard deviation of three independent replicates.

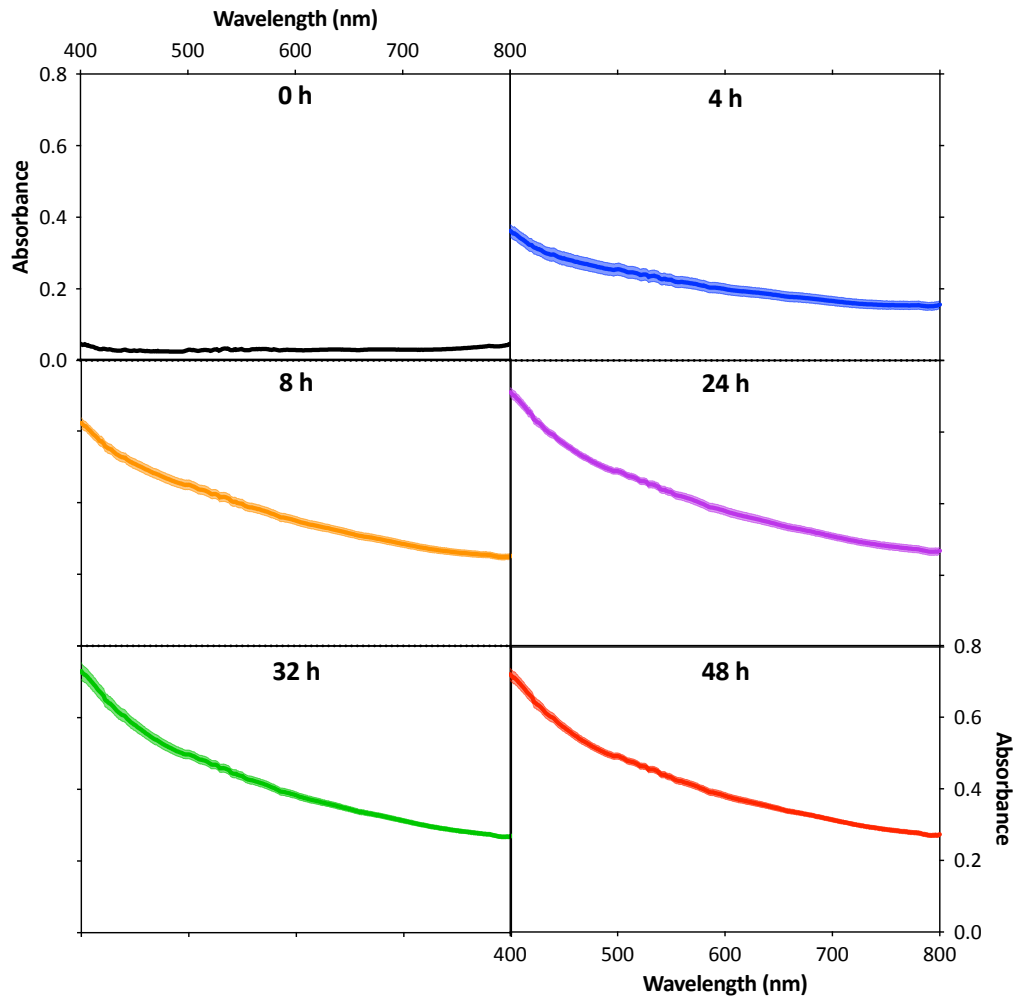


**Figure 12.65:** Visible spectra from graph a) of **Figure 7.5** divided into individual measurements. Results are average of three independent replicates. Some error bars cannot be visualised because they are smaller than the thickness of the curves.

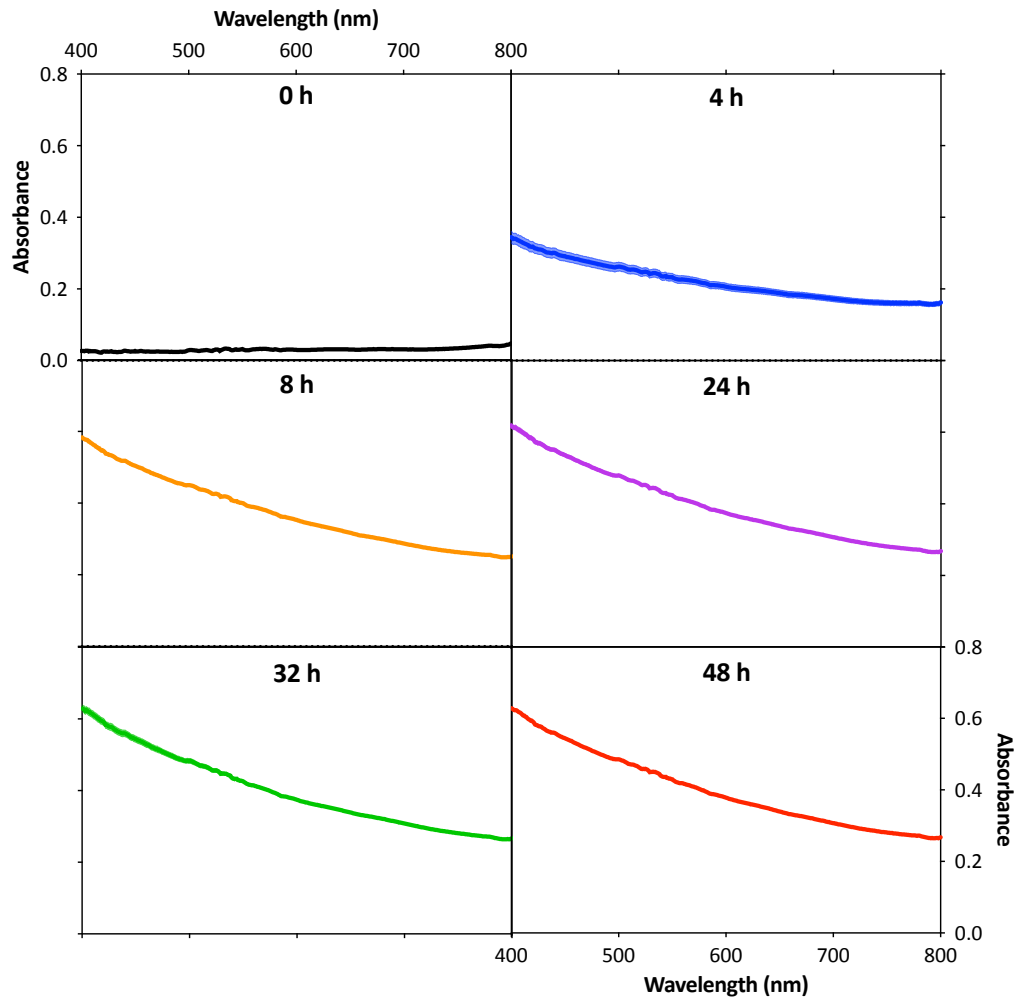


**Figure 12.66:** Visible spectra from graph b) of **Figure 7.5** divided into individual measurements. Results are average of three independent replicates. Some error bars cannot be visualised because they are smaller than the thickness of the curves.



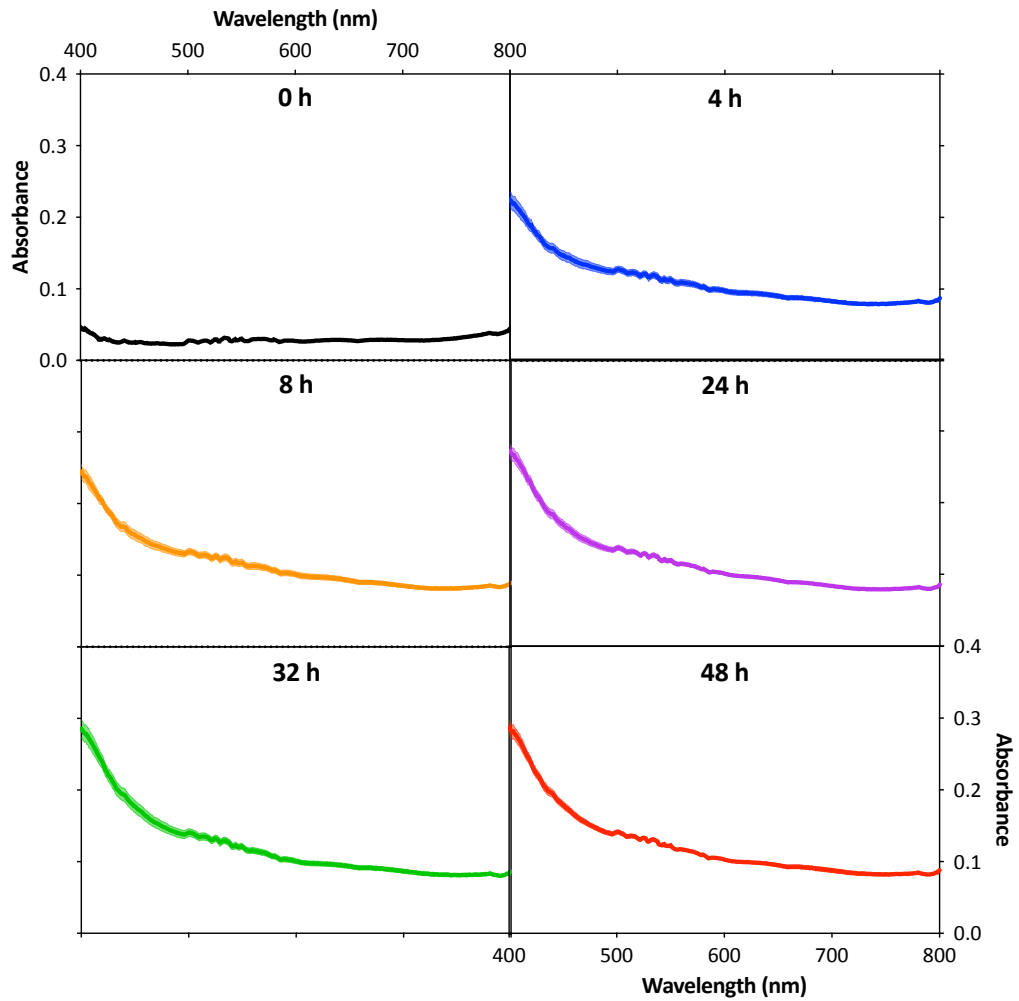


**Figure 12.67:** Visible spectra from graph c) of **Figure 7.5** divided into individual measurements. Results are average of three independent replicates. Some error bars cannot be visualised because they are smaller than the thickness of the curves. For improved clarity of the graphs, the scale in the y-axis was modified in relation to the scale in **Figure 7.5**.

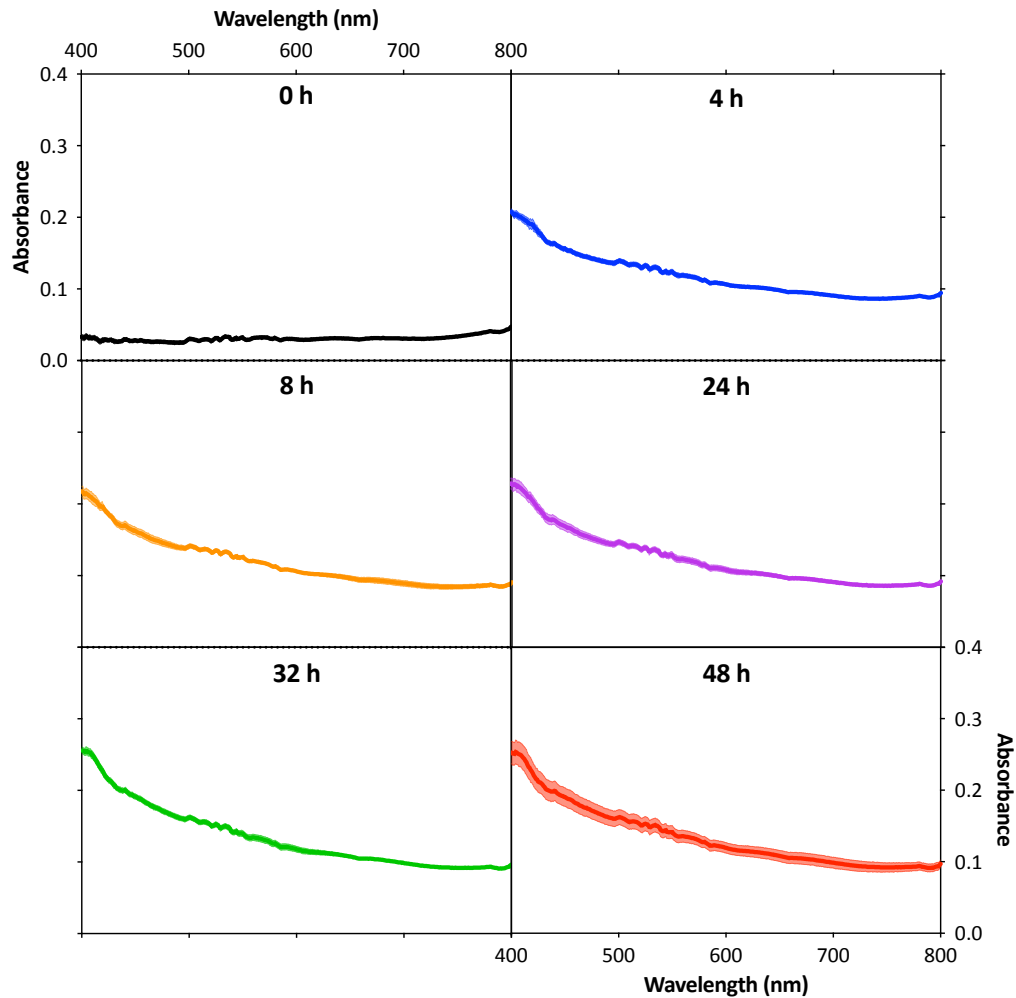


**Figure 12.68:** Visible spectra from graph d) of **Figure 7.5** divided into individual measurements. Results are average of three independent replicates. Some error bars cannot be visualised because they are smaller than the thickness of the curves. For improved clarity of the graphs, the scale in the y-axis was modified in relation to the scale in **Figure 7.5**.

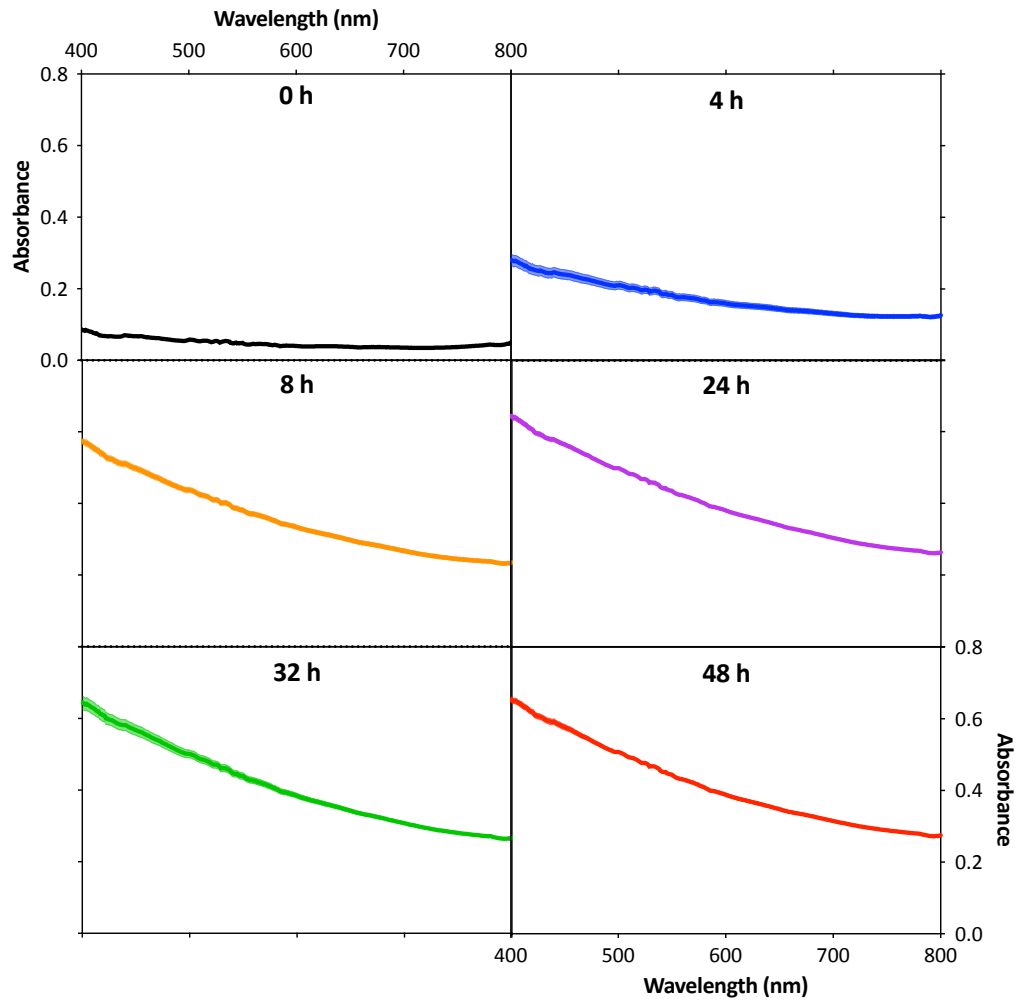


**Figure 12.69:** Visible spectra from graph e) of **Figure 7.5** divided into individual measurements. Results are average of three independent replicates. Some error bars cannot be visualised because they are smaller than the thickness of the curves.

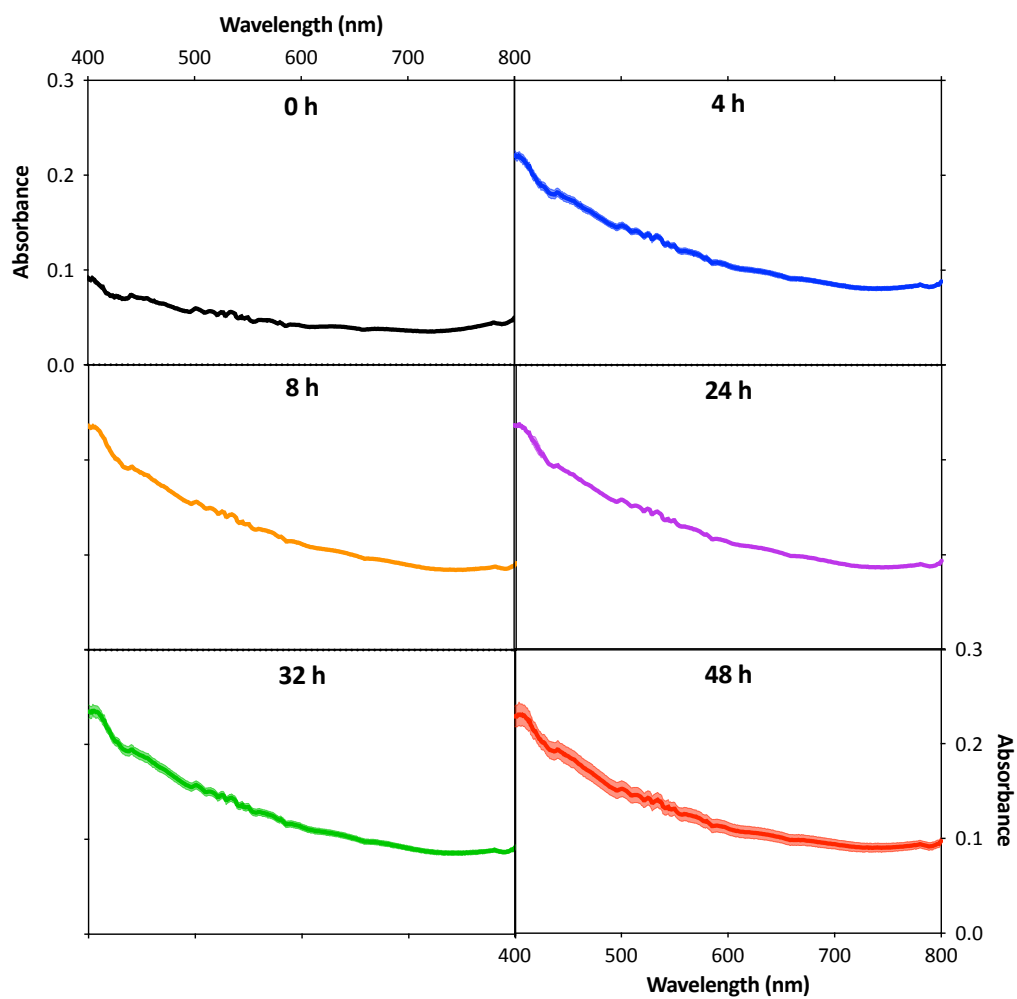


**Figure 12.70:** Visible spectra from graph f) of **Figure 7.5** divided into individual measurements. Results are average of three independent replicates. Some error bars cannot be visualised because they are smaller than the thickness of the curves. For improved clarity of the graphs, the scale in the y-axis was modified in relation to the scale in **Figure 7.5**.

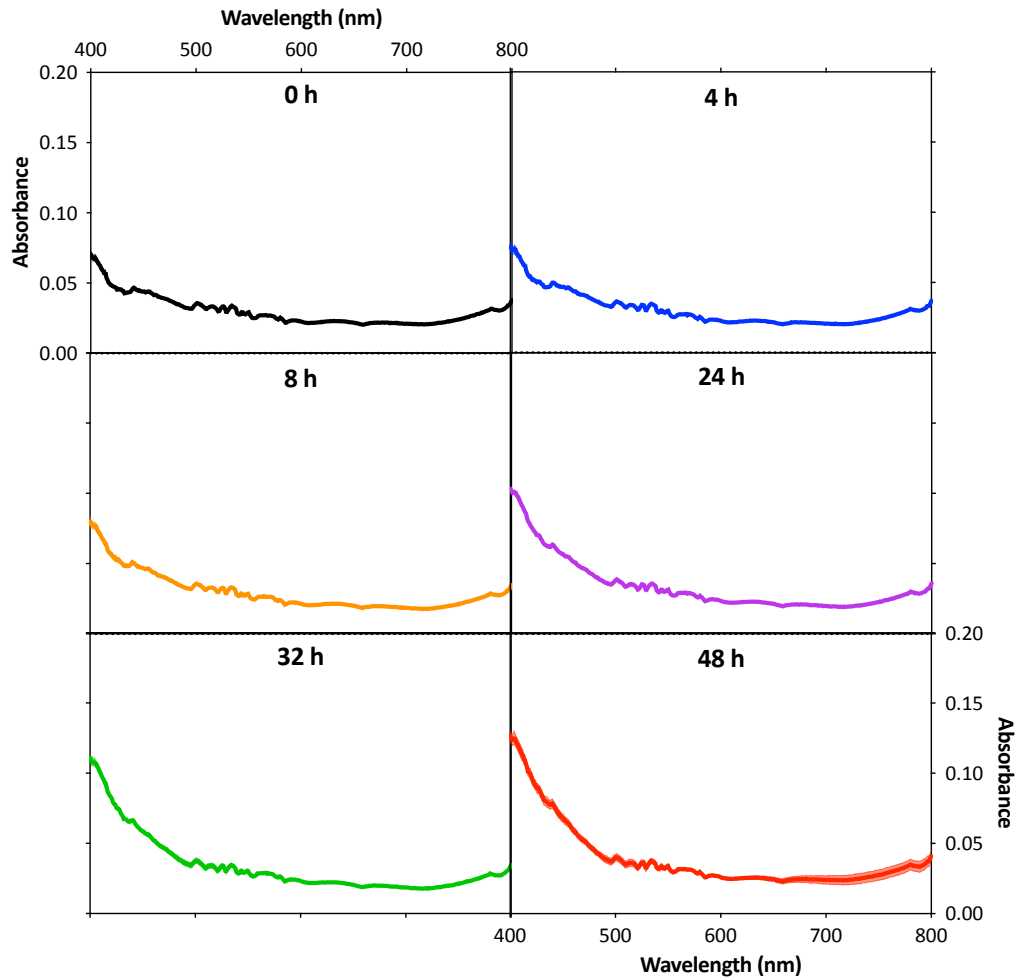


**Figure 12.71:** Visible spectra from graph g) of **Figure 7.5** divided into individual measurements. Results are average of three independent replicates. Some error bars cannot be visualised because they are smaller than the thickness of the curves. For improved clarity of the graphs, the scale in the y-axis was modified in relation to the scale in **Figure 7.5**.

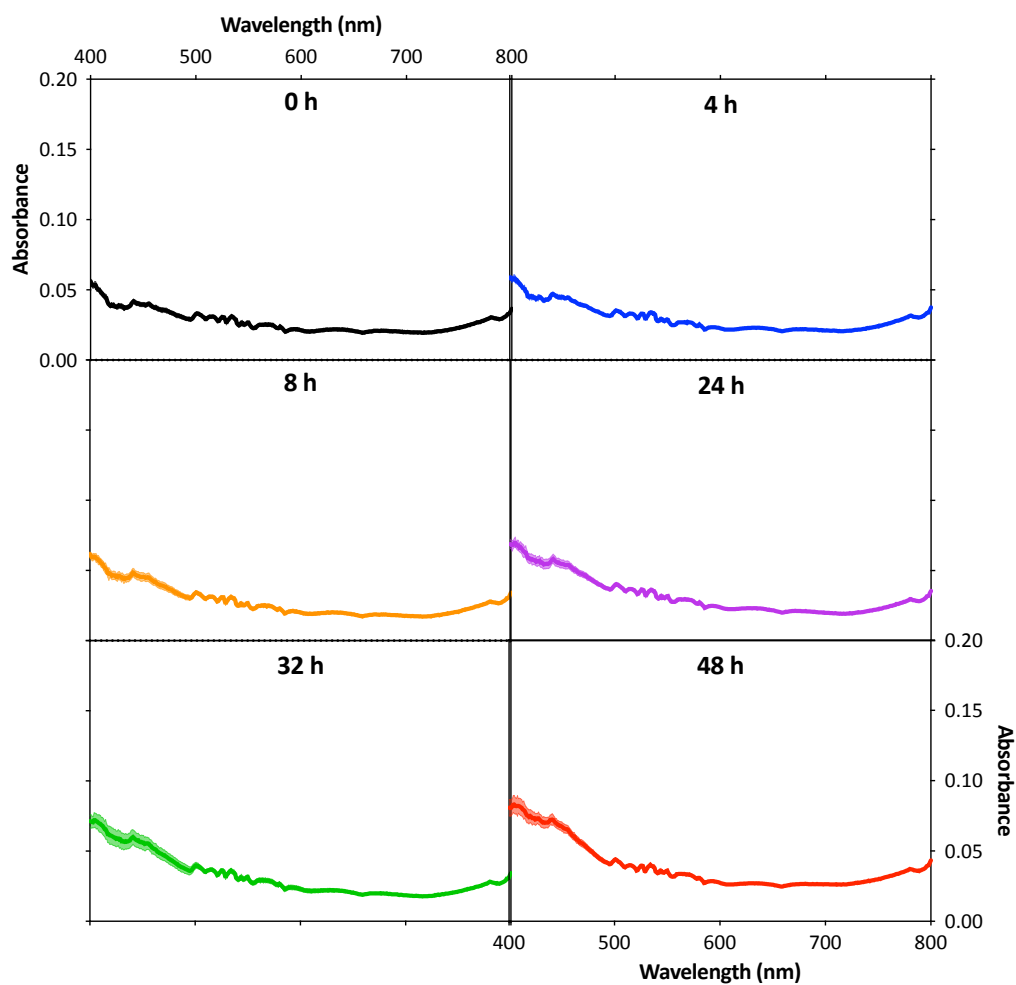


**Figure 12.72:** Visible spectra from graph h) of **Figure 7.5** divided into individual measurements. Results are average of three independent replicates. Some error bars cannot be visualised because they are smaller than the thickness of the curves. For improved clarity of the graphs, the scale in the y-axis was modified in relation to the scale in **Figure 7.5**.

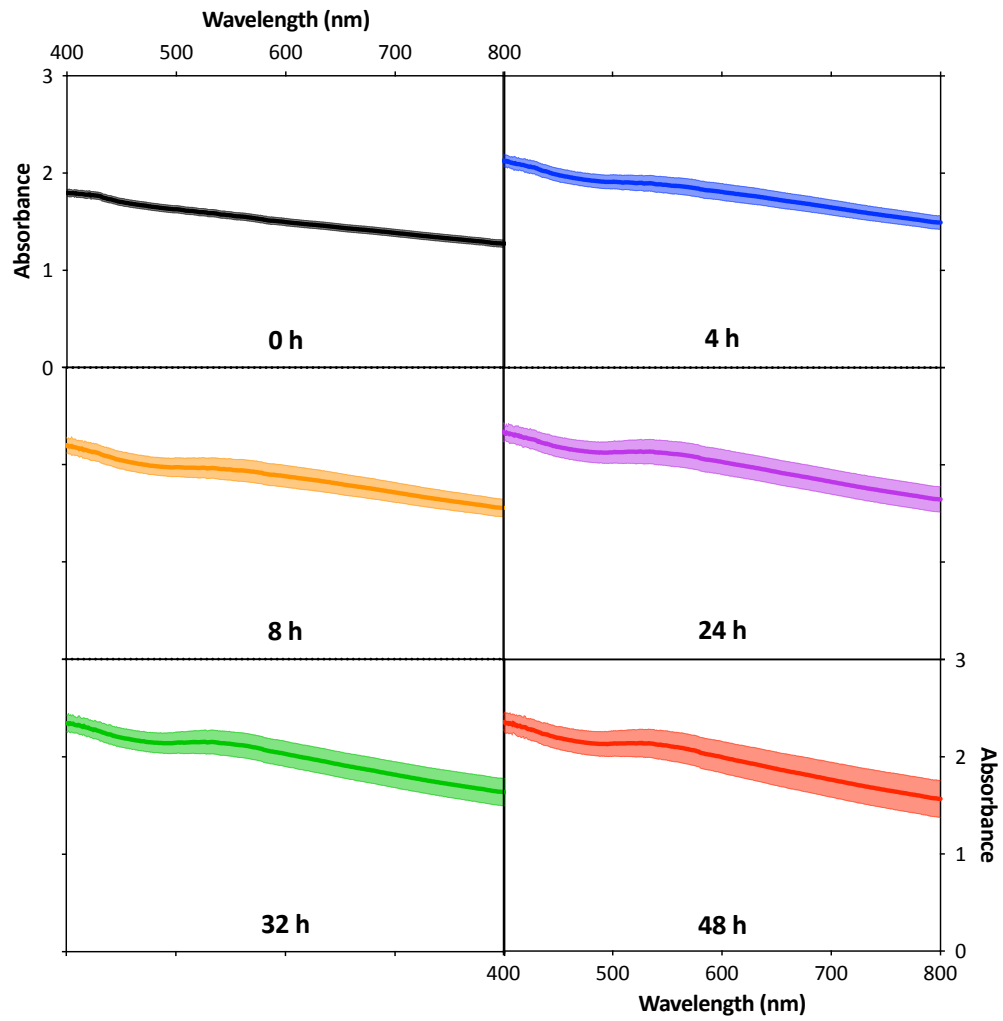


**Figure 12.73:** Visible spectra from graph a) of **Figure 7.6** divided into individual measurements. Error bars indicate the standard deviation of three independent replicates.

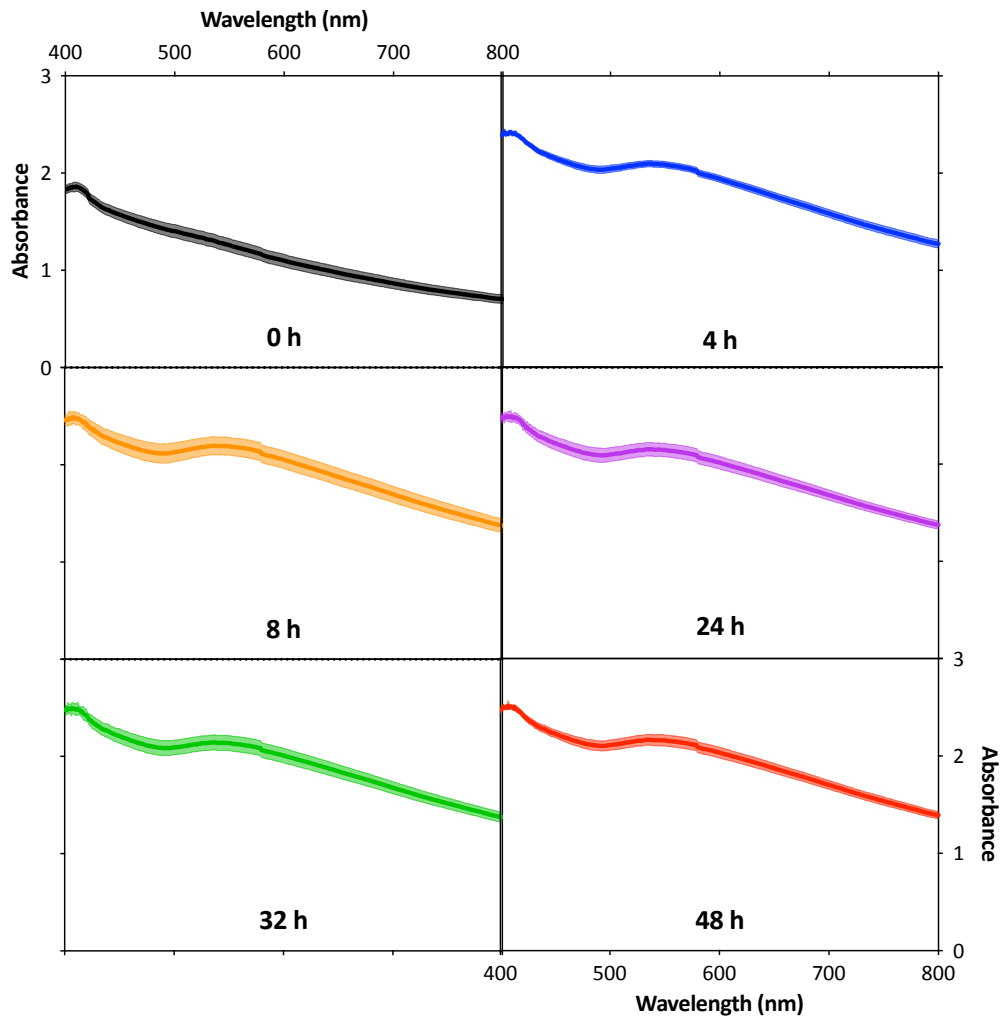


**Figure 12.74:** Visible spectra from graph b) of **Figure 7.6** divided into individual measurements. Results are average of three independent replicates. Some error bars cannot be visualised because they are smaller than the thickness of the curves.



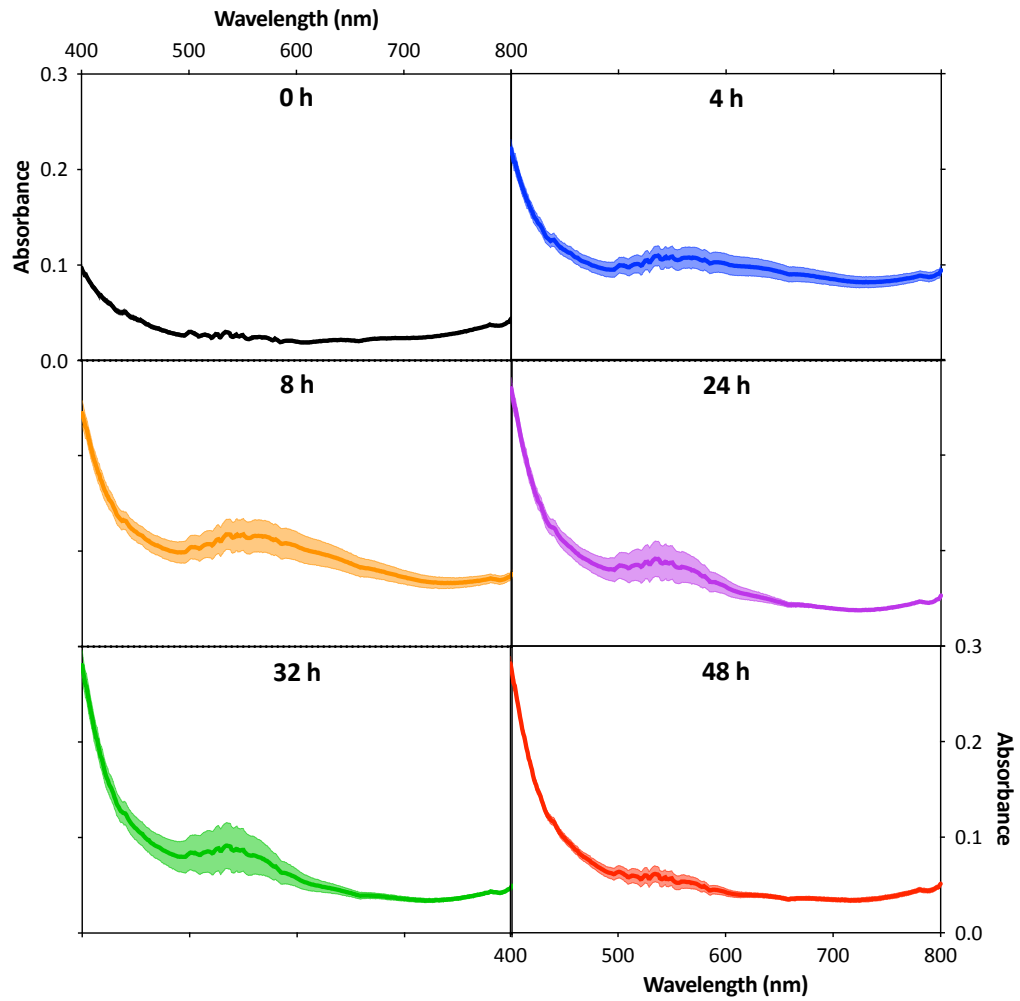


**Figure 12.75:** Visible spectra from graph c) of **Figure 7.6** divided into individual measurements. Results are average of three independent replicates. Some error bars cannot be visualised because they are smaller than the thickness of the curves. For improved clarity of the graphs, the scale in the y-axis was modified in relation to the scale in **Figure 7.6**.

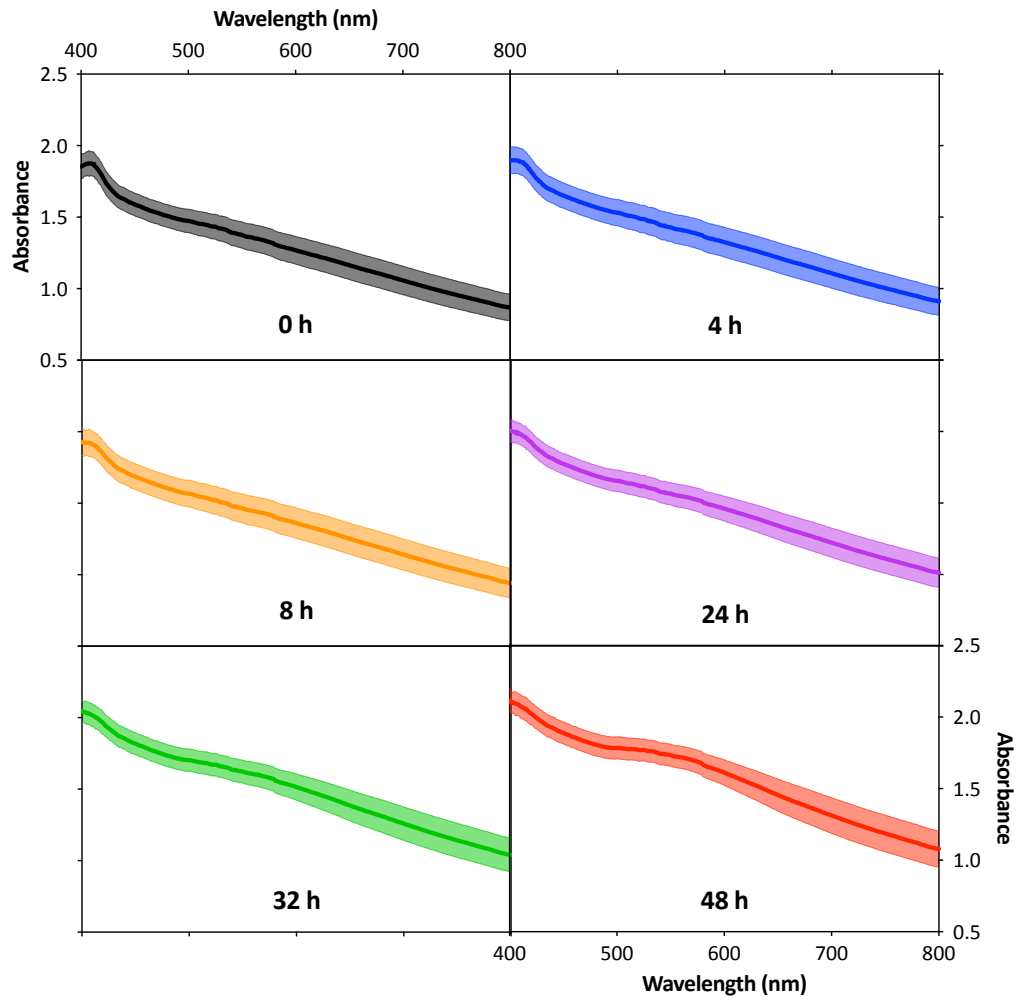


**Figure 12.76:** Visible spectra of MR-1 monitored during the implementation of method I with the variation of cells being resuspended and incubated in gold solution which had the pH corrected to 7. Error bars indicate the standard deviation of three independent replicates.

## 13 Appendix III

---

This appendix section presents growth monitoring of bacteria cultured under aerobic and anaerobic conditions. The tests made were aerobic growth of BL21(DE3) and MR-1 in LB and M9, and anaerobic growth of *S. oneidensis* wild-type and mutants in LB supplemented with sodium lactate and ferric citrate.

### 13.1 Materials and methods

#### 13.1.1 Microorganisms and culture media

All strains listed in **Table 4.1** were used for the experiments in this appendix section. For aerobic experiments, LB, LB agar and M9 were the culture media used. For anaerobic tests, anaerobic LB supplemented with 50 mM sodium lactate and 50 mM ferric citrate with pH 7.4 was the medium applied. The recipes for LB and M9 are the same as explained in section 4.1.2. The preparation of anaerobic LB supplemented with sodium lactate and ferric citrate also followed the same recipe as described in section 4.1.2, but ferric citrate solution did not pass through the centrifugation step after pH correction.

#### 13.1.2 Procedures for growing the cells

For bacterial growth under aerobic conditions, 250-mL shake flasks containing 50 mL of culture medium (LB or M9) were inoculated with 1 to 3 bacterial colonies in LB agar. The flasks were then incubated at 30 °C and 180 rpm. For anaerobic growth, 1 to 3 colonies in LB agar were inoculated into 10 mL LB in 50-mL centrifuge tubes, which were then incubated at 30 °C and 180 rpm for ca. 16 h. After the overnight growth  $OD_{600}$  was measured and an amount equivalent to 1 mL of cells at an  $OD_{600}$  of 1 was withdrawn with a syringe. The cultures were then injected into serum bottles containing 100 mL of the anaerobic LB supplemented with sodium lactate and ferric citrate and the bottles were left incubating at 30 °C and 180 rpm.

### 13.1.3 Monitoring growth

Aerobic growth of BL21(DE3) and MR-1 in LB was monitored by OD<sub>600</sub> and colony counting; aerobic growth in M9 was monitored with OD<sub>600</sub>; and anaerobic growth in LB supplemented with sodium lactate and ferric citrate was monitored with pictures of the cultures and microscope images. More details are given below:

#### 13.1.3.1 Optical density

Growth monitoring through OD<sub>600</sub> was carried out exactly as described in section 4.3.1. The only difference was that measurements were made in a Helios Epsilon spectrophotometer (Thermo Spectronic, US).

It is important to note that due to variations in alignment, detectors and light scattering measurements among instruments, different spectrophotometers can present different readings. For that reason, a calibration curve correlating OD<sub>600</sub> measurements in UV-10 and Helios Epsilon was developed (**Figure 13.1**). The calibration curve showed good correlation between both instruments, and according to the linear regression equation in **Figure 13.1**, an OD<sub>600</sub> of 0.5, 1 and 2.5 measured by the UV-10 machine give an OD<sub>600</sub> of 0.436, 0.870 and 2.175 in the Helios device, respectively. It is also important to clarify that all standard OD<sub>600</sub> values used throughout this thesis refer to values obtained with the UV-10 device.

#### 13.1.3.2 Colony counting

In the case of colony counting, the conventional serial dilution method was applied. LB broth was used for diluting the samples and colony forming units were counted on petri dishes with LB agar after overnight incubation at 30 °C.

#### 13.1.3.3 Camera pictures and microscope images

This type of monitoring allowed only a qualitative evaluation of growth. For the monitoring through pictures, samples of 10 mL were withdrawn from the cultures and inserted into 15-mL centrifuge tubes. The samples were then

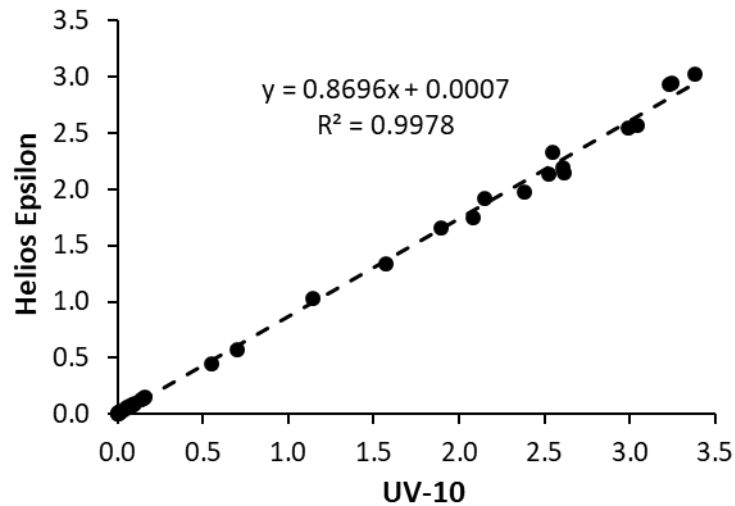


**Figure 13.1:** Regression analysis comparing OD<sub>600</sub> measurements carried out with Helios Epsilon by Thermo Spectronic and UV-10 by Thermo Scientific. The data points were collected from three different experiments in duplicate: BL21(DE3) growing in LB and in M9, and MR-1 growing in LB. The dashed line corresponds to the linear regression.

centrifuged at 4,000 ×g and 4 °C for 10 min and the bottom of the tubes (containing pellets) were photographed. For microscope images, samples of 10-μL were pipetted onto a metallised hemacytometer (Reichert Bright-Line model 1492, Hausser Scientific Company, Horsham, PA) which was then analysed under a BX51TF optical microscope (Olympus, Tokyo, JP) connected to a CCD camera (ProgRes® C5, Jenoptik Optical Systems GmbH, Jena, Germany) operated by the ProgRes® CapturePro 2.6 software (Jenoptik Optical Systems GmbH, Jena, Germany). Pictures and images were taken at times 0 h, 6 h and 24 h after the inoculation of the cells into the serum bottles containing the anaerobic medium. In the cases where growth was not observed at the 24 h measurements, an extra measurement was taken at 48 h.

## 13.2 Results

### 13.2.1 Aerobically grown cultures

The results of the aerobic growth of BL21(DE3) and MR-1 in LB and M9 are depicted in **Figure 13.2**. It can be seen in graphs a) and c) that *E. coli*

reached an OD<sub>600</sub> of 3.4 within 12 h of growth, the same time that  $1.5 \times 10^8$  cfu/mL were counted. After that time, the cultures stabilised at an OD<sub>600</sub> of ca. 2.6 and colony counting of  $1.05 \times 10^8$  cfu/mL. The regression analysis in graph e) comparing OD<sub>600</sub> and colony counting for the first 16 h of growth revealed a reasonable correlation ( $R^2 = 0.83$ ) between the two techniques. Graph g) shows that BL21(DE3) reached a maximum OD<sub>600</sub> smaller in M9 in comparison to LB. The growth pattern of *S. oneidensis* monitored through OD<sub>600</sub> – as depicted in graph b) – was somewhat different than the one for *E. coli*. MR-1 had a two-stage growth, the first stage – with a steeper slope – started at ca. 3 h after inoculation and ended at 8 h of growth; the second one then took over, at a slower rate, and ceased at the 32-h measurement. No proper stationary phase was seen because cell density started to decrease right after the culture reached maximum absorbance. Nevertheless, the most interesting curve was the one depicted in graph d). Colony counting did not follow the normal trend expected for a bacterium, since after 16 h of steady growth the number of colonies counted decreased rapidly, reaching levels lower than  $10^3$  cfu/mL. Although it appears that cells started to die after 16 h of growth, some factors do not corroborate this hypothesis. First, and most importantly, the OD<sub>600</sub> data show a different trend – although to a lower extent, cells continued to develop after 16 h. Then, the visual aspect of the cultures (not shown) did not present clear demonstration of cell death, as the turbidity of the cultures were high after 16 h of growth and formation of clumps of precipitated (dead) biomass was not detected in the flasks. One possible explanation for the phenomenon is that after a period of growth cells lost their capacity to develop in solid medium, turning them into a viable but not culturable state (Brennan et al., 2013). Because of this unusual behaviour of MR-1, regression analysis was carried out only for the period from 0 h to 16 h (graph f), yielding a high R-squared value – 0.99. Also interesting was the lack of growth of MR-1 in M9 (graph h)). It is not entirely clear why this is not a suitable medium for *S. oneidensis* development, however some previous studies already showed growth of MR-1 in M9 supplemented with extra nutrients (Learman et al., 2009).

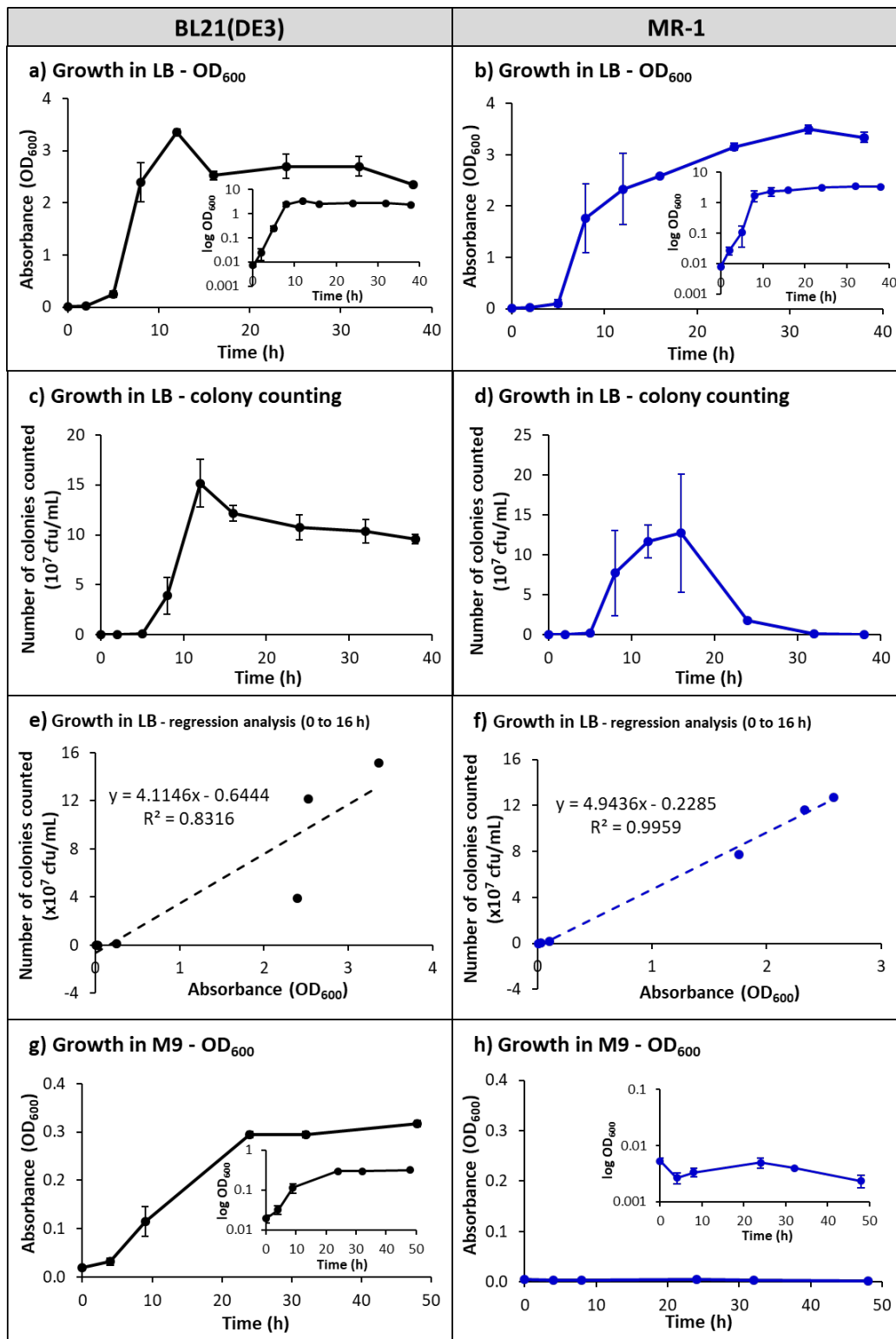


**Figure 13.2:** Monitoring growth of BL21(DE3) and MR-1 in LB and M9 at 30 °C and 180 rpm. Graphs a), c), e) and g) show data for BL21(DE3) and graphs b), d), f) and h) show data for MR-1. Graphs a) and b) show growth in LB monitored through OD<sub>600</sub>; graphs c) and d) show growth in LB monitored through colony counting; graphs e) and f) show regression

analyses comparing the data of OD<sub>600</sub> and colony counting in LB; and graphs g) and h) show growth in M9 monitored through OD<sub>600</sub>. The insets in graphs a), b), g) and h) present the same data as in the original graphs, but as log OD<sub>600</sub> vs. time. Error bars indicate the standard deviation of three independent replicates.

Solving the linear regression equations from graphs e) and f) of **Figure 13.2** for an OD<sub>600</sub> of 2.175 (equivalent to 2.5 in the UV-10, as shown in section 13.1.3.1), we find the concentrations of  $8.30 \times 10^7$  cfu/mL for *E. coli* and  $1.05 \times 10^8$  cfu/mL for *S. oneidensis*. Therefore, both strains can be considered to have similar concentrations at this OD<sub>600</sub> value, which is used as a standard value for the biosynthesis of gold nanoparticles in the present study.

### 13.2.2 Anaerobically grown cultures

The techniques of colony counting, OD<sub>600</sub> and dry cell weight were attempted for monitoring anaerobic growth of *S. oneidensis* wild-type and mutants, but, unfortunately, they were not successful. Colony counting was not feasible as the cells growing under anaerobic conditions did not form colonies in solid medium, possibly because anaerobic conditions triggered the viable but not culturable state. Optical density did not work because ferric citrate is dark, and, consequently, the culture medium with ferric citrate becomes dark. As cells grow, iron(III) ions are respired by the bacteria and get reduced to iron(II), clearing the medium. Since these changes in colour of the medium affect optical density readings, it was not possible to correct this background interference and obtain reliable results. Dry cell weight was also not successful because undissolved ferric citrate pelleted down with bacteria and influenced the weight of the dried samples. Therefore, as the aim of these tests was mainly to determine the strains that grow under anaerobic conditions in LB supplemented with lactate and ferric citrate, the visual monitoring through pictures of the bacterial pellets and images of the cells under the microscope was found to be valid to reach this goal. The results are given in **Figure 13.3** to **Figure 13.12**.



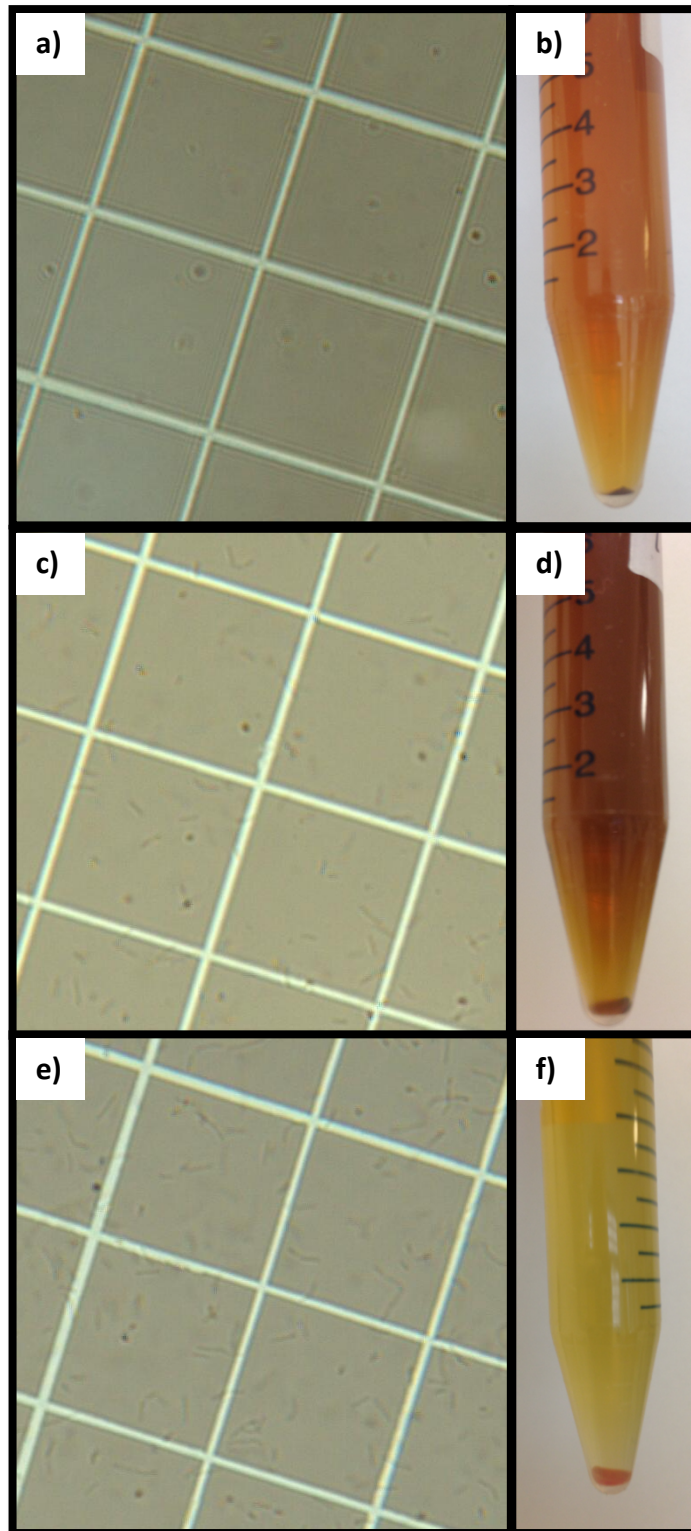


**Figure 13.3:** Monitoring growth of MR-1 in anaerobic media. a), c) and e) are images of cells under the microscope and b), d) and f) are pictures of the cultures after centrifugation. a) and b) show samples at time 0 h, c) and d) show samples at time 6 h, and e) and f) show samples at time 24 h.

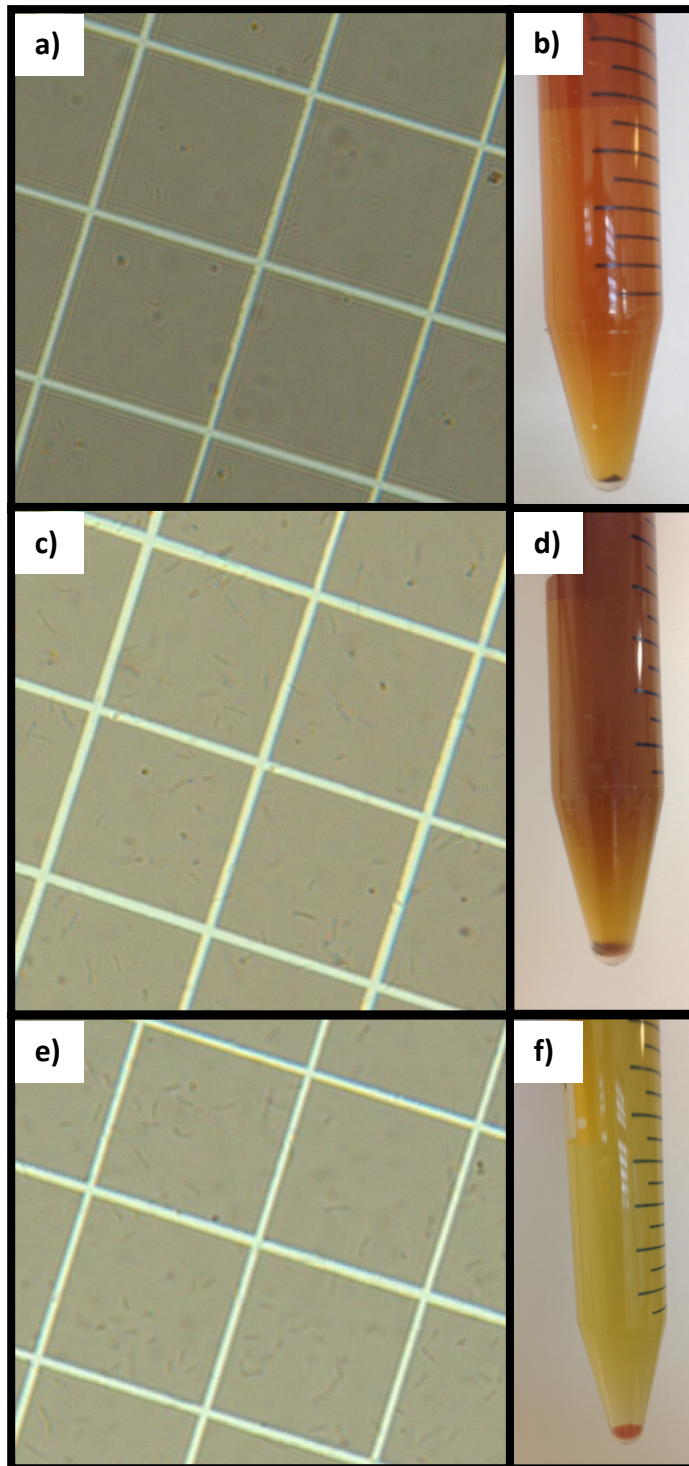


**Figure 13.4:** Monitoring growth of SmA in anaerobic media. a), c) and e) are images of cells under the microscope and b), d) and f) are pictures of the cultures after centrifugation. a) and b) show samples at time 0 h, c) and d) show samples at time 6 h, and e) and f) show samples at time 24 h.

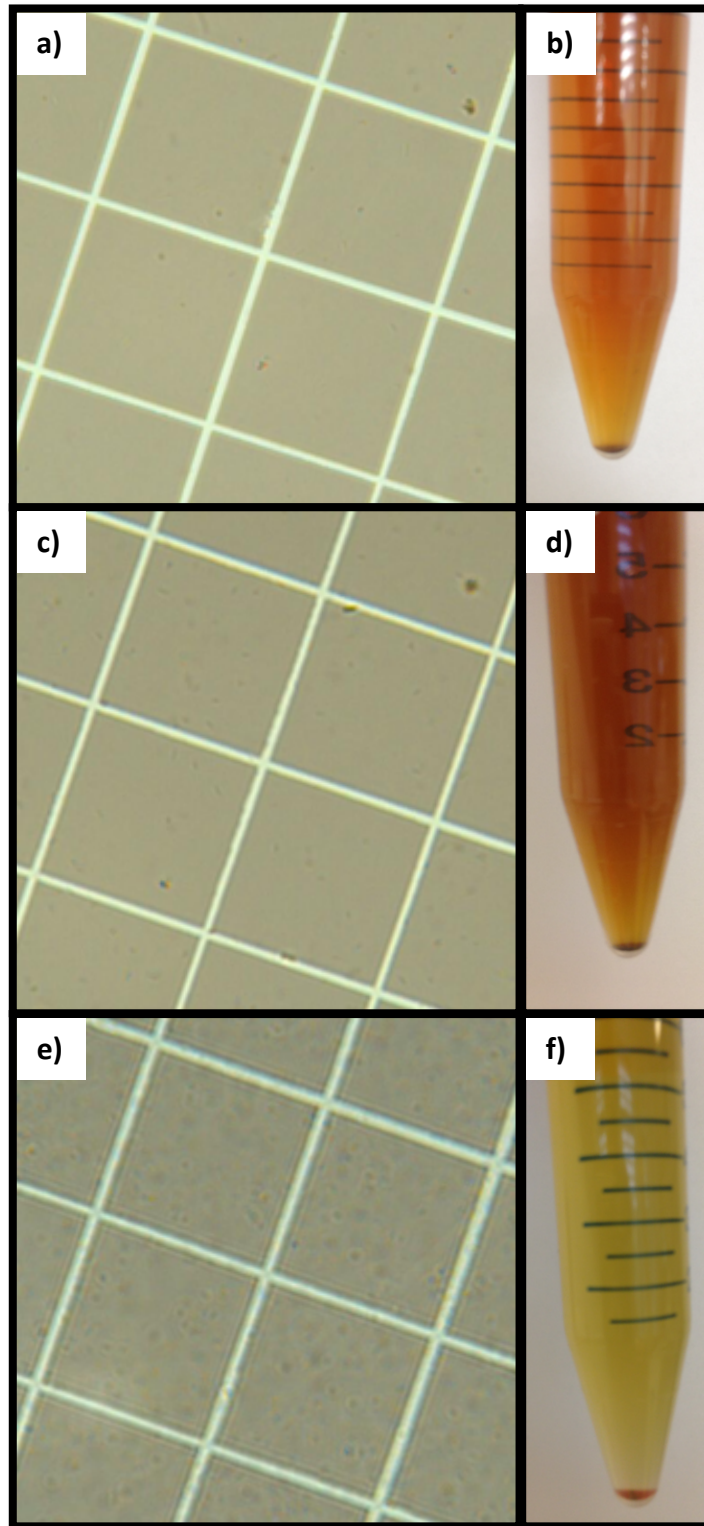


**Figure 13.5:** Monitoring growth of SmC in anaerobic media. a), c) and e) are images of cells under the microscope and b), d) and f) are pictures of the cultures after centrifugation. a) and b) show samples at time 0 h, c) and d) show samples at time 6 h, and e) and f) show samples at time 24 h.

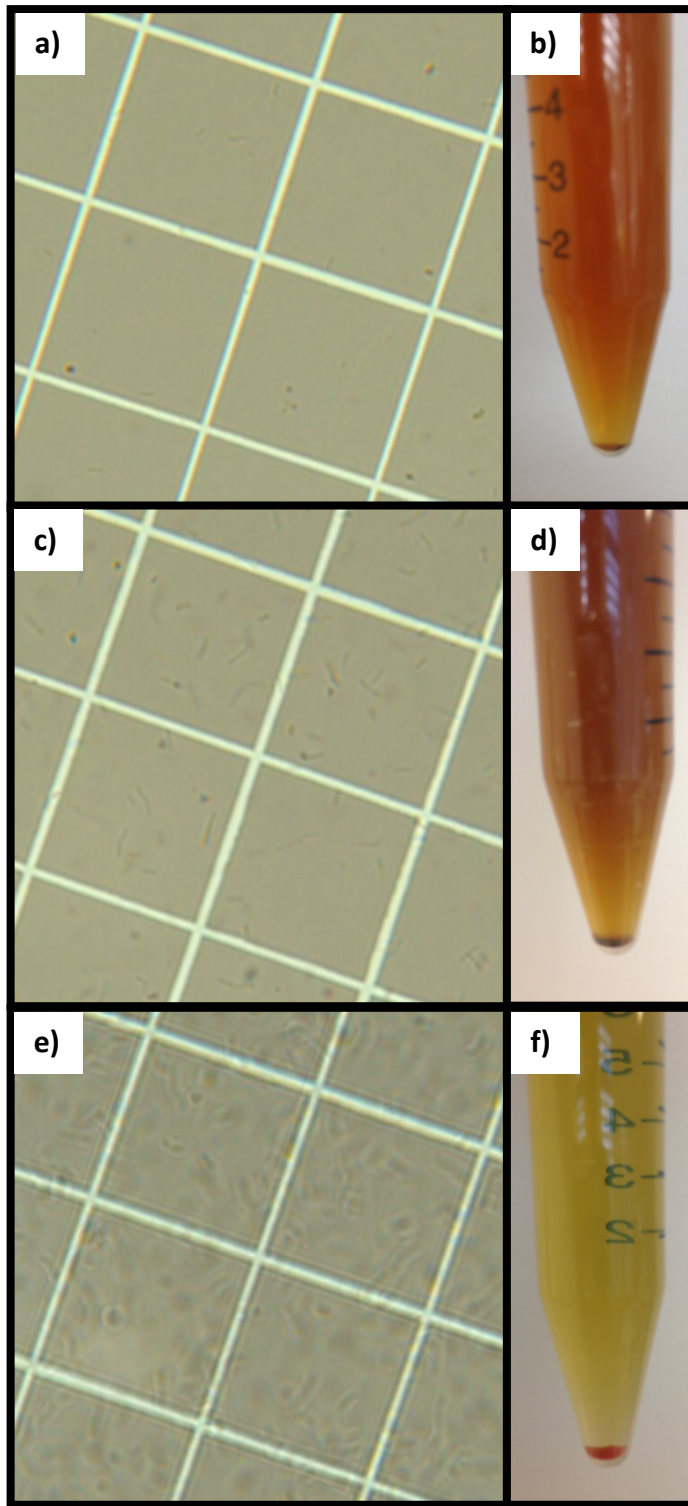


**Figure 13.6:** Monitoring growth of SmF in anaerobic media. a), c) and e) are images of cells under the microscope and b), d) and f) are pictures of the cultures after centrifugation. a) and b) show samples at time 0 h, c) and d) show samples at time 6 h, and e) and f) show samples at time 24 h.

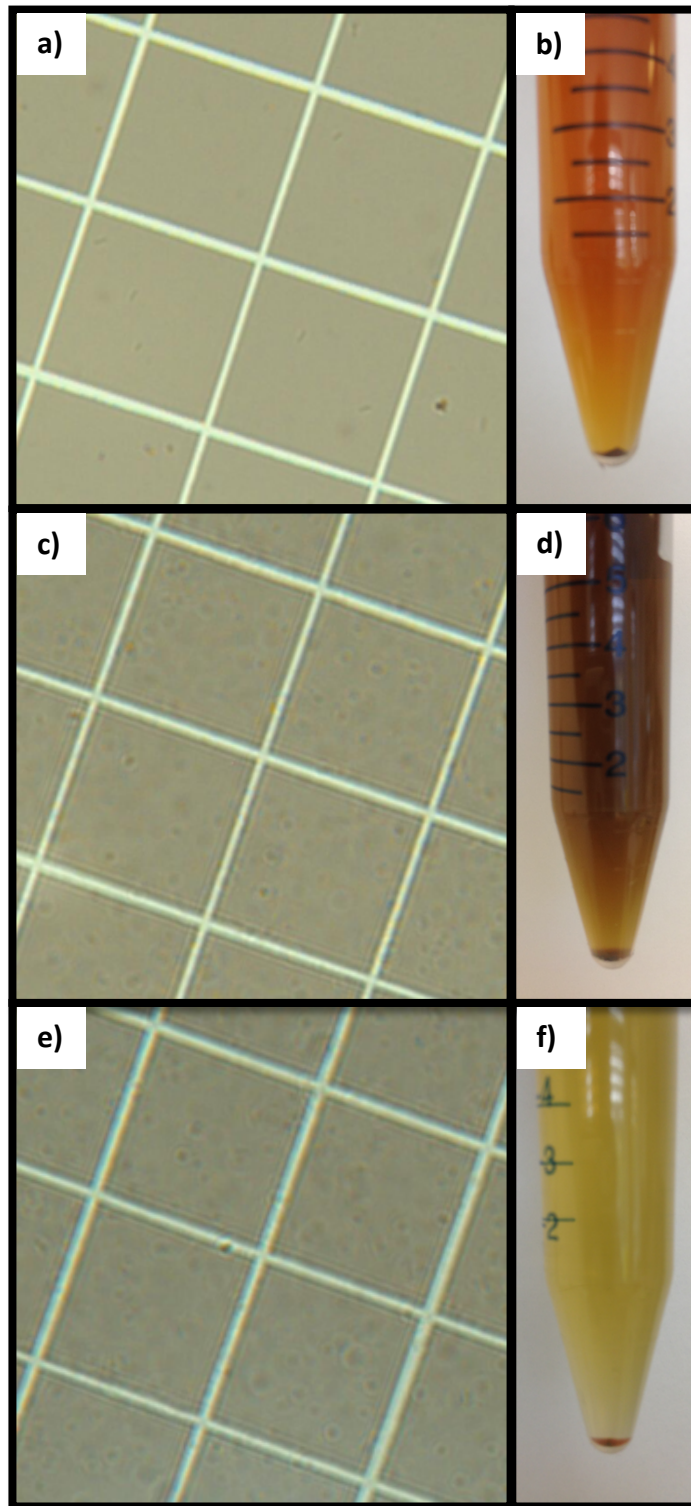


**Figure 13.7:** Monitoring growth of DmAC in anaerobic media. a), c) and e) are images of cells under the microscope and b), d) and f) are pictures of the cultures after centrifugation. a) and b) show samples at time 0 h, c) and d) show samples at time 24 h, and e) and f) show samples at time 48 h.

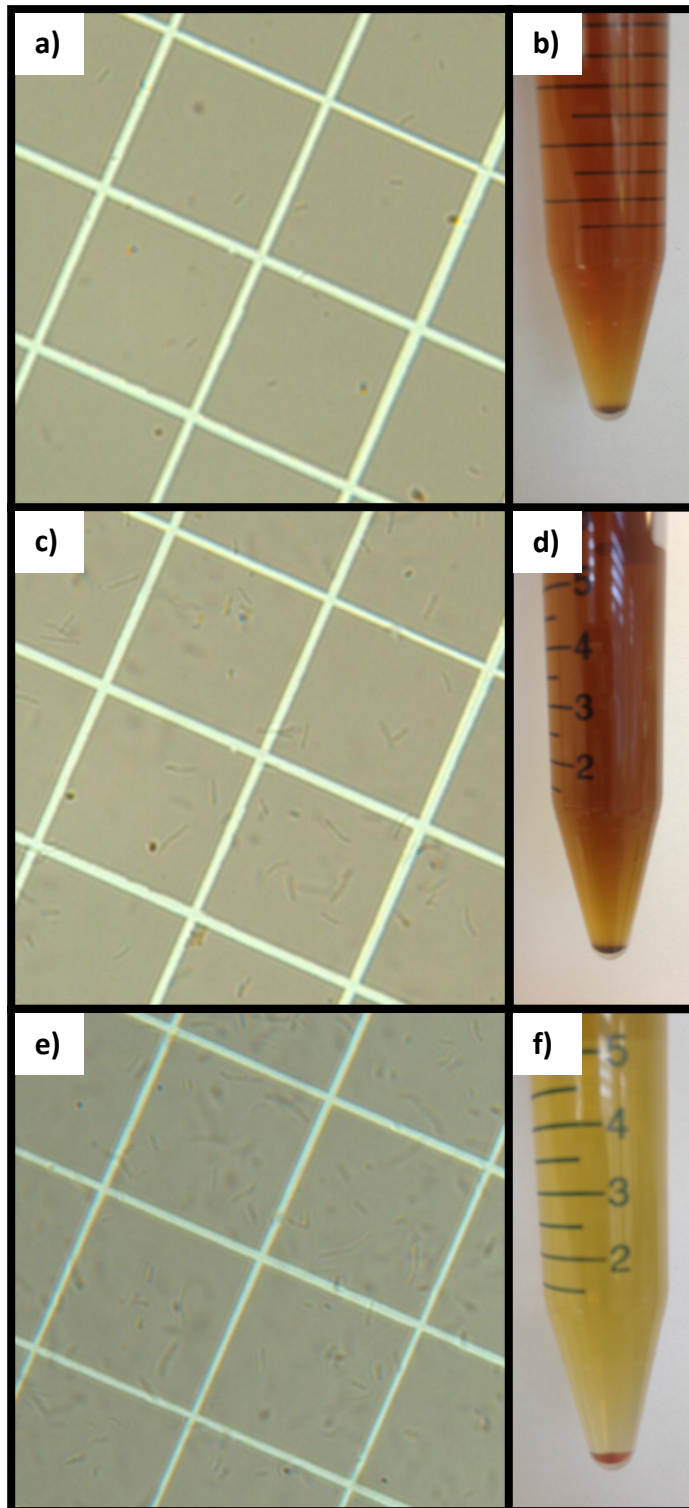


**Figure 13.8:** Monitoring growth of DmAF in anaerobic media. a), c) and e) are images of cells under the microscope and b), d) and f) are pictures of the cultures after centrifugation. a) and b) show samples at time 0 h, c) and d) show samples at time 6 h, and e) and f) show samples at time 24 h.

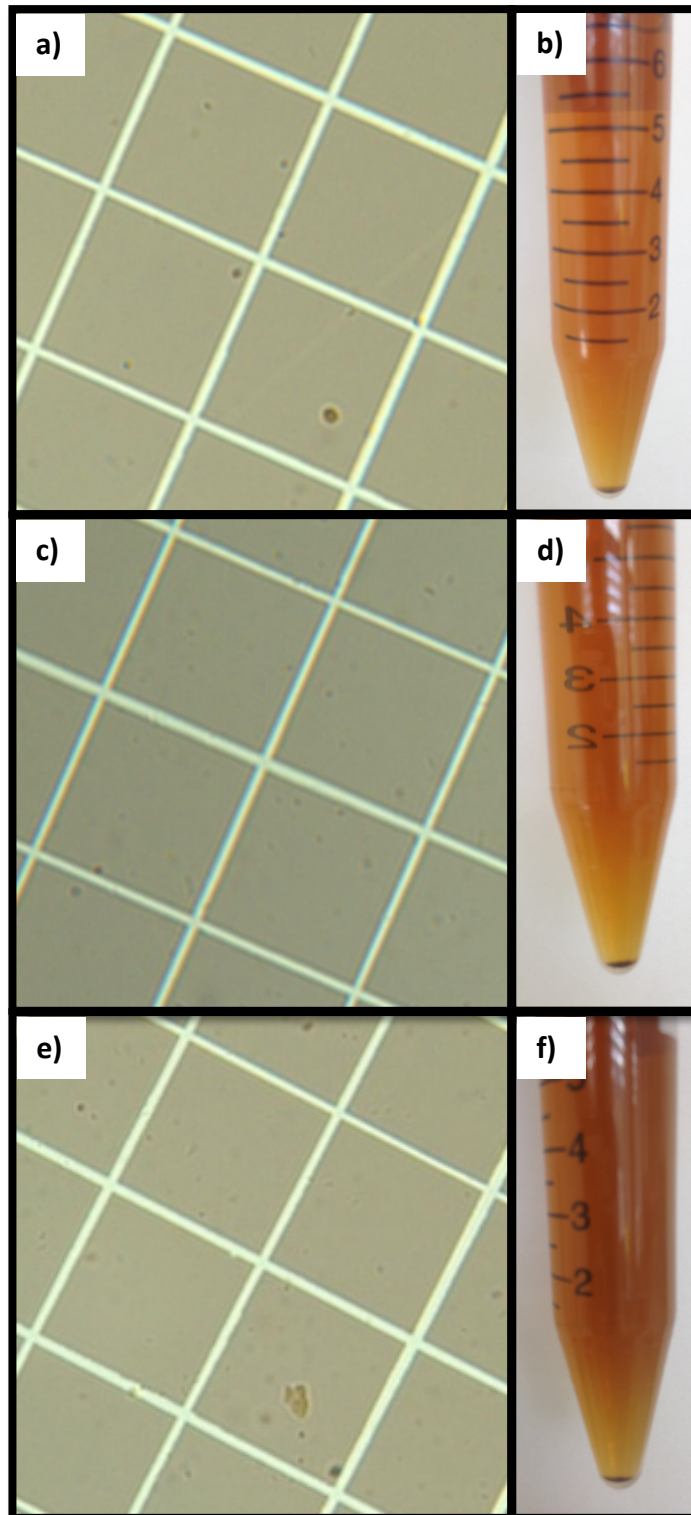


**Figure 13.9:** Monitoring growth of DmCF in anaerobic media. a), c) and e) are images of cells under the microscope and b), d) and f) are pictures of the cultures after centrifugation. a) and b) show samples at time 0 h, c) and d) show samples at time 24 h, and e) and f) show samples at time 48 h.

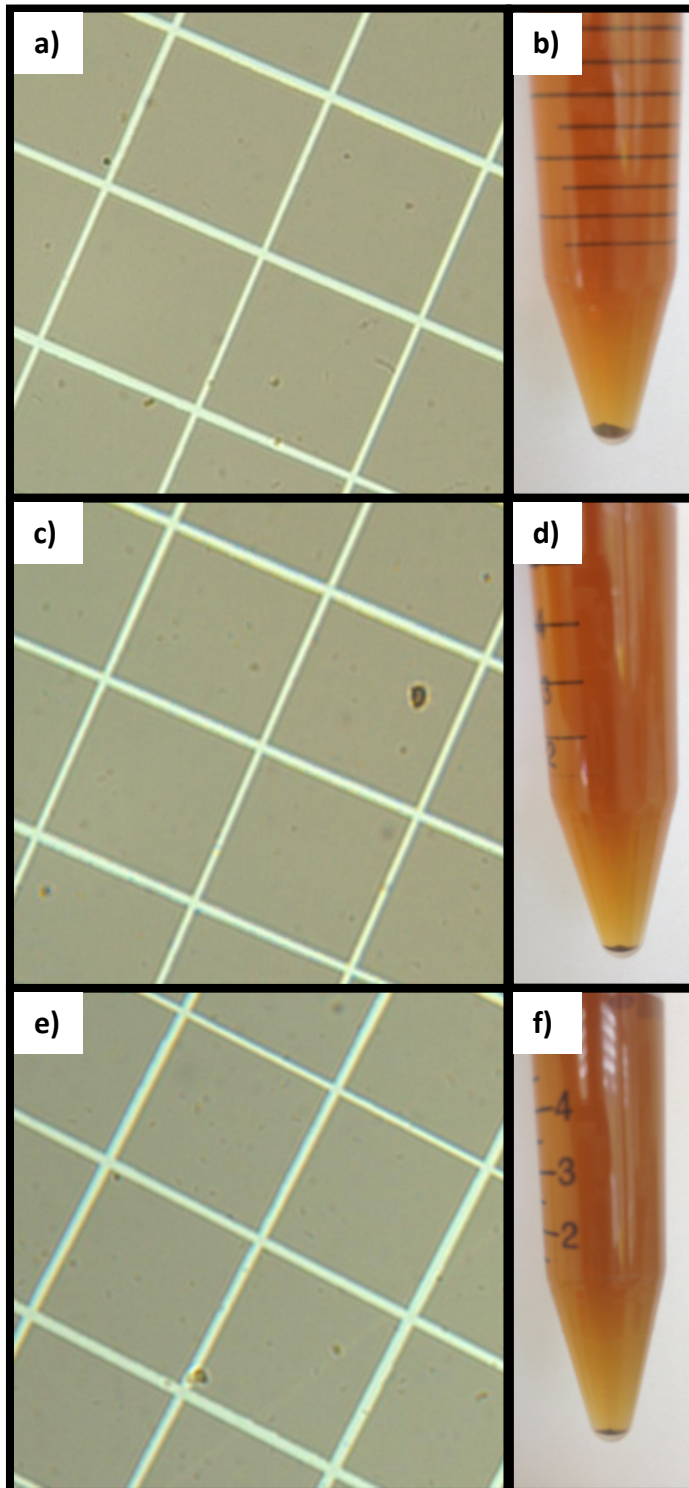


**Figure 13.10:** Monitoring growth of TmACF in anaerobic media. a), c) and e) are images of cells under the microscope and b), d) and f) are pictures of the cultures after centrifugation. a) and b) show samples at time 0 h, c) and d) show samples at time 24 h, and e) and f) show samples at time 48 h.



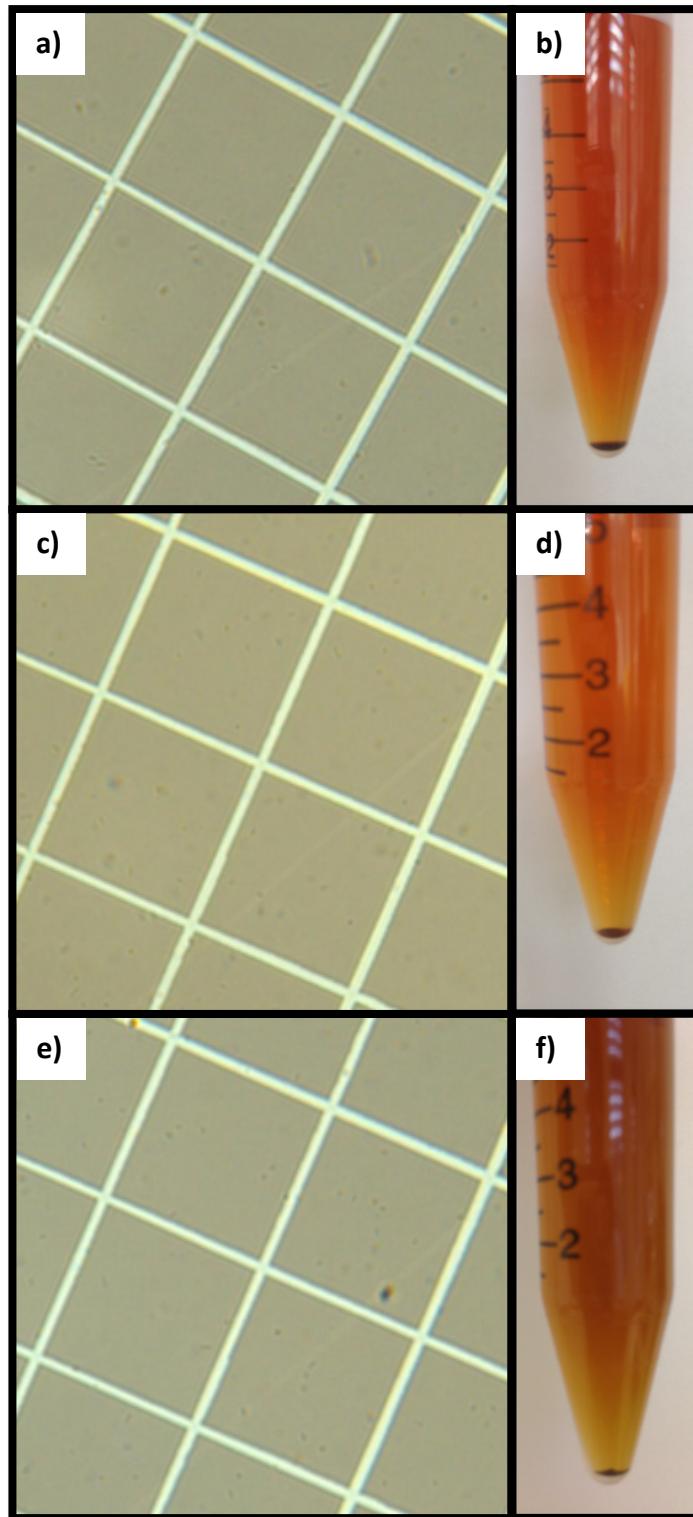


**Figure 13.11:** Monitoring growth of MmOP in anaerobic media. a), c) and e) are images of cells under the microscope and b), d) and f) are pictures of the cultures after centrifugation. a) and b) show samples at time 0 h, c) and d) show samples at time 24 h, and e) and f) show samples at time 48 h.

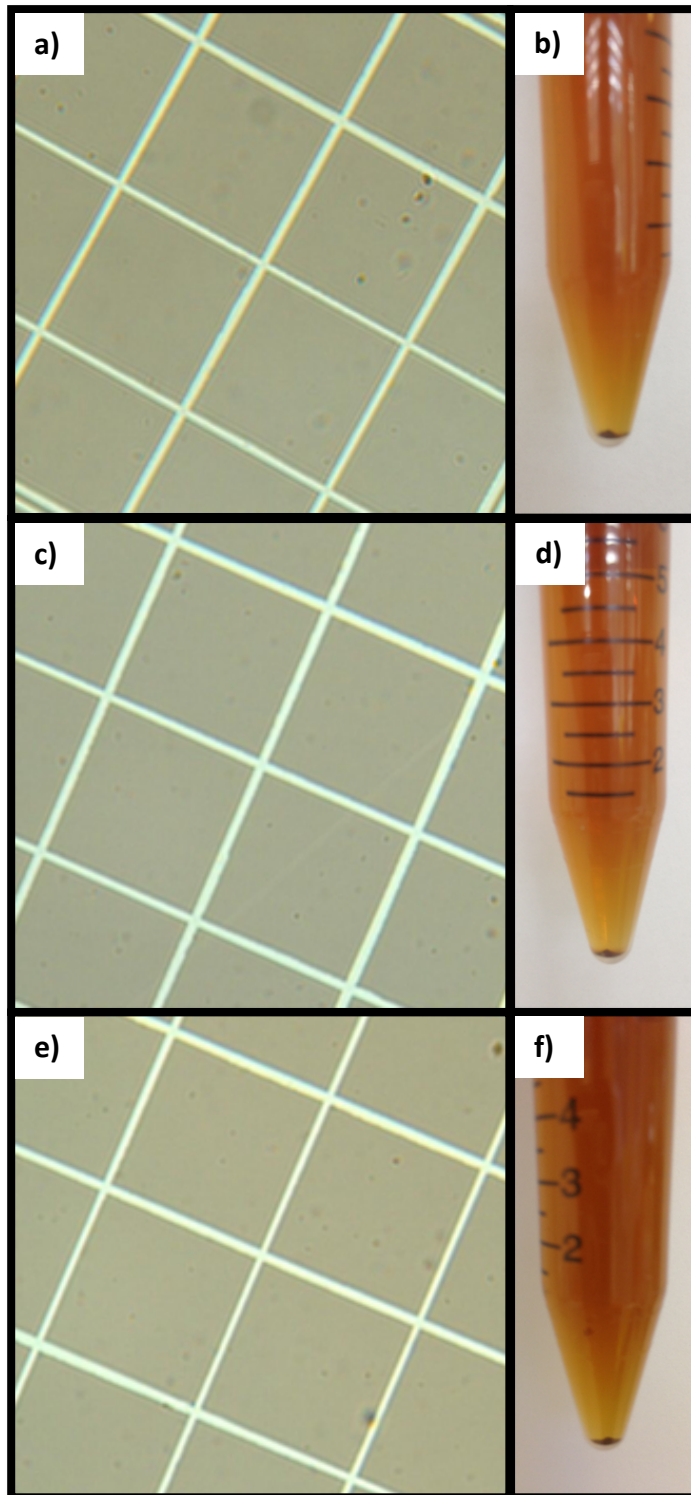


**Figure 13.12:** Monitoring growth of  $CcmC^-$  in anaerobic media. a), c) and e) are images of cells under the microscope and b), d) and f) are pictures of the cultures after centrifugation. a) and b) show samples at time 0 h, c) and d) show samples at time 24 h, and e) and f) show samples at time 48 h.

It is important to clarify that although three independent replicates were measured, only one replicate is depicted (the other replicates all yielded the same results).

The images and pictures shown in **Figure 13.3** to **Figure 13.12** reveal that out of the 10 strains tested, only MR-1, SmA, SmC, SmF, DmAC and DmAF were capable of growing in anaerobic LB supplemented with lactate and ferric citrate. The most obvious manner to determine the growth of the strains was the change in colour of the medium (pictures f) of the figures). The colour of the pellets was another evidence of growth – pellets of *S. oneidensis* growing under anaerobic conditions are reddish. The dark pellets seen in the pictures correspond to undissolved ferric citrate (examples of small rocks of undissolved ferric citrate can be seen in image e) of **Figure 13.9** and image c) of **Figure 13.10**). The images taken with the microscope reinforced the observations from the pictures, i.e. in all cases where colour changes took place the grids of the hemacytometer were filled with bacteria.

One curious fact observed from the figures is that all strains that grew presented change in colour at the 24-h measurement, with the exception of DmAC – which revealed a clearing of the medium only at the 48-h measurement. This observation shows that lack of *omcA* and *mtrC* reduces the rate of respiration of ferric citrate.

## 14 Appendix IV

---

This appendix section presents a series of control data collected to prove that BL21(DE3) and MR-1 are indeed capable of forming AuNPs with method I. The plasmon bands observed in graphs a) and b) of **Figure 5.2**, **Figure 12.2** and **Figure 12.3** already gave a substantial indication that gold nanoparticles were synthesised by the cells, especially because the wavelength of the peaks (around 550 nm) match with what is expected for AuNPs – as explained in section 3.4.1. However, it is important to perform additional control experiments to further confirm that the nanoparticles synthesised are indeed AuNPs.

The first additional evidence for the synthesis of gold nanoparticles by the bacteria is presented in **Figure 14.1**. As demonstrated in section 3.4.1.13.4.1, because of the LSPR phenomenon, when gold atoms aggregate to form particles within a certain size range, these structures reflect colours different than the colour of the bulk metal. Such change in colour is revealed in **Figure 14.1** – pictures d) and e) show that the colours of the cultures after incubation in gold solution are different than the colour of 1 mM H<sub>AuCl</sub><sub>4</sub> solution (picture a)) and the colour of biomass after incubation in DI water (pictures b) and c)). Curiously, BL21(DE3) and MR-1 did not present the same colour after incubation in gold solution, with *E. coli* displaying a purple-brownish colour (picture d)) and *S. oneidensis* displaying a purplish colour (picture e)).

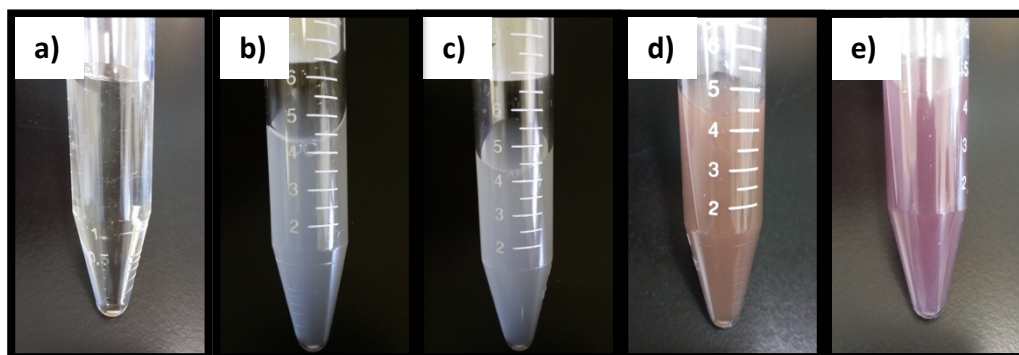


**Figure 14.1:** Pictures of a) 1 mM H<sub>AuCl</sub><sub>4</sub> solution (abiotic control) after incubation at 30 °C and 180 rpm for 48 h; b) BL21(DE3) biomass after

incubation in DI water at 30 °C and 180 rpm for 48 h; c) MR-1 biomass after incubation in DI water at 30 °C and 180 rpm for 48 h; d) BL21(DE3) biomass after incubation in 1 mM H<sub>AuCl</sub><sub>4</sub> solution at 30 °C and 180 rpm for 48 h; e) MR-1 biomass after incubation in 1 mM H<sub>AuCl</sub><sub>4</sub> solution at 30 °C and 180 rpm for 48 h.

The TEM images shown in **Figure 12.10** have provided further proof that AuNPs were formed when cells were incubated in H<sub>AuCl</sub><sub>4</sub> solution, and were not formed when incubated in DI water. However, when gold(III) chloride solution at 1 mM was analysed under the TEM after incubation, as an abiotic control, non-amorphous nanoparticles somewhat similar to the bacterial-made particles were identified (**Figure 14.2**). The same patterns of particles were seen in the three independent replicates analysed. The results reported in **Figure 14.2** is actually an alarming indication that the microorganisms might not be the agents responsible for the formation of nanoparticles, although NPs were more abundant when bacteria were present.

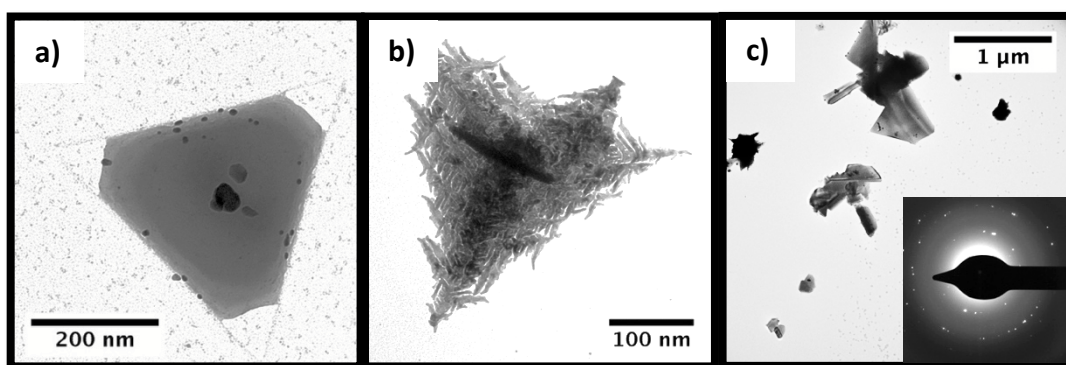


**Figure 14.2:** TEM images of nanoparticles present in 1 mM H<sub>AuCl</sub><sub>4</sub> solution after incubation for 48 h at 30 °C and 180 rpm (abiotic control of method I). The inset corresponds to the SAED measurement of image c).

When the carbon grids are plasma-treated some free radicals can be formed on the surface of the grids and these could, to a low extent, act as centres for chemical reactions. Therefore, there is a possibility that the glow discharged carbon grids are reducing the gold ions of the specimen and turning

them into the nanoparticles observed in **Figure 14.2**. It is unlikely that this phenomenon is taking place, yet this hypothesis was verified through TEM analyses of 1 mM gold(III) chloride solution on grids that were not plasma treated. The results can be found in **Figure 14.3**. As expected, the same type of nanoparticles as in **Figure 14.2** can be found in **Figure 14.3**, ruling out the hypothesis that carbon grids were the agents for nanoparticle formation.

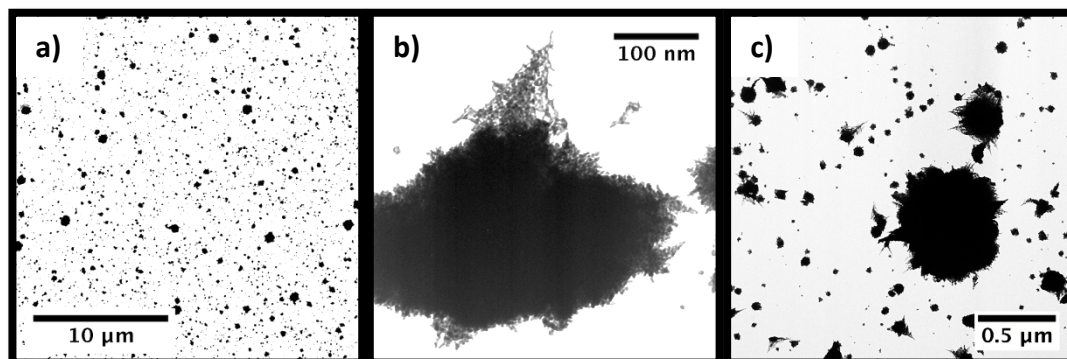


**Figure 14.3:** TEM images of nanoparticles present in 1 mM  $\text{HAuCl}_4$  solution after incubation for 48 h at 30 °C and 180 rpm (abiotic control of method I). The carbon grid was not plasma treated for these analyses.

DI water, after incubation in shake flasks at 30 °C and 180 rpm for 48 h, was also analysed under TEM (**Figure 14.4**). This analysis was made to check whether the particles observed in **Figure 14.2** and **Figure 14.3** were actually contaminants that originated from the water. Although **Figure 14.4** does show nanostructured contaminants, they do not resemble the nanoparticles present in **Figure 14.2** and **Figure 14.3**. These results provide an indication that the particles in **Figure 14.2** and **Figure 14.3** were formed during the incubation of chloroauric acid solution. Intriguingly, according to the SAED result in image b) of **Figure 14.4**, the contaminant in the figure was also non-amorphous. SAED analysis performed for image c) of **Figure 14.4** was a control for electron diffraction, as it was carried out in a selected area without any contaminant.

Since the  $\text{HAuCl}_4$  solution is composed of hydrogen, oxygen, gold and chloride, it is possible that the composition of the particles in the abiotic control is different from composition of the particles attached to the bacteria. In order

to test this, the samples were submitted to EDS analyses. **Figure 14.5** contains the results of the EDS analyses of the particles from the abiotic control as well as from the samples with microorganisms (the measurements were made in the images of **Figure 5.3**).

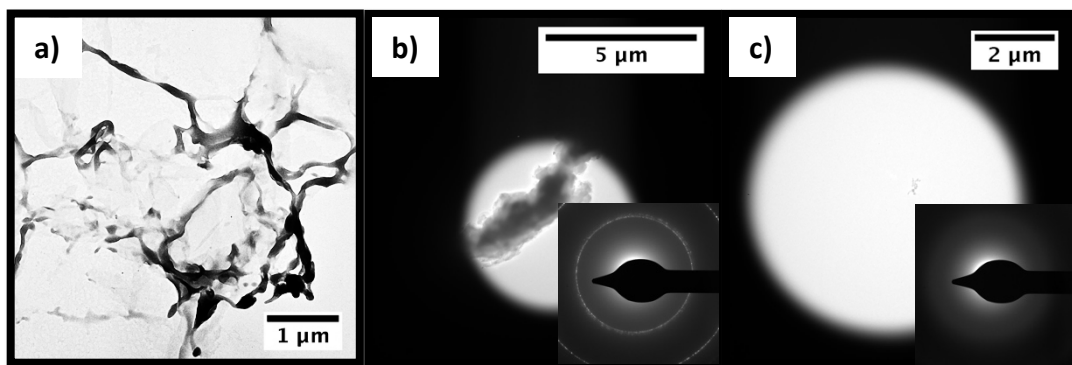


**Figure 14.4:** TEM images of DI water after incubation for 48 h at 30 °C and 180 rpm. The insets in images b) and c) correspond to the SAED measurements of images b) and c), respectively.

The results contained in graph a) of **Figure 14.5** confirms that the particles seen in the control solution are not AuNPs. A substantial peak for chloride and a smaller one for carbon were detected. The composition of the particles made by *E. coli* (graph b)) and *S. oneidensis* (graph c)) is the same, AuNPs. The peaks for copper correspond to the grids supporting the carbon films.

Altogether, these results confirm that method I applied to *E. coli* and *S. oneidensis* allows the formation of gold nanoparticles. Change in colour of the solution, development of surface plasmon bands, TEM and EDS analyses all confirmed that crystal nanostructures of gold were biosynthesised from precursor gold ions; and control experiments revealed that the reduction process was caused by the bacterial cells.

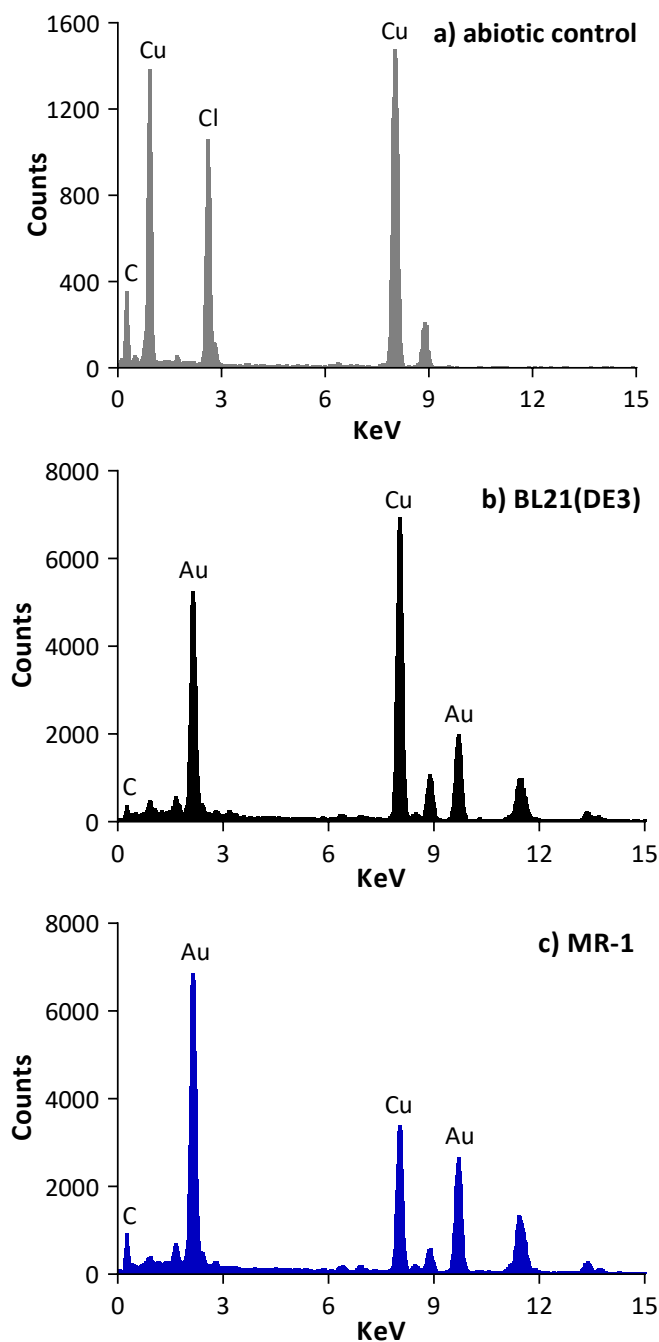


**Figure 14.5:** EDS measurements of a) nanoparticles present in 1 mM  $\text{HAuCl}_4$  solution after incubation for 48 h at 30 °C and 180 rpm (abiotic control of method I); b) nanoparticles made by BL21(DE3) after incubation in 1 mM  $\text{HAuCl}_4$  solution for 48 h at 30 °C and 180 rpm; c) nanoparticles made by MR-1 after incubation in 1 mM  $\text{HAuCl}_4$  solution for 48 h at 30 °C and 180 rpm.